Measurement of energy performance : Analysis of QUB method

Naveed Ahmad

N° d'ordre NNT : 2020LYSEI051

THESE de DOCTORAT DE L'UNIVERSITE DE LYON
opérée au sein de
Institut National des Sciences Appliquées de Lyon
École Doctorale N° ED 162
Mécanique, énergétique, génie civil, acoustique (MEGA)

Spécialité / discipline de doctorat :
Énergétique

Soutenue publiquement le 08/07/2020, par :
Naveed AHMAD

Measurement of Energy Performance: Analysis of QUB method

Devant le jury composé de :

SAELENS, Dirk :	**Professeur des Universités, KU Leuven, Belgique, examinateur**	Président

JIMENEZ, Maria Jose :	Directrice de recherche, CIEMAT, Espagne, rapporteuse
IBOS, Laurent :	MCF, HDR, CERTES, Université Paris-Est Créteil, France, rapporteur
SAELENS, Dirk :	Professeur des Universités, KU Leuven, Belgique, examinateur
GHIAUS, Christian :	Professeur des Universités, INSA Lyon, France, Directeur de thèse

This page is intentionally left blank

Département FEDORA – INSA Lyon - Ecoles Doctorales – Quinquennal 2016-2020

SIGLE	ECOLE DOCTORALE	NOM ET COORDONNEES DU RESPONSABLE
CHIMIE	**CHIMIE DE LYON** http://www.edchimie-lyon.fr Sec. : Renée EL MELHEM Bât. Blaise PASCAL, 3e étage secretariat@edchimie-lyon.fr	**M. Stéphane DANIELE** Institut de recherches sur la catalyse et l'environnement de Lyon IRCELYON-UMR 5256 Équipe CDFA 2 Avenue Albert EINSTEIN
E.E.A.	**ÉLECTRONIQUE, ÉLECTROTECHNIQUE, AUTOMATIQUE** http://edeea.ec-lyon.fr Secr. M.C. HAVGOUDOUKIAN	**M. Gérard SCORLETTI** École Centrale de Lyon 36 Avenue Guy DE COLLONGUE 69 134 Écully Tél : 04.72.18.60.97 Fax 04.78.43.37.17
E2M2	**ÉVOLUTION, ÉCOSYSTÈME, MICROBIOLOGIE, MODÉLISATION** http://e2m2.universite-lyon.fr Sec. : Sylvie ROBERJOT Bât. Atrium, UCB Lyon 1 Tél : 04.72.44.83.62	**M. Philippe NORMAND** UMR 5557 Lab. d'Ecologie Microbienne Université Claude Bernard Lyon 1 Bâtiment Mendel 43, boulevard du 11 Novembre 1918 69 622 Villeurbanne CEDEX
EDISS	**INTERDISCIPLINAIRE SCIENCES-SANTÉ** http://www.ediss-lyon.fr Sec. : Sylvie ROBERJOT Bât. Atrium, UCB Lyon 1 Tél : 04.72.44.83.62	**Mme Sylvie RICARD-BLUM** Institut de Chimie et Biochimie Moléculaires et Supramoléculaires (ICBMS) - UMR 5246 CNRS - Université Lyon 1 Bâtiment Curien - 3ème étage Nord 43 Boulevard du 11 novembre 1918 69622 Villeurbanne Cedex
INFOMATHS	**INFORMATIQUE ET MATHÉMATIQUES** http://edinfomaths.universite-lyon.fr Sec. : Renée EL MELHEM Bât. Blaise PASCAL, 3e étage	**M. Hamamache KHEDDOUCI** Bât. Nautibus 43, Boulevard du 11 novembre 1918 69 622 Villeurbanne Cedex France Tel : 04.72.44.83.69 hamamache.kheddouci@univ-lyon1.fr
Matériaux	**MATÉRIAUX DE LYON** http://ed34.universite-lyon.fr Sec. : Stéphanie CAUVIN Tél : 04.72.43.71.70 Bât. Direction	**M. Jean-Yves BUFFIÈRE** INSA de Lyon MATEIS - Bât. Saint-Exupéry 7 Avenue Jean CAPELLE 69 621 Villeurbanne CEDEX

MEGA	**MÉCANIQUE, ÉNERGÉTIQUE, GÉNIE CIVIL, ACOUSTIQUE** **http://edmega.universite-lyon.fr** Sec. : Stéphanie CAUVIN Tél : 04.72.43.71.70 Bât. Direction	**M. Jocelyn BONJOUR** INSA de Lyon Laboratoire CETHIL Bâtiment,Sadi-Carnot 9, rue de la Physique 69 621 Villeurbanne CEDEX
ScSo	**ScSo*** **http://ed483.univ-lyon2.fr** Sec. : Véronique GUICHARD INSA : J.Y. TOUSSAINT Tél : 04.78.69.72.76	**M. Christian MONTES** Université Lyon 2 86 Rue Pasteur 69 365 Lyon CEDEX 07 **christian.montes@univ-lyon2.fr**

*ScSo : Histoire, Géographie, Aménagement, Urbanisme, Archéologie, Science politique, Sociologie, Anthropologie

Abstract

Le QUB est une méthode d'essai de caractérisation thermique in situ dynamique qui a le potentiel d'être menée sur une courte durée d'une à deux nuits. La méthode a été testée sur des bâtiments à petite échelle, sur une maison à grande échelle avec un environnement contrôlé et une maison à grande échelle avec des conditions météorologiques réelles. La valeur globale du coefficient de transfert de chaleur (H) mesurée à l'aide de la méthode QUB se situe généralement à ± 15% de la valeur mesurée à l'état d'équilibre. Avec une telle variance, il est important de comprendre comment les résultats QUB varient avec les conditions aux limites (radiations solaires, température extérieure, température extérieure pendant la nuit de test QUB) et les conditions initiales (puissance initiale avant l'expérience QUB). L'expérience QUB, c'est-à-dire la puissance de chauffage et la durée, sont optimisées en utilisant une connaissance a priori (c'est-à-dire une valeur supposée) du coefficient de transfert global du bâtiment, H_{ref}. La robustesse de la méthode QUB avec l'incertitude du niveau de puissance (pendant la phase de chauffage QUB), l'incertitude du coefficient de transfert de chaleur global à l'état d'équilibre, H_{ref}, et les températures extérieures en fonction des saisons doivent être établies pour les bâtiments réels.

Il est coûteux d'effectuer des expériences QUB sur une vraie maison pendant une longue période avec des conditions limites et initiales variables, différents niveaux d'isolation et des saisons. Afin de faire des expériences numériques, un modèle dynamique d'état-espace est développé et testé dans cette thèse. La modélisation espace-état consiste à générer un circuit thermique pour chaque composant du bâtiment (murs, fenestration, système de ventilation, etc.). Les circuits thermiques sont ensuite assemblés pour générer un seul circuit pour l'ensemble du bâtiment. Le modèle de l'espace d'état est validé en utilisant les caractéristiques thermiques et les données mesurées d'une maison à grande échelle (la maison jumelle) fournies par l'Annexe 58 de IEA EBC Caractérisation fiable de la performance énergétique du bâtiment basée sur des mesures dynamiques à grande échelle. L'erreur de la température intérieure simulée de toute la maison (sept zones thermiques) pour un pas de temps de 10 min. est de l'ordre de ± 2 °C, avec trois quartiles des erreurs se situant à ± 1 °C. Le modèle espace-état développé dans ce travail nous aide à analyser les valeurs propres et les constantes de temps du bâtiment. Ils sont utilisés pour optimiser le maillage utilisé dans la

modélisation, pour attribuer les conditions initiales, pour concevoir une expérience QUB optimale et pour expliquer pourquoi des expériences à temps relativement court peuvent être utilisées pour déterminer la valeur globale du coefficient de transfert de chaleur, qui est une caractéristique en régime permanent.

Des expériences QUB ont également été menées sur la maison mentionnée ci-dessus. Les différences entre les mesures et les simulations numériques étaient de ± 1 ℃. En utilisant le modèle numérique, les expériences QUB montrent que la méthode ne présente que de légères variations avec une incertitude de puissance; par exemple, une erreur de 30% de la puissance optimale peut provoquer une erreur à moins de 3% de la valeur de référence. Par conséquent, la méthode QUB peut être considérée comme robuste avec la variation de puissance. Une analyse d'erreur a posteriori est effectuée en prenant soin des expériences QUB dans des situations où l'enveloppe réelle a des caractéristiques différentes de celles supposées dans la conception de l'expérience pour la méthode QUB. Ces résultats sont ensuite comparés à des erreurs a priori, une situation dans laquelle des expériences QUB sont effectuées avec la connaissance de l'enveloppe réelle. L'analyse d'erreur montre qu'avec une erreur de 50% du coefficient de transfert de chaleur global (c'est-à-dire une situation d'isolation de paroi manquante), la méthode QUB entraîne une erreur accrue de seulement 3%.

La précision de la méthode QUB a également été testée avec la variation du rayonnement solaire. Les résultats QUB les jours nuageux montrent une variation moindre par rapport aux jours ensoleillés. Il a été démontré que le transfert de chaleur des radiations solaires retardées entrant à travers les murs du bâtiment a un effet sur l'évolution de la température au cours de l'expérience QUB. Cela peut entraîner une augmentation de l'erreur dans la méthode QUB. Une méthode est proposée dans cette thèse pour estimer la contribution du rayonnement solaire et du facteur correctif solaire pouvant réduire l'erreur de la méthode QUB. L'impact du facteur correctif dépend du rayonnement solaire pendant la veille de l'expérience QUB et de la diffusivité de l'enveloppe du bâtiment.

Les expériences QUB sont simulées en été et en hiver pour déterminer l'impact des saisons sur la précision de la méthode. La saison d'hiver montre des résultats plus robustes que les mois d'été. Les mois d'été montrent une plus grande variation des résultats. Il est vérifié que la grande variation est due à une petite différence de température entre les conditions intérieures et extérieures pendant certaines nuits d'été. Les expériences en saison estivale peuvent être améliorées en augmentant la température de consigne avant l'expérience QUB.

Abstract

QUB is a dynamic in-situ thermal characterization test method that has the potential to be conducted in a short duration of one to two nights. The method was tested on small scale buildings, on a full-scale house with controlled environment and a full-scale house with real weather conditions. The overall heat transfer coefficient value (H) measured using QUB method usually lies within ± 15 % of the value measured in steady state. With such a variance, it is important to understand how the QUB results vary with the boundary conditions (solar radiations, outdoor temperature, outdoor temperature during QUB test night) and the initial conditions (initial power before QUB experiment). The QUB experiment, i.e. the heating power and time duration, are optimized by using a priori knowledge (i.e. a supposed value) of the overall transfer coefficient of the building, H_{ref}. The robustness of QUB method with uncertainty in power level (during QUB heating phase), uncertainty in overall heat transfer coefficient at steady state, H_{ref}, and the outdoor temperatures a function of seasons needs to be established for real buildings.

It is expensive to perform QUB experiments on a real house for a long time with varying boundary and initial conditions, different levels of insulation and seasons. In order to make numerical experiments, a dynamic state-space model is developed and tested in this thesis. The state-space modelling involves generating a thermal circuit for each component of the building (walls, fenestration, ventilation system, etc.). The thermal circuits are then assembled to generate a single circuit for the entire building. The state-space model is validated using thermal characteristics and measured data of a full-scale house (the twin house) provided by IEA EBC Annex 58 *Reliable Building Energy Performance Characterisation Based on Full Scale Dynamic Measurements*. The error of the simulated indoor temperature of the entire house (seven thermal zones) for a time-step of 10 min. is in the range of ± 2°C, with three quartiles of the errors being within ± 1°C. The state-space model developed in this work helps us to analyse the eigen values and the time constants of the building. They are used to optimize the meshing used in modelling, to assign the initial conditions, to design an optimal QUB experiment and to explain why relatively short time experiments can be used for determining the overall heat transfer coefficient value, which is a steady-state characteristic.

QUB experiments were also conducted on the house mentioned above. The differences between the measurements and the numerical simulations were within ± 1℃. By using the numerical model, the QUB experiments show that the method has only slight variation with uncertainty in power; for example, 30% error in optimum power can cause an error within $3\,\%$ of the reference value. Therefore, QUB method can be considered as robust with the variation in power. A posteriori error analysis is performed by caring on QUB experiments in situations in which the real envelope has different characteristics than those assumed in the design of the experiment for QUB method. These results are then compared with a priori errors, a situation in which QUB experiments are performed with the knowledge of the real envelope. The error analysis shows that with $50\,\%$ error in the overall heat transfer coefficient (i.e. missing wall insulation situation), the QUB method results in an increased error of only $3\,\%$.

The precision of QUB method was tested also with the variation of solar radiation. QUB results on cloudy days show lesser variation as compared to sunny days. It was shown that the heat transfer from the delayed solar radiations entering through the walls of the building has an effect on the temperature evolution during the QUB experiment. This can lead to an increased error in QUB method. A method is proposed in this thesis to estimate the contribution of solar radiation and of the solar corrective factor that can reduce the error of QUB method. The impact of the corrective factor depends on the solar radiation during the day before the QUB experiment and the diffusivity of the building envelope.

The QUB experiments are simulated during summer and winter to determine the impact of seasons on the accuracy of the method. The winter season shows more robust results as compared to summer months. The summer months show larger variation of results. It is verified that the large variation are due to small temperature difference between indoor and outdoor conditions during some of the summer nights. The experiments in summer season can be improved by increasing the set point temperature before the QUB experiment.

Table of contents

List of figures

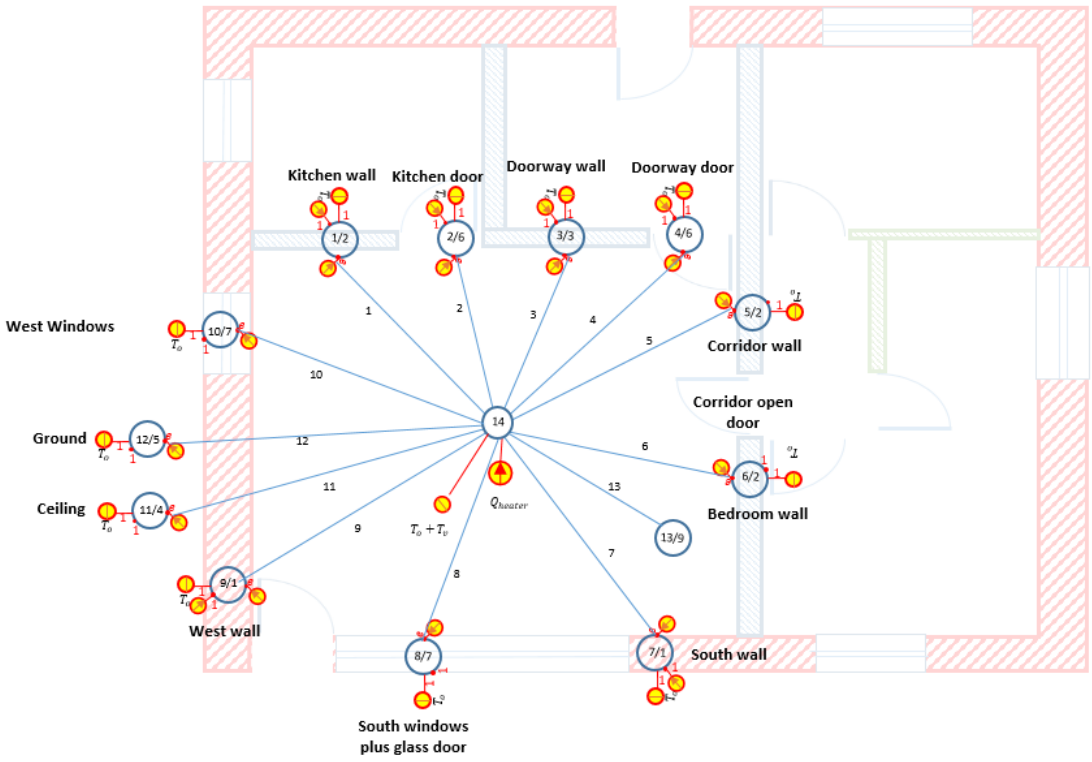

List of Tables

List of abbreviations

ANN	Artificial Neural Networks
ASHRAE	American Society for Heating, Refrigerating and Air-conditioning Engineers
BREAM	Building Research Establishment Environmental Assessment Method
BWM	Box Whisker Mean Plots
CEN	Comité Européen de Normalisation
DT	Delta Test
DOE	Department of Energy, US
ECM	Energy Conservation Measures
EPA	Environmental Protection Agency, US
EPBD	EU Energy Performance of Buildings Directives
EPC	Energy Performance Certificates
EPI	Energy Performance Indicators
EVO	Efficiency Valuation Organization
EIA	Energy Information Administration
EU	European Union
EUI	Energy Utilization Index
GA	Genetic Algorithms
GHG	Greenhouse Gas
IPCC	Intergovernmental Panel on Climate Change
HERS	Home Energy Rating System
HVAC	Heating, Ventilation and Air Conditioning
ICC	International Code Council
ICT	Information and Communication Technology
IECC	International Energy Conservation Code (buildings)
IEA	International Energy Agency
IEO	International Energy Outlook
IPMVP	International Performance Measurement and Verification Protocol
ISO	International Standardization Organization
LEED	Leadership in Energy and Environmental Design

MOAT	Morris Once-at-a-Time
MC	Monte Carlo
SA	Sensitivity Analysis
STEM	Short Term Energy Monitoring
SVM	Support Vector Machine
PMEP	Performance Measurement and Evaluation Plan
UMP	Uniform Methods Project

List of symbols

Capital letters	
A_s	surface area, m^2
C	internal thermal capacity, J/K
H	over-all heat transfer coefficient, W/K
H_{ref}	steady state over-all heat transfer coefficient, W/K
H_{QUB}	over-all heat transfer coefficient measured using QUB method
P_1	power measured during the heating phase of QUB experiment, W
P_2	power measured during the cooling phase of QUB experiment, W
T	temperature, K or C^o
T_o	ambient temperature, K or °C
T_i	boundary temperature, K or °C
T_1	temperature difference between outside and inside of the building during heating phase of the QUB method, °C
T_2	temperature difference between outside and inside building during the cooling phase of the QUB method
K_p	steady state gain for power
K_i	steady state gain for boundary temperature
U	heat transfer co-efficient, $W/m^2/K$
Greek letters	
$\bar{\theta}$	mean temperature, K or °C
θ_i	indoor temperature, K or °C
τ	time constant, hour or seconds
φ	heat input, W
α_1	temperature slope during heating phase of the QUB experiment
α_2	temperature slope during cooling phase of the QUB experiment
Vectors and matrices	
A	state matrix in state space model
B	input matrix in state space model
C	output matrix in state space model

D	feed through matrix
u	input vector
$\mathbf{u}_{ss}$	steady state input vector
x	state vector
y	output vector
$\mathbf{y}_{ss}$	steady state output vector

This page is intentionally left blank

1 Introduction

1.1 Socio-economic relevance

World energy consumption has shown a consistent growth. *International Energy Outlook* 2019 (IEO 2019) has projected an annual growth of 3 %, between 2018 and 2050, leading to an increase in energy consumption from 600 quadrillion BTU to 911 quadrillion BTU [1]. Energy in building is the major source of greenhouse gas emissions and the sector with highest growth in emissions in future scenario [2]. Building sector therefore risks to increase the CO_2 emissions but at the same time has the opportunity to reduce greenhouse gas emissions. Reduction in energy sector focuses on two sides: supply-side reduction by switching to renewable energy sources and demand-side reduction by improving energy efficiency.

Buildings offer a promising opportunity to reduce greenhouse gas emissions via demand-side reduction/management through energy efficiency improvement. In 2010, buildings (residential and commercial) accounted for 32 % of the total greenhouse gas emissions and one third of black carbon emissions worldwide. Buildings consume 21 % of the total energy worldwide. It is projected as the sector with the highest growth in energy consumption of 1.4 % per year between 2018 and 2050 [1].

The projected increase in building energy consumption is due to improvement in living standards, changing lifestyles, population growth and rapid urbanization. United Nation's *World Urbanization Prospects* reports that presently 54 % of the total world population is living in urban centers, that is expected to grow to 66 % by 2050 [3]. Increasing number of commercial and residential buildings in developing countries will increase energy consumption and associated emissions.

In absence of mitigation strategies and policies, it is expected that building energy consumption will increase two to three folds, by 2050 [4]. With 32 % of the total world GHG emissions, buildings offer an immense opportunity of improvement. This is the reason why building energy consumption sector is receiving significant attention for improvement in energy efficiency. Paris Agreement on climate change (COP21) and Montreal protocol have included buildings as important resources to reduce greenhouse gas emissions [5]. The IPCC (UN Intergovernmental Panel on Climate Change) working group III works on GHG mitigation strategies in different sectors, including buildings (IPCC, 2018).

The increase in building GHG emissions, by two to three folds as projected, can be stabilized at its 2005 level and can even be reduced further. Energy efficiency policies, mitigation strategies, awareness campaigns and efficient technologies will play key role to reduce energy consumption in buildings. GEA [6] has projected that with broad based application of existing energy policies and technologies, 45 % reduction in heating and cooling loads is achievable in buildings.

Significant savings can be achieved in both new and existing buildings. Depending on the level and type of retrofit (deep or shallow) and the type of building, the potential savings achieved can range from 25 % to 90 % [4]. Due to this potential, building energy efficiency sector received highest percentage (58 %) of investments in energy efficiency, in IEA member countries (including six major emerging economies Brazil, China, India, Indonesia, Russian Federation and Mexico)[5].

Monetary benefits from savings are coupled with other benefits, referred as co-benefits. If the impacts of co-benefits are counted, then the actual benefits from retrofit are double the indicated economic benefits. Common co-benefits include:

1. health benefits from improved indoor and outdoor conditions,
2. ecological benefits due to reduce carbon footprint,
3. employment creation,
4. service provision benefits (reduction of transmission and distribution losses,

5. social effects (e.g. reduction in energy poverty, improved control on indoor environment) [5].

To meet the GHG mitigation goals using potential savings from buildings, some barriers are yet to be overcome. These include improvements on availability of direct data from buildings, gaps in knowledge to understand the buildings behavior, lack of comprehensive measured data from real occupied buildings, difficulty to predict occupants' behavior and life styles, inclusion of energy efficiency in building decisions, continuous and dissemination of available resources, knowledge and policies to the public [2].

Variation and uncertainties in building energy consumption at building level, and consequently at the aggregated level of cities and regions, make it difficult to forecast the future of building energy consumption (and hence GHG emissions) within narrow confidence interval. Reason for such variations and uncertainty are the uncertainties in accurate determination of envelope properties of building, changing operating schedules, stochastic occupant behavior, changing weather patterns and discrepancies in understanding/modelling accurate relations between inputs and corresponding output building energy consumption [7].

1.2 Thermal regulations

1.2.1 Introduction

Building thermal regulations provide the basic description of how buildings should be constructed in order to save energy. Some building regulations are specifications of different building components, such as minimum heat transfer coefficient value (U-value), thermal resistance (R), solar transmittance for windows (g-value) and roof insulation level [8]. Building regulations are not strict in terms of specifications, but define overall minimum energy efficiency or maximum level of energy consumption that must be maintained in new and existing buildings. An illustrative figure representing buildings heat transfer with environment is presented in Figure 1.1.

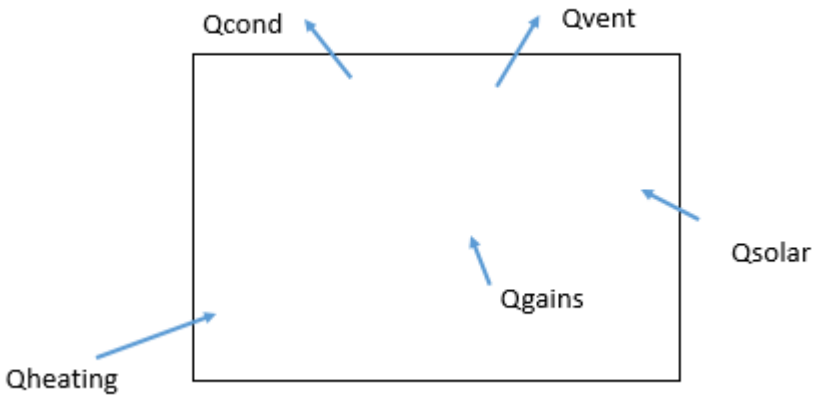

Figure 1.1: Energy balance for building/room in the heating modes [9]

The steady-state energy balance for heating the air inside a building is:

$$Q_{heating} = Q_{cond} - Q_{vent} + Q_{gains} - Q_{solar} \quad (1.1)$$

where

$Q_{heating}$ is the amount of heat supply required to maintain the maintain the temperature inside;

Q_{cond} - heat conduction fom the walls;

Q_{vent} - heat exchange due to ventilation;

Q_{solar} - solar radiation;

Q_{gains} - internal heat gains due to occupancy and electrical loads.

The indoor temperature T_i is kept at desired level against the fluctuations of outdoor temperature T_a. In absence of an external heating or cooling, the indoor temperature variation (at steady state) from equation (*1.1*) is given as [9]:

$$T_i = T_a + \frac{Q_{gains} + Q_{solar}}{UA + \dot{m}c} \quad (1.2)$$

where

U is the conduction heat transfer coefficient;

$\dot{m}$ - mass low rate of ventilation/infiltration air;

c - specific heat capacity of air.

The building regulations aim to maintain comfortable conditions inside building with least possible input energy i.e. $Q_{heating}$ or $Q_{cooling}$ (mechanical or electrical) in equation (*1.1*) by manipulating the second term in equation (*1.2*), i.e. by regulating losses through envelope and ventilation/infiltration etc. [9].

Regulations provide a framework or path under which building codes are implemented [10]. Most regulations are now defined in line with international, regional or national goals of greenhouse gas (GHG) reductions; for example, EU target of reduction of GHG emissions by 20 % by 2020 is reflected in energy performance of building directives (EBPD). In such case, building regulations define maximum allowable CO_2 per square meter. This provides designers and constructers sufficient freedom to work within the regulatory framework to achieve this target. Building energy codes cover lighting, insulation, glazing, heating and cooling equipment and other energy efficiency measures.

1.2.2 History of building thermal regulations

Building energy regulations were developed during the 1970s oil embargo when developed countries realized the need to reduce their dependence on foreign oil [11]. In US in 1975, ASHRAE published the first ASHRAE Standard 90.1 for energy conservation in new buildings. This standard was regularly updated and formed the basis for the implementation of Energy Policy Act (EPA) in 1992 which required all states to adopt the ASHRAE 90.1 Standards as a minimum level for building efficiency [12]. In 1994, International Code Council (ICC) was formed; it introduced the International Energy Conservation Code (IECC) for buildings. Both IECC and ASHRAE 90.1 Standard served as baseline standards or codes at state and federal level in US. IECC and ASHRAE codes for buildings are updated every three years. States are asked to comply with the codes within two years of issuance of new codes [13]. The energy policy act 2005 requires all federal buildings to reduce energy consumption by 20 % in 2015 as compared to 2003 level [14].

In UK (England and Wales), energy conservation part of the building regulations became effective in 1979. The part "L: Conservation of Fuel and Power" of the building regulations formed the building energy conservation part, with L1A dealing with conservation in new buildings and L1B with existing buildings. In 2005, UK also complied with EU Energy Performance of Building Directives (EPBD) for buildings by including EPBD directives in its energy regulations [15].

Building energy consumption is Europe is high as compared to other parts of the world because of weather based loads. European Union (EU) building energy consumption is 40 % of total energy consumption and 36 % of total GHG emissions. EU has set a target of reducing building energy consumption by 20 % by 2020. To achieve this target, EU issued two main legislations: Energy Performance of Buildings Directive (2010) and Energy Efficiency Directive (2012) [16]. This legislation provides a framework for EU countries to adopt different mitigation strategies relevant to building energy consumption. Under the energy performance directive, the member countries need to take steps to the set targets, such as target for all new buildings to be zero energy by 31st December 2020, setting minimum energy standards for retrofits, inspection schemes for heating and cooling systems [16].

1.2.3 Performance and prescriptive building regulations

Building regulations have two philosophies:

1. performance based,
2. prescriptive based.

Performance based regulations set maximum target for either energy consumption per square meter in heating and/or cooling and range of allowable internal temperature in free-running. They leave the designer the freedom to choose between different sets of parameters. **Prescriptive** based regulations set minimum values of building material properties like minimum U-value, infiltration level, glazing values etc. They are easy to follow. Performance based regulations directly target emissions or energy consumption and are usually preferred

over prescriptive based regulations [9]. A combination of two approaches are also used in building regulations.

Building regulations are set based on the dominant climatic conditions (summer or winter) of a country or region. This provides a challenge to set specifications that operate with optimal energy in every season. For example, in EU countries the building regulations are based on winter conditions; the summer or the mid-season conditions are ignored for optimal performance [9]. However, regardless of the designed weather conditions for building regulations, they bring reduction in energy consumption and therefore should be implemented despite imperfections, with continuous search for improvement.

Standard for comfort conditions inside buildings are usually set and regulated by bodies like ASHRAE, ISO and CEN. These standards categorize or evaluate buildings based on the closeness with which internal building conditions are maintained and controlled. The buildings are labelled accordingly, for example category **A** building is the building with best comfort control. Some authors argue that following comfort standards closely leads to high energy consumption [17]. These standards, on one hand, control indoor environment through mechanical or electrical heating and cooling but also set minimum standards on energy consumption (building fabric and ventilation). These goals are at times in conflict in the sense that following the set point temperature strictly results in high consumption.

One of the criticisms on thermal regulations is the declaration of universal set point temperature. The thermal comfort conditions for different people are different based on their age, activity level and regional climate. Therefore, the thermal comfort conditions should not follow a universal set point temperature. It should vary based on localized comfort conditions at the level of personal comfort. Substantial savings can be achieved by giving to the occupants control over their comfort [17]. In this way, satisfaction level of occupants is enhanced and the energy consumption is reduced, allowing occupants to use fresh or free cooling and heating as available from natural environment.

Simulation studies suggest that new building codes with energy efficiency improvements bring substantial savings. McKinsey in his study of 2009 IECC building codes estimates that code issued in 2009 has the potential to improve energy efficiency by 12 % to 15 % as compared to codes of 2006 [14]. The question of whether building energy regulations bring substantial reduction in reality is addressed in different research works. A comparison study between billing data of Florida state for buildings constructed before and after implementation of newbuilding energy codes (2002), was conducted [11]. It was found that electricity consumption per year was reduced by 4 % and gas consumption per year was reduced by 6 % after codes were implemented. As code changes are implemented with substantial investments, the payback period for the investments were 6.4 years for private buildings and between 3.5 to 5.4 years for public buildings. The conclusion that building regulations bring similar reductions in other regions needs further investigation [11].

1.2.4 Performance measurement (certificate of performance)

The building performance measurement or certificate provides information on "the thermal characterization of a building that is measured using set procedures. The certificate provides information on the energy used for different purposes (heating, cooling, lighting etc.); on how well (efficiently) the building is using energy; and the opportunities to improve energy efficiency" [18]. A typical energy performance certificate is a shown in (Figure 1.2).

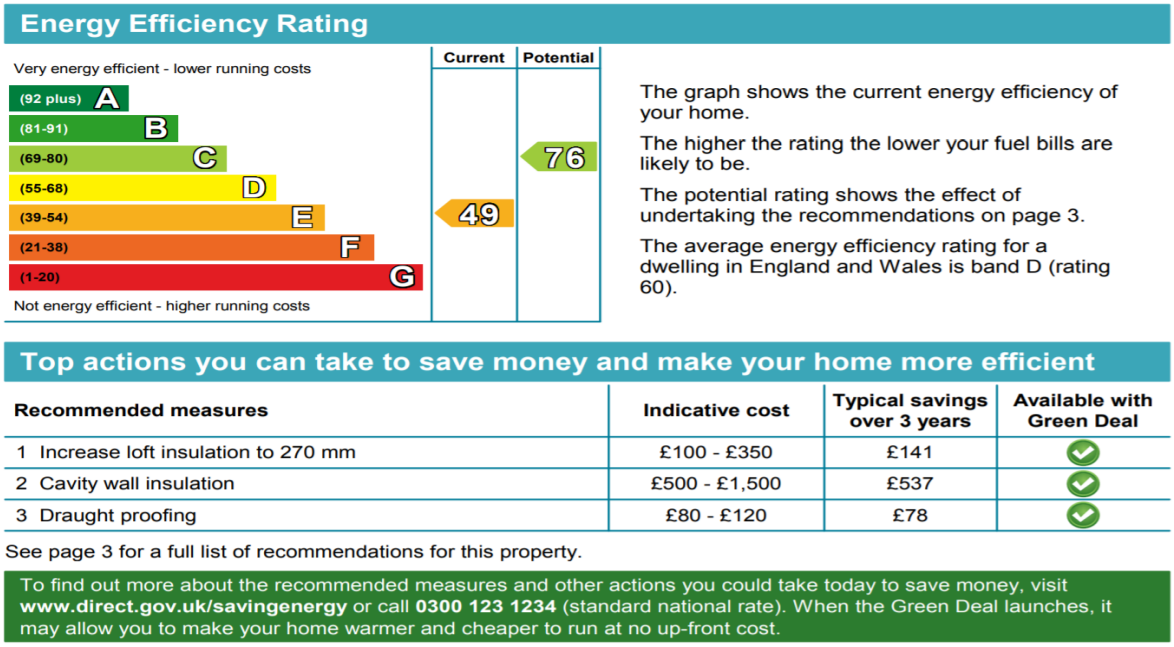

Figure 1.2: An Energy Performance Certificate (EPC), UK [19]

Energy performance of buildings is assessed based on energy and water consumption required to meet the typical operational demands of a building [20]. Energy performance is expressed in terms of performance index such as normalized energy consumed per square meter per year, also called Energy Utilization Index (EUI) or CO_2 emissions per unit area per year.

Energy performance certificate are awarded based on the energy consumption of a building and its relative position in comparison to consumption of buildings at national, state, or regional level. The building performance is assessed and expressed using any or the combination of the three terms or methodologies known as [18]:

- energy rating,
- benchmarking process,
- energy labelling.

Energy rating is the specific method of performance assessment of a building that presents the energy performance with an index or number. It is a methodology of performance assessment, energy use prediction and rating score based on level of energy consumption. For example, Energy Performance Certificate (EPC), Leadership in Energy and Environmental

Design (LEED), Building Research Establishment Environmental Assessment Method (BREAM), Home Energy Rating System (HERS) etc., present different rating systems based on slightly different methodologies [18]. The rating system is categorized into *asset* rating and *tailored* rating. The asset rating evaluates building performance based on climate and energy consumption, irrespective of occupant's behavior or other factors that may affect building energy consumption. The tailored rating systems take into account all the factors that affect the energy consumption, such as changes in occupancy, operation schedule etc., [18].

Benchmarking process is based on comparison of building energy performance indicator (EPI) with a sample of similar buildings. The similarity is based on type of use, climate, location, shape, etc. Benchmarking of buildings involves four steps that are [18]: 1) development of database of similar buildings; 2) performance evaluation of building (Energy Performance Indicator, EPI); 3) comparison analysis with database of similar buildings; and 4) recommendations for efficiency improvements. Figure 1.3 presents the steps for benchmarking.

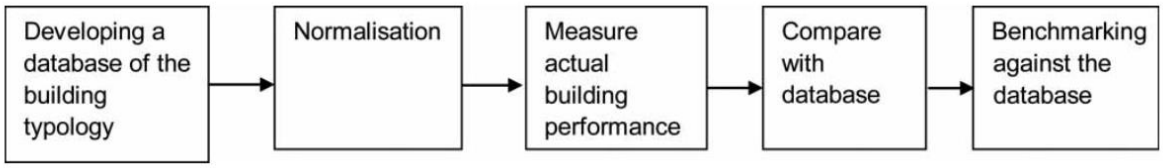

Figure 1.3: Benchmarking process [21]

Energy labelling is based on points achieved by building against a set of criteria set by certifications such as LEED and BREAM etc. For example, LEED labels a building as Silver, Gold or Platinum, if the building achieves sufficient points to be eligible for labelling. The criteria for LEED are based on energy and environmental sustainability. The labelling can also be developed based on the bell curve distribution of energy consumption of a similar stock of buildings. Building labelling identify the position of building in the bell curve of similar buildings [22]. According to performance of the building, a certificate is awarded such as **A** to **G** (EU) or score of 1-100 depending on the score of the building and the rating system being used (EPA, 2000).

.

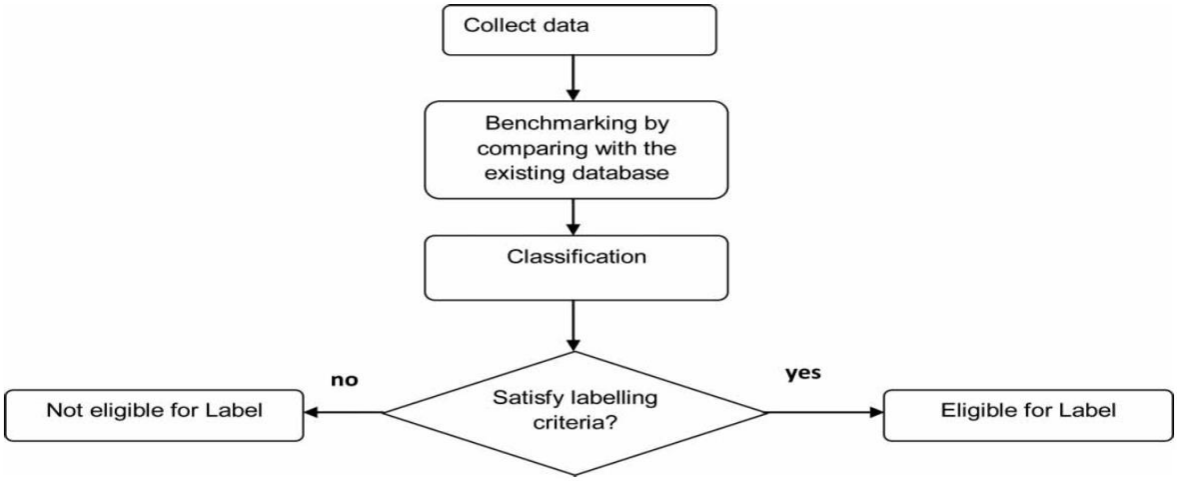

Figure 1.4: A typical labelling system procedure [22]

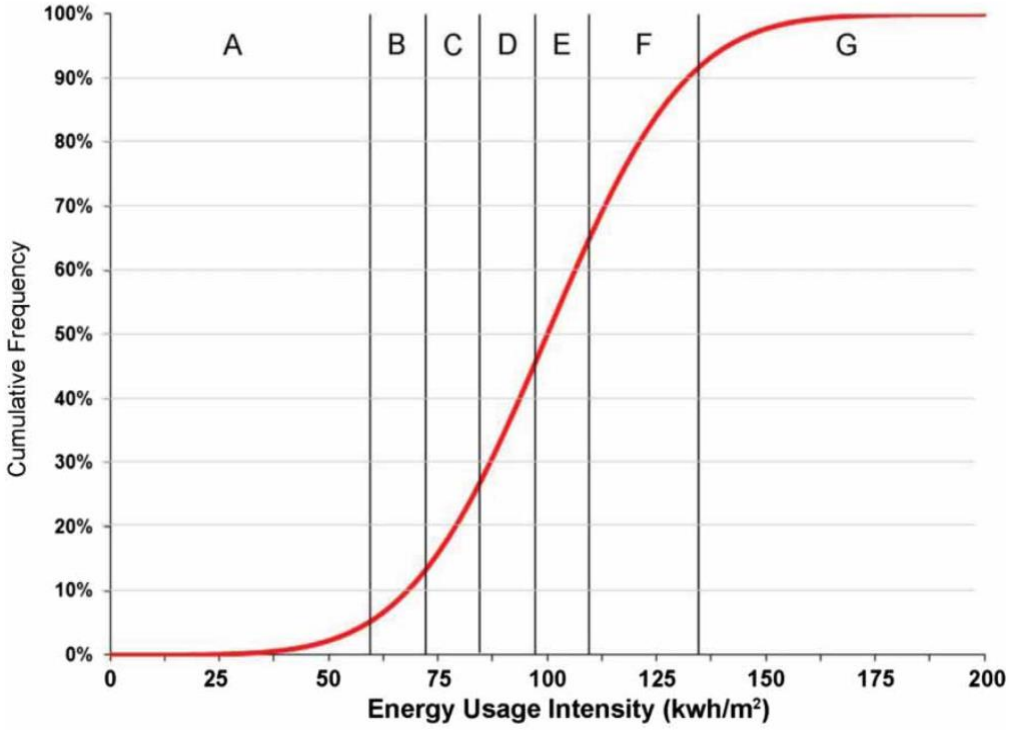

Figure 1.5:Building energy labelling system [22]

Figure 1.4 presents a general flow of building labelling system. The performance assessment can be done online using billing data and building specifications. Alternatively, performance assessment is performed by certified auditors using measurement surveys at building level. After the building is assessed and the score is achieved, it is compared with either similar buildings (percentile score) or with a standard score set in certification criteria.

The comparison score based on Energy Utilization Index is shown in Figure 1.5. The score achieved by the building places it in a range of percentile score. Accordingly, the building will be eligible for a label. A label of '**A'** achieved by building (based on EUI) means that building is in top 25 % buildings [22].

1.2.5 Performance certificates in US, EU and UK

Building performance certificates have gained prominence within the last 15 to 20 years. Majority of the developed countries are now using building rating systems [20]. In some countries, it is mandatory to have an energy performance certificate (European Union) whereas in other countries, it is voluntary or a combination of voluntary and enforced (United States).

In US, different performance or building rating systems exist. These include mandatory state level programs like New York City, California, Washington DC that have mandatory performance certificate programs. The voluntary national level certification programs include LEED (Leadership in Energy and Environmental Design) certification program (for new and existing buildings) and the ENERGY STAR Portfolio Manager. For residential purposes, RESNET, HERS and ENERGY STAR are common labelling schemes [14]. ASHRAE's building Energy Quotient rates both new buildings (as designed) and existing buildings (ACEEE, 2002). Existing buildings are rated after conducting an ASHRAE Level 1 audit [14].

In European Union countries, Energy Performance Certificates (EPC) were introduced in 2002 through the 'Energy Performance Building Directive (EPBD)' which requires all EU countries to introduce performance certificate scheme according to the local weather conditions. Different updates (2010 and 2013) to EPC have been added for further improvements [19]. EPBD

requires all states to have an EPC scheme for all new buildings or buildings undergoing major renovations, for all standalone houses or apartments, sold or rented.

EPC certificates must be available at the time of building construction, mentioned in any advertisement selling or renting building; EPC certificate must be handed over to tenant or person purchasing the building. Countries with local EPC scheme need to update their scheme as per Energy Performance Building Directives [19]. The building directive set qualification standards for personal involved in EPC calculations, set calculation methodology, recommendations for software and the obligatory information provided by EPC. The EPC should include technically feasible recommendations for improvement in energy efficiency, breakup of heating and cooling energy and its impact on energy consumption and emissions and an estimate of payback period (for recommended improvements).

BREAM (Building Research Establishment Environmental Assessment Method) developed by UK in 1990 is the earliest building rating system. Like LEED certification, it has a holistic approach towards sustainability and evaluates building on points accrued, rather than on comparison with other buildings. The sustainability is assessed with respect to a number of categories such as energy, water, innovation in building (design, construction and operation), and sustainable land use, materials, management, pollution, transport and waste. A certified BREAM assessor evaluates each category for a given building and gives credits; these credits are multiplied with environmental weights given for each category. The accumulated credits provide a score for the building that categorizes it as unclassified, pass, good, excellent and outstanding building [23].

1.3 Performance gap

1.3.1 Energy quantification methods

Significant difference exists between the predicted energy consumption of buildings and the actual or measured energy consumption; this is known as performance gap [24]. Predicted energy consumption is the estimation or simulation of future energy consumption of building over a specific time horizon (day, month or year). However, simulation can also be used to

assign the measured energy consumption to different uses/sources such as heating, cooling and lighting etc. Simulation methods used for energy prediction are calculation based methods, measurement based methods and a combination of calculation and measurement approaches that is hybrid methods [20]. Different methods of quantification are as shown in Figure 1.6.

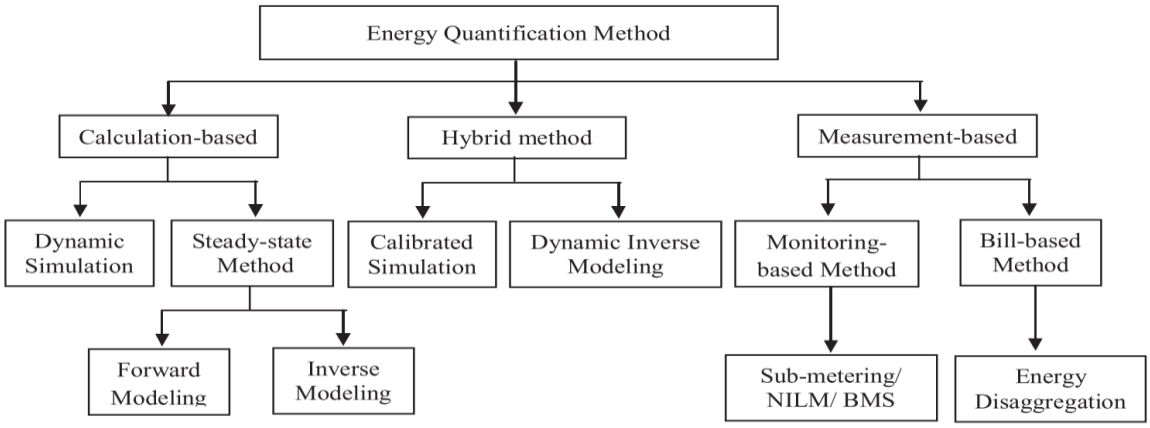

Figure 1.6:Building energy quantification methods [20]

All the three methods, i.e. calculation-based, measurement based, or hybrid based methods, predict future consumption of building energy against uncertain weather conditions, occupant's behavior, operating schedules, and are therefore prone to errors. The calculation based methods suffer from significant errors between predicted and actual energy consumption, the measurement based and hybrid based methods can also be erroneous due to observation/measurement errors, as measurements themselves rely on equations that may not present the true relationships [25].

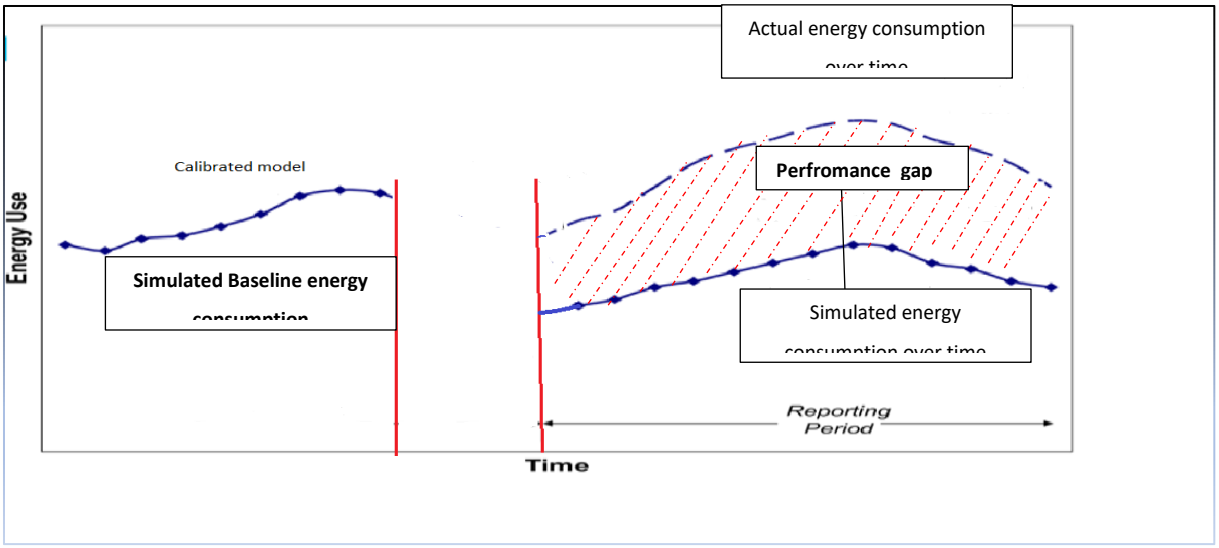

Figure 1.7: Performance gap between predicted energy consumption and the actual energy consumption over a period of time[26]

1.3.2 Magnitude of performance gap

The magnitude of the gap between predicted and actual consumption can be significant. Some authors estimated a performance gap of 2.5 times of predicted energy consumption [25]. A study of 600 buildings carried out by Carbon-buzz in UK indicates that actual energy consumption was 1.48 to 1.9 times higher than the simulated energy consumption [27]. Figure 1.8 shows the results of a study that highlights the difference between predicted and actual energy consumption in schools, offices and campus buildings.

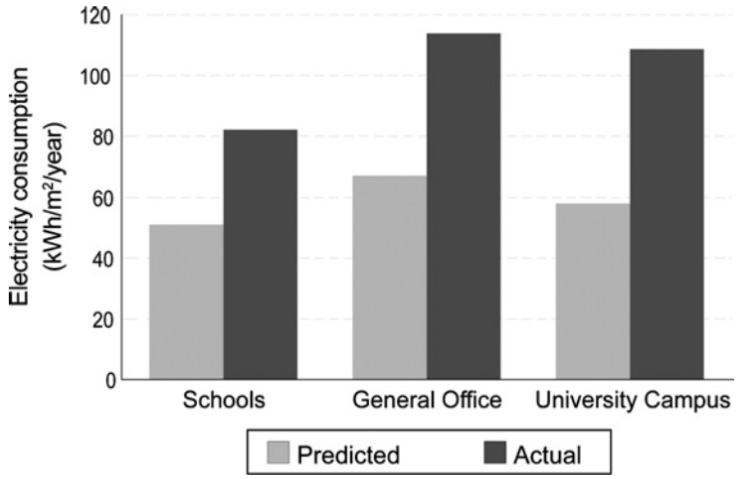

Figure 1.8:Carbonbuzz study on median electricity in different sectors predicted vs actual [19]

Energy Utilization Index (EUI) is usually used as a prediction indicator that is used for performance comparison between new and existing buildings. Majority of the building performance certification awards are based on EUI. Figure 1.9 shows a spread of EUI data presenting the difference between simulated and measured EUI. This difference reflects in significant increase in actual energy bills compared to expected energy bills based on designed EUI.

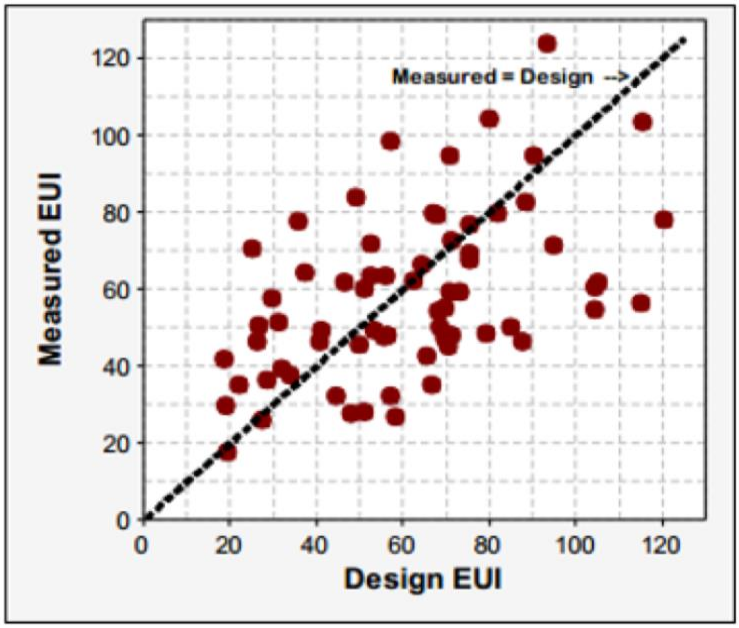

Figure 1.9: Difference between measured and predicted EUI [28]

The performance gap becomes important when forecasting payback period for investments based on Energy Conservation Measures (ECM). The ECM savings are always either under-predicted or over-predicted. Empirical evidences in UK, Austria, Norway, US and Canada show that actual energy savings from heating retrofits were 68 % less than predicted savings [27]. A study of German dwellings indicates an over estimation of energy consumption by 30 % as predicted by Energy Performance Rating (EPR) [29].

The Efficiency Valuation Organization (EVO) has developed the International Performance Measurement and Verification Protocol (IPMVP) to standardize the quantification of energy

savings and manage the risks and associated benefits with energy efficiency projects in buildings [26].

Savings predicted from energy conservation measures (ECM) can be misleading if the savings are based on post ECM billing data only (Figure 1.7). The increase or decrease in energy can be attributed to many reasons other than ECM, for example the increased or reduced level of activity, change of weather, change of occupant's behavior, etc. IPMVP recommends adjustments to original baseline in case of any change in the conditions of the original baseline.

1.3.3 Causes for performance gap

The gap between predicted or simulated energy consumption of building and actual energy consumption for buildings is called performance gap. The three categories of root causes for performance gap are design, construction and operation [25]. Study for a school in revealed that operational issues were responsible for 75 % of the performance gap and procurement issues (construction and equipment malfunction) were responsible for 25% of the performance gap [27].

The design stage causes include miss-communications about performance targets of building, inability to accurately predict the future operations and condition of buildings, over specification of building equipment, lack of thermal concepts at design stage and assumptions due to lack of data [19].

The construction causes include inability to construct as per design specifications of building and non-uniform properties of building materials due to manufacturing defects. Building materials specification are generally quoted for standard conditions and may change behaviour due to change in climate conditions. A detailed inspection is required to confirm the building construction as per design specifications [30].

The operational causes for performance gap come into play once the building is commissioned for use. The operational causes include difference in occupants' behavior, which is always

difficult to predict. Occupant behavior is considered as one of the main reasons of the performance gap [29]. Simulation is based on standard operating conditions, i.e. standard heating and cooling set points, ventilation rates and operation schedules. The control and operation of building HVAC equipment, different from the simulation values, lead to significant performance gap [31]. The building staff responsible of running the equipment may not run it according to the designed control values.

Most of the simulations consider constant internal temperature which is misleading as indoor condition differ over the year. The weather conditions can change significantly from the data used for predictions. This will result in significant gap in case of building with significant weather-based loads. Acquisition of accurate weather data poses a problem and suffers from uncertainties even if data from dedicated weather stations is used. In contrast to weather based loads, the uncertainties in electrical loads, especially the ICT based loads, may cause performance gap [27]. With rising living standards, the electrical loads (ICT) will factor significantly in building energy use in future.

One of the reasons for performance gap is the inability of simulation process to fully understand the relationships between various inputs and output energy consumption of buildings. Building physics is complex process whereas most of the simulation programs are based on equations that are the approximate representation of actual process. The operation and control of an HVAC system is not fully understood with significant performance deviations from modelling equations [32]. This is the reason current research focus also on data-based analysis, like black box and grey box modelling. The output of any simulation also depends on the skills and the knowledge of the expert. Two experts using the same simulation tool may produce different results. This leads to the conclusion that it is extremely difficult to model building energy consumption accurately.

The measurements of inputs and outputs that are used to find the performance gap may be erroneous due to uncertainty of data from sensors. Figure 1.10 shows the sources and the possibility of errors with each source that can lead to performance gap. The most revealing fact from the figure is that dwellings with similar ratings differ significantly in energy

consumption with a difference of more than 13 times between the least and the most consuming dwelling [33]. Sources of difference are inability to mark space heating and water heating, variations in weather conditions, occupant behavior, model simplifications, performance gaps of installations and modelling faults.

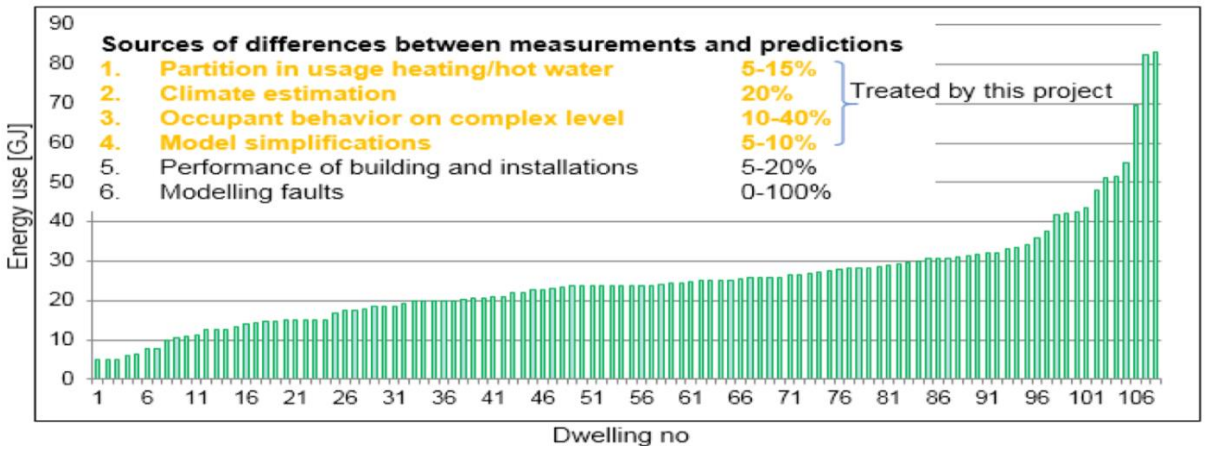

Figure 1.10: Sources of error between measurements and predictions [34]

The technical reasons of performance gap may be exacerbated by the effects known as pre-bound and rebound effects. The pre-bound presents a situation before retrofit meaning that in inefficient houses with higher energy bills people tend to use less energy than expected or modelled; for example, people may choose to live in comparatively colder conditions. The rebound effect represents a situation where the savings are overconsumed by the increased energy use after retrofits. Both present an important source of performance gap in EU countries as mentioned in [29].

One of the issues with benchmarking is to classify buildings based on single parameter, i.e. type of use (e.g. school, hospital or single home), as practiced in benchmarking programs like *Energy Star Portfolio Manager*. Studies suggest that this can be misleading as a school with less amenities and services might score higher then another school using more energy efficient technologies [24]. A single floor commercial building will be always rated lower than a commercial building with multiple floors but the same per floor area. It is recommended to search for similarities other than type of use only, like height and shape, age, equipment and operation schedule, internal loads and other features of the building. It is recommended to

take into account multiple features for realistic a realistic topology, e.g. the building typology using 'data based unsupervised' clustering techniques generate better results [24].

1.4 Intrinsic performance measurement

The main causes of performance gap, as discussed in section 1.3, are constructional and operational. The operational causes constitute the equipment efficiency and the operational schedule of equipment. It is relatively easy to measure the equipment efficiency; however, the operational schedule depends on occupant behavior, changing weather conditions and thermal performance of building.

The thermal performance of building, also known as the intrinsic performance of building, is the ability of the building to maintain the comfort conditions without energy or as low energy as possible. The thermal performance is important for energy consumption of the building as it affects both the occupant behavior and the operational hours of heating and cooling equipment.

A common parameter that quantifies the thermal performance of building is overall heat transfer coefficient (H). It represents the amount of heat required to maintain the indoor environment at a given set point temperature against the varying outdoor temperature. The overall heat transfer coefficient can be determined using the stated values of building envelope. However, the material properties deteriorate with time and does not give the correct estimation of the overall heat transfer coefficient. The parameters, such as overall heat transfer coefficient, can be determined using parameter identification and onsite test methods.

The parameter identification models, like energy signature, PRISM methods, RC-identification etc., are based on energy consumption as a function of outdoor temperature, solar radiation, wind speed, occupants, etc. These parameters can be determined as coefficients of regression analysis (in case of black box models). The identification models can be both dynamic and

static models, depending on the intended purpose of model and the sampling time of the available data. The identification models can be either based on pre-designed/supervised onsite (in-situ) experiments such as co-heating or they can be based on unsupervised experiments, such as smart metering data.

The pre-designed/supervised onsite test methods are categorized as long term and short term methods. The long term methods are based on steady state analysis and are considered accurate. The results of long term test methods, such as co-heating, are used as reference or standard methods. The results of these methods are used as a benchmark for other methods. The issue with long term methods is their duration, which makes it difficult to apply them in commercial sector. The short test methods, such as QUB (Quick U-Value for Buildings), ISABELE etc., are fast methods that can be performed in short time.

The QUB method is the shortest of all methods. However, the results of test show variations and the method is not tested with varying building types, weather conditions, etc. The number of QUB tests data conducted are limited. The aim of the current work is to analyze the influence of boundary and initial conditions on QUB method (change in input power and time duration) and the influence of weather conditions (such as winter and summer) on QUB results.

1.5 Thesis outline

The thesis begins by presenting the importance of building consumption and the potential savings, building energy regulations, the performance gap analysis, causes of performance gap and need for the performance measurement.

The parameter identification models can be used to determine the intrinsic performance measurement, i.e. overall heat transfer coefficient. In chapter 2, the state of art on the modelling of intrinsic thermal performance measurement is discussed; the chapter details the classification of models, black box and grey box model structures and principles, calibration

and sensitivity analysis, statistical techniques to remove or reduce the errors, model order selection and data analysis techniques.

In chapter 3, long term thermal characterization tests are presented, such as calorimetric and co-heating methods. The standard tests and test setups conducted to as part of IEA, EBC Annex-58 are discussed. The potential errors of the methods and data analysis techniques with long term thermal characterization methods are also discussed.

In chapter 6, the short term thermal characterization methods are discussed. The focus is on the analysis of QUB method, its theoretical background, analysis of QUB experiments performed, shortcomings of this method and the need for future work.

In chapter 5, a state space model for analysis of the QUB method is developed. The chapter discuss the assembling of individual thermal circuits and the extraction of state space from thermal circuit of the building components. The model is validated using data from the house as discussed in IEA, EBC annex-58.

In chapter 6, the model developed is used to design QUB experiments using different values of initial (power during heating phase) and boundary conditions (solar radiation). The impact of solar radiation on QUB method is analyzed. The impact of time duration on QUB experiments is also analyzed.

In chapter 7, the a-posteriori error analysis of the QUB method is performed. The ideal conditions for QUB method are discussed. The QUB experiments for non-ideal conditions are performed and analyzed. The QUB experiments are performed for two seasons i.e. summer and winter. The errors are analyzed by observing the evolution of temperature during heating and cooling phases of QUB experiment.

In chapter 8, the conclusions for the entire thesis are summarized and directions for future work are given. Chapter 9 forms the annexure of the thesis and is composed of discussion on effective capacity and model order reduction.

2 State of the art for intrinsic building energy performance measurement

In the first chapter, the main causes of performance gap were identified as uncertainty in input data, inability to correctly measure/identify the building parameters, changes in building operations and the occupant's behavior. The building parameters, such as overall heat transfer coefficient, time constant, solar aperture etc. also known as the intrinsic building performance measurements, provide efficiency measures that do not change with occupant's behavior and weather patterns.

This chapter discusses different modelling methods used for parameter identification (intrinsic performance measurement). There are number of methods used for this purpose. Each one has its own application, advantages and disadvantages. From the point of view of parameter identification, it is important to know the methodology for characterization of models, the data pre-processing steps, the interpretation of results, identification and removal of modelling errors. A discussion of different methods of modelling, their advantages, disadvantages and necessary data analysis steps is given below.

2.1 Classification of modelling methods

Due to complexity of building energy consumption, there is a continuous search to improve the performance of existing simulation methods and introduce new techniques. Different modelling methods and approaches currently exist. Some of the common methods are: engineering methods, statistical methods (black box), intelligent methods such as genetic algorithms (GA), artificial neural networks (ANN), support vector machine (SVM) and hybrid methods (grey box). The classification is not strict; different researchers provide different techniques of classification [35]–[38]

A brief categorization of modelling methods into forward approach (classical) and inverse approach (data driven) is [38]:

- **Forward approach (classical method)**: The objective of these methods is to predict an output variable based on specified model structure and known input variables [38]. An interesting explanation in case of forward modelling is that the modeller has the complete description of building to model the peak demand and operational energy required [39]. These methods use engineering and thermodynamic principles to model energy consumption. They require complete description of buildings, including geometrical shape, location, properties of building fabric, HVAC equipment and plug loads, occupancy data and operating schedules. They can be used to predict the peak demand, annual energy consumption and savings from retrofits. The effectiveness of these methods depends on details added to model that are inclusion of different heat transfer phenomenon and their quantification that affects building energy consumption. This adds complexity to the model and is the reason why a number of sophisticated software tools, like BLAST, ENERGY PLUS, EQUEST, TREAT and ESP-r etc., are used for forward modelling. When interactions between inputs, outputs and parameters get complex, results of forward modelling method may divert from actual energy consumption. Physical models have the advantage that they can be extrapolated beyond the data, i.e. based on first principles they can model for a set of completely unobserved conditions [40].
- **Data driven (inverse approach)**: In data driven approach, the output (that is the energy consumption or indoor temperature) and inputs (such as outdoor conditions) are known by measurements. The model of the building is built based on input-output relation. An interesting definition for data driven model is: “Given a set of input and output vectors of measurements, a supervised learning generates a function that builds an input-output relation” [41]. The method is used to estimate system parameters, such as building thermal mass, thermal resistance, effects of occupancy behaviour etc. It can also be used to determine energy consumption with reference to single variable, such as outdoor temperature, or multiple variables, such as wind, solar radiation and occupancy [37]. The objectives of an inverse model are to answer the questions concerned with existing building energy use, such as how much energy a

building is consuming compared to design predictions, how parameters (such as change of thermostat settings or ventilation rate) will effect energy consumption and, in case of retrofit settings, the question that whether the savings were due to weather conditions or due to retrofit [39]. They require a minimal set of input variables for modelling [40]. The inverse models help identify building parameters with improved accuracy, as they are deduced from actual building data. The system parameters thus obtained can be used for better energy modelling in future. The data for modelling can be **intrusive data,** i.e. obtained through controlled experiments, or **non-intrusive data,** i.e. data from normal building operation. The model is built with fewer parameters in aggregated form, such as overall heat transfer co-efficient and time constants etc. The inverse modelling is data intensive and the uncertainty and quality of data affects the modelling accuracy. They help us to understand better the effects of different parameters on energy consumption and can be used to build a better building energy baseline against which the savings from retrofits can be evaluated. However, no extrapolation can be made beyond the valid data range; only interpolation is allowed with data-based models.

Both the forward and data-based approaches can be static or dynamic depending on the time domain and the analysis approach. The **steady state** methods are based on degree-days and bin temperatures [38], whereas **dynamic** methods are based on transfer functions and solution of differential equations. In general, the steady state methods are based on monthly, weekly and daily data, whereas dynamic models are based on hourly or sub hourly measurements [37]. The dynamic models consider the transients effects due to thermal mass of the building that influences the duration of building warm up or cool down. They are appropriate for peak load determination and building load control. In contrast, the **steady state** models do not have any time lagged terms and are used for overall monthly or annual energy consumption.

The data driven approach can further be classified into three categories:

- **Empirical or black box method.** These are pure statistical techniques where simple or multiple variable regression is used to find parameters from relationship established

between input and output data. The model offers no description of the parameters identified and leaves it to user to recognize them.

- **Hybrid method (grey box).** Hybrid methods are semi-physical or semi-statistical approaches used to identify parameters or dynamical characteristics of buildings. Unlike black box modelling, the parameters have direct physical interpretation. This enable us to add prior physical knowledge, in addition to the statistical model to identify parameters of building. A controlled experiment data is used to apply this approach [42]. .
- **Calibrated simulation method (white box).** The calibration method is a two-step method. A model of the building is generated based on first principles or engineering method. The model is then tuned with data to arrive at energy consumption in line with the billing/consumption data. Different methods of tuning are applied to various parameters of significance [42].
- **Artificial intelligence** based methods such as genetic algorithms (GA), artificial neural networks (ANN) and support vector machine (SVM) are advanced approaches that are coupled with black box, grey box or calibrated simulation to improve the outcome of these methods. It may be noted that with the advancement of research, the distinction between these methods has blurred [36].

Figure 2.1 provides the classification of modelling methods.

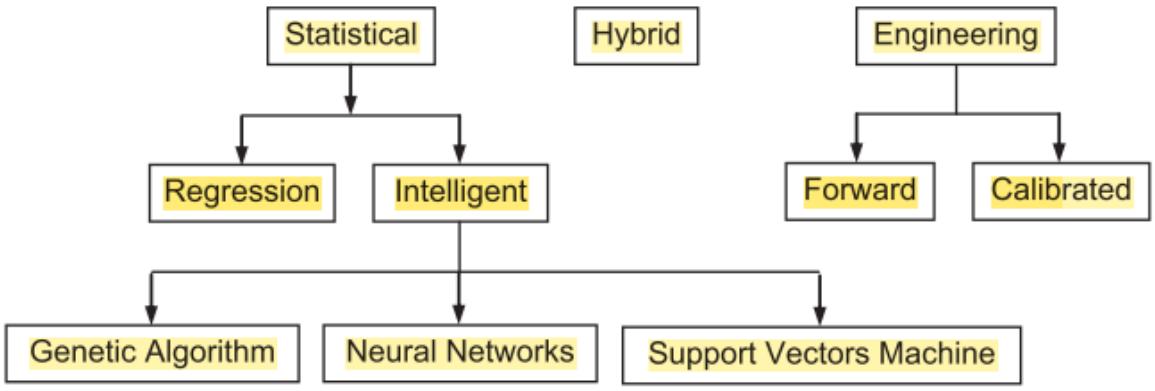

Figure 2.1:Clasification of modelling methods [36].

A comparison between two modelling approaches can be observed in Figure 2.2. It shows that the aim of the inverse approach is to estimate model parameters. Since the subject of the thesis is the measurement of intrinsic performance, parameter identification for buildings is discussed in more detail in the next section.

Physical system		Types of modelling problems		
		Direct	Inverse	
		$f(\cdot\|a)$	$f(\cdot\|a)$	$f(\cdot\|a)$
		$y \leftarrow f(x\|a)$	$a \leftarrow \{y, f(x\|\cdot)\}$	$x \leftarrow \{y, f(\cdot\|a)\}$
		Simulation	Identification	Control
$f(\cdot\|\cdot)$	Model structure	known	known	known
a	Model parameters	known	output	known
x	Inputs of the physical system	input	input	output
y	Outputs of the physical system	output	input	input

Figure 2.2: A comparison of modelling approaches (forward and inverse methods)

2.2 Parameter identification

Parameter identification is the establishment or correction of mathematical models with real world data [43]. It has applications in versatile fields of science and engineering, such as statistics, econometrics, health science, biological sciences, geophysics and thermal sciences. The system identification theory has been developed independently and therefore finds applications equally in all fields [44]. For any system of interest, parameter identification can be used for dynamic or static modelling aimed at prediction, control, simulation, reconstruction of measurement data etc. [45].

Parameter Identification is based on relationships generated with historical set of input and output observations, also known as regression analysis. Regression analysis can be used for two purposes: 1) determination of output energy in relation to a single or multiple variables and 2) estimation of system parameters, such as total heat loss coefficient, total heat capacity,

gain factor etc. [37]. Data acquisition and analysis are essential components of parameter estimation and the quality of the results from parameter estimation are highly dependent on the performance of these two steps.

Since the subject of this research is measurement of energy efficiency in buildings the next section discusses the applications of Parameter Identification methods as applied to thermal characterization of buildings. In case of buildings, parameter identification is used for improved estimation of parameters, for finding the impacts of different parameters on building energy consumption, for improved estimation of building energy consumption with changing inputs such as weather, occupancy and for optimal control of HVAC equipment.

2.2.1 Principles of parameter identification

Various methods of parameter identification are based on choice of independent variables, applied constraints, criterion for goodness of fit and choice of linear or nonlinear algorithms [39]. Parameter identification is done in more step: data measurement and acquisition, selection of model structure, optimization algorithm and estimation of parameters, and model validation.

The steps for parameter identification are:

Data measurement and acquisition depends on the nature of analysis and involves steps such as:

- Design of Experiment (DOE) procedure indicating the necessary instrumentation, measurements, accuracy, type of experiments. For example, the standard ISO 9869:2014 (on measurement the overall conductance of a wall in steady state) provides complete details for the measurement equipment, installation, calibration and measurement procedure and analysis of data [46].
- Sampling rate for data acquisition that defines the time between two measurements.
- Data filtering for removing noise to receive the desired signal only (preliminary data analysis).
- Segregation of data into training data, test data and validation data.

Selection of model structure determines the type of model as applied/fitted to data for the purpose of identification. Selection of model is a complex decision because of the large number of available models, the lack of a single criteria for the best model selection and the conflicting criteria between the simplicity of the model and its capability of explaining the observed data. The model structure can be black box that is purely based on data that do not require any description of physical nature of system or parameters, or grey box, that uses physical description of system. The grey or black box model selected can be dynamic or static. The models range from simple linear regression to complex models such as artificial neural networks (ANN), genetic algorithms (GA), etc.

Parameter estimation is an inverse problem and is said to be well posed if the following conditions are fulfilled:

Existence: For all data, solution exists for the problem posed.

Uniqueness: For all data, there exists a unique solution.

Stability: The solution depends on continuously available data.

Parameters are estimated against criteria that optimize the solution. A common criterion used is the least square minimisation criteria that minimizes the gap between observations and estimated model [46].

Model validation is done on data which was not used for model training. Cross validation is achieved by comparing with the known or expected values or with results of other models. Based on validation results, the model is rejected, accepted or further improved [47].

Performance of parameter estimation or system identification depends on how well these steps are applied and how well the principles governing the system are understood and incorporated. Crassidis and Junkins summarized these steps as [45]: decisions regarding which variables need to be measured, the frequency of data acquisition, accuracy of measurements and selection of the best mathematical models. Principles of estimation theory are developed

separately from consideration of any particular physical system and the success of the method lies in understanding of estimation theory and principles governing system.

A variable of interest can be quantified in terms of three values i.e., true value say $y(t)$, measured value $\tilde{y}(t)$ and estimated value $\hat{y}(t)$. True value is the actual value that is known either via measurement with some measurement error or via estimation with some estimation error such that the true value is never known with hundred percent accuracy [45]. The errors arise due to errors in measurement, wrong selection of parameters and modelling errors (inadequate presentation of actual phenomenon). Mathematically, the measured value is:

$$\tilde{y}(t) = y(t) + \nu, \tag{2.1a}$$

where ν represents the measurement errors, and the estimated value is:

$$\hat{y}(t) = \tilde{y}(t) + e, \tag{2.1b}$$

where e represents the modelling or the estimation errors. Simple linear regression will be taken as a sample model to illustrate the methodology of parameter estimation. Let's assume we have a set of measurements y_j taken as time series data with time interval t_j presented as

$$\{y_1, t_1;\ y_2, t_2; \dots \dots \dots . y_m, t_m\} \tag{2.2}$$

True value ideally can be presented as

$$y(t) = x^T h_i(t), \quad m \geq n \tag{2.3}$$
$$x = [x_1, x_2 \dots . . x_m]^T$$

where x_i represents the parameter values and $h_i(t)$ presents the basis function that can be expressed as:

$$h_i(t) \in \{h_1(t), h_2(t) \dots \dots ., h_n(t)\} \tag{2.4}$$

Relationship between measured $\tilde{y}(t)$, true value $y(t)$ and estimated $\hat{y}(t)$ can be presented as

$$\tilde{y}_j \equiv \tilde{y}(t_j) = x^T h_i(t_j) + v_j, \quad m \geq n$$
$$x = [x_1, x_2 \ldots . . x_i]^T \tag{2.5}$$

$$\hat{y}_j \equiv \hat{y}(t_j) = \hat{x}_i{}^T h_i(t_j) + v_j, \quad m \geq n$$
$$\hat{x} = [\hat{x}_1, \hat{x}_2, \ldots \hat{x}_i]^T \tag{2.6}$$

$$\tilde{y}_j = \hat{x}^T h_i(t_j) + e_j, \quad m \geq n$$
$$\hat{x} = [\hat{x}_1, \hat{x}_2, \ldots \hat{x}_m]^T \tag{2.7}$$

where residual error e_j is given by

$$e_j \equiv \tilde{y}_j - \hat{y}_j \tag{2.8}$$

This can be written in compact matrix form as

$$\tilde{y} = H\hat{X} + e \tag{2.9}$$

The least square optimization criterion is used to find the parameter values $\hat{X}$ as

$$\hat{X} = (H^T H)^{-1} H^T \tilde{y} \tag{2.10}$$

These set of equations forms the fundamental basis of estimation theory. Further improvements in estimation theory can be regarded as extensions, modifications or generalization of linear regression analysis to adapt to different measurement techniques and mathematical models [45]. For example, further improvement to this method are sequential estimation to update/improve model with receiving data, weighted least square solution, constrained least square solution, differential correction procedures for application to

nonlinear problems, nonlinear estimation techniques, minimum variance and Bayesian estimation [45]. Solution criteria, other than least square criterion (LS), are minimum mean square error criterion (MMSE), prediction error methods (PEM), subspace identification methods (SIM) and the maximum likelihood criterion (ML). Recently, new criteria are introduced based on information theory descriptors of entropy and dissimilarity (Badong Chen, 2013).

2.2.2 Model structure

Model structure provides a framework in which Identification algorithms work to generate a model. In certain cases, such as black box modelling, model structure and identification algorithm are considered as synonymous [48]. Data based modelling structures are identified with one of the two model structures i.e., **black box** pure statistical approach and **grey box** model, a combination of statistical and physical method.

2.2.2.1 Black box structure

Black Box models consider building as a model for which the parameters can be inferred from inputs, such as outdoor temperature, humidity, solar radiations etc. and outputs such as indoor temperature, energy consumption etc. [39]. It is a pure statistical approach where fitting a statistical model to data is used for identification. The coefficients identified have no physical meaning [49]. They are regression models (regression techniques identify relationships between dependent and independent variables) with complexity of regression model equations ranging from simple linear equations, to exponential forms, Fourier series, artificial neural networks (ANN), fuzzy logic and genetic algorithms. ARX, ARMAX, state space, impulse response and transfer function models are some of the most common black model structures for dynamic systems [49].

As an example, consider simple black box **linear auto regressive with exogenous (ARX)** models that can be used to estimate thermal load. The ARX models are recommended for linear time invariant dynamic systems (stationary). ARX models are used for estimation of

over-all heat transfer co-efficient H, solar radiations gA, and the time constants τ of the system. It consists of outputs that are related to inputs in linear form using coefficients. A general equation of an ARX model is given as:

$$y(t) + a_1 y(t - \Delta t) + \cdots + a_r y(t - r\Delta t) = b_0 u(t - b\Delta t) + \cdots + b_s u(t - (b + s)\Delta t) + e(t) \quad (2.11)$$

where $y(t)$ represent the model output related linearly to number 's' of the past inputs via coefficients 'b' and to the past output readings 'y' via coefficients 'a'. A parametrized form of the ARX model to building thermal load can be of the form:

$$Load_t = W_1 T_t + W_2 H_t + W_3 Wind_t + W_4 Rad_t + W_5 Occ_t + W_6 Load_{t-1} \quad (2.12)$$

where $Load$ is the building thermal load, T is the dry bulb temperature H is the outdoor humidity, $Wind$ is the wind speed, Rad is the direct radiation, Occ is the occupancy and W_{1-6} represents estimated parameters.

The black box models are also called **external models**. They are based on external relation between input and output and hence can be used for external properties of buildings, such as H and gA values [46]. They cannot estimate internal properties, such as internal resistance and heat capacities, although they can be inferred using dynamics of actual system.

Sampling time, for any black box model, depends on whether it is dynamic estimation or steady state estimation. For H and gA, estimation of the sampling time ranges between 1 and 6 hours for normal buildings. However, sampling can be longer for heavily insulated buildings. For the purpose of control, the sampling time usually ranges from four minutes to an hour [46].

Model Parametrization. The output for the model can be either heating power or Internal temperature [46]. In case of heating power as output, the temperature is thermostatically controlled by supplying heat. The parametric form of the time series model is:

$$\phi(B)\Phi_t^h = \omega_i(B)T_t^i + \omega_e(B)T_t^e + \omega_{sol}(B)I_t^{sol} + \varepsilon_t \quad (2.13)$$

where

$\phi(B)$ is an output polynomial of order p in the backshift operator B;

T_t^i, T_t^e are internal and external temperatures respectively;

$\omega_i(B), \omega_e(B), \omega_{sol}(B)$ are polynomials co-efficients of order S_i, S_e and S_{sol} respectively.

In ARX modelling, where heating power is considered as output, the internal temperature is kept constant and hence the order of the internal temperature polynomial is set to zero. In case of change in internal temperature, the linear ARX model with heating power as output is not valid. The order of input polynomials S_e= S_{sol} is set equal to $p-1$, where p is the model order. In case of model order $p = 0$, the order of all input polynomials is set equal to p which is a special case of linear steady state condition. In complex cases, different models are considered [50].

Model order selection. The model order p (of output) is selected by the following criteria;

(a) The model order is set to zero initially ($p = 0$).
(b) Estimate model parameters.
(c) Evaluate noise residuals using autocorrelation function (ACF) and partial autocorrelation function (PACF) functions

The model order is increased until both ACF and PACF show white noise only [46].

Calculation of H, gA-vaues and time constants. In case of heating power as output, the heat transfer coefficients H_i, H_e and gA_{sol} (solar aperture) are calculated using the equation (2.13) [46]:

$$H_i = \frac{\omega_i(1)}{\phi(1)} \quad (2.14)$$

$$H_e = -\frac{\omega_e(1)}{\phi(1)}$$

$$gA_{sol} = \frac{\omega_{sol}(1)}{\phi(1)} \tag{2.15}$$

Time constant. Time constant of the system is calculated as [46]:

$$\tau_i = -\Delta t_{smp} \frac{1}{\ln(p_i)'} \tag{2.16}$$

(

where p_i is the i'th non-negative real pole determined as roots in charactersitic equation and Δt_{smp} is the sampling time.

Advanced model forms can be considered with the objective to improve model accuracy. These include separate model orders (for each input in contrast to output), including **Moving Average (MA)** term in the model, i.e. historical values of residuals, **additional input variables** other than T_i,T_e and I_{sol} like the long wave radiation, wind speed, wind speed multiplied with temperature differences, precipitation, transformed input variables like T^4 for radiative heat transfer, methods like pre-whitening and ridge regression, and adding cross-correlation functions between residuals and various candidate variables [46].

Improvements in **solar radiations** modelling can also be added. Some of the improved modelling effects are adding a parametrized gA-curve that is function of solar elevation and azimuthal angle (as gA is not constant) or simply as function of time of day (for short periods), splitting total solar radiations into direct and diffuse radiations, transformation of solar radiations on the surface of buildings and use of semiparametric functions such as modelling gA-curve using spline function [46].

Box-Jenkins transfer function model. In transfer function form, the input series U_t can be related to the output series Y_t as

$$\Upsilon_i = h_k^T . U_{t-k} + N_t, \text{ where } h_k = [h_1, h_2, \ldots . h_k] \quad (2.17)$$

where N_t, is correlated noise process. The parametrized form in Box-Jenkins form can be written as

$$\phi(B)\Upsilon_t = \omega(B)U_t + \epsilon_t \quad (2.18)$$

where ϕ, ω and θ are polynomials in B. The effect of other inputs can be included, such as solar radiation and heat supply. The assumption of the Box-Jenkin models is that output process does not influence the inputs [46].

State space model in discrete time is used to model input_output relations but also focus on the internal states of the system. A linear state space equation relating the state vector X_t (m-dimentional, latent and random in case of black box modelling), input vector U_t , via known matrices B and C, can be expressed as:

$$X_t = AX_{t-1} + BU_{t-1} + e_{1,t}\,\epsilon_t \quad (2.19)$$

The measurement equation can be given as

$$\Upsilon_t = CX_t + e_{2,t} \quad (2.20)$$

Kalman filter (Kalman smoother) can be used to estimate the state vector. The two elements of the output state vector defined in case of building modelling can be the temperature of indoor air and heat accumulating concrete floor. The input vector consists of ambient air temperature, solar radiation and heat input. When only indoor temperature is observed, Υ_t it consists only on indoor temperature.

Black box models are easy to build and are computationally savvy. However, they require extensive training data and long training period. They are applicable to specific building conditions, for which they were developed and can generate prediction errors if the training data do not cover all the conditions that building undergoes [51]. One issue with black box modelling is the parameter interpretation. The model in itself does not offer any explanation; physical interpretation is not transparent and can change drastically as the model order increases [39]. Grey box models are used as improvement of black box model and are further explained in the next section.

2.2.2.2 Grey box model structure

Grey Box models are empirical models based on simplified physical description to simulate building energy behaviour [51]. They are combination of physical and empirical models and potentially compensate for the deficiencies in both approaches [52]. These are semi-physical or semi-statistical approaches for identifying internal parameters or internal dynamic characteristics of buildings. Unlike black box, the grey box parameters have direct physical interpretation [46]. This enables us to add prior physical knowledge in addition to the statistical model to identify parameters of building. The simple semi physical models reduce the requirement of training data set (up to two weeks) and computation time [51].

The steps for implementation of grey box model are [51] :

- Development of model based on simplified physical expression.
- Putting rough bounds on physical parameters from prior description of building.
- Application of identification algorithm for identification of parameters.
- Validation of model with test data and external validation.

A simple explanation of these steps can be given in terms of resistance capacitance network RC. The RC network represents a highly simplified form of physical/thermal behaviour of the building with a high computational efficiency. The RC network is able to simulate the thermal dynamics of building via two elements, i.e. thermal mass represented by the capacity C and building envelope presented by resistance R. The resistances and the capacities are then identified using different statistical techniques.

Grey box models can take into consideration both linear, non-linear, stationary and non-stationary effects. The nonlinear and time varying approaches provide better explanation of complex phenomenon at the cost of high computation time. The linear methods are easy to implement. However, they leave much of the scatter in the data unexplained. An example of the effectiveness of grey box models is that they can model the variation in thermal capacity of building with change in moisture (a time varying phenomenon) where building moisture show high variation with temperature, radiation and season of the year [53].

There are different methods for presenting the physical grey box model expression such as Thermal Netwrok Models of resistances and capacities, Auto Regressive Moving Averages (ARMA), differential equation and modal analysis [39]. The thermal network models are easy to understand and construct. However, a systematic decision regarding the number of resistors and capacitors in model, presents a problem [39]. The differential equation or ARMA model are recommended as in both methods the ease of implentation is coupled with systematic addition of parameters. The ARMA is solved via numerical methods but differntial equation offer the ease of analysis with analytical methods and therfeore some authors recommend to use differential equation to ARMA [39].

A differential equation in state space form is used to parametrize physical system described by linear differential equation lumped form (limited number of parameters). A deterministic linear model in continuous time of the states X of the system:

$$\frac{dX}{dt} = AX + BU \tag{2.21}$$

where matrices A and B presents how parameters transform the state and inputs respectively. The matrices A and B are described by physical equations such as RC formulation.
Since the deterministic linear equation cannot predict exactly the future states of the system, the deviation is usually dealt with by introducing a noise term in the differential equation. The stochastic linear state space model can be given as:

$$dX = AXdt + BUdt + d\omega(t) \tag{2.22}$$

where $\omega(t)$ is n dimensional stochastic process. Reason for introducing $\omega(t)$ are:

- inability of matrix A to present the dynamics of system due to approximations,
- some inputs may not be measured but have impact on dynamics of system,
- measurements are noisy due to measurement errors.

Since practically all systems are non-linear and a non-linear presentation is a better approximation of the system, in **non-linear** form the equation can be written as ordinary differential equation (ODE) as

$$dX_t = f(X_t, U_t, t)dt \;\; t \geq 0 \tag{2.23}$$

where f is a deterministic function of time t. The equation is deterministic and parameters can be estimated.

Stochastic differential equations, as continuous description of physical phenomenon such as dynamics of heat transfer, are coupled with a set of discrete data measurement equations. These models are called continuous-discrete stochastic (SDE) state space model. A general non-linear (continuous) SDE for stochastic process is given as:

$$dX_t = f(X_t, U_t, t)dt + G(X_t, U_t)dW_t \tag{2.24}$$

where $X_t \, \epsilon \, R^n$ is the n-dimensional state vector, $U_t \, \epsilon \, R^m$ is m-dimensional input vector, G is the stochastic drift term and W_t is the Wiener process of dimension n with incremental covariance Q_t.

And the discrete set of measurements are given as:

$$Y_{t_k} = h\left(X_{t_k}, U_{t_k}\right) + e_{t_k} \tag{2.25}$$

where $Y_{t_k} \epsilon R^m$ is the m-dimensional vector of measurements at time t_k, h is the measurement function and $e_{t_k} \epsilon R^m$ is a Gaussian white noise with covariance $\sum t_k$[46].

Depending on study objectives, grey box can be steady state and dynamic state where dynamic state models are characterized by differential equations. The dynamic grey box modelling is explained with reference to [49] who used 6 days data of a single story test building (Flex House) to test the performance of grey box models of increasing complexity. Thermal networks were used as physical model for building. These models can be presented as stochastic linear state space model with dynamic states written as

$$d\boldsymbol{T} = \boldsymbol{AT}dt + \boldsymbol{BU}dt + d\omega \tag{2.26}$$

where $\boldsymbol{T}$ represents the state vector, $\boldsymbol{U}$ the input vector, and matrices $\boldsymbol{A}$ and $\boldsymbol{B}$ consist of combinations of parameters such as C_i and R_i . Depending on the complexity of the model, the number of C_s and R_s may change accordingly. For example, in the simplest model there will be a single R and C representing thermal resistance and heat capacity of the entire building. ω is the standard Wiener process. Input vector $\boldsymbol{U}$ can be represented as:

$$\boldsymbol{U} = [T_{\boldsymbol{a}}, \Phi_{\boldsymbol{s}}, \phi_h]^{\boldsymbol{T}} \tag{2.27}$$

where $T_{\boldsymbol{a}}$ is the ambient temperature, $\Phi_{\boldsymbol{s}}$ are solar radiations and ϕ_h is the heat input from building heat source. Parameters were estimated using maximum likelihood function where observations are presented by

$$y_{\boldsymbol{n}} = [Y_N, Y_{N-1}, \ldots\ldots, Y_1, Y_0] \tag{2.28}$$

The likelihood function is given by the joint probability density:

$$L(\theta; y_{\boldsymbol{n}}) \prod_{k=1}^{N} p(Y_k/y_{k-1}, \theta) p(Y_0/\theta) \tag{2.29}$$

where:

$L(\theta; y_{\boldsymbol{n}})$ is the Likelihood function of parameter θ given the observations y_n

$p(Y_k/y_{k-1}, \theta)$ is the probability density of observations given the parameter θ

The maximum likely estimate of the parameters is then:

$$\hat{\theta}=arg\max_{\theta}\{L(\theta; y_{\boldsymbol{n}})\} \tag{2.30}$$

Likelihood ratio test was used to evaluate the performance of different combination of models of same order. The model with highest log-likelihood is chosen. After this stage, the extended models are compared with lower order (subset) models using likelihood ratio test and improvement with increasing order is estimated from p value (where p is a significance of test, a lower value of p indicates the hypothesis that both full order and reduce order are the same should be rejected) [49]. A lower p value indicates improvement with increasing model order. The iteration is repeated until no more improvement is visible. The models are evaluated by data fitting and evaluating residuals using auto correlation function (ACF) and the cumulated periodogram (CP). Any pattern in residuals indicate that the model does not fit the data and it should be further extended [49]. The analyses initiated with simplest building model consisting of single state T_i (indoor air temperature only). The order was increased and in each order the performance of every sequence was evaluated. The model with highest order was $T_i\ T_m\ T_e\ T_h\ T_s\ A_e$, where

T_i is the temperature of the indoor air,

T_h is the temperature of heater

T_m is the temperature of the walls and furniture (Indoor medium)

T_e is the temperature of building envelope

T_s is the temperature of the sensor.

Based on the result of the fitted data, parameter estimation (using CSTM-R) and the autocorrelation and cumulated periodogram plots, it was inferred that a third order or three state model order $T_iT_eT_h$ generated acceptable results. A similar estimation procedure was applied to data from smart grid experimental facility SYSLAB at DTU Elektro, Denmark, and the third order model $T_iT_eT_h$ was found suitable [46].

The following measurements were done for the identification of the grey box modelling as discussed in the previous paragraph [46]:

- Indoor air temperature. A time series of the average temperatures of the indoor air.
- Heat input. A time series of the heating output value of heaters in building.
- Ambient temperature. A time series of the outside air temperature.
- Global radiation. A time series of global radiations measured close to building.
- Wind speed and direction. A time series of wind speed and direction around building.
- Excitation signals to estimate the dynamic response of building. Usually ROLBS or PRBS sequential signals are used.

The typical parameters estimated using grey box models are the overall heat transfer coefficient or thermal resistance, effective heat capacities of parts of building, effective solar aperture (effective area for solar radiations), parameters representing effects of wind such as wind induced infiltration [46]. The parameters are estimated using maximum likelihood with Kalman filter. Kalman filter reduces the impact of noisy measurements that are included in model on the estimation of parameters.

2.2.3 Steady state models

Steady state methods assume that both the system and the variables are constant in time. The measurement time considered is sufficiently long to average out indoor and outdoor variations, i.e. constant during duration of observation [38]. This is called down sampling, where data is averaged over longer periods of time so that auto-correlated noise/residuals are filtered out (becoming white noise).

These methods are used for describing linear and stationary steady state relations between the input and the output. They do not consider thermal storage in building or the transient skin behavior of the building that can cause temperature transients. ISO (9251:1987) gives description of steady state methods [50]. These methods are less suitable to represent real experimental conditions and utilize data on sub-optimal level. These methods can be used for estimation of overall heat transfer co-efficient (H) and gA-values (product of solar transmittance and effective solar aperture).

Single variate models are steady state models where only a single variable is considered as driving agent. For example, in case of buildings, it is common to consider outdoor dry bulb temperature as a variable. A number of parameters (P), ranging from single parameter (1-P) to 5-P are used. Number of parameters considered vary with type of study, building i.e. commercial, residential and weather based or non-weather based [50]. Single variable models are applicable to buildings where single variable, such as outdoor temperature, is the dominant driving force for energy consumption (e.g. residential buildings). In case of commercial buildings with multiple driving factors, the model may not truly represent or relate energy consumption to single variable. Their advantage of use is to single out weather based loads, compare pre-and post-retrofit normalized (weather) energy consumption in buildings and provide an overall easy visualization of energy consumption [38]. These models ignore effects of variables such as solar radiation, thermal mass and effects of humidity.

Multivariate models are extension of single-variate models and take into consideration other variables such as internal loads (heat given by people and electrical devices), solar radiation and humidity effects. They can take the form of **Fourier series** models (for seasonal diurnal effects) and **standard multiple-linear** or **change point** regression models. Parameters that are difficult to estimate or measure, such as internal heat given by occupants, are usually lumped. The problem of linear correlation of some variables i.e., **multi collinearity,** can lead to poor model predictions. Multi collinearity may be overcome by principal component analysis (PCA). However, it should be used with caution [46].

A simple steady state energy balance equation for a building is given as:

$$\Phi_h = H(T_i - T_e) - gA_{sol}I_{sol} \tag{2.31}$$

where Φ_h is heating power supplied, H is the parameter representing overall heat transfer coefficient (both transmission heat coefficient and ventilation heat transfer coefficient) and gA_{sol} is the parameter that is the product of solar transmittance g and affective solar collecting area(solar aperture) representing is the heat transfer coefficient, T_i and T_e are external and internal temperatures I_{sol} is the solar radiation received by the building [46]. This equation is used to parametrize the linear regression model

$$\Phi_t^h = \omega_i T_t^i + \omega_e T_t^e + \omega_{sol} I_t^{sol} + \varepsilon_t \tag{2.32}$$

where

- ε_t is independently and identically distributed white noise with zero mean and variance σ^2, expressed as $(0, \sigma^2)$, called white noise;
- ω_i and ω_e represent the H, from the two estimates of H the best estimation is obtained using a linear minimum variance method;
- ω_{sol} is the estimate of gA_{sol}, it should be noted that this estimate is obtained from the available solar radiations measurements such as global solar radiations and since the incoming solar radiations are different from the measurements care must be taken while estimating gA_{sol} [46].

All the estimates must be stated with the standard error of estimates for better comparison with physically judged results.

Sampling time for steady state. In case of buildings where data is available as time series, it is important to consider proper sampling time for measurements. The sampled data is usually averaged out and is denoted as function of time indicating the hour at which it is averaged out. A sampling time of one or two hours is taken in case of standard insulated buildings whereas for heavy insulated buildings the averaging time may be increased. For small

buildings, 6 hours average time is considered as appropriate. An Auto Correlation Function (ACF) method is used to select appropriate time that will avoid significant cross-correlation between different inputs, such as solar radiation [53].

A steady state method that can be used for estimation of long-term energy consumption of buildings is the energy signature method. This method is based on determination of overall heat transfer coefficient (H) of buildings from the measured energy consumption (bills) and mean outdoor temperature. The overall heat transfer coefficient (H) appears as regression coefficient in relationship between outdoor temperature and energy use [46]. The overall heat transfer coefficient determined by using steady state (energy signature method) is also known as the *building heat loss coefficient* and includes envelope transmission losses, ventilation losses and infiltration losses [54]. The general expression of the heat transfer between building and environment can be presented approximately as:

$$H(T_i - T_0) = Q_{hs} + Q_{el} + Q_P + Q_{sol} - Q_{dyn} \quad (2.33)$$

where Q_{hs} is the heat supplied from heating system, Q_{el} represents the heat gains from electricity, Q_P is heat gain from people, Q_{sol} are solar gains and Q_{dyn} presents heat storage corrective factor. For steady state methods, heat transfer due to solar radiations, intermittent building operation, occupancy behavior and the dynamic storage (building envelope) are ignored. H is estimated using the first three terms of equation (2.33) only. As a result, overall heat transfer coefficient H is estimated with low determination constant leading to low precision [55].

In order to improve steady state methods, the dynamic effects are incorporated using correction factors. Danov *et al*., introduced a methodology to include both the dynamic effects (effective capacitance) and the solar gain effects as correction factors for improved estimation of H [56]. Results indicated that considering both dynamic and solar effects as correction factor improved linear relationship resulting in an increased value of determination constant.

The estimation of overall heat transfer coefficient is based on linear regression. The results of linear regression are valid if temperature follows the normal distribution and the residuals follow a normal distribution with zero mean [57]. Both the outdoor temperature and energy load should follow an identical distribution. Temperature is usually normally distributed. However, energy load does not follow the distribution of the outdoor temperature at tails. The model from this simple linear regression may generate acceptable results for the data for which it was generated, but it is much less precise when used for other set of outdoor temperatures. A new method was proposed that uses a regression model based on quantile q-q plot. The model based on q-q regression can be used with equal precision for a data set different from the data for which the original model was developed [57].

2.2.4 Energy signature and degree-day

One of the simplest ways to measure the energy performance of the building is to evaluate energy consumption against the outdoor weather conditions. A correlation between the energy bills (electricity or gas) and outdoor temperature, is used to predict energy demand. This method is known as **energy signature** method. It has the capability to predict within 90 percent confidence interval of the actual demand [57]. Degree day method is simpler as compared to dynamic method and is used in energy management of buildings. This method simplifies the weather conditions by expressing them as a single variable: outdoor temperature. The energy performance system are based on degree day method for assessments [58]. It provides a simple and cost-effective method of benchmarking similar buildings by comparing the energy bills and weather data only.

Heating degree days is the summation of temperature difference between the outdoor air and indoor air (base temperature) over a period (year, day or season), where base temperature is defined as maximum or minimum outdoor temperature for which no internal heating is required. The base temperature can be expressed as:

$$q_{gain} = K_{tot}(T_i - T_{bal}) \tag{2.34}$$

where

q_{gain} are the total heat gains (internal and external)

K_{tot} - overall heat transfer coefficient (ventilation and conduction)

T_i - indoor temperature

T_{bal} - temperature for which no heating or cooling is required

T_e - temperature of building envelope

T_s - temperature of the sensor

The base or balance temperature can be given by:

$$T_{bal} = T_i - \frac{q_{gain}}{K_{tot}} \tag{2.35}$$

The energy loss or heating energy required can be given as:

$$q_h = \frac{K_{tot}}{\eta_h}[T_{bal} - T_o]^+ \tag{2.36}$$

where

T_o is the outdoor temperature

This can be integrated over a time t to determine/predict energy consumption provided that the overall heat transfer coefficient and thermal efficiency of the heating system η_{th} are known as

$$q_{h,yr} = \frac{K_{tot}}{\eta_h}\int [T_{bal} - T_o]^+ dt \tag{2.37}$$

Depending on how the integral is approximated by summing over average values of daily or hourly temperatures, the method is termed as **degree day** or **degree hour**. The base temperature in majority of the cases is taken as $18.3℃$ [38] in US and $15℃$ in UK [58]. The base temperature can be adjusted to include solar, ventilation and losses to ground as well.

The overall heat transfer coefficient and the balance temperature varies with occupancy, internal heat gains, time of day (activity level) and outdoor temperature. In order to improve estimation using energy signature method, the base or balance temperature is calculated based on bin hour where average temperature and periods of interval are stated simultaneously to account for activity level and efficiency of heating equipment [26]:

$$q_{bin} = N_{bin} \frac{K_{tot}}{\eta_h} [t_{bal} - t_o]^+ \tag{2.38}$$

where N_{bin} presents number of hours in a bin. The bins are usually measured and stated in interval of 2.8 K and eight hours shift [38].

The energy signature method is based on number of heating degree days that are based on base temperature. The consideration of fixed base temperature is misleading as it varies with type, age, size, operational schedule and percentage of heated space [58]. For further improvement the measurement of indoor set temperature is required [59]. The base temperature is determined by energy signature method or performance line method where performance line method requires small sampling periods as compared to energy signature method.

Different regression methods used for energy signature are change point (CP), Gaussian process regression (GPR), Gaussian mixture regression (GMR) and artificial neural network (ANN). GMR offers a slightly better statistical performance compared to rest of the three methods. However, CP is preferred because of its simplicity and less computational requirements to predict energy consumption [60].

Meng and Mourshed analyzed energy consumption of 199 non-domestic buildings in UK using change point regression analysis [58]. The variation of base temperature was analyzed with respect to building type, age, location and operational schedule. It was concluded that the actual base temperature was 1.2 ℃ higher than the value used for UK regulations (15.5℃).

Park *et al.* used a four parameter change point regression model to analyze energy bills for 128 apartments [61]. A three-year billing data 2009-2011 was used where bills provided data on electricity, natural gas and district heating consumption. The model parameters were able to characterize the energy use of thermal buildings with hydronic radiators. The slope of the regression model represents the heat loss from the building and efficiency of the space heating (kWh/m^2C).

Lakatos discussed the variation of balance temperature with difference in location of the city, solar gains, apartment house or standalone house, level of refurbishment, level of insulation and heat island effect for a city in Hungary [62]. The assumption of base temperature of $12℃$ (Hungary) can mislead to over estimation or under estimation of heating energy demand. The number of degree days vary depending on the assumed balance point temperature [63].

Anjomshoaa used daily consumption data of Kerman city to estimate the change over time and the base temperature for heating and cooling. Gas consumption was analyzed for heating and electricity consumption for cooling [64]. The base temperature estimated was 15.42 ℃ for cooling and 21.18 ℃ for heating. A linear relationship between base temperature and heating energy consumption was inferred based on sensitivity analysis. It was found that changing the base temperature by $1℃$ changes heating energy by 5 MJ.

Energy performance estimation using degree day methods is based on steady state analysis. They have the advantage of simplicity and can provide long term scenario analysis for different energy efficiency measures [65]. One of the limitations with steady state method is that they neglect the effects of inertia as the method is based on building envelope characteristics only (steady state). This leads to prediction errors and inability to correctly model short term variations. Several methods have been suggested that add corrective terms to the original steady state methods.

Transient thermal models can be used to overcome the shortcomings (inertia) of steady state degree day methods. De Rosa used lumped RC model for a building energy simulation using MATLAB the tool Building Energy Performance Simulator (BEPS) [65]. Building energy

consumption was then analyzed for different climate zones and several cities in Europe. The model was able to predict energy demand for all cities and climates. It was found that for heating degree days HDD, the heating demand was linearly related to difference between external and internal temperature. For cooling demand, the relationship is not linear for cooling degree days (CDD< 200) as the data scatter cannot be explained [65]. This is due to inertia of building related to solar radiations. A correction factor added was used to improve the linear relationship between cooling energy demand and temperature difference between internal and external environment [65].

The degree day and degree hour methods cannot model dynamic effects (thermal inertia, solar radiations etc.) on building energy consumption. This leads to poor estimation. However, these methods have their advantages. They are based on utility billing data (electricity and gas consumption) and weather data that are easily available. They do not require any experimentation or detailed input data as required in case of forward models. They can predict long term energy consumption for buildings and cities with weather variations [61]. Physical parameters can be estimated using degree day method and the fitted parameters are then able to predict energy consumption.

2.3 Calibrated simulation

In building energy modelling, considerable discrepancies exist between the predicted energy consumption and the actual energy consumption. The reasons for such discrepancies are modelling simplifications and assumptions (also called model inadequacies), uncertainties in indoor conditions and operating schedules, weather conditions and building material properties. Calibration of simulation model is used to remove the errors between predictions and observations [7]. Calibration is the process of tuning the simulation model so that the gap or error between the predicted and actual energy consumption can be reduced [36].

Building energy simulation is an integral part of energy audits required by country or state laws for energy performance assessment of buildings. Building simulation is used to develop

a baseline energy for buildings, i.e. average annual energy consumed by the building in absence of any energy conservation measures (ECM). The baseline helps to determine the contribution of heating/cooling loads, water heating, lighting, plug loads, building fabric (thermal performance), solar radiation, ventilation and occupancy on the total building energy consumption.

Savings from any energy conservation measures are estimated against the simulated baseline. It is difficult to simulate a representative baseline that can take into account the impact of all parameters. Discrepancies in baseline are more pronounced in existing buildings because of deterioration of building thermal properties, reduction in efficiency of equipment, operation off the designed values, changing weather pattern, changes in operation schedule and occupancy [66]. Majority of energy conservation measures are adapted to existing buildings. They require investment by building owners that have to be guaranteed against predicted savings by Energy Service Companies (ESCOS). Uncertainty in predicted savings make it difficult to gain the confidence of investors in savings from energy conservation measures.

Due to discrepancies in modelled energy, different energy performance certificates have set minimum acceptable error between simulated and actual energy consumption [40]. ASHRAE Guideline 14 [67], International performance measurement and verification protocol (IPMVP) [26], US Department of Energy's (DOE) Performance Measurement and Evaluation Plan (PMEP) and Guideline and Uniform Methods Project (UMP) provide the procedures for ECM saving calculations, measurement verification of savings from energy conservation measure, and minimum criteria for simulation/model fitness [67]. Calibration is therefore a requirement for energy auditors to bring simulated energy consumption close to actual energy consumption. In absence of calibration, the discrepancies can be in the range of ± 30% for an entire building whereas for components, such as HVAC equipment, the discrepancies can rise up to ± 90 % [37, 41].

Calibration is considered as an overdetermined problem i.e. too many parameters to support with observed data [68]. This can result in non-unique solutions [40]. One of the major issues with calibration guidelines, such as IPMVP, is the criterion for estimating prediction errors

without specifying procedure or methodology of calibration [68]. There are many published methods for calibration. However, there is a lack of standardized, uniform method for calibration. The following paragraphs explains the principles of calibration along with the issues and advancements in this field.

2.3.1 Principles

Calibration for building energy models is carried using the following steps:

- Collect data
- Enter data and run simulation
- Find error between simulation and actual data
- Tune the parameters until the desired accuracy is achieved [68].

The method of error determination and tuning can be used to further classify the calibration techniques. For example, a broad classification is

a) **Manual calibration,** where tuning of parameters is performed manually by the user utilizing their knowledge and experience.
b) **Automatic calibration,** which is performed by automated process or tools that assist in calibration, e.g. using mathematical and statistical techniques.

A more detailed classification is given by [40], [68].

i. Calibration based on manual, iterative and expert-based intervention.
ii. Calibration based on suite of graphical or visualization techniques.
iii. Calibration based on empirical tests and analysis.
iv. Calibration based on analytical and mathematical techniques.

It may be noted that a single method of calibration cannot work alone. Therefore, a combination of two or more techniques is used. A brief description of error criteria between simulated and actual energy consumption is explained in the following paragraphs.

2.3.2 Error criteria for calibration (objective function)

In order to reduce the gap between simulation output and measured energy consumption (billing data), it is necessary to quantify the error between simulation and measured data. Different terms are used in literature for this purpose.

A simple method to calculate the simulation error is to find percent difference between actual energy consumption and simulated energy consumption also known as Mean Bias Error [38]:

$$MBE(\%) = \frac{\sum_{i=1}^{N_P}(M_i - S_i)}{\sum_{i=1}^{N_P} M_i} \tag{2.39}$$

where M_i and S_i are measured and simulated data at instance i; P is the period of interval (e.g., monthly, weekly, daily and hourly); N_P is the number of values at interval period P (i.e., N_{month} = 12, N_{day} = 365, N_{hour} = 8760). This is practiced in energy audits of multi residential buildings. However, error computed using this method gives a false perception of reduced error due to compensation from over and under estimation over an year [38].

To overcome the under estimation of error, Root Mean Square Error (RMS) is used making all the $(M_i - S_i)$ terms positive before addition thereby cancelling the effect of over and under estimation in estimated error [26]. The RMS is indexed by introducing an error term called coefficient of variance of Root Mean Squared Error (CVRMSE):

$$CVRMSE_{(P)} = \frac{\sqrt{\sum_{i=1}^{N_P}((M_i - S_i)^2/N_P)}}{\overline{M_P}} \tag{2.40}$$

where

$$\overline{M}_p = \frac{\sum_{i=1}^{N_p} M_i}{N_P} \tag{2.41}$$

In contrast to error coefficients (MBE, CVRMSE), Index of agreement d gives a direct measure of the fitness or agreement. The value of d varies between 0 and 1, with higher value indicating good fit [69]:

$$d = 1 - \frac{\sum_{i=1}^{n}(O_i - P_i)^2}{\sum_{i=1}^{n}(|P_i - \overline{O}| + |O_i - \overline{O}|)^2} \quad (2.42)$$

where O is the observation and P is the prediction value for the corresponding instances.

The acceptance criteria for simulation error is based on CVRMSE and RMS with models achieving minimum values for CVRMSE and MBE are considered as 'fit'. The fitness shows the acceptance criteria as per ASHRAE Guideline 14, IPMVP and FEMP. CVRMSE is used as a cost function or objective function criteria against which parameters are optimized during calibration [7]. As the minimum error criteria can be achieved through many non-unique solutions, constrain on parameter values can be used as an additional criteria to reduce number of possible solutions [7].

In case of model output with a specific distribution, the closeness with measured distributions is calculated using Continuous Rank Probability Score (CSPR) [7]. If distributions are obtained using Monte Carlo Simulation, then CSRP is given as:

$$CRPS(F, Y) = E_F|Y - y| - \frac{1}{2}E_F|Y - Y'| \quad (2.43)$$

where F is the predictive distribution of random variable Y, y is the observation, E_F is the expectation over F and Y' is an independent random variable with identical distribution as Y. A larger distribution means a larger discrepancy between predicted and observed distribution.

Table 2-1: Error acceptance criteria for building energy model [40]

Standard/guideline	Monthly criteria (%)		Hourly criteria (%)	
	MBE	CVRMSE	MBE	CVRMSE
ASHRARE Guideline 14	5	15	10	30
IPMVP	20		5	20
FEMP	5	15	10	30

2.3.3 Calibration methods

The methods of calibration require building construction and operation details. The details are either provided by owner or obtained by a detailed survey of the building for which the simulation is developed, known as **characterization technique,** to know the physical and operational characteristics of buildings. Standardized methods of characterization have been developed that are known as energy audits or energy surveys [70]. According to the level of detailed survey, they may be characterized as:

Level 1-walkthrough audit. It involves a visual inspection of the facility to know the building and its operations. It usually does not involve extensive data collection.

Level 2-standard audit. It involves extensive inspection and data collection. All energy consumption equipment is noted in detail and is broken down as per type of energy consumption such as heating, cooling, lighting loads etc. building geometry, shape, structure, fenestration and roof etc. are inspected [67].

Level 3-investment audit. It involves measurements of energy consumption equipment along with extensive detailed inspection of facility, detailed interviews with facility managers to know the building operations. These audits serve the purpose of providing guaranteed ECM savings for investments [67].

Depending on the level of audits, simulations are carried out by using data from facility. Simulation ranges from simple excel macros to detailed software analysis using market software such as BLAST, EnergyPlus, ESP-r, Equest etc. After simulation, the results are compared with actual billed data of building to find any prediction or simulation errors. Simulations are calibrated to remove the errors based on any or combination of the following methods explained [71].

2.3.3.1 Calibration based on manual, iterative and expert-based Intervention

Field calibration is performed manually by experts through steps such as selection of significant parameters and tuning or “fudging” the values of significant parameters (parameter estimation). The process is repeated by iteratively changing values of set of

parameters and running simulation until the desired closeness of gap between the simulated energy consumption and actual energy consumption is achieved [66]. This method of calibration is labor intensive, time consuming and subjective, depending on the skills and experience of the expert. This can result in unrealistic values of parameters, different values of parameters leading to the same results (identification issue), poor optimization of parameter and unrealistic fitting between actual data and simulation [66]. The unrealistic closeness between simulation and actual energy consumption can lead to saving predictions that are never achieved. Some of the discrepancies in manual calibration can be resolved by assisting it with mathematical/analytical and advanced graphical techniques.

2.3.3.2 Advanced graphical techniques for calibration

A simple form of graphical analysis is to compare the simulation time series of energy consumption versus the measured energy consumption using time series graphs. The scale of time can be months, days or hours; parameters are tuned to reduce the difference between measurements and simulation results. Advancement in graphical data presentation has improved the comparisons. Some of the advanced graphical comparisons are:

- **3-D comparative plots**: These are surface plots created using 3-dimensional data such as hourly and daily axes against vertical energy consumption axes. When plotted as function of difference between simulated and actual energy consumption, they can identify even very small discrepancies. The valleys and peaks of 3-D graph make visible the departure that can be tuned further. 3-D graphs are also used to view any unusual peaks in energy consumption [40].
- **Graphical statistical indices**: Plots like Box Whisker Mean Plots (BWM) are used to indicate statistical indices in graphical format. This helps in easy understanding of data and elimination of data overlaps. They express data in the form of mean, median, 10^{th}, 25^{th}, 75^{th} and 90^{th} percentile for each data bin (month, week or day) [40].
- **Other Plots**: Other plots (Figure 2.3,Figure 2.4) include colored contour plots showing error propagation, superposed and juxtaposed binned box and scatter plots [68].

One way to use graphical analysis is using signature method, i.e. **Calibration Signature** and **Characteristic Signature** in which a normalized plot of difference between simulated versus

actual energy consumption is plotted as a function of outdoor temperature. This graphic signature can then be tuned by changing different parameters. A characteristic signature for each building can be generated for heating and cooling loads. These signature graphs serve the purpose of baseline for evaluating any energy conservation measure [68].

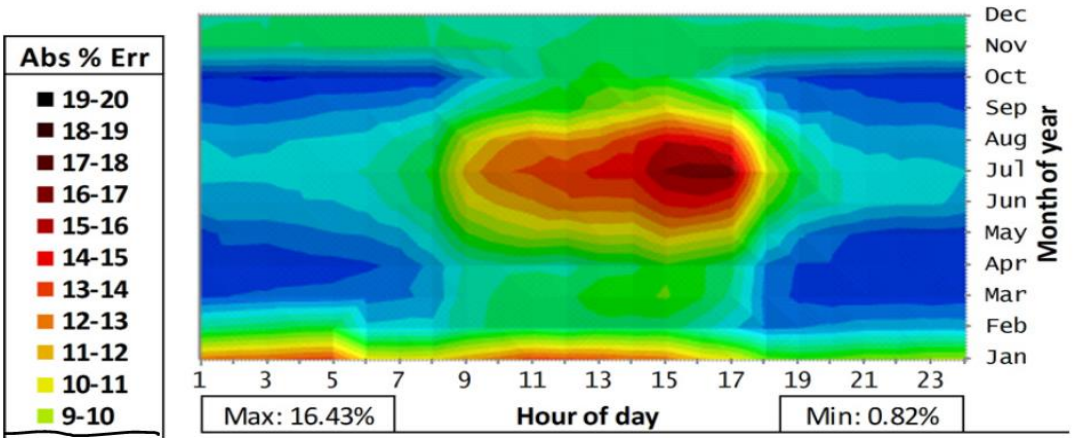

Figure 2.3:Colour contour graphs showing error between simulated and actual energy consumption [71]

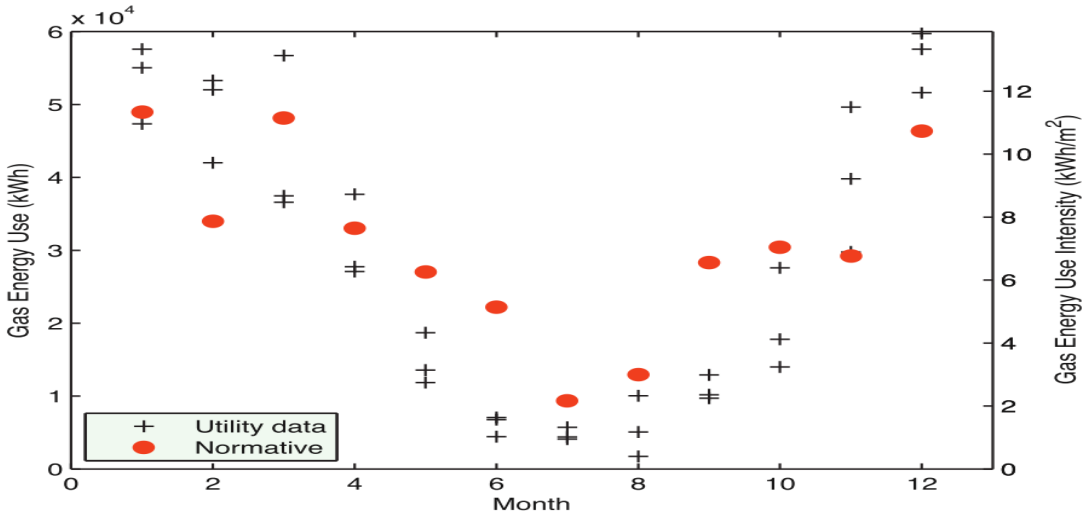

Figure 2.4 Scatter Plot for Calibration [66]

2.3.3.3 Calibration based on tests

The total building energy consumption can be modelled as the summation of energy consumption from heating, cooling, domestic hot water, lighting and electronic equipment consumption. The energy bills do not provide the segregation of different loads. Simulation

uses operation schedules and energy relations to find the impact of each load on overall energy consumption. One of the simple ways is to perform on site tests for this purpose. The different test methods explained in this section are used for calibration and parameter identification.

Intrusive blink tests: These tests include turning on and off load equipment for a short interval of time usually one to five minutes. This help to identify the impact of selected parameters effect on hourly energy consumption that can be averaged over longer period. Usually loads are turned on and off sequentially for a short interval of time. The incremental energy consumption can accurately quantify the impact of these loads. Two to four weeks of testing is considered enough for calibration purposes [68].

STEM tests: The short-term energy monitoring (STEM) test is a calibration test to segregate energy consumption into end use profile such as cooling energy, heating energy, lighting energy and plug loads. STEM test involve intrusive and non-intrusive controlled heating and cooling tests for a period of two to four weeks. The method was developed by Subbarco (1988) [72]. The test protocol consists a period when temperature is kept constant by application of heating or cooling followed by a period where temperature is allowed to float freely. The co-heating is usually carried at night time and is used to determine the overall heat transfer coefficient in case of buildings where heat loss through building shell is significant. The cool down/free floating time is used to determine building time constant. Building heat transfer coefficient 'U' is a significant parameter influencing building energy simulation, the calibrated value determined effectively reduces discrepancy between simulated and actual energy consumption.

2.3.3.4 Calibration based on analytical and mathematical techniques (automatic calibration)

The mathematical and analytical calibration can be defined as an optimization process with an objective function to reduce the gap between the simulated and actual energy consumption for buildings [68]. These methods find the important parameter to tune and decide on how much to tune. An analytic framework for automatic calibration using tools (steps) such as Sensitivity Analysis (to determine the most significant parameters),

Identifiability Analysis (to find parameters that can be tuned), numerical optimization (to find the best parameter sets that can reduce discrepancies) and uncertainty analysis (variation space of parameters) is provided in [73]. An exhaustive literature is available on each of these tools. This section provides an overview of important issues relevant to the work of this thesis.

2.3.3.5 *Uncertainty in inputs*

Simulation output depends on the quality of the data (measured and calculated) used for simulation. The quality of input data varies largely due to many reasons. Uncertainty in data is due to stated values based on laboratory tests (standard conditions only), manufacturing defects and errors during measurement process. For example, in real working conditions the properties such as thermal transmittance, density and specific heat are reported to have a standard deviation of 1 %, 5 %, and 25 % as compared to stated values [66]. The area weighted thermal capacity C (kJ/m^2 K) of concrete can have variation between 160 to 257 (kJ/m^2 K). Significant variations occur in actual ventilation and infiltration values when compared to the standard values used in simulation.

A study on naturally ventilated buildings showed that estimated normal values used for naturally ventilated office buildings range between 5.0 to 10.0 m^3/h at 50 Pa whereas actual values ranged between 8.3 and 32.0 m^3/h at 50 Pa. Similar discussion of uncertainty applies to other parameters, such as infiltration due to window openings, number of window openings, variation in efficiency of HVAC equipment, heat losses in distribution system, heat gain from occupants (3-7 W/m^2), plug load per occupant (124-229 W/person), weather conditions, etc.

Simulation model may fit actual data even with incorrect inputs or parameters. This is misleading as is evident in many projects where savings were either over estimated or under estimated, despite initial simulation agreement [40]. Confidence in simulation output depends on the quality of input data. It is therefore important to perform uncertainty analysis to reflect the impacts of uncertainty in inputs on output simulation. One way is to express uncertainty of each input as statistical distribution and run simulations to generate an output with statistical distribution [41].

Simulation involves large number of parameters and running simulations for every input parameter with its statistical distribution is time consuming. It is therefore important to select parameters with significant importance using Sensitivity Analysis techniques.

2.3.3.6 Sensitivity analysis (parameter selection)

Any calibration process involves a number of parameters that need to be tuned to match simulation and actual data. Tuning each parameter is time consuming and computationally expensive. Different techniques are developed to segregate parameters that have significant effect on the output. This is called Sensitivity Analysis (SA). A typical sensitivity analysis method requires the steps shown in Figure 2.5.

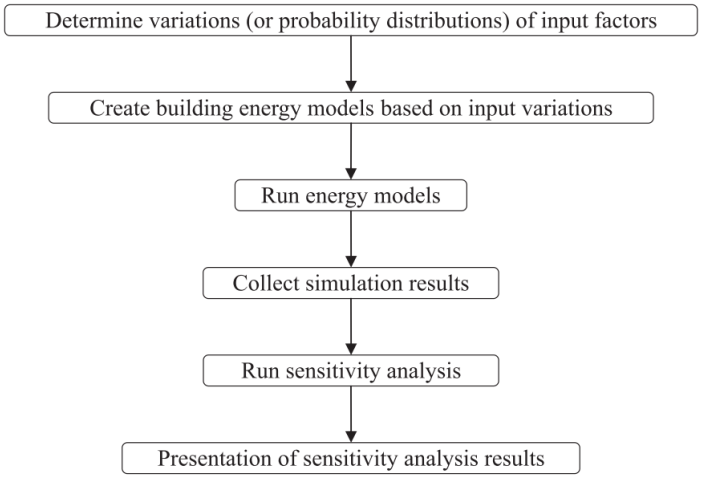

Figure 2.5: Sensitivity analysis steps [74]

Sensitivity analysis methods can be broadly classified as local and global. Local sensitivity analysis, also referred as one-factor-at-a-time methods, explore the relationship of individual input by keeping the other inputs constant. It is a simple method compared to the global sensitivity analysis that considers the effect of uncertain inputs and the correlation between inputs on the entire input space as well. Global methods are more reliable, but require high number of computations. Several techniques have been recommended in literature for sensitivity analysis, such as Correlation Analysis, Regression Analysis (RA), Morris One-at-a-

Time (MOAT), Multiple Adaptive Regression, Splines (MARS), Delta Test (DT), Monte Carlo (MC), Fourier Amplitude Sensitivity Test (FAST), etc. [75].

First step for sensitivity analysis is to define inputs with probable variation. Different methods used for this purpose are known as sampling techniques. Sampling techniques are used to generate sample size of parameters or inputs, the range or variation of each data input and distribution for each value, such as normal, uniform, lognormal and triangular distribution. Plack-Burman (PB), Monte Carlo (MC), Extended Sobol etc., are some of the Sampling techniques [75]. Embedded Latin Hypercube Design (LHD) with Monte Carlo simulation technique for generating samples was used in [7]. The advantage of this method is that it reduces sample size and all desirable properties of input are retained as it.

The global sensitivity analysis can classified into regression based, Morris design (screening based), variance based and meta-modelling [76]. A brief explanation of each method is given in below.

Regression based is one of the fastest methods that has low computational costs and is easy to interpret. However, the effects of some parameters may be left unexplained when using this method. Many improved versions of the original method are used now. The common methods used are Standardized Correlation Coefficient (SRC), Partial Correlation Coefficient (PRC), Standardized Rank Regression Coefficient (SRRC) and Partial Rank Regression Coefficient (PRRC) [76]. The SRRC and PRRC methods, also called rank transformation methods, are used when there is a nonlinear relationship between input and output. The SRC and PRC methods are used in case of linear relationships between inputs and outputs, with the difference that SRC do not consider interrelation effects between inputs. The statistics used for selection of important parameters are t-statics, F-statics and R determination coefficient (R^2) [76].

Morris design (screening based) is a global sensitivity analysis method that changes one input at a time whereas the other inputs are kept constant at initial value and the variation in output with respect to output is calculated. The process is repeated, and the inputs are ranked

according to their variation impact on output. Input factors are selected from levels rather than distributions [76]. The sensitivity index μ is used to present direct effects of input on output, another index δ indicates the correlation effects between various inputs, and another index μ^* indicates the total effect. This method requires lesser simulations and is recommended for projects with small number of significant parameters and large number of insignificant parameters. The disadvantage of this method is that it is qualitative and cannot quantify the impacts of input variations on output [76].

Variance based methods decompose the effects of input on output into easily interpretable fractions such as main effects of an input on output (first order) and the total effects due to both main effects and non-linear effects such as correlation between the inputs. The difference between main and total effects give fraction of correlation effects due to interrelation between two or more inputs. Two common methods used in variance-based methods are Fast Amplitude Sensitivity Test (FAST) and Sobol. The FAST method considers the nonlinear effects only, whereas the Sobol method fractions variations of output into nonlinear and correlation effects. The methods are recommended for complex nonlinear systems. However, they are computational expensive, e.g., a model with 6 input factors will require minimum 608 simulation runs [41].

Meta-modelling sensitivity analysis analysis require multiple simulation runs depending on the number of inputs. With inputs in hundreds can lead to simulation runs in thousands. With detailed building energy software like EnergyPlus, ESP-r, Equest this is computationally expensive and time consuming. A replica of the original model, with reduced computational requirements, called meta-model or emulator, is generated to emulate the parent model. This reduces both computation steps and time consumed for running simulations [41].

Meta model is reduced order approximate predictor for complex model generated through supervised learning, training and testing. The meta model may work as classifier (discrete values) or as a regressor (continuous values). Variance based sensitivity analysis methods can then be applied to meta-modelling. The meta models reported in literature are Multiple Adaptive Regression Splines (MARS), Adaptive Component Selection and Smoothing Operator

(ACOSSO), Support Vector Machine (SVM), Gaussian Process (GP) and Treed Gaussian Process (TGP).

Choice of sensitivity analysis methods depend on the intended purpose of research, computation time and cost and number of input variables [76]**.** The sensitivity analysis take much lower time as compared to energy simulation time required for multiple runs with different input sets [76]. Linear regression-based methods are first choice based on their simplicity and computational cost. However, they can leave variation in output unexplained. A meta-model can be better solution in this case. In case of large number of inputs, Morris method is preferred based on smaller number of simulations required, especially for qualitative analysis. Variance-based method is more reliable. However, it has high computational cost [76].

2.3.3.7 Meta modelling (linear regression)

Model calibration is essentially an optimization problem. Building simulation calibration has a number of parameters to tune by using observations. However, it is a problem with multiple non-unique solutions [40]. The first step therefore is to put constraints on the number of solutions by reducing the number of parameters, as explained in the previous section. The next step is to calibrate it with significant parameters using automated optimization criteria.

Let us assume that $G(\cdot)$ represents a model with x as observable inputs and θ as numerical parameters and unobservable inputs. The model output y can be given as:

$$y = G(x, \theta) \tag{2.44}$$

Suppose the number of experimental observations d_i are obtained representing the actual output:

$$d = d_1, d_2 \dots \dots \dots, d_n \tag{2.45}$$

Discrepancy ε_i between model output y and observations d can be represented as:

$$d = G(x, \theta) + \varepsilon_i \tag{2.46}$$

One way to calibrate this model is to perform non-linear regression between model output and observation and then optimize parameters in a way that minimizes the squared difference between model output and observation. The Root Mean Square Error (RMS) is given as:

$$RMS = \sqrt{\frac{1}{n}\sum_{i=1}^{n}(d_i - G(\theta, x_i))^2} \tag{2.47}$$

Using this calibration method has some drawbacks as calibration requires multiple simulation runs, sometime running into thousands. Using detailed energy models for this purpose is time consuming and computationally expensive [40]. The meta models, also known “model of the model”, of reduced order can be used as a short cut to long, detailed simulations. It is simple and computationally fast generated based on input/output data relationship, also called supervised learning. The simplest way of modelling based on supervised learning is linear regression with equation:

$$h(x) = \sum_{i=0}^{m} \theta_i x_i = \theta^T x \tag{2.48}$$

where m is the number of input variables, x the observations and θ parameters. Linear regression calibration minimizes the difference between modelled $h(x_i)$ and output observation y_i using least square as cost function:

$$J(\theta) = \sum_{i=1}^{n}(h(x_i - y_i)^2 \tag{2.49}$$

The cost function $J(\theta)$ is minimized by:

$$\theta = (X^T X)^{-1} X^T y \tag{2.50}$$

where X represent training input data and y represents training output data in matrix form. Fitness criteria used for this purpose is RMSE and/or coefficient of determination R^2 given as:

$$R^2 = 1 - \frac{\sum_{i=1}^{n}(y - y_i)}{\sum_{i=1}^{n}(y - y_{mean})} \tag{2.51}$$

Distribution of residuals is analyzed for any pattern which is an indication of imperfect modelling. T-test and F-test are used to verify that residuals are identically identified and independently distributed (i. i. d.). Further details can be introduced to linear regression to improve the model and its calibration [41]:

- Expressing linear relationship in probabilistic form.
- Introducing relation/interaction terms i.e., $x = x_1 x_2$ or in polynomial form i.e., $x_2 = {x_1}^2$.
- Using nonlinear functions that are linear in their parameters.
- Using kernel functions.

Some advanced meta models are MARS (Multiple Adaptive Regression Splines), ACOSSO (Adaptive Component Selection and Smoothing Operator), Support vector machine (SVM), Gaussian Process(GP) and Treed Gaussian Process (TGP) [41]. These models can be used within Bayesian frame work. The Bayesian calibration is explained in next section.

2.3.3.8 Bayesian calibration

It is a well-established fact that energy conservation measures (ECM) for buildings are either under estimated or overestimated due to discrepancies in modelling, uncertainties in inputs and variation in parameter values. ECMs are potential investment risks and that is the reason why ESCOs usually down grade the potentials savings. One way to overcome this issue is to express the energy conservation measures savings with uncertainties or confidence interval by taking into account all the uncertainties of the inputs and model outputs. Bayesian

statistical inference provides a systematic way to consider uncertainties in inputs and their propagation in model output [70].

Bayesian inference collects and generates the uncertainty in parameters in the form of probability distribution. This distribution is then mapped into the output by generating probability distribution for model output. These model output and prior parameter distributions are updated by using Bayes rules to generate posterior distributions [70]. Bayesian calibration incorporates three sources of uncertainty that are parameter uncertainty θ in model output $\eta(x, \theta)$ [77]:

$$y(x) = \eta(x, \theta) + \delta(x) + \varepsilon(x) \tag{2.52}$$

where x is input, $\delta(x)$ is the discrepancy between model output and observations where $y(x)$ are the observations, and $\varepsilon(x)$ is the observation error.

An emulator, such as Gaussian process, is used to model the simulation output ($\eta(x, \theta) + \delta(x)$), as a reduced order model. Probability distribution function for parameters is generated by using Markov Chain Monte Carlo algorithm. As models are always based on approximations, they will never be able to match the observations. Bayesian calibration avoids the problem of over estimation by keeping the discrepancy term $\delta(x)$ [66].

Under Bayesian framework, different modelling techniques have been used for calibration purposes. **Normative modelling** [66] and **Artificial Neural Networks (ANN)** [40] were used to calibrate a building model for retrofit analysis to quantify risks associated with retrofits. Data from a building at University of Sao Paulo were used for simulation of building energy consumption using ANN and EnergyPlus [40]. It was found that ANN generated building energy model with 10 % error compared to 13 % error by EnergyPlus. The ANN requires less manual inputs but requires extensive data for training. The ANN models, however, do not provide any physical understanding of the process. The author suggested that the use of this method should be further investigated for air conditioned buildings [40].

Three models, i.e. piecewise linear regression, Gaussian process (GP) meta modelling and detailed simulation are used to simulate energy consumption for office building using Bayesian calibrantion [41]. All these models were found in agreement with observation data, with the reduced order GP providing additional benefits of ease of use and computational cost reduction in all three steps: optimization, uncertainty and sensitivity analysis. GP method has the potential to provide promising results in terms of continuous commissioning, model predictive control, monitoring of energy consumption and detection of faults, and power peaks, especially in the field of smart grid and district energy systems [41].

Four linear emulators using Bayesian calibration were tested on building energy data from Georgia Tech University [7]. The corresponding four linear emulators were GP emulator, Linear-main (LM) emulator, that includes only main effects, Linear-interaction emulator (LI), that includes main effects and the interaction effects, and Linear-quadratic (LA) emulator, that takes into consideration main effects, interaction effects and quadratic effects. The emulators were used for calibration of physical model and for generating calibrated meta-model. The emulators LI or LQ showed a promising result in parameter estimation when used for physical model calibration and provide accurate predictions when used as meta-model. Use of emulators saved time and computational cost without compromising accuracy.

An important point mentioned by is that emulators can fit the building data and generate an acceptable model [7]. However, different emulators generate agreeably similar results, even with different parameter sets. In case of ECM predictions with changes in parameter values, an emulator may not be flexible enough to consider the sole effects of parameter change. This can result in wrong predictions. The author therefore prefers the calibration of physical model by modeler as compared to relying on emulators.

2.4 Data pre-processing

Parameter identification (both black and grey box) are based on data. The estimated results depend largely on the quality of measurements, sampling and analysis of data. A well-known

term used in modelling literature with reference to input data is “GIGO” that is garbage in garbage out. In order to ensure the acquisition and utilization of quality data, International Energy Agency (IEA), EBC (energy in buildings and communities) Annex-58 has recommended necessary pre-processing steps [53].

Pre-processing. It is important to analyze data for any abnormalities and errors before using it for modelling. This process is known as data pre-processing. Understanding the data requires knowledge of measurement system and principles of phenomena to be measured. It is important to plot data on different time scales such as time of day, week, month and yearl. These plots help find any abnormal tendencies, missing sensor data, outliers, irregularities. Averages or quantiles that may be calculated to single out unusual phenomena, Box plots and time series plots can also be useful in this regard [50]. Pre-processing can lead to rejection of measurements, correction of experimental setup or repetition of experiments [78]. Time synchronization of data acquired from different measurement systems should be dealt with care.

Sampling. An important question regarding data acquisition is the sampling rate of data, i.e. the time interval between acquisitions of two data samples. Measurement is a continuous process but is registered at discrete time interval. This is known as sampling the signal or simply sampling [79]. Discrete sampling for a continuous measurement can be represented as shown in Figure 2.6

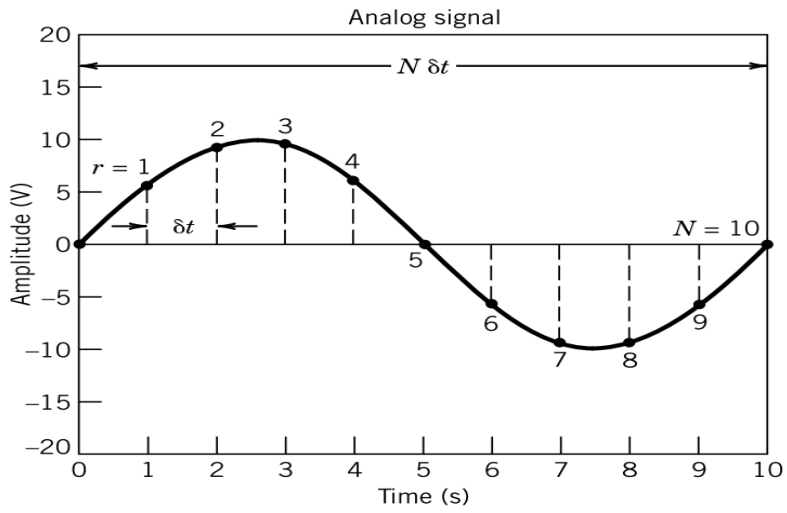

Discrete time signal $\{y(r\delta t)\}$	
r	Discrete data
0	0
1	5.9
2	9.5
3	9.5
4	5.9
5	0
6	–5.9
7	–9.5
8	–9.5
9	–5.9
10	0

Figure 2.6: Sampling of continuous signal [80]

Sampling rate depends on the time constant or dynamic response of instrument, i.e. time required by instrument for stable readings, dynamics of the measured process (frequency of analog signal) and sampling requirement of modelling or interest. The frequency with which a sample is measured at time interval δt is given by:

$$f_s = {}^{1}/_{\delta t} \tag{2.53}$$

Sampling theory states that the signal should be sampled at a rate more than twice the highest frequency (f_m) in input signal i.e.

$$f_s > 2f_m \text{ or } \delta t < {}^{1}/_{2f_m}. \tag{2.54}$$

Aliasing. When a signal is measured or sampled at a rate $f_s < 2f_m$, this can cause removal of high frequency signal/data and the resulting sample will show false lower frequency, a misinterpretation of the original signal. This is called aliasing and the sampled frequency as alias frequency [80]. Nyquist frequency f_N is a term used with alias frequency f_a is given by:

$$f_N = {}^{f_s}/_{2} = {}^{1}/_{2\delta t} \tag{2.55}$$

It shows that all the frequencies in the input signal above the Nyquist frequency will appear as signals of lower frequency equal to alias frequency f_a less than f_N. A folding diagram can be used to predict the alias frequency. In order to overcome the problem of aliasing, the sampling rate should be based on the maximum frequency of interest and the signal should be passed through a low pass filter (anti-aliasing filter) to remove signal content at or above the f_N [80]. One way to overcome the issue of aliasing is to select a sampling frequency such that the majority of the frequency content is lower than the Nyquist frequency, f_N. There is a trade-off between accurately depicting a signal using as high frequency as possible but at the same time reducing the measurement noise.

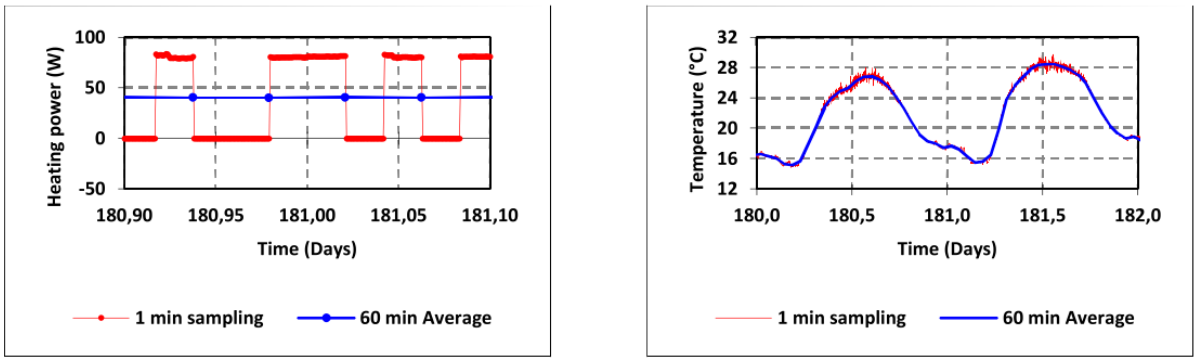

Figure 2.7: (a) 60 minutes average data removes important information; (b) 60 minutes average removes noise.[78]

Filtering. Filters are used to remove undesirable frequencies/information form an input signal. A filter allows the desired range of frequencies to pass through, known as the pass band and blocks the undesirable frequencies known as the stopband. Depending on the requirement, a filter can be low-pass, high-pass and band-pass. In case of high frequency in input data, the measurement system cannot respond with the frequency of input data and becomes a filter by itself. This is the case of undesirable filtering. In certain cases, the input signal comes with noises and disturbances and the filter has to be used to obtain the desired data only. A moving average or smoothing filter is used for removing noise or trends. A self-correcting filter can

remove the current faulty data point based on the average or weighted average of the previous data points:

$$\dot{y}_i = (y_{i-n} + \cdots .. + y_{i-1} + y_i + y_{i+1} + \cdots + y_{n+1})/2(n+1) \quad (2.56)$$

where $\dot{y}_i$ is the average value used. The average smoothing can be both forward-moving and backward-moving.

In advanced form, various Kalman filtering techniques are used directly for state estimation by filtering noisy measurements. Kalman filtering can be used for decisions regarding the type, location and orientation of sensors, pre-filtering methods for smoothing sensor noise and data sampling rates for sensors. Kalman filter achieves a better estimate of variables by estimating a joint probability distribution, using series of measurements that may be corrupted by statistical noise and other inaccuracies [81]. Extended Kalman filter, colored noise Kalman filtering and adaptive filtering are the advanced forms of the original Kalman filtering [45].

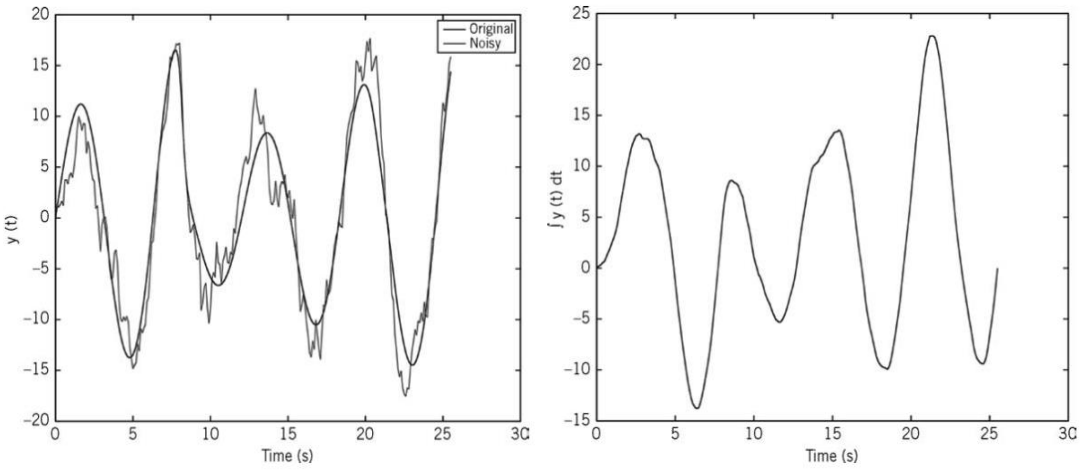

Figure 2.8: The effect of filtering on noisy signa l[80]

Averaging and filtering. Averaging is sometimes required to obtain a consistent sample whereas filtering is used to remove any unwanted information from the input signal. Both can be used in case they do not hide any useful information from the signal. These techniques may

be used to remove information that is not relevant to the phenomenon being studied. However, care must be used not to wipe relevant information while using these methods. Special care should be practiced in case of averaging signals with extreme low and high values [53]. In case of two measurement systems with different data sampling rates, the data for one instrument must be averaged out. This can create the issue of aliasing or weaning out of the relevant information from one of the signals [78]. In case of down sampling (longer sampling), the same method should be used for all inputs.

A relevant example of the advantages and disadvantages of averaging can be seen in Figure 2.7. The energy consumed by the heater can be measured by measuring the time for on and off of the heater. Sampling the on and off data over 60 minutes can mislead into wrong measurement of the energy consumed as shown in Figure 2.7(a) by the blue line. A one minute sample is better approximation of the process [78] as it can be seen from the red line. For outdoor air temperature (Figure 2.7(b)), the sampling data of one minute does not provide a clear picture of the outside temperature and simulation over this sample can lead to measurement noise. As can be seen in Figure 2.7(b), averaging over a period of one hour reduces measurement error.

2.5 Conclusions

This chapter details the theory for parameter identification, simulation models used and the statistical analysis techniques. Since the subject of current thesis is the analysis of models used for parameter identification, this chapter forms the theoretical foundation for the analysis of results. The models are broadly classified as classical (forward approach) and data driven (inverse approach). These types are further discussed in detail. The chapter discussed the calibration principles and techniques used to reduce the gap between predicted and measured energy consumption. The sensitivity analysis and a discussion on the advantages and disadvantages of each method were presented.

A detailed study on the parameter identification includes the different type of model structures, sampling time, model order selection, application of identification methods. The data analysis techniques and effect of data sampling, filtering and aliasing are discussed. The material in the chapter can be used as a guideline for building modelling, parameter identification and data analysis.

In the next chapter, the techniques discussed are applied with reference to experiments used for thermal characterization of buildings and building components. The next chapter explains in detail the standard thermal characterization test methods, experiments and data analysis techniques as applied to these test methods. These test methods provide construction data, weather data and measurement data that can be used to verify any model. The data from one of the test sites (twin house) is used for modelling in thesis.

This page is intentionally blank

3 Long-term identification test methods

Two common approaches to reduce building energy consumption are: to improve energy efficiency of the equipment inside the building, such as lighting and HVAC etc., and to improve the performance of the building envelope, such as adding insulations, reducing infiltration etc. It is relatively easy to measure the equipment efficiency in comparison to the performance measurement of building envelope [82].

Some of the common indicators of envelope performance measurement are: overall heat transfer coefficient (H), thermal inertia, thermal resistance, solar factor, time constant etc. The overall heat transfer coefficient (H) is considered as the most popular indicator of energy efficiency of building envelope. It represents the heat flow rate due to temperature difference between building and environment and is expressed as W/K. The overall heat transfer coefficient includes losses due to transmission (transmission losses through building physical surfaces) and infiltration losses (due to ventilation and infiltration) [82].
The overall heat transfer coefficient of building with a steady state heat rate of $\dot{Q}$ that maintains a steady state temperature difference ΔT between inside of the building and surroundings is:

$$H = \frac{\dot{Q}}{A\Delta T} \tag{3.1}$$

A number of methods are used to measure the over-all heat transfer coefficient:

- Calculations based on quoted thermo-physical properties of building and steady state or dynamic model of building.
- Measurements using long testing methods, such as co-heating tests, PSTAR. Usually, statistical techniques are employed to dissociate the measured value from the effects of occupant's behavior, weather conditions and efficiency of building;
- Long-term test identification methods like energy signature, PRISM methods, RC-identification; that are based on energy consumption as a function of outdoor

temperature and are occupant-based methods. The heat transfer co-efficient is determined by regression analysis. The long term identification methods are better suited for estimation of savings from deep retrofits over long period of time as these methods cannot identify the short term dynamic effects;

- Methods that are short enough to limit the effects of occupancy and weather conditions (tests carried with no occupants inside)

For long term identification methods, it is difficult to dissociate the impact of occupant's behavior, energy efficiency of systems, hot water consumption, infiltration rate, impact of solar radiations etc., from envelope performance.

The short-term parameter identification methods are dynamic methods based on lumped parameters and can be used to identify suitable models that can describe thermal characteristics of building structure and its systems (HVAC equipment etc.). These methods are useful for grid optimization that can respond to changing energy needs of buildings (based on dynamic model of buildings) [83].

The calculated or designed H value of building is validated using different tests. Long term methods, such as co-heating tests, are zero occupancy steady state method and measure the H value as a function of the daily energy consumption and average outdoor temperature. Linear regression is used to identify U-value.

The long term test methods are aimed at thermal performance verification of building envelope using measurements and estimation techniques (as discussed in chapter 2) [46]. A simple explanation of how these methods work can be given by the equation presenting estimation of overall heat loss coefficient [46]:

$$H = \sum U_i . A_i + H_{TB} + \rho . c_p . Q_v$$

$$Q_v = \sqrt{{Q_s}^2 + {Q_w}^2} = \frac{A_l}{1000} . \sqrt{C_s . \Delta T + C_w . {U_w}^2} \qquad (3.2)$$

where

H_{TB} is the heat loss from thermal bridges,

$U_i A_i$ - envelope losses,

$\rho c_p Q_v$ - infiltration losses.

The overall heat loss coefficient is based on the experimental measurement of the terms in equation (3.2). As the tests, such as co-heating tests, are conducted throughout the day, multiple linear regressions are performed to identify H and solar aperture. The identification relationship for co-heating test is:

$$Q_{heating} + g\, A_{solar} = H\, \Delta T \qquad (3.3)$$

where

$Q_{heating}$ is steady state heat flow rate (W)

g are the measured solar radiation (W/m^2)

A_{solar} is the identified solar aperture (m^2),

H is the identified overall heat transfer coefficient

ΔT is the temperature difference between building (internal) and external environment

The estimated H value is considered as accurate enough to be used as a reference value. Two co-heating tests conducted for the same building by two different teams have generated the same results [83].

The in-situ parameter Identification methods starts with the collection of data based on experiments. The experiments conducted are either:

- long term
- short term
- intrusive (non-controlled experiments)
- non-Intrusive (controlled experiments)

- experiments based on building components such as walls, roofs etc.
- experiments based on entire buildings.

Depending on the available data and purpose of measurement, the parameter identification can be based on:

- steady state analysis
- dynamic analysis

This chapter discuss long term test methods discussed in literature.

3.1 Long-term methods for building components (walls)

The **heat flow meter** test method (**ISO 9869**) is used to measure the thermal properties, such as thermal resistance and conductance, of building components, such as opaque walls [84]. The measurements involve heat flux measurement across wall surface using heat flow meter and the temperature measurement of the two surfaces using thermocouples [46]. Thermal resistance is evaluated by dividing the mean temperature difference by the heat flux:

$$\mathrm{R}_{N,S\ to\ S} = \frac{\sum_{K=1}^{N}(T_{i,s,K} - T_{e,S,K})}{\sum_{K=1}^{N} q_{i,,S,K}} \tag{3.4}$$

where

R is the thermal resistance (m^2K/W);

N Is the number of measurements starting from $K = 1$;

$T_{i,s}$ is the internal surface temperature (K);

$T_{e,s}$ is the internal surface temperature (K);

$Q_{i,s}$ is the heat rate per meter square (W/m^2).

Both static and dynamic analysis are used to measure the thermal characteristics using data obtained from the tests. The potential sources of error in this method are measurement

errors, boundary condition errors and data analysis errors. It is difficult to meet the data analysis conditions in steady state analysis. The steady state analysis does not provide any insight into dynamic properties and requires long time to arrive at accurate results. ISO 2014 outlines the standard procedure [46]:

- test duration should be at least 72 hours;
- measured value should be within 5 % of the value estimated at the end of the test period;
- the value estimated during first period (up to 2/3rd of the time from the beginning) should be within 5 % of the value estimated during last period of the test (up to 2/3rd from the end)
- internal energy in wall/component should not increase by more than 5 % of the initial value.

It is usually difficult to achieve these steps during the tests, especially for unknown components. However, they are recommended as a first estimation. For light components, this method can achieve reasonable accuracy. In a simple case, for a wall with insulation of 20 cm, U-value was averaged over eight days to arrive at value, consistent with reference value [46].

The dynamic analysis requires less testing time and is used for estimation of both static and dynamic properties with reasonable accuracy [46]. A lumped RC model is used for dynamic analysis of the wall. The standard form of energy balance equation for any node inside the wall can be written as:

$$\mathrm{C}_2.\frac{dT_2}{dt} = \ (T_1 - T_2)H_{1-2} + \ (T_3 - T_2)H_{2-3} + q_2 \tag{3.5}$$

Where T_1, T_2 are temperatures of nodes, H_{1-2} and H_{2-3} represent thermal conductance of wall partitions and q_2 represents an external heat flux such as solar radiations or external heating or cooling. With the dynamic model, both static (conductance) and dynamic properties (capacitance) can be estimated provided that data such as outdoor temperature, indoor temperature and solar radiation are given. The identified parameters such as thermal

resistance or capacitance are compared with measured values. The identified parameters can be further optimized using an objective function with the aid of specialized software such as LORD or CSTM [46]. The estimation and validation process for the identified parameters is shown in Figure 3.1.

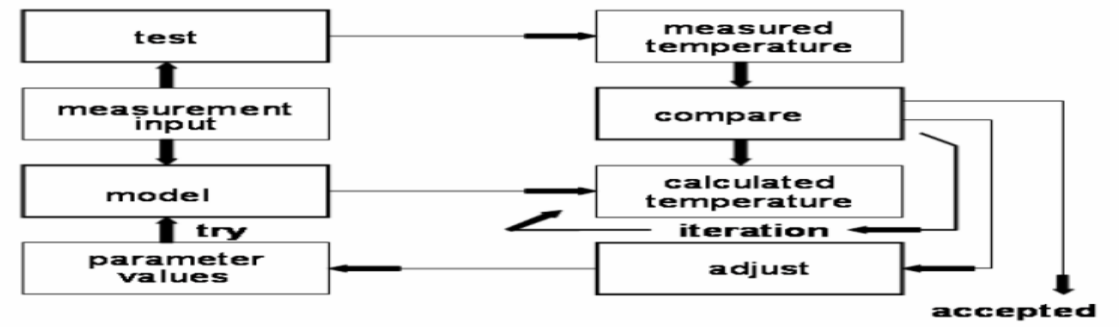

Figure 3.1: Parameter Identification and validation process for parameters of a wall [46]

The flow meter method was applied to a triple glazing and an insulated concrete wall to validate the claims of manufacture about the U values. Both the wall and the glazing were oriented towards North [46]. The data obtained every five minutes was averaged over 5 hours. Interesting results for glazing and wall can be observed as shown in Figure 3.2.

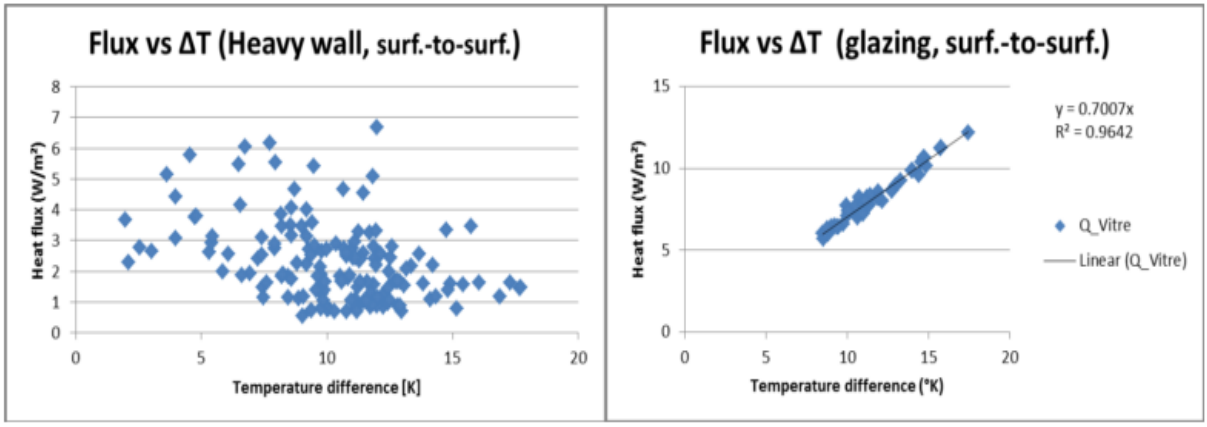

Figure 3.2: Heat flux relationship for insulated concrete wall and glazing in flow meter testing [46]

Figure 3.2 shows a strong relationship between the heat flow through glazing and temperature difference. The U-value can be easily determined from the relationship. However, in the case of insulated heavy wall, the data is scattered and U-value cannot be

determined from the measurement. An increased averaging time of up to 72 hours or dynamic relationship can be used to determine U-value in this case [46].

A light wall with strong insulations (high resistance) on two sides was tested using heat flow meter method. Both static and dynamic methods were used for estimation of thermal properties. For steady state estimation, the observation length was increased to one day per sampling. The period necessary to obtain an accurate U-value was between 5 to 6 days. In total, observations for 8 days were used.

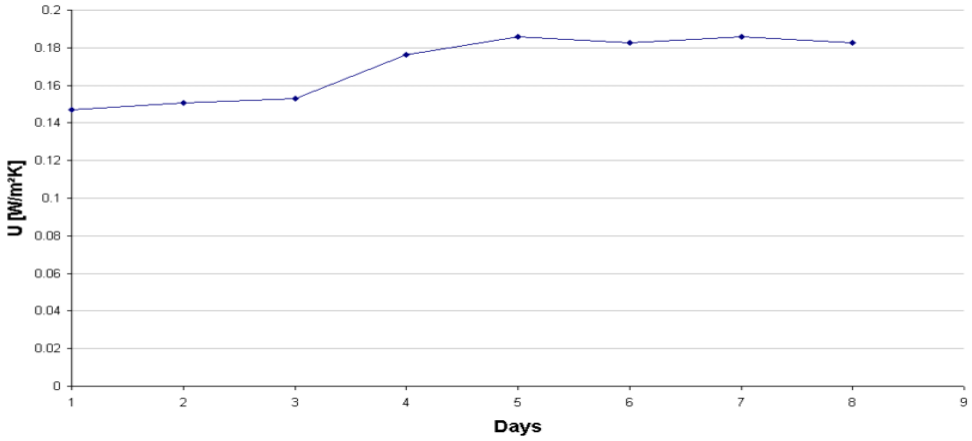

Figure 3.3:Varaition and stability of U value over time [46]

A dynamic model was generated by using 3R2C model with an approximate 72 hours of test data. The observed surface to surface U value was measured as 0.179 W/m^2K with a standard deviation of 0.4. Both the steady state and dynamic conductance values (U) were close to each other [46].

An interesting comparison of steady state and dynamic analysis methods is provided by [63] for a cavity wall located in Belgian climate. The thermal resistance calculated from thermos physical properties of walls is 4.002 m^2KW^{-1}. The weather conditions, temperature variation of wall and heat flow through wall is modelled for a period of one year and simulation step of one minute. The methods tested with data were steady state methods; the simple ISO 9869 (average method), ISO 9869 method with rectification/correction for storage (also known as semi stationary method) and dynamic methods; using Anderlind's regression (regression with correction for dynamic effects), ARX and the stochastic state space GREY BOX methods. The ARX model of order 18 and grey box model of order 3 were found suitable [63].

The dynamic methods generated an improved performance compared to the stationary methods. Different dynamic methods performed more or less equally well. The anderlind's regression (improved black box) method converged quickly to accurate estimates as compared to ARX and grey box methods. The state space grey-box modelling was more labor intensive as compared to ARX and Anderlind's regression method. In winters, both semi stationary and dynamic methods performed equally well. In summers, only dynamic methods generated reliable results. Dynamic models are more versatile. However, they are complex to use in contrast to semi-stationary methods, which provide reliable results in winters only [63].

The flow meter (ISO 9869) testing for thermal characterization can take from 3 days to a week, depending on the thermal mass of the wall and the weather conditions [84]. The value estimated using this method is used as a reference value and is considered as accurate. However, the long-time duration of this method makes it impractical to be employed at a large scale. A new transient short term method called Excitation Pulse method was proposed, based on the theory of the response factors (RFs) [85].

This method involves the application of triangular excitation pulse to a wall for a short duration and the measurement of heat flow and temperature on both sides of wall. The measurement time took one and half hour for readings to converge. The schematic of the experiment is shown in Figure 3.4.

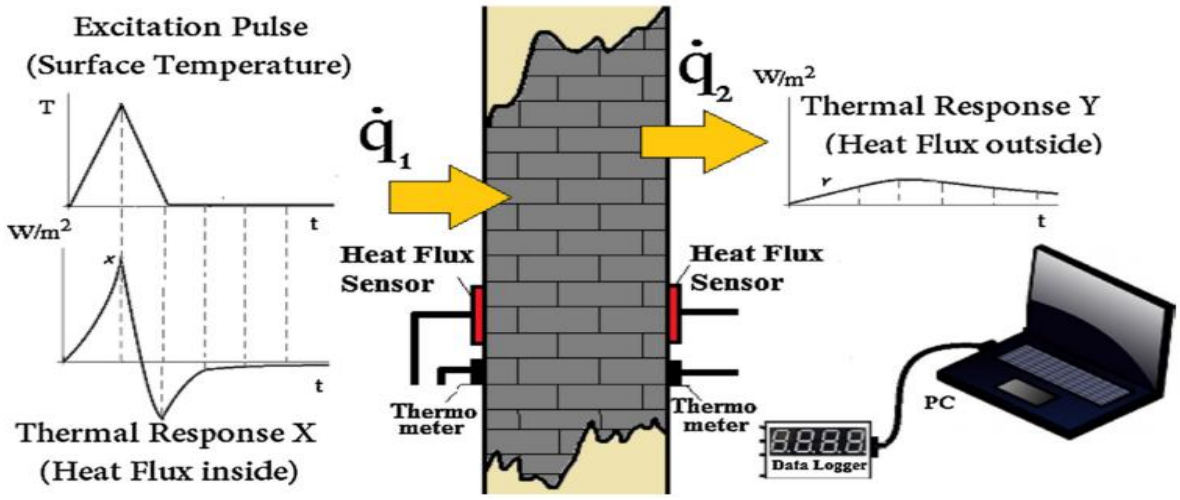

Figure 3.4:The experimental setup for Excitation Pulse Method[85]

The response factors X and Y are calculated as

$$\mathrm{X}_i = \frac{q_1}{\delta}, \mathrm{Y}_i = \frac{q_2}{\delta} \tag{3.6}$$

where q_1 and q_2 are the heat fluxes measured at inner and outer surfaces of the wall, respectively and δ is the magnitude of triangular pulse. The resistance value of the wall can be measured as:

$$R_c = 2 \times \left(\sum_{i=0}^{n} (X_i + Y_i) \right)^{-1} \tag{3.7}$$

The Excitation Pulse Method (EPM) method was applied for different case studies (walls) [85]. It was found that the measured R_c values were close to the values obtained by ISO-9869 during the same experiment. A difference of less than 2 % was found between ISO-9869 and EPM. It was recommended to test EPM method for different constructions and to standardize the testing method using automatic controls [85].

Calorimetric methods are used to determine both thermal and solar characteristics of building components [46]. Calorimetric method is based on the principle that heat flow through any component is based on its thermal properties and boundary conditions (internal temperature,

global radiations, wind speed direction etc.). Hence, if the time series of heat flow and boundary conditions are measured, the thermal properties can be estimated [46]. The test cell for calorimetric method is a rectangular box (PASLINK Test cell) with front surface used to test wall specimens (Figure 3.5).

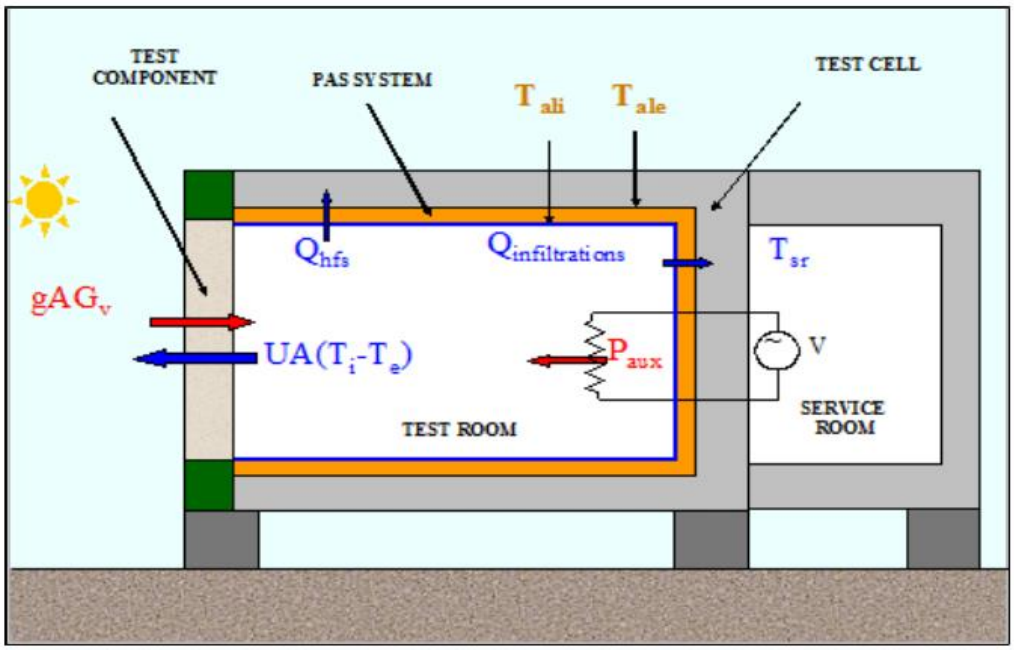

Figure 3.5: A view of calorimetric test cell and heat transfer surfaces [46]

A general form of heat transfer equation for the test cell can be given as:

$$\Phi_{net,c} = \quad P_{aux} - \Phi_{tc} - \Phi_{sr} \tag{3.8}$$

where $\Phi_{net,c}$ is the net heat flow through the test component, P_{aux} is the net heat supplied, Φ_{tc} is the heat transfer to the exterior across the boundaries/walls of the cell and the Φ_{sr} is the heat transfer with service room. The measured $\Phi_{net,c}$ from the experiment is used to estimate the thermal properties by using equation:

$$\Phi_{net,c} = \quad H(T_i - T_e) - A_{sol} I_{sol,v} \tag{3.9}$$

where

T_i is the internal box temperature (K);

T_e is the external temperature (K);

$I_{sol,v}$ is the solar radiations (W/m^2);

A_{sol} is the solar aperture (m^2);

One week of test data is usually required for determination of all thermal properties. For linear regression, the following equation is used where H and A_{sol} form the intercept and slope of regression line:

$$\frac{\Phi_{net,c}}{(T_i - T_e)} = H - A_{sol}\frac{I_{sol,v}}{(T_i - T_e)} \quad (3.10)$$

The above equation can be used for steady state analysis. The steady state methods require a long testing time, sometimes more than 10 days, and is unable to provide information on dynamic properties of the building. In order to overcome these issues, dynamic analysis are used using software tools such as LORD or Continuous time linear stochastic modelling (CSTM). CSTM considers uncertainties in both measurements and calculations during estimation. This software tool can be used for identification and performance assessment of the entire building, building components and heat exchangers, etc. However, there are two issues with this method: the correct assignment of variables as inputs and outputs and its dependence on user experience, as with same data, different users can generate different results [86]. One week of measurement is recommended for majority of the tests.

Jimenez and Madsen applied different models of varying complexity for estimating characteristics of building components such as UA and gA values [87]. A wall with double glazed window was used as a sample in PASLINK test cell and data was collected during tests for two orientations of wall, i.e. towards South and North. The test cell was excited using randomly ordered logarithmically distributed binary sequence (ROLBS).

Different mathematical models were used for data fitting and validation [47]:

Linear Model 0: with assumption of no infiltration air and no heat transfer via test cell boundaries.

Linear transfer function Model 1: with none of the assumptions of Model 0 and the assumption that heat transfer between the surroundings and test cell are linear.

Non linear Transfer Model 2: same as model 1 with addition of nonlinear term for radiation heat transfer between the test cell and finally.

Nonlinear continuous time state space model 3: with the same assumptions as Model 2 but expressed in form of dynamic state and consideration of difference between room temperature and sensor.

A linear ARX model was used to estimate parameters for Models 0 to 2 using MATLAB toolbox for System Identification. Parameters for Model 3 were estimated using CSTM (Continuous Time Stochastic Modelling) software. UA and gA values were estimated for an opaque wall with a double-glazed window. The model was validated using a separate data set. The performance was measured by comparing the estimated values of UA and gA against the reference values in literature (for each model) and by analyzing residual characteristics such as mean, standard deviation and autocorrelation function and cumulated periodogram. The test results confirmed that **Nonlinear Continuous Time State Space Model 3** is the best model among the four models for opaque wall with double glazing.

Naveros conducted further studies on calorimetric method on real sized building components to analyze the limitations of average linear regression, such as minimum data integration time required and minimum number of terms required in energy balance equation for steady state methods. It was observed that the results were improved significantly if the average period of data integration is increased from one to five days and the wind speed is included as variable (Naveros, 2012). Jimenez performed statistical analysis for calorimetric test using RC network, transfer functions and state space modelling. It was concluded that better results can be obtained by using state space model with inclusion of non-linear long wave radiations [47].

The overall heat transfer coefficient and heat capacity for a building with integrated solar panels was estimated using one and two state grey box model [88]. Evaluation of one state

and two state showed that two-state model was able to model the system dynamics very well and further improvement to the model can be made by adding terms for solar radiation and PV module temperature to the noise term. The statistical evaluation of the two-state model shows that this model describes the dynamics of the system very well. A possible model improvement could be the introduction of a dependency of the solar radiation and the PV module temperature in the noise term.

3.2 Co-heating method

Co-heating method is used for measuring heat transfer coefficient $H(\frac{W}{K})$ and solar aperture $A_{sol}(m^2)$ for an entire building. It is a quasi-static method in which a building is heated to a uniform and constant temperature of 25 °C, with the varying external weather conditions [89]. Electric heaters and fans are used to achieve uniform temperature. Heat input, indoor and outdoor temperatures, solar radiations, wind speed and direction and relative humidity are observed during the experiment. The experiment timing and data averaging is selected in a way to reduce the effect of charging and discharging of building.

The data is collected over five-minute interval with the advantage that data can be utilized to analyze the dynamic effects. The data is aggregated over long time span such as 1 day, 2 days or one week. The data aggregation methods include averaging, resampling and decimating [89]. The controlled indoor temperature and appropriate sampling of data help to reduce the effects of dynamic effects [90].

The total heat loss coefficient is the combination of both fabric and ventilation losses. The ventilation loss coefficient can be segregated from envelope heat loss coefficient using common tests such as pressurization tests, tracer gas decay method and constant concentration test method. For co-heating test, at least 10 K temperature difference is recommended. This is the reason why it is preferred to conduct the co-heating tests during

winters when temperature difference between indoor and outdoor temperature is sufficient. A recommended duration of the test is from two to four weeks [46].

The energy consumption of building is analyzed against the indoor and outdoor conditions using regression analysis. The coefficients of regression give the building thermal characteristics such as total heat loss coefficient and solar aperture [89]. Steady state conditions are achieved by keeping the indoor temperature constant during analysis when the outdoor temperature can be considered as constant. The heat balance equation used for regression analysis of the data is:

$$\Phi_p + A_{sol} I_{sol} = H(T_i - T_a) \tag{3.11}$$

where

Φ_p is the power supplied for keeping the indoor temperature constant (W)

A_{sol} is the solar aperture (m^2);

$I_{sol,v}$ is the solar radiations (W/m^2);

H Overall heat transfer coefficient (W/K);

T_i is the internal box temperature (K);

T_a is the external temperature (K);

The solar aperture A_{sol} can be calculated from the building geometry, orientation, properties of walls and fenestration and solar measurements. Alternatively, it can be estimated by using linear regression analysis. Different methods of analysis to estimate H and A_{sol} are:

- Calculating A_{sol} from building features and average measured I_{sol} and use equation to estimate H value only. However, it is recommended not to calculate A_{sol} on the basis of orientation and shape as this term includes complicated terms not presented by geometrical dimensions only [90].
- Multiple regression analysis where H and A_{sol} are considered as independent variables and Φ_p (heating power) as dependent variable.
- Rearranging equation so that in regression analysis H appears as intercept and A_{sol} as the slope of linear regression line (Figure 3.6).

$$\frac{\Phi_p}{\Delta T} = H + A_{sol}.I_{sol}/\Delta T \tag{3.12}$$

The graph shows determination of heat loss coefficient based on calculation of A_{sol}, where the equation is forced through zero intercept and heat loss coefficient is determined as slope of the regression line (Figure 3.6). The plot on right of Figure 3.6 is based on A_{sol} and H as independent variables and determined as intercept and slope of the graph respectively.

The validity of results from co-heating experiments depend on three factors that are repeatability of results, systematic errors due to neglecting solar radiation and thermal lags [89]. The errors can be further reduced by observing separately thermal bridging and local infiltration losses.

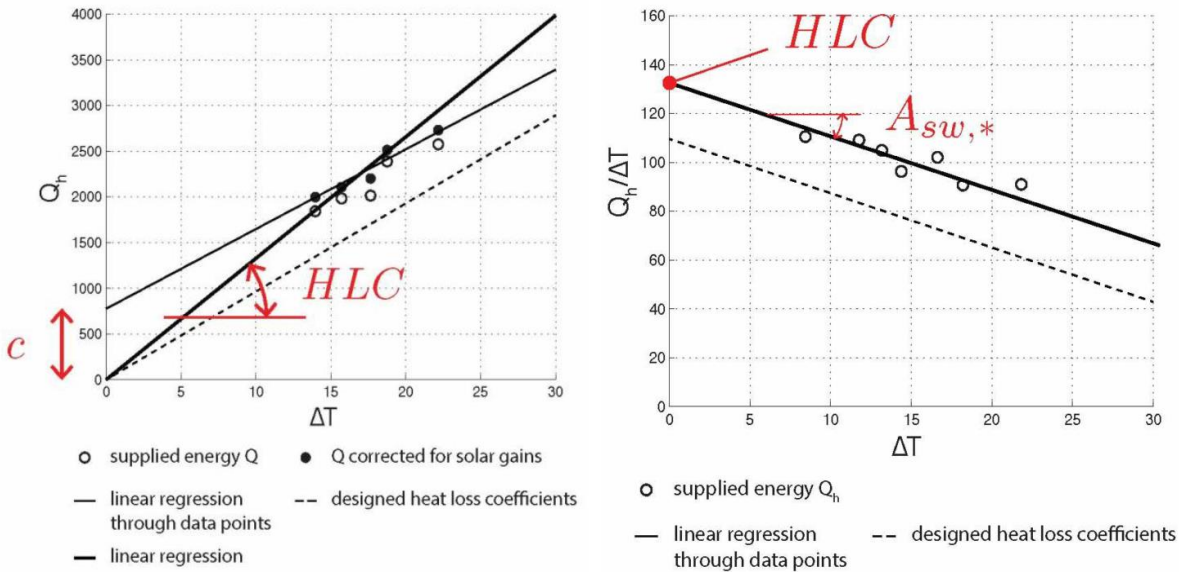

Figure 3.6: Estimation of H and Solar aperture, using simple linear regression [46]

A regression analysis on three axis is recommended for co-heating data analysis as it helps visualize the estimates under the influence of different boundary conditions (weather), as shown in Figure 3.7 [90].

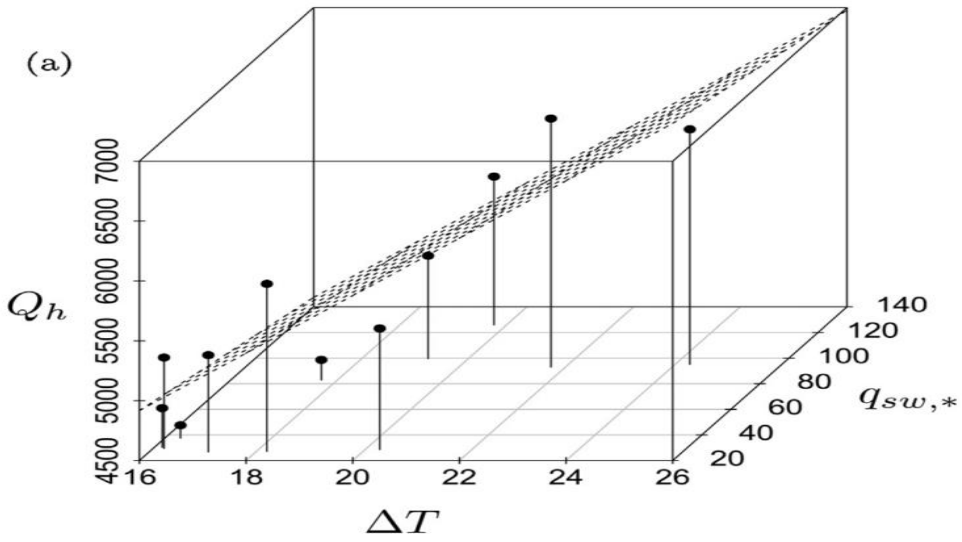

Figure 3.7: Three dimensional presentation of linear regression of co-heating data [89]

One of the issues with co-heating method is the measurement of solar radiation, i.e. whether vertical measured radiations should be considered or horizontal radiations [91]. Majority of the tests have reported horizontally measured radiation. The heat lost through adjoining buildings or spaces is another issue and usually requires heating the adjoining building or space to equal temperatures. These issues, together with the long periods of testing and with testing periods specifically limited to the cold seasons of the year have reduced the popularity of co-heating methods [91].

The normal period for coheating test ranges recommended testing duration can be reduced up to 3 days. Within 72 hours of testing period, the value of H can reach within $\pm$ 10 % of the reference value, as demonstrated for 12 out of 16 cases [91]. Monitoring beyond this period improves results to a smaller extent. The range of suitable testing period depends on dwelling type. The suitable testing period is 2/3 of the year for buildings built as per UK 2012 regulations, 40% of the year for buildings built to national standards, 20 % for Passivhaus and 12% for apartments [91].

3.3 Conclusions

The long term test methods, such as co-heating, calorimetric and flow metric tests (ISO 9869) are utilized for in-situ thermal characterization of buildings. The thermal values estimated using these tests are precise compared to raw model values (based on simulations or calculations only) and can be effectively used to reduce performance gap. However, certain shortcomings make these methods impractical to be employed in field tests at large scale. These methods require a long testing period, that can range from two to four weeks, with the shortest reported period being 3 days [85].

There are many reasons why the long-term methods cannot be applied on a large scale in field tests. The season of the year during which the tests can be conducted is limited to heating season only, when external temperatures are low and effects of solar radiations are minimal [92]. The range of suitable testing duration depends on type of dwellings. The methods also require a long testing period with no occupancy. It is usually difficult to obtain a facility for such a long period.

The long-term test methods, as discussed in this chapter, have a shortcoming: they are too long to be employed on commercial scale. To overcome this shortcoming, short term thermal characterization test methods were developed. The short-term test methods, with focus on QUB method is discussed in the next chapter.

This page is intentionally blank

4 Short-term test method: QUB method

Short term methods were developed to overcome the shortcomings of long term methods, i.e. the long testing time. PSTAR, ISABELE (In Situ Assessment of Building EnveLope pErformance) and QUB (Quick U-value of Buildings) are some of the short test methods.

PSTAR is a dynamic testing method that uses system identification techniques to estimate building parameters. The test is performed in three nights and four days: the first night is to achieve steady state conditions; the second night is to let the temperature decay and the third night is to calibrate the heating system. One or more solar days are included to account for solar aperture. Overall heat transfer coefficient is estimated in last two nights. The method requires strict experimental conditions and has repeatable accurate results. The errors result from the inability to achieve steady state conditions and the sensitivity to solar radiations. The methods also require building to be modelled as single zone.

ISABELE (In-Situ Assessment of the Building envelope performancEs) is a dynamic thermal characterization method based on the response of building temperature to controlled heating input. This method is based on French Thermal Regulation RT2012 and identifies thermal transmission and thermal inertia. The identification process involves fitting a thermal model to the observed temperature response. ISABELE method models uses five resistances and one capacitance and identifies the parameters from the response curve [93]. The experiment involves the observation of the building temperature when no power is injected, followed by power injection and finally no power is supplied. The required measurements are internal temperature, heating power injected, air infiltration rate and external climate conditions. The test takes 5 to 15 days to be completed, depending on thermal inertia of building [83]. The method is sensitive to air infiltration rate and solar radiation.

QUB is a short term testing method that measures the heat loss co-efficient in one to two nights. It has the shortest duration among the short term methods, with results of the test ranging in ± 15 to $\pm 20\%$ of the reference value. As the focus of the thesis is on QUB method,

its development, basic principles and experimental validation is discussed in details in the next sections.

4.1 Introduction to QUB method

QUB is quick method for testing, introduced by Saint-Gobain, to measure the heat loss coefficient (H) within a single night. The method has the potential to reduce the testing time from 8 hours to 1 hour in some cases [46], [91], [92], [94].This method involves application of two levels of excitations, i.e. different levels of power. Usually, a high power period is followed by low level or no power period, as shown in Figure 4.1. The duration for both excitations is the same. The experiment is performed at night without any occupants to avoid external gains [59]. The response of building is estimated by measuring indoor and outdoor temperatures and the power levels.

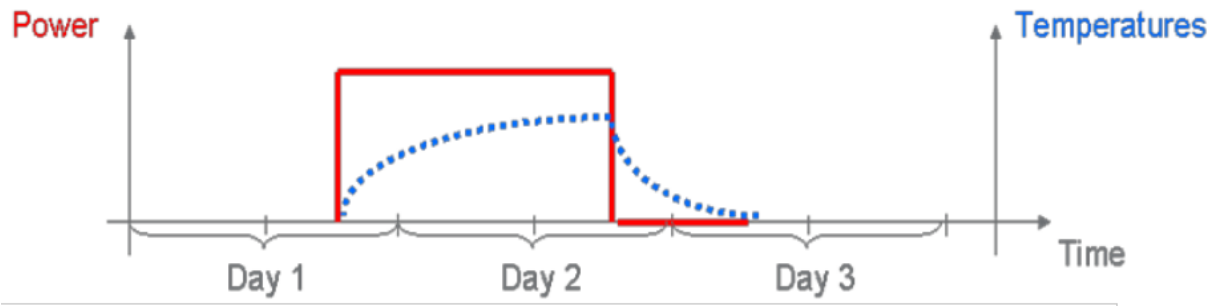

Figure 4.1: Schematic presentation of QUB method [46]

The building is represented by a RC network (Figure 4.2). The temperature inside the building is considered as homogeneous and represented by a single node. The evolution of the internal temperature with input power is modelled with respect to indoor and outdoor temperatures, over-all heat transfer coefficient and the capacitance of building. The power injected is:

$$\dot{Q}_h = H(T_{in} - T_{out}) + C\frac{dT_{in}}{dt} \tag{4.1}$$

where $\dot{Q}_h$ is the power supplied, H is the over all heat transfer coefficient, T_{in} and T_{out} are the indoor and outdoor temperatures respectively, and C is the capacitance. The temperature evolution is expressed as time constant with product of resistance and capacitance as exponents of decay.

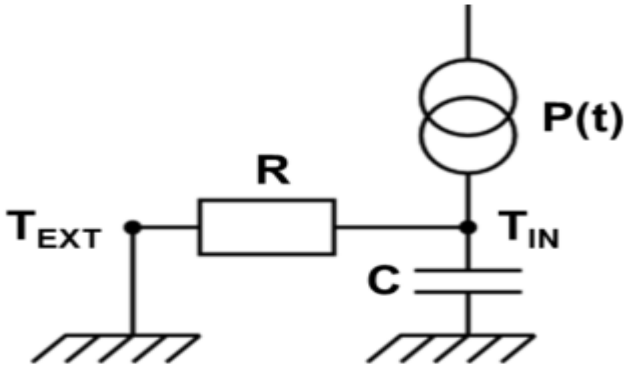

Figure 4.2: RC-Network Model used in QUB method [59]

The overall heat transfer coefficient is estimated by

	$$H_{QUB} = \frac{\alpha_2 P_1 - \alpha_1 P_2}{\alpha_2 \Delta T_1 - \alpha_1 \Delta T_2}$$	(4.2)

where

α_1	slope of the measured indoor temperature at the end of heating phase;
α_2	slope of measured indoor temperature at the end of cooling phase;
P_1	input power during heating phase;
P_2	Input power during cooling phase;
T_1	temperature difference between indoor and outdoor temperature at the end of heating phase. The outdoor temperature is estimated by taking the mean temperature during QUB night;

T_2	temperature difference between indoor and outdoor temperature at the end of cooling phase. The outdoor temperature is estimated by taking the mean temperature during QUB night;

Taylor series method for uncertainty is used for estimate uncertainty with estimation of H_{QUB}. It is recommended to carry out the test when the building is empty and there is no power in the second period of the test [92]. This one night testing method has the potential to be an effective tool for energy measurement. Since the method is relatively new, it requires further validation by repeating method on virtual buildings, test buildings and actual buildings.

The QUB test requires instruments for measuring zone air temperatures, external air temperature and power input. The power measurement requires special care during QUB test. To estimate the influence of weather parameters, such as wind speed, solar radiations etc., a weather station may also be used [94]. Heat flux meters may be used to measure the U-value for building components, such as walls, during the QUB test.

QUB method is sensitive to the homogeneity of the input temperature in the measurement zone and care must be taken to ensure that uniform temperature is maintained. Saint-Gobain recommends to use mat heaters for this purpose. The duration of heating and cooling should be the same. The data analysis period must be the same. For example, when heating duration starts at 7 PM and ends at 1 AM and two hour analysis period is selected between 11 AM and 1 AM, then the same data analysis period must be selected for the cooling period, that is from 4 AM to 6 AM [46]. To avoid effects of solar radiation, the test is conducted during the night in empty building with power measurements (electric heating).

A dimensionless parameter α is used as a check on the estimated value of overall heat transfer coefficient, known as α-criterion:

$$\alpha = 1 - \frac{H_{ref}\Delta T_0}{P_1} \tag{4.3}$$

where H_{ref} is the reference heat loss coefficient determined earlier using co-heating test method or the stated/assumed value available [92], ΔT_0 is the initial temperature difference between indoor and outdoor temperature at the start of the test and P_1 is the power supplied during the first phase of test. The value of α is an indirect measure of certainty on the estimated value of H_{QUB}. An H_{QUB} value for which α lies between 0.4 and 0.7 is considered within the limits of reference value. Any α greater than 0.7 indicates that H_{QUB} value is overestimated. A value smaller than 0.3 indicates an underestimation. In case of overestimation, the test period is increased.

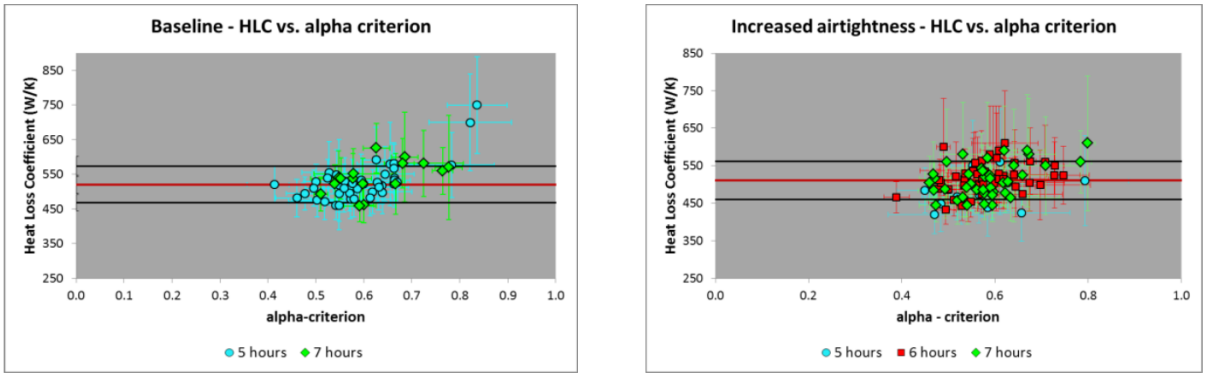

Figure 4.3: Variations of overall heat transfer coefficient values with alpha [92]

For equal heating and cooling times ($t_1 = t_2$), constant external temperature and no power dissipation during the second phase of the test, the H_{QUB} can be given as function of theoretical H by the equation:

$$H_{QUB} = \frac{H}{1 - \alpha^2 f(\alpha)} \tag{4.4}$$

where function $f(\alpha)$ depends on α, on resistance R_i and capacitance C_i of the model. This equation shows that H_{QUB} is equal to the theoretical H at lower values of α. However, at higher values of α, H_{QUB} overestimated as shown in Figure 4.3.

A simple R-C model with internal heat generation is used to model the entire building for QUB data analysis

	$C\ dT = (\Phi_P - H.\Delta T)\ dt$	(4.5)

where C, is the heat capacity of the building representing the amount of heat required to bring 1 K temperature difference, Φ_P is the heat supplied, H is the overall heat transfer coefficient and ΔT is the temperature difference between internal and external temperature. The assumptions of this model are uniform/homogeneous internal temperature and constant external temperature.

The QUB test results can be expected to show a maximum standard deviation of 20 % compared to the co-heating tests, numerical studies showed a deviation of 11 % (for specific study), experiment in a controlled climate chamber a deviation of 4% and a real building showed a deviation of 11%. The method is tested successfully for few buildings and the results obtained were verified with reference values. The experimental tests and simulation tests show a variation in QUB results for the same house under relatively identical conditions [92]. The variation of the method with varying levels of insulation in not verified. The impact of changing weather conditions on QUB tests needs to investigated. The QUB method do not take into consideration heat losses to building ground floor losses , this can be a source of error that warrants experiments with and without the consideration of losses through ground floor.

4.2 State of the art on QUB method

In order to understand the QUB method, it is useful to discuss a previous work concerning the estimation of overall heat transfer coefficient of complex house [95]. The overall heat transfer coefficient is determined via three methods i.e.

- Thermo physical properties only;
- Free cooling and heating experiments in a house (short term);
- using energy signature method.

This work provides a good opportunity to understand the theoretical framework of QUB method.

The overall heat transfer coefficient K_o value using thermos physical properties for building envelope is calculated as a sum of heat loss coefficients via building surfaces/envelope and heat loss via transmission/infiltration and ventilation losses using:

$$K_o = K_{01} + fC_a \tag{4.6}$$

where K_{01} is the building envelope loss, f is the mass flow rate of air and C_a is the total air capacity. The conductance of the building is calculated as:

$$K_{01} = \left(\sum_i A_i\right) U_{bat} = \sum_i U_i A_i + \sum_j \psi_j l_j + \sum_k \chi_k \tag{4.7}$$

where $\psi_j(\frac{W}{m*K})$ is the linear coefficient for thermal bridge junction j, l_j is the length of the thermal bridge and χ_k is the punctual coefficient of 3D thermal bridge $(\mathrm{W/K})$. The calculated H value was 497 $(\mathrm{W/K})$ [95].

For a heating or free cooling experiment, assuming no occupancy, homogeneous internal temperature and no internal power generation, the behavior of building with the active heating source such can be described by equation:

$$CdT = (P - K_o T)dt \tag{4.8}$$

Where C is the apparent heat capacity, P is the heating power and T is the temperature difference between outside and inside building.

Taking the Laplace transform of equation (4.8) (free cooling) we get :

$$\Delta T^c = \Delta T_o^c(\exp(-t/\tau)) \tag{4.9}$$

Linearization of this equation generates:

$$\Delta T^c = \Delta T_o^c(1 - t/\tau) \tag{4.10}$$

where $\tau = C/K_o$, is the characteristic time of the building. In “heating case”, with constant power P, the temperature evolution obtained by using Laplace transform is:

$$\Delta T^h = (\Delta T_o^h - P/K_o)\exp(-t/\tau) + P/K_o \quad (4.11)$$

Linearization of this equation (4.11) generates:

$$\Delta T^h = (\Delta T_o^h - P/K_o)(1 - t/\tau) + P/K_o \quad (4.12)$$

The theoretical evolution of temperature can be validated by following the experimental evolution of temperature inside a real house for heating and cooling. Measurement of experimental slope of temperature and fitting a line/curve generates:

$$\Delta T^c = \Delta T_o^c - \alpha_c t \quad (4.13)$$

where

$$\alpha_c = \Delta T_o^c K_o/C \quad (4.14)$$

For heating experiments:

$$\Delta T^h = \Delta T_o^h + \alpha_h t \quad (4.15)$$

where

$$\alpha_h = P - \Delta T_o^h K_o/C \quad (4.16)$$

Both coefficients α_c and α_h are measured during experiments of heating and cooling. The heat loss coefficients and the capacitance of the building can be estimated by

$$K_o = P/(\Delta T_o^h + \Delta T_o^c \frac{\alpha_h}{\alpha_c}) \tag{4.17}$$

and

$$C = P/(\alpha_h + \Delta T_o^h \frac{\alpha_c}{\Delta T_o^c}) \tag{4.18}$$

The experiments for free cooling and heating as explained are conducted during the months of February and April. The experimental curves used for derivation of equations are shown in Figure 4.4.

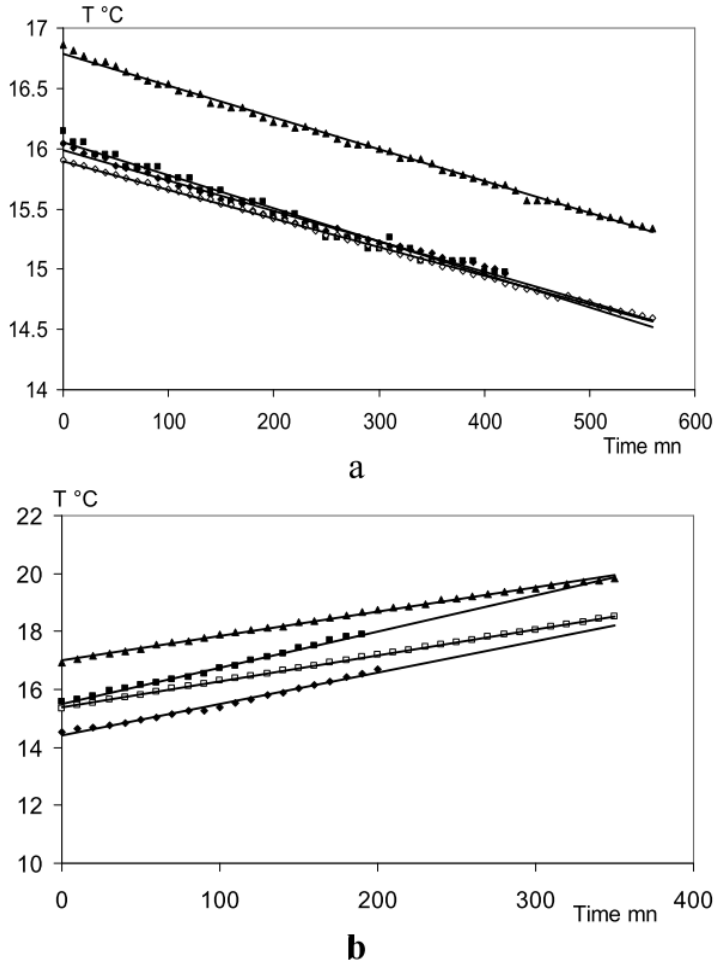

Figure 4.4: Fitted curves to experimental data during cooling and heating of building [95]

From the slopes of the fitted curves, the values of α_c and α_h are measured. They are inserted in equations (4.17) and (4.18) to estimate values of K_o and C as

a. $K_o = 462$ W/K and $C = 112\ MJ/K$

b. $K_o = 466$ W/K and $C = 104\ MJ/K$.

The time constant τ for building is almost 3 days.

In the third stage, the energy consumption of the building is measured along with weekly outside temperature data when the indoor temperature is maintained at 20 ℃ [95]. The fitted line of the graph is shown in Figure 4.5.

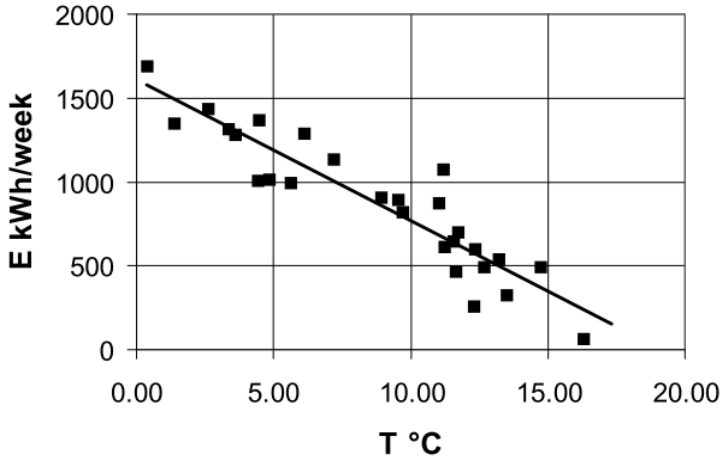

Figure 4.5: Energy consumption as a function of weekly averaged outside temperature [95]

The H value estimated in this case using using regression analysis:

$$E = 503(20 - T_{outside}) - 453W \qquad (4.19)$$

where 453 Watts, is the corrective factor for solar gains and heat generated due to occupancy.

The three values for overall heat transfer coefficient estimated using the three methods i.e. based on thermos physical properties, short term heating and cooling experiments and energy

signature/annual energy consumption are shown in Table 4-1. The three values for overall heat transfer coefficient estimated using three methods are in relative agreement with each other as shown in Table 4-1. The overall heat transfer coefficient during short term heating and cooling experiments is slightly underestimated, this may be attributed to zero occupancy and no solar radiations due to closed shutters, however this needs further investigation [95]. The short term method as explained in this section can be considered as precursor to more sophiticated QUB method.

Table 4-1: Overall heat transfer coefficients estimated using three tests [95]

Calculations (thermo-physical properties)(W/K)	Measured yearly energy consumption(W/K)	Heating and cooling experiments(W/K)
497	503	464

4.3 Influence of time constants of building for QUB method

QUB method assumes homogeneous internal temperature, constant external temperature and equal heating and cooling duration. The assumption of single RC network is too simplistic and the number of resistances and capacitances can be increased to n nodes to present the real behavior of the building [96]. In such a case, the temperature decay can be presented as n exponential terms. In steady state when the decay is considered for a time long the temperature can be given as: $\lim_{t\to\infty} T(t) = \varphi / H_{tot}$. Where φ is the heating power and H_{tot} is the steady state overall heat transfer coefficient.

The general solution for temperature evolution during the heating or cooling phase of the QUB experiment can be represented by equation :

$$T(t) = \frac{\varphi}{H_{tot}} + \left[T(0) - \frac{\varphi}{H_{tot}}\right] \sum_{i=1}^{n} a_i e^{-\frac{t}{\tau_i}} \tag{4.20}$$

where τ_i are time constants in increasing order such that τ_n represents the longest time constant and a_i represents the constants that depend on model resistance, capacitance and initial conditions. The steady state value H_{tot} will be equal to H_{QUB} only if [82]

$$\frac{\sum_{i=1}^{n}\left[a_{i.(1)}/\tau_i\right]e^{-\frac{t_{(1)}}{\tau_i}}}{\sum_{i=1}^{n}\left[a_{i.(1)}\right]e^{-\frac{t_{(1)}}{\tau_i}}} = \frac{\sum_{i=1}^{n}\left[a_{i.(2)}/\tau_i\right]e^{-\frac{t_{(2)}}{\tau_i}}}{\sum_{i=1}^{n}\left[a_{i.(2)}\right]e^{-\frac{t_{(2)}}{\tau_i}}} \quad (4.21)$$

The above equation holds true when we consider the temperature evolution: as a function of single time constant i.e. $n = 1$, this happens when the time duration for two phases $t_{(1)}$ and $t_{(2)}$ increase to such extent that all the time constants except the highest time constant decays This is considered as sufficient time for QUB experiment and if this time is shorter than single night, than QUB experiment can be performed during a night without the influence of solar radiations [82].

The accuracy of the QUB method as a function of longest/highest time is discussed in [93]. The time constants are determined as eigen values of state space matrix A of the building. The response of the building temperature is exponential due to the cumulative effect of all time constants. However, the matrix A has a number of time constants (negative inverse of eigen values) categorized as short, medium or long time constants (significant or non-significant time constants) [93]. The coefficient of time constants determines whether they are dominant or insignificant time constant.

The medium time constants with large coefficients determine the exponential response of the building [93]. The response of the building is exponential after the small time constants (insignificant) have decayed and before the effect of large time constants have set in. The slope of the response curve should be determined at this stage.

The QUB experiment is performed without any occupancy at night so that influence of solar radiation and any other power input (due to occupants) can be eliminated. The thermal power

has strong influence on the result of QUB experiment and should be applied as a constant value known with accuracy. To ensure accuracy, it is advisable to use two electric heaters with low inertia. Any other sources of heat, such as wood, boiler, gas etc., require conversion and efficiency factors. This can lead to errors. A small deviation such as 5% deviation in voltage measurement, can lead to larger deviation in power measurement and a 10% deviation in measured H_{QUB} [97].

It is important to keep temperature homogeneous across the buildings. This can be a problem in case of buildings with multiple rooms. Heaters with small power (100 W) designed to maximize convection can be used to ensure this. This problem can also be resolved by using heaters according to the thermal parameters of the room. G. Pandraud recommended to use heating mats of 112.5 W placed in vertical position over floor to ensure homogeneous temperature distribution. Vertical position results in lesser heat transfer to the ground and generates a smoother temperature curve [97]. The analysis period must be long enough to average out the measurement noise but still be representative of the dynamic conditions.

It should be mentioned here that the formulas for H_{QUB} are derived using single RC network, which is a crude approximation of the actual temperature evolution. The exact evolution of temperature during a QUB experiment can be modelled by considered the wall with n layers (an RC network with n nodes). The temperature evolution during QUB experiment can then be presented as $[T^*] = \sum_{i=1}^{n} c_i [X_i]\, e^{-\frac{t}{\tau_i}}$, that is a sum of n time constants [97]. By simple derivation, it can be proved that

$$\frac{T_I^{*\cdot}(t)}{T_I^*(0) - q/K_o} = -\frac{1}{\tau_n}\frac{T_I^*(t) - q/K_o}{T_I^*(0) - q/K_o} \tag{4.22}$$

This equation leads to the QUB equation for H

$$H_{QUB} = \frac{\alpha_1 q_2 - \alpha_2 q_1}{\alpha_1 T_2 - \alpha_2 T_1} \tag{4.23}$$

where $\alpha = \frac{dT}{dt}$ is the temperature gradient and T^* is the temperature difference between internal building and external environment. The equation with n nodes can be simplified to single RC network as after some time when the multiple time constants decay and the temperature evolution is the function of single time constant only. The capacitance is then calculated as a function of the largest time constant i.e. $C = \tau_n . K_o$.

Since single RC network is a crude presentation, H. Madsen [98] proposed that two time constants are sufficient to model a simple building. Since QUB method simplifies analysis by conducting experiments at night (no solar radiations) and no occupancy, it can be assumed that the model in this method can be represented by two time constants. Two-time constants translate into two capacitances, three resistances and two nodes as shown in Figure 4.6, where R_{EW} and R_{IW} are wall resistances, R_{IE} is the ventilation/infiltration resistance and T_E is the external temperature, respectively.

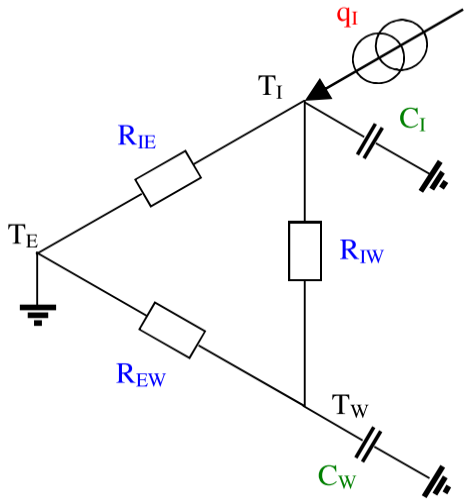

Figure 4.6:3R-2C representation of QUB model [99]

The model (3R2C) can be solved both numerically and analytically and can be presented by the equation

$$\frac{T_I^*(t) - q/K_o}{T_I^*(0) - q/K_o} = \frac{\left(A_1 - \frac{1}{\tau_1}\right) e^{-\frac{t}{\tau_1}} - \left(A_1 - \frac{1}{\tau_2}\right) e^{-\frac{t}{\tau_2}}}{\frac{1}{\tau_2} - \frac{1}{\tau_1}} \quad (4.24)$$

where the values of A_1,τ_1 and τ_1 are given as functions of capacitance, resistance and different temperatures of the circuit [99]. The influence of the exponential $\exp(-t/\tau_1)$ disappears quickly, leaving temperature evolution as a function of single time constant τ_2, that leads to the simple QUB equation for H. The method can thus be applied to complex buildings.

Experiments conducted in Energy House in Salford were used to validate both QUB method (single RC), and the 3R2C model. The 3R2C fits the temperature evolution curve with two-time constants, as shown in Figure 4.8. The temperature evolution after four hours becomes a simple exponential decay. The H values from the four methods, i.e. steady state experiments, QUB method, 3R2C and estimation via basic energy modelling software SAP are compared in [99]. The estimates of H from different methods given in table are close to each other.

Table 4-2: Comparison of three method of overall heat transfer estimation [99]*)*

Case	No roof insulation		Insulated roof
Test Number	1	2	3
K_0 steady-state	262.7		215.4
K_0 QUB	274.5	263.8	229.8
K_0 3R-2C model	270.9	250.5	227.6
K_0 SAP	386.4		332.9

Results of these estimations validate QUB method. There are two sources of uncertainty: the uncertainty underlying the model due to the simplicity that is difficult to estimate; the choice of time period during which data is analyzed, especially the time for slope determination. The change in slope period during different test periods causes the dispersion in H value ($\pm$ 10 W/K). The suggested direction for future work is that the range of uncertainty of QUB method under different test conditions needs to be established (though it is in range of $\pm 10 - 15\%$) [99].

The heating power should be high enough to ensure the significant temperature difference between interior and exterior. The required power levels can be obtained by optimizing the value of power ratios α given be equation (4.3). The QUB method involves application of two levels of power: a heating power followed by no power. There are two ways to conduct these experiments: either applying both levels of power in a single night (8-12h) or applying two stages separately in two nights (36-48h). The experiment should be as long as possible. If initial conditions are similar, i.e. the two constants $\alpha_{i.(1)=}a_{i.(2)}$ in equation (4.21) then overall heat transfer coefficient estimated by QUB method (H_{QUB}) will be equal to steady state heat transfer coefficient provided that the time for heating and cooling durations is equal i.e. $t_{(1)=}t_{(2)}$,. The values are calculated at the end of each test period [82].

4.4 Validation experiments for QUB

An experiment to validate the measurement of H by QUB method was conducted at energy house of Salford University [82]. In this experiment, H value was measured first by conducting a steady state experiment where H was estimated using $H_{tot} = \varphi/(T_2 - T_1)$ from Figure 4.7 where values are averaged over a period of 12 hours. H_{tot} is used as a reference value.

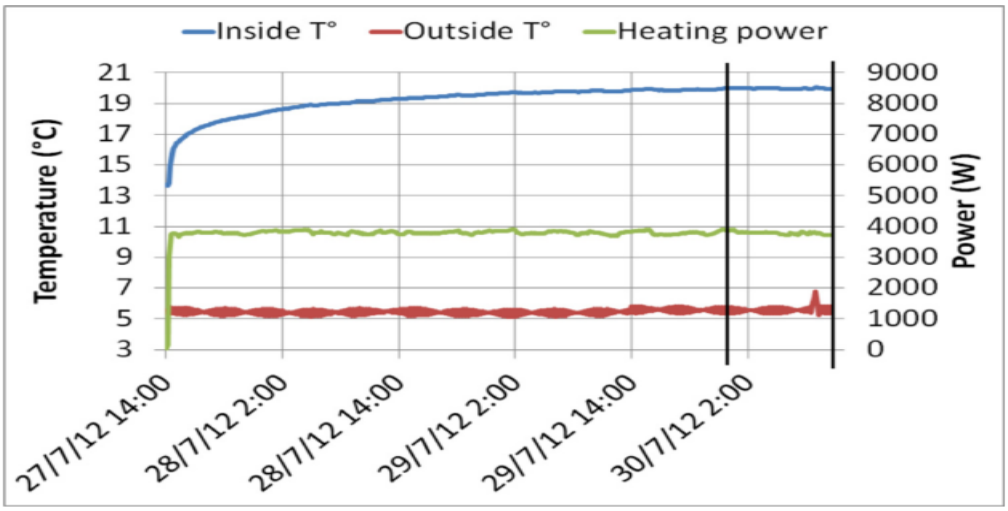

Figure 4.7: Steady state experiment for H value. The solid black line shows measurement values for estimation of H [82]

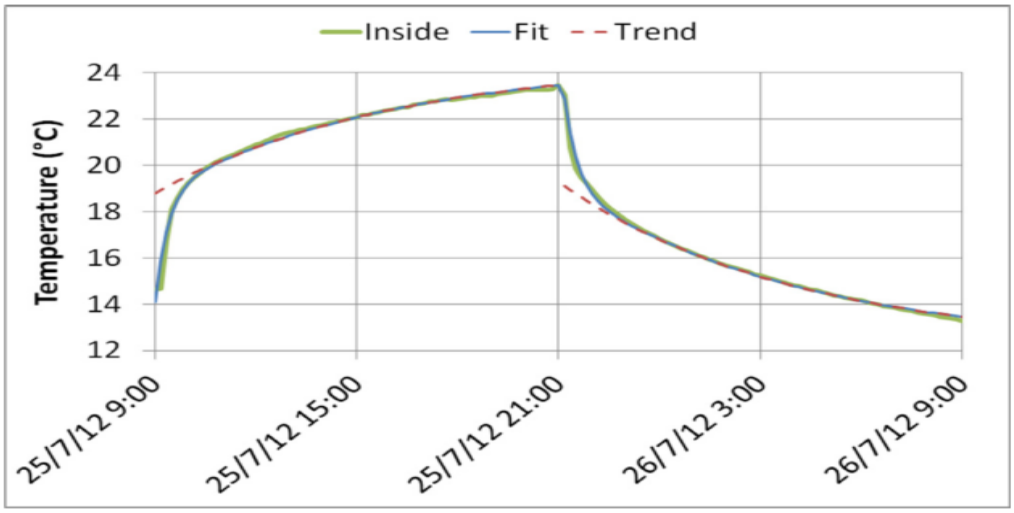

Figure 4.8:Evolution of internal temperature (green curve) and various fits as applied to the measured(green) curve [82]

The measurement of H in steady state is followed by a QUB test. The evolution of the internal temperature is as shown in (Figure 4.8). The red dotted line in Figure 4.8 shows the fit with single time constant from the RC model also called *trend*. The blue line represents the same single RC model but with two-time constants, also called *fit*. Both the *trend* and *fit* models are derived using the same equation but with different number of time constants. The model with two-time constants corresponds to a model with two capacitances and minimum two resistances. Two time constant model seems to fit data very well [100]. The first-time constant

is shorter and dies out in 23 minutes or within an hour. After this time, temperature evolution can be presented by a single time constant. The results of QUB tests for H are compared in Table 4-3. The table shows that QUB results are in good agreement with H_{ref}.

Table 4-3: Results of three measurements from QUB test and steady state test [82]

Case	1	2	3
$t_h = t_c$ [h]	12	8	12
Roof insulation?	No		Yes
H_{ref} [W/K]	263.9 ± 2.7		209.5 ± 2.3
H_{QUB} [W/K]	255 ± 9	264 ± 8	216 ± 7

There are some questions that still need to be answered despite a good agreement between QUB test values and steady state values, s. a. the relationship between error, building characteristics and test duration. It is evident from the experimental results, that QUB test can give better results even with shortest possible time (0.5h). The question of sufficient time for QUB test is still unanswered [96].

QUB method was tested virtually using TRNSYS software for a virtual single family house of 109 m^2 (with internal insulation) with weather data from city of Rennes [101]. Fifty-two tests were condcuted for a single year. The values obtained from QUB test were compared with the reference value 143 W/K obtained from TRANSYS model. The values obtained by QUB tests were between 136 and 167 W/K, with a mean value of 150 W/K and maximal deviation of 17%. The estimated QUB value was within $\pm 10\%$ for 90 to 95% values [101].

University of Salford has built a controlled testing house known as Salford Energy House. It is a two-bedroom house built inside a controlled environment chamber where different weather conditions can be replicated. The house has sensors for multiple measurements in which fenestration, doors, and envelope insulations can be changed [94]. A number of in situ measurements were conducted at Salford Energy House [101]. Temperature sensors, power meters and heat flow plates were used for generating a data set of QUB test. When heat flow

plates are used, the QUB test it is referred to as QUB/e. With QUB/e test, U values of walls can be measured as well. It was inferred from the test that:

- the H values obtained for QUB tests with one-hour heating duration yield values within 10% of the steady state reference values;
- for heating duration less than half an hour, H values showed dispersion with a difference of up to 40 % with steady state reference values;
- U values measured with QUB/e method were found within the recommended uncertainty bounds of steady state methods (co-heating methods ISO 9869-1).

It should be noted that these conclusions were obtained for a reference test house and may not represent the real conditions of a living house in a community.

A number of in situ tests were conducted for a detached uninsulated house in UK with heating duration of 5, 6 and 7 hours [92]. The tests were conducted starting from end of September till end of April. The tests were conducted for two different configurations of air tightness. It was concluded that:

- QUB method provides reasonable results within 10 % error, provided that α lies between 0.4 and 0.7;
- tests with 5, 6 and 7 hours generated similar results, though for 5 hours heating duration results were at the lower limit;
- no significant relation was found with wind speed, with a possible explanation that the building was sheltered from wind from three directions;
- with tests extending from October to late September, a relation between H and external temperature was found.

4.5 Test duration and power levels for QUB test

The test duration for QUB experiment should be as long as practical and for identical initial conditions i.e. $a_{i(1)} \approx a_{i(1)}$, the heating and cooling test durations should be equal. There is no optimal duration and for each experiment the test duration should be dealt on case to case

basis [82]. However, the period should be long enough to average out measurement noise but short enough to be representative of dynamic conditions.

In order for $H_{QUB} \approx H_{ref}$, it is important that $t_h = t_c > t_l$ where t_l is the sufficient time for all the small time constants to become zero, except the highest one. The quadrupole analysis shows the relationship between H_{QUB} and H_{ref} (steady state) [82]:

$$H_{QUB} = H_{tot} \frac{1}{1 - \alpha^2 \frac{\sum_{i>j} s_i s_j \beta_i \beta_j (\tau_i - \tau_j)(\beta_i - \beta_j)}{R_T \sum_i (1 - \alpha\beta_i) s_i \beta_i}} \quad (4.25)$$

where $\alpha = 1 - T_o/R_T P_h$ and $\beta_i = e^{-\frac{t_h}{\tau_i}}$. The value of α is of particular importance in case of QUB test and represents the range of thermal load applied to building. There are two ways that can lead to $H_{QUB} = H_{tot}$:

- If t_h is increased such that its value is higher than the second largest time constant, then all the β_i terms except one are zero and the second term in the denominator of equation (4.25) tends to 0.
- It is possible to make $\alpha = 0$. This can be achieved by $p_h = p_o$, that is the building stays at steady state, the temperature slope is zero and and $H_{QUB} = \varphi/T$ [82]. However, it is practically not possible to make $\alpha = 0$, although its value can be reduced. As the value of α increase, the corrective factor in denominator increases as well.

Using Quadrupole numerical analysis, the error in H_{QUB} was analyzed as a function of α, using time durations of 1,6 and 12 hours respectively [82]. As shown in Figure 4.9, for a given α, the error reduces as test duration increases.

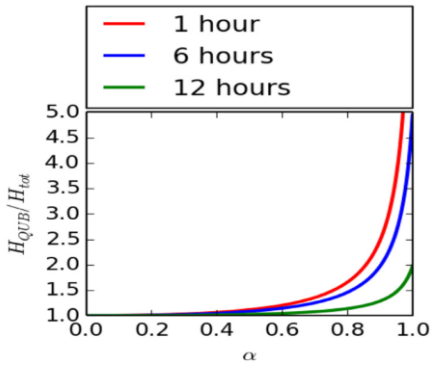

Figure 4.9: The error in QUB as a function α and time duration

Another simulation, with varying initial conditions and different durations of cooling periods before QUB test, showed strong dependence of the test on α, showing that reliable results can be obtained (within 10% of the reference value) even with shorter durations provided that α is kept at low values.

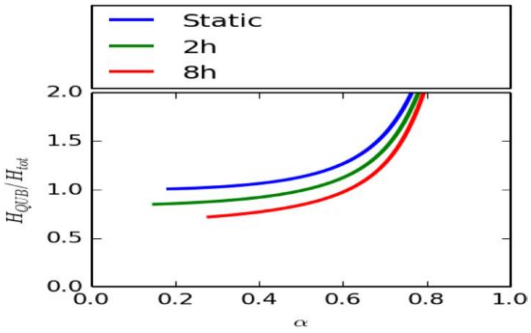

Figure 4.10:H_QUB as a function of initial conditions[82]

G. Pandraud conducted both numerical and experimental analysis to optimize power levels and duration of the test. The purpose is to decrease both time duration and uncertainty of QUB test [97]. Results of QUB test depend on duration of the test: the longer the test period, the more accurate/closer is the H_{QUB} to the refence value. It is possible to obtain an accurate value from QUB test by using one night per test (heating and cooling). This is evident from the expression $[T^*] = \sum_{i=1}^{n} c_i [X_i]\, e^{-\frac{t}{\tau_i}}$, or from the expression 3R2C (function of two time constants) where after sufficient time, the temperature evolution is function of single time constant. With temperature as a function of a single time constant, the equation for QUB test can be used to estimate H

$$H_{QUB} = \frac{\alpha_1 q_2 - \alpha_2 q_1}{\alpha_1 T_2 - \alpha_2 T_1} \quad (4.26)$$

The uncertainty of QUB test therefore increases with decrease in duration of the test. However, it is important to understand the relationship between the length of the test and the uncertainty in strict terms (numerical or analytical) in order to optimize the test duration, i.e. to reduce the test duration with minimal loss of accuracy.

QUB tests were simulated with different durations of test, a 3D surface as function of all heating and cooling times was generated [97] as shown in Figure 4.11:

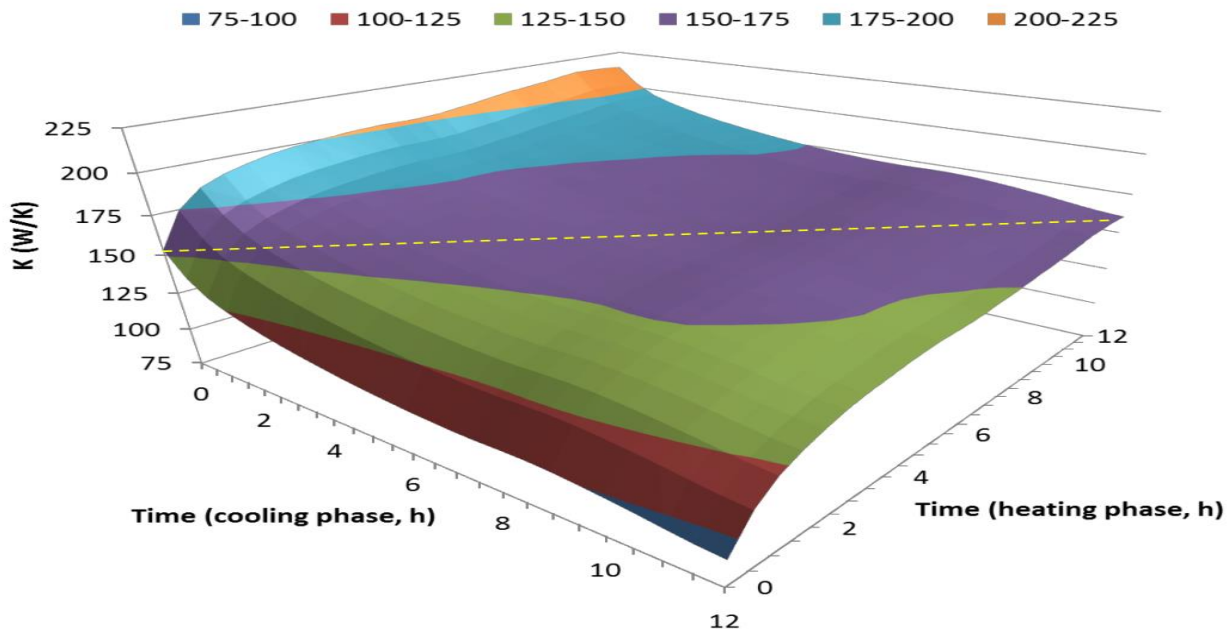

Figure 4.11: H_{QUB} as a function of position of heating and cooling duration [97]

It is concluded from the Figure 4.11 that after 6h, the H_{QUB} flattens out, i.e. no further improvement is obtained by increasing the test duration. The second conclusion is that accurate estimation of QUB in time lesser than one night can be achieved by keeping both heating and cooling durations equal [97].

These results were confirmed by experiments at Energy House Salford University (for case of uninsulated house) as shown

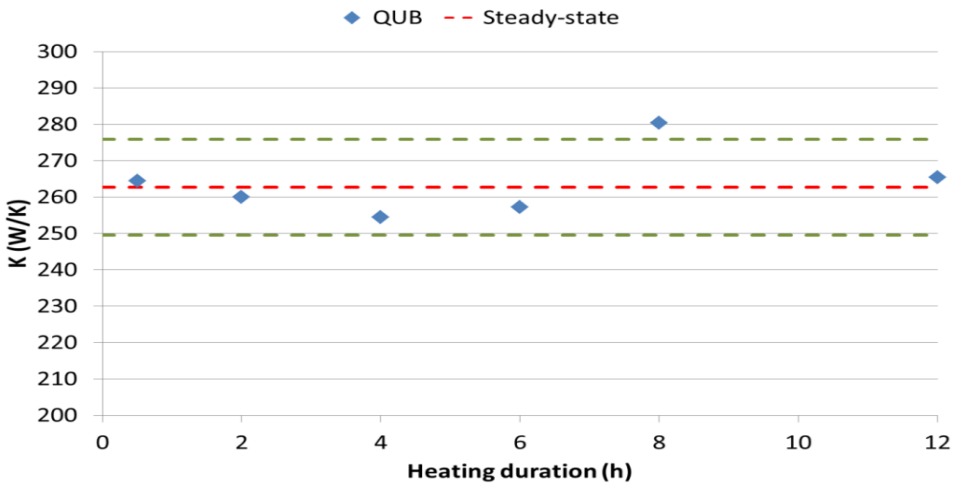

Figure 4.12:QUB tests as function of test duration [97]

Figure 4.12 shows that accurate results can be achieved even with small durations, such as an hour. The accurate result for test lesser than an hour (0.5h) may be sheer luck as it is not supported by theoretical evidence.

A special case for quadrupole analysis is considered where the precise value of initial conditions, initial power P_o and temperature, are known, external temperature is constant, heating and cooling durations are equal and power dissipated during cooling phase in nil [97]. These assumptions lead to a semi analytical expression of H_{QUB} as a function of theoretical value K_o, heating duration t_h and the resistance R_i and C_i of the network as:

$$H_{QUB} = K_o \frac{1}{1 - \left(1 - \frac{P_o}{P_h}\right)^2 . f\left(\left(1 - \frac{P_o}{P_h}\right), \exp(-t_h), R_i, C_i\right)} \quad (4.27)$$

where f is a function of infinite sums of different products of resistances and capacitances and exponentials of time duration and ratios of power levels (during heating and cooling). Although f cannot be expressed analytically, it decreases exponentially with time and hence the denominator gets closer to 1 and the K_{QUB} value gets closer to reference value K_o. As it is

evident from the equation, the second way to optimize the H_{QUB} independent of time duration is to keep the ratio $\frac{P_o}{P_h}$ in equation (4.27) close to 1, i.e. to keep the low thermal load during heating phase relative to initial conditions [97], [99].

The initial conditions during QUB test refer to the steady state conditions before the experiment. The power required to keep initial conditions in steady state is given as

$$P_o = H_o \Delta T_o \tag{4.28}$$

where $\Delta T_o = (T_{io} - T_{e,h})$, i.e. the difference between initial indoor and external temperature. The ratio of powers can be presented as $\alpha = 1 - K_o \Delta T_o / P_h$. For a fixed duration of time, we can write the equation:

$$H_{QUB} = H_o \frac{1}{1 - \alpha^2 \varphi(\alpha)} \tag{4.29}$$

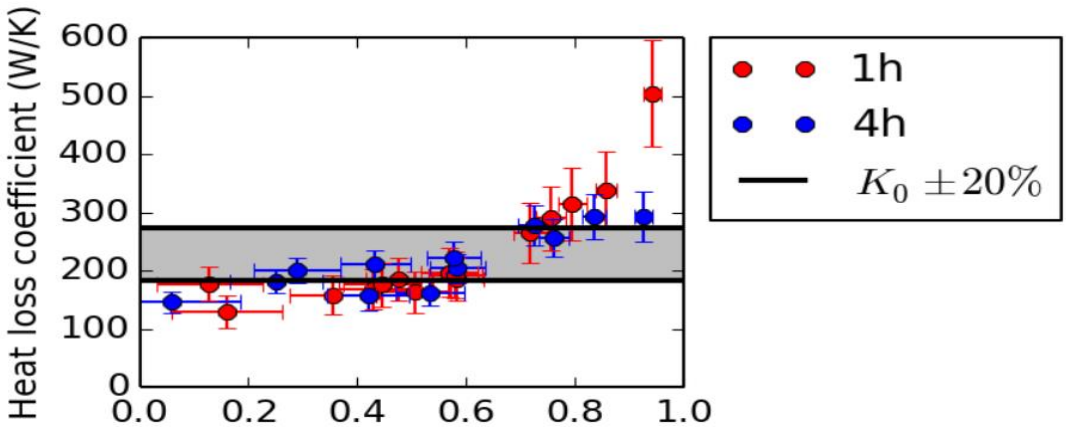

Figure 4.13:H_{QUB} as a function of α [97]

Thus, a value of $H_{QUB} = H_o$ can be achieved by keeping α between 0.5 to 0.8. This is confirmed from experimental evidence for tests conducted at Energy House at Salford University as shown in Figure 4.13

Three conclusions can be drawn from the experiments at Salford University:

- H_{QUB} increases as a function of α and generates an overestimated value of H_{QUB}.
- Overestimation can be reduced by increasing the test duration.
- Low values of α can also lead to errors in H_{QUB}, i.e. is under estimations.

Numerical simulations were performed by changing initial conditions and observing the variation of H_{QUB}. The variation of H_{QUB} with α was also observed as shown in Figure 4.14.

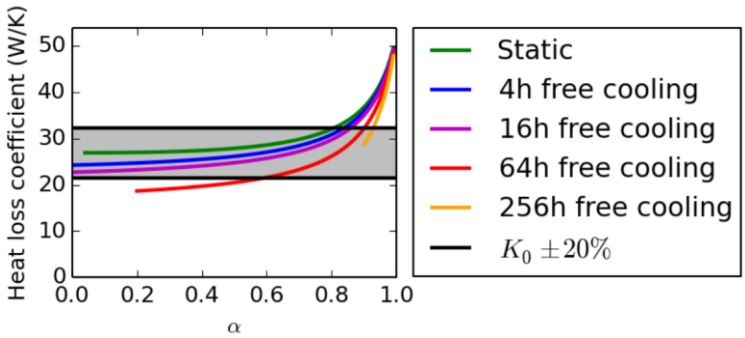

Figure 4.14:Kqub Vs variation in initial conditions and α[97]

It can be a delicate task to control α in practical situations. However, simulation results show that satisfactory results (H_{QUB}) can be obtained with α values (4.3) between 0.2 and 0.8; α values between 0.3 and 0.7 generate best results. This help us identify the optimized value of α. The value of $\alpha = 1 - H_o \Delta T_o / P_h$ is based on H_o which might not be known in advance. This requires the prior estimation of H_o that can be estimated using thermophysical values or some software such as SAP [97].

It is highly probable that the estimated value of K_o will always be known with error. G. Pandraud showed that as long as the error in $K_o \Delta T_o$ stays within $40\ \%$, the value of α can be kept in range of 0.3 to 0.7, as shown in Figure 4.15

Figure 4.15: Value of α as function of input Power [97]

To quantify, for a targeted value of $\alpha = 0.5$, an error of 10% on P_h leads to an error of 5% on α, which leads to an error of 2 to 5% on K_{QUB}.

The QUB method can also be used to find out the apparent capacitance C_{QUB} as is evident from equation

$$q = C_{QUB}\frac{dT_{int,i}}{dt} + K_{QUB}(T_{int,i} - T_{int,e}) \tag{4.30}$$

This equation can be used to determine C_{QUB} during as

$$C_{QUB} = \frac{q_1 T_2^* - q_2 T_1^*}{T_1' T_2^* - T_2' T_1^*} \tag{4.31}$$

Value of C_{QUB} evolves/increases with time and is know as effective capacitance. C_{QUB} represents the aggregate capacity of different elements of building. Increase in value is due

to the fact that initially air temperature increases and later the air temperature warms the walls (at this point the capacitance of walls come into play) until the limiting value of capacitance is reached that can be given as $C_o = K_o \tau_o$, where τ_o is the largest time constant of building. The evolution of effective air capacity is shown in Figure 4.16

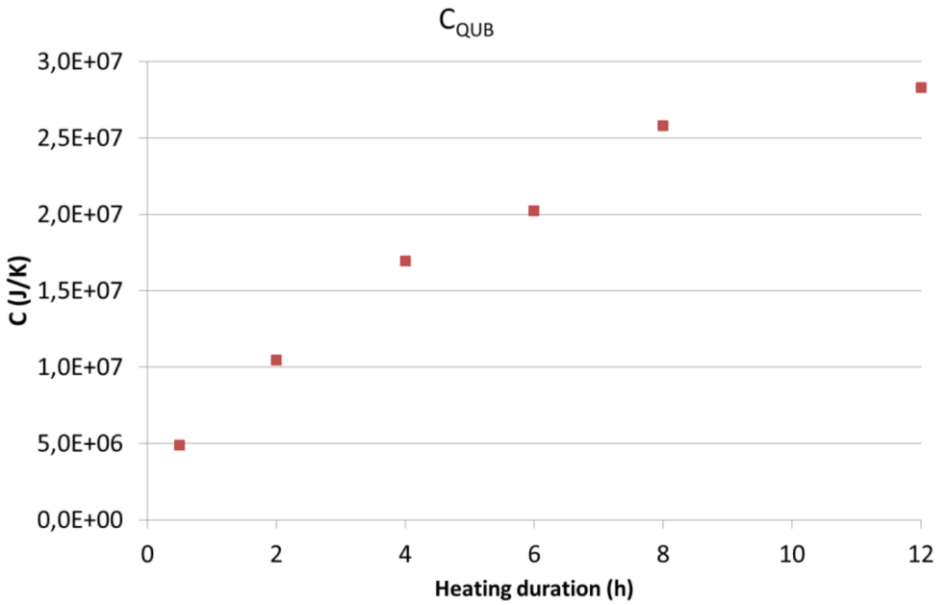

Figure 4.16:Effective heat capacity as function of time[97]

4.6 Results of QUB Experiments

Three test houses were used to validate the numerical results, as shown in numerical simulation section. The three test houses were: small scale building in real climate (Saint-Gobain), real scale building in controlled climate (energy house at Salford University) and real scale building in real climate (Twin houses at Fraunhofer Institute of Building Physics IBP). In all the tests, the steady state H was measured using the standard co-heating test method followed by QUB test. Reliable QUB results are therefore obtained with increased time duration for QUB test; the optimized value of α for QUB test is between 0.4 and 0.7 [82].

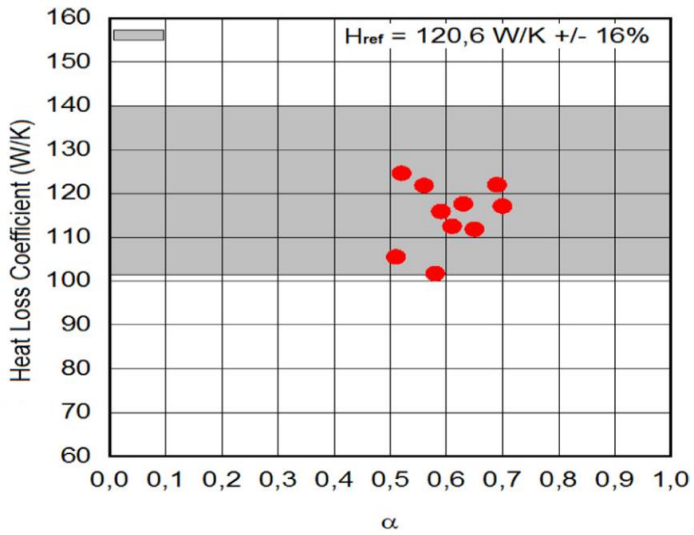

Figure 4.17:QUB values for Twin house Germany [82]

The nonconformity of some QUB experimental results with numerical simulation can be attributed to the following reasons:

- non-homogeneous temperature due to stratification, stack effects (a temperature difference of 2 K is observed between ground floor and attic space);
- changed air infiltration rate and wind pressure conditions between the two tests, i.e. QUB test and steady state test;
- inability to control H_{QUB} α-value in practice.

Reliable results for QUB test can be obtained provided that good air tightness is maintained. During the tests, the conditions of airtightness and infiltration must be considered. It is important to use more sophisticated techniques (tracer gas measurements) for air infiltration measurement and its impact on heat transfer coefficient [82]. The error depends on α, building structure and test duration, that can be reduced by choosing α carefully. A low value of α leads to an underestimated H_{QUB} whereas high value leads to an overestimation of H_{QUB}. An optimal value of α (between 0.4 and 0.7) can lead to a reliable H value.

With short duration of QUB test it is possible to conduct as many as 20 QUB tests in comparison to single co-heating test that can take two to three weeks. Due to short duration

and dynamic nature of the QUB test, it offers an opportunity to find the impact of weather conditions, such as wind velocity, on the value of the H-value of the building H [82].

QUB method is relatively new and needs further validation, both theoretically and empirically. It is important to know the nature of uncertainty of QUB value, variations in uncertainty with test duration, building/wall type and experimental conditions. The information provided by QUB test are not diagnostic and should be further added with additional infiltration tests, thermal bridges, window types etc. [82].

4.7 Conclusions

The QUB method can be used as a tool to quickly estimate U-value of building. This U-value can be used for labelling, certification, control or research purposes. However, QUB results are based on interpretation of data that can be user dependent. This can result in erroneous values that cannot be used with certainty (for certifications or research purposes).

There are two sources of uncertainty:

1. model complexity (single RC or 3R2C due to simplicity of the model) that is difficult to estimate;
2. choice of time period during which data is analyzed, especially the time for slope determination.

The change in slope period during different test periods causes the dispersion in H value ($\pm\ 10\ \mathrm{W/K}$). Determination of temperature slope is a serious problem and should be determined with mathematical and experimental precautions that leads to reproducible results. It is advisable to analyze temperature evolution for a long period and determine temperature slop at or near the end of test (end of heating or cooling period). Aother technique is to determine the slope for a set of points along the temperature evolution curve. It is also possible to model temperature evolution by a model function such as exponential, polynomial or spline, and then calculate the temperature slope once again at or near the end of the period.

The direction for future work is that range of uncertainty of QUB method under different test conditions needs to be established [99]. The limitations of QUB method (due to simplicity and short duration) need to be quantified. Measurements under different conditions, such as weather, type of constructions and variation in H_{QUB} and the determination of time when the temperature evolution become a simple exponential decay. These experiments should be coupled with numerical simulations as well.

It is important to understand the variation of error when the QUB experiments are repeated in succession for a number of days. The variation in QUB value with power level and time duration has been already explored [93]. However, the variation in H_{QUB} value with real boundary conditions (solar radiation, outdoor temperature) and initial conditions (initial power and initial conditions of building) with experimental data needs to be further investigated.

There are two possibilities to perform the detailed analysis of QUB under different set of weather conditions, construction types etc. One is to perform real experiments at different sites, with different construction types, under different set of weather conditions. This can be both expensive and time consuming. Several experimental setups are presented in Chapter 0.

The second possibility is to design simulation experiments with different condition sets. This is less expensive and can be performed in relatively short time but needs adapted models. To simulate and design QUB experiments, it is important to have a modelling tool that has the ability to generate the evolution of indoor temperature under different set of power, time duration and weather conditions. A state space modelling technique with its developed is presented in Chapter 6. The techniques for generating thermal circuits for individual components of buildings, assembling of thermal circuits, generating state space model from the assembled circuits and the advantages for using this modelling technique are discussed in next chapter.

5 Experimental setups for testing the measurement methods

Building thermal characterization or building energy models need to be validated before their general application. It is important to obtain a data set with known conditions and accuracy that can be used to validate and calibrate building energy models. This section explains the experiments, experimental setups and data analysis techniques that are documented as part of IEA, EBC Annex 58 'Reliable building energy performance characterisation based on full scale dynamic measurements'[50].

5.1 Round-robin box

A round-robin test is an experimental methodology aimed to repeat a single test (or group of tests) on a specimen in multiple laboratories or in multiple conditions with different sets of instruments, assumptions and experts. The purpose of the test method is to verify the repeatability of results, validity of new methods, analyze the effect of varying conditions and varying techniques on the results test.

A sample test box was prepared as a simplified representative of building to be tested at different locations. The box was shifted to different locations and tested under real climatic conditions. Data representing the measurements were then sent to different research organizations for analysis. Based on similarity with round-robin test methodology, it was named as Round-robin box [53].

The aim of the test was to establish the state of the art on design of experiments, measurements, dynamic data analysis and dynamic characterization. The experiments provided an opportunity to look into capabilities, limitations and reliability of in situ full scale:

- testing methods
- dynamic data analysis
- influence of different variables on characterization results.

The thermal characteristics selected for these analysis are overall heat transfer coefficient H, solar aperture gA and dynamic characterization, such as dynamic response of building to changing boundary conditions (temperature and solar radiations) and effective capacitance [46].

Round-robin box a cubical box with external dimensions of $120 \times 120 \times 120$ m^3 and internal dimensions of $96 \times 96 \times 96$ m^3. The façade of the box is made in three layers with an internal façade of light weight material, a middle heavy weight and final light weight façade on the outside. The box rests on 50 cm high stand. There are three different designs of the box: a box with no window, with window and with a façade layer material that can be changed. The box had no heating or cooling equipment to allow different experts select equipment as per their design of experiment. An opening with a pipe at the base is provided as an outlet/inlet for instruments and equipment wiring [46].

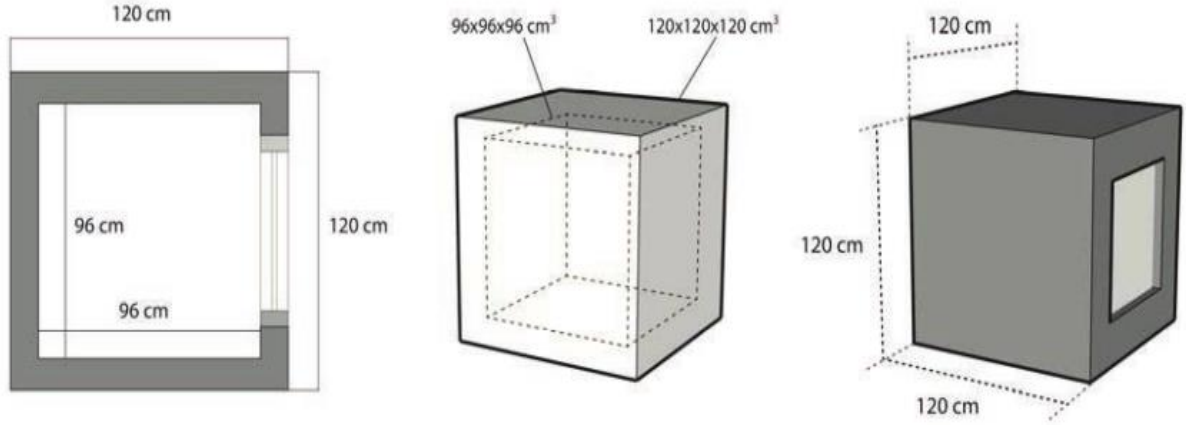

Figure 5.1: An overview of the Round-robin box [46]

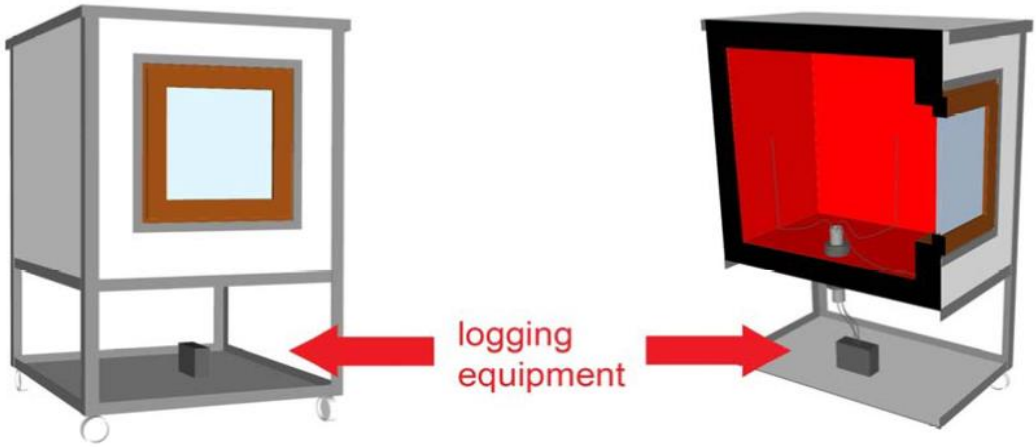

Figure 5.2: Box outlook with sensor and equipment arrangements [53]

Virtual simulation of the box was performed before the actual test to estimate the thermal properties of the box. A 3D steady state model was generated with indoor conditions of 25℃ and outdoor conditions of 0℃ . The H-value was evaluated as 4.08 (W/K). Under real test conditions (co-heating test,) the H-value measured was 3.75 (W/K) [50]. It was estimated that with changing wind speeds, the overall heat transfer coefficient may exhibit an uncertainty of $\pm$ 10 %. The resistance values for opaque walls were estimated to be between 1.927 to 2.2 m^2K/W (this change is attributed to glue or thin air film between the layers) [50]. The change in convection heat transfer co-efficient with air velocity is given as:

$$V < 5\ \frac{m}{s}, h_c = 5.6 + 3.9.V$$
$$V > 5\ \frac{m}{s}, h_c = 7.2V^{0.78} \quad (5.1)$$

The measurements during Round-robin tests require the following instruments:

- Climate boundary conditions: a weather station that can measure outdoor temperature humidity, solar radiation (diffuse and direct), wind speed and wind direction.
- Test box measurements: surface temperature measurement, indoor temperature measurement, heat flux measurement.
- Co-heating tests: heating equipment and power measurement instrument [46].

Different tests were performed at different locations. The first test was conducted at a site in Belgium Building Research Institute (BBRI) in the lee of wind and solar radiation. The test site weather is maritime weather with mild winters and cool summers, generally rainy, humid and cloudy [46]. For the co-heating test, the box is heated using a 188 W heater. The following experiments were conducted

1. constant indoor temperature of 26 C for 5 days;
2. constant indoor temperature of 21 C for 5 days;
3. constant indoor temperature of 31 C for 5 days.

A simple linear regression between outdoor temperature and power input was used for an initial estimate of H and wall thermal resistances. The estimated value was 3.4 to 3.5 W/K.

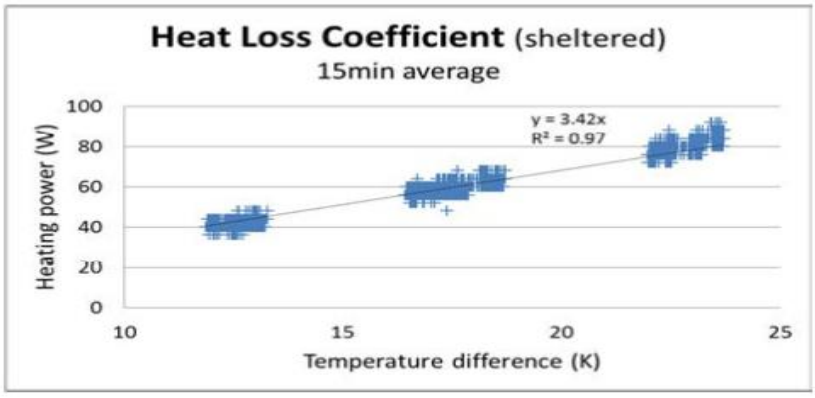

Figure 5.3: A linear regression to estimate H value[53]

A second series of tests was carried out outdoors in Belgium with the following set of experiments [46]:

1. co-heating test with constant indoor temperature of 25 for 2 weeks;
2. free-floating internal temperature for 2 weeks;
3. ROLBS sequence test for 3.5 days (dynamic heating test).

The measurements taken during the experiments included:

- ambient air temperature;
- vertical global solar radiations for glazing;
- horizontal longwave radiations;

- horizontal global solar radiations;
- horizontal diffuse solar radiations;
- vertical long wave radiations;
- wind velocity and direction;
- relative humidity.

Experiments at Belgium Building Research Institute (BBRI) were repeated in a different climate (extremely hot and dry) at Plataforma Solar de Almeria, South of Spain [50]. The weather of this region is characterized by a large temperature fluctuations between day and night and strong horizontal solar radiation (summers) and strong vertical solar radiation (winters). With the strong weather fluctuations the estimates of overall heat transfer coefficient H was between 3.75 to 4.08 W/K and thermal resistance R- is between 1.927 to 2.2m^{2}K/W [50]. This shows that overall heat transfer coefficient and thermal resistance can be reliable measurement of building performance even with strong fluctuating weather conditions [53]. The weather, indoor temperature variation and construction data can be used for model validation.

A third experiment on Round-robin box was conducted at University Centre for Energy Efficient Buildings (UCEEB) Prague. Experiment was conducted in a controlled weather chamber [46]. The internal, surface, external and power dissipated were measured during the experiments. The conditions were maintained until steady state conditions were achieved for each step. Time constant for box was measured to be approximately 24 hours and the time calculated to reach steady state was approximately 3 days.
H was estimated after steady state is achieved using the steady state equation

$$\Phi_p - H(T_i - T_e) = 0 \tag{5.2}$$

As the climate chamber can keep the external temperature constant, it is relatively easy to use an average uniform temperature. The spatial internal temperature T_i measured with different sensors should be representative of temperature of heating surface (of heat source),

indoor air and internal surface of the box [46]. A representative temperature with weight factor for each

$$\mathrm{T}_{i,1} = \frac{K_c T_{ai,1} + K_{r1} T_s + K_{r2} T_{s,2-6}}{K_c + K_{r1} + K_{r2}} = w_1 T_{ai,1} + w_2 T_{s,2-6} + w_3 T_s \tag{5.3}$$

where K_c and K_r are convective and radiative conductance and $T_{ai,1}$, $T_{s.2-6}$, T_s are temperatures of air, the representative temperature of six surfaces and the temperature of the surface considered [50].

The following uncertainties are important for determination of H;

- error in sensor measurement (e.g. manufacturing uncertainty od $\pm$2W for power);
- error in installation of sensors;
- fuzzy representation of internal and external temperatures (assumed value of ± 2℃ for outdoor and indoor temperature);
- assumption of steady state [46].

The propagation of uncertainty in internal temperature was evaluated by generating samples using Latin hyperbole technique where uncertainty in both weights and measurement was evaluated [46]. The uncertainty in each surface was evaluated and finally the total internal temperature for each sample was calculated. The uncertainty in H was calculated using

$$\mathrm{u}_c = \sqrt{(c_1 \delta \Phi_p)^2 + (c_2 \delta \mathrm{T}_i)^2 + (c_1 \delta \mathrm{T}_e)^2} \tag{5.4}$$

where c_i is the sensitivity coefficient determined with respect to the partial derivative of the respective terms. The data from this test is availabe be used for validation of building energy models.

5.2 The Twin House experiment (IEA, EBC annex-58)

The Twin House experiments were conducted as part of IEA, EBC Annex-58 project aimed to provide data for validation of building simulation models used in performance measurement. The two houses, named N2 and O5, are located on a plane area in Holzkirchen, Germany, at a altitude of 680 meters. As shown in Figure 5.4, both the houses are unshaded. The houses have an attic, a living space and loft [102].

Figure 5.4: Views of twin houses from East and West house[102]

Figure 5.5: Views from South and North[102]

The two houses are identical in construction and thermal properties. A baseline generated in October 2012 for both houses indicated that the difference in energy performance is only 1-2 % at the start of the experiments and remains 0.5 % throughout the experiment. The experiments were conducted with the following conditions; building heated to a constant temperature of 25 C with electric heating, no internal heating generation and blinds closed [102].

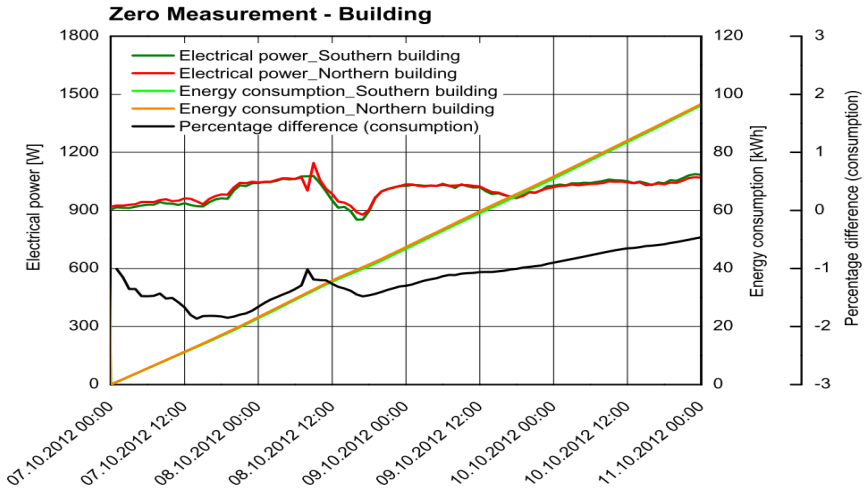

Figure 5.6: Comparative baseline of the twin houses[102]

The measurement experiments were conducted in the ground floor of the building with attic and loft temperatures used as external boundary conditions. Experiments were conducted in August and September with rollers on the southern sides of one building down and the other up. As experiments were conducted in hot season, a high ventilation rate was used to avoid overheating. Electric heaters are used for heating the indoor space. Each building was divided virtually into north (boundary zone) and south zones. The south zone consisted of living room, bedroom, bathroom and corridor that were sealed from the boundary zone that consists of cellar, attic, kitchen, north bedroom, hall and outdoor ambient as shown in Figure 5.7. The boundary space is kept at constant temperature of 22 °C.

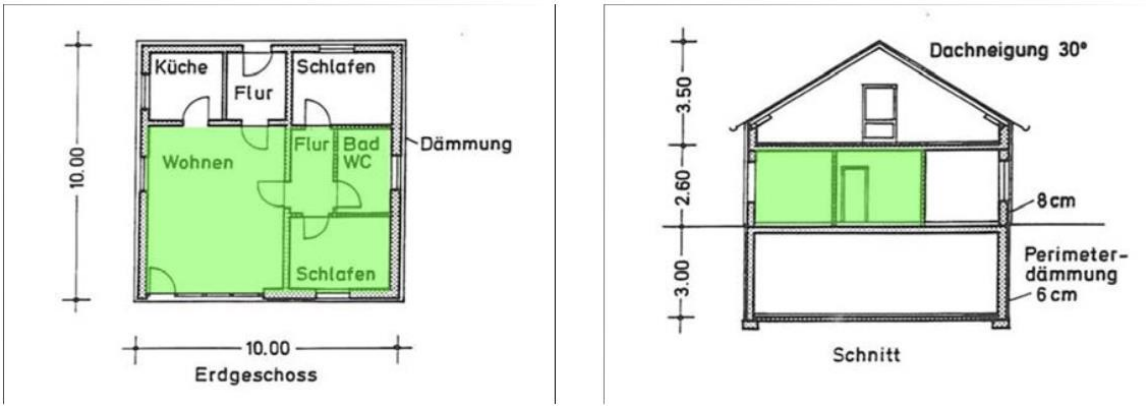

Figure 5.7: Cross-and vertical sections of controlled boundary conditions (Strachan et al., 2016)

Before running the experiment, air leakage was measured using blowing door test. The specifications for the thermal properties of the construction and the details of measurements, such as ground reflectivity and leakage data are provided [102]. Weather data was measured on the site by using a weather station. The experiments were conducted simultaneously in two buildings, with the sequence of heating as shown in Figure 5.8.

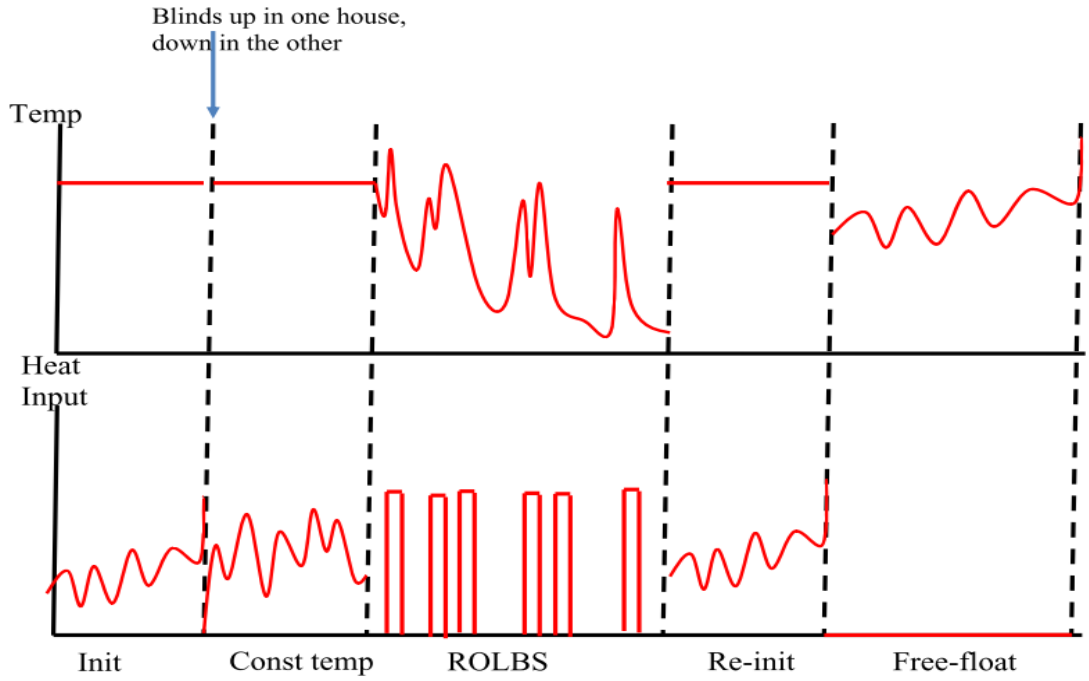

Figure 5.8: Sequence of application of heat during experiments (Strachan et al., 2016)

The experiments were performed with two houses, named as O5 and N5. The experiments in O5 house differ from those in N5 house by the operation of the southern windows. In N5, the roller blinds of the southern windows remain open during the initialization period. The experiment has two phases:

- **phase one**: temperature is kept constant with the objective to obtain the required input heat necessary for keeping temperature constant.
- **phase two**; temperature is allowed to float freely (no application of internal heat) and the objective is to simulate variation of indoor temperature with time.

The stepwise description of the experiments is:

1. Seven days initialization period when temperature was set at 30 °C in both houses. The south façade blinds were kept close during the initialization period.
2. Further 7 days the temperature was kept at 30 °C and the blinds in one house (N2) were lifted to let the solar radiations enter building.
3. Two weeks of randomly order logarithmic binary sequence for heating input was used in both buildings. The purpose of the ROLBS is to avoid any correlation between heating input and solar radiation for study purpose. The heat pulses ranged from 1 hour to 9 hours to ensure the entire range of time constant for building to be covered. The heat pulses were of 500 W in magnitude.
4. Seven days of a second re-initialization period to keep indoor temperature at 25 °C.
5. Seven days of free-floating (i.e. no heating) of both houses.

A ventilation rate of 120 m^3/h was maintained during the test period to avoid over heating of space. The data set provided with the twin house experiment can be used for model validation and design of experiments.

5.3 Conclusions

This chapter discussed the thermal characterization experiments conducted as part of IEA-EBC Annex 58 'Reliable building energy performance characterisation based on full scale dynamic measurements' [50]. It also discussed the data analysis procedures used to obtain reliable results. The analysis steps together with the data from the experiments can be used as a validation data for modelling and thermal characterization. The experiment and construction data used in the twin houses are used for validation of the model developed in this work (chapter 6) and for design of QUB experiments (chapters 7 and 9).

6 A new simulation model for testing the short-time measurement methods

A state space model presents a physical system in terms of inputs, outputs and state variables that are related to each other by first order differential equation. State-space representation is largely used in the theory of dynamic systems. The state space model can be used to model building in terms of a set of inputs such as outdoor temperature, solar radiations, wind speed, indoor heating etc. and outputs such as building indoor temperature with state variables such as the internal temperature of building components.

This chapter introduces a methodology for obtaining state-space representation from the thermal models of elementary components of a building in three steps:

1) generating thermal circuits for each component,
2) assembling thermal circuits,
3) extraction of state-space model from the thermal circuit.

This model is generated for the Twin Houses presented in Chapter 5.2 and tested with measurement data obtained from the IEA-ECB Annex 58 experiment. The model thus developed can be used for the analysis of the QUB method. With this modelling technique it is possible to estimate the time constants of the building and find the influence of increasing or decreasing the time duration of the QUB method. It allows us to increase or decrease the number of partitions of the building components and allows for ease of weather data with different sampling time.

6.1 Introduction

Thermal networks are graphic representations of systems of differential algebraic equations (DAE) which model heat transfer by conduction (described by the weak form of the heat equation [103]), convection (described by Newton law) and long wave radiative exchange

(described by using radiosity [104]). The resistor-capacitor (RC) models have physical meaning that allows the evaluation of the modelling hypothesis considered for buildings and their urban environment [105].

Thermal networks are used for defining the models of elementary components (e.g. walls, floors, doors, windows, etc.) in energy balance method [105 ,106]. Energy balance method is the recommended method of ASHRAE [108] and the basis of the CEN standard for calculation of the design heat load [109] as well as of other CEN standards related to thermal performance of buildings [109, 110]. Other procedures are seen as variants or simplifications of the heat balance method. In this method, the set of equations is integrated numerically, generally by using existing solvers. It is the case of many commercial simulation software [112] such as TRNSYS [113], EnergyPlus [114], IDA ICE [115], of research oriented tools, like ESP-r [116], CODYRUN [117] or of tools developed "in house" [118]–[122]. Another approach is to use equation-based modeling. In this case, the computational causality (i.e. the input – output relation) is defined after the model was constructed and can be changed. Then a simulation engine performs the calculations [121], [123], [124]. This has the advantage of using the same model for different sets of inputs and outputs but can generate ill-posed problems [125].

State-space is the most used input-output representation of linear models, as shown by recent reviews on modelling of building energy systems [116], [126] and on strategies for building energy management [127], [128]. State-space representation is widely used for model identification and calibration. In model identification, the structure of the model is proposed and then the parameters are identified by minimizing the error between the output of the model and the measured data. An essential issue is the structure of the model on which the experimental data is projected. This is done mostly empirically by using models with a variable number of states [129]–[132]. The procedure of model calibration is very similar to parameter identification: use optimization techniques to fit the model to data by changing the values of the parameters. The main difference is that the parameters obtained by calibration of physical models have physical significance [133]–[136].

State-space representation is widely used for model order reduction, which can be done numerically, when the state-space model is known, as is the case for walls, or by projecting the results obtained by simulation on a given structure [137]. A key point in model order reduction is the model order selection [138].

State-space model is the most used representation in modern control theory. One approach to obtain the state-space representation is to use a thermal network for the model of the building [139] and to identify the parameters of the state-space representation from input-output data [140][141][142][143]. Usually, the model used for controller synthesis has one state variable: the indoor temperature [143]–[149], although state-space models were obtained from the thermal network of a room for 4 states [150], 6 states [151] or for 17 states[152].

Since thermal networks are widely used for modelling heat transfer and state-space is the most used representation in control theory, state-space extraction from thermal networks is of the highest interest. A solution to obtain systematically the state-space representation is by using nodal/mesh analysis to reduce the number of undesired variables [153]. Another state-space extraction method uses the concepts of tree (a sub-graph of the original graph containing no loops) and co-tree (a sub-graph of the original graph containing the edges removed to form the tree) but it requires symbolic manipulation [153]. Commercial implementations of the state-space extraction are not documented [93].

6.2 Obtaining thermal circuit for state space modelling

All load calculation software, whether simulating variation of air temperature or estimating heating or cooling loads, are based on heat balance method [154]. Heat balance is essentially the first principle of conservation of energy, which states that “the total energy of an isolated system remains constant”. Since, in real world, no isolated system exists, the law of conservation of energy is stated in terms of net balance of energy entering, leaving, generated and stored in the system.

For an air volume inside a facility, such as building or room, load estimation is based on heat balance of air, which states that [154]

$$m_a c_a \frac{d\theta_a}{dt} = q_{ci} + q_v - \dot{Q}_g - \dot{Q}_{HVAC} \tag{6.1}$$

where

$m_a c_a \frac{d\theta_a}{dt}$ time variation of the heat stored in mass,

q_{ci} heat transfer from the enclosure surfaces/walls, such that:

$$q_{ci} = \sum_i S_i h_i (\theta_{si} - \theta_a) \tag{6.2}$$

where

S_i surface area;

θ_{si} surface area temperature;

q_v heat transferred by outdoor air infiltration and ventilation, such that $q_v = \dot{m}_v c_a (T_o - \theta_a)$;

$\dot{Q}_g$ longwave radiatios, sensible and latent heat from people, lights, home appliances, etc.;

$\dot{Q}_{HVAC}$ heat input from air-conditioning equipment, heaters, etc.

6.3 Thermal network models

The thermal model of a room, or any building, is represented by linear algebraic equations. Though the actual heat transfer is non-linear, it can be written as an infinite sum of linear algebraic equations. The set of linear equations representing the heat transfer of a room are combined in state-space form [154]. For ease of manipulation and comprehension, it is

convenient to present heat transfer equations in form of thermal resistance circuits, analogous to electrical circuits Figure 6.1.

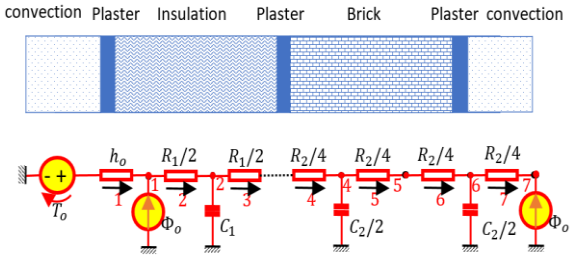

Figure 6.1 Representation of a wall heat transfer by a thermal circuit

The elements of thermal circuit represent thermal resistance, capacitance, flow rate sources, such as solar radiation, and temperature sources, such as outdoor temperature. The difference between thermal and electric circuits is that thermal circuits do not contain any inductance [154]. As an example, the temperature difference across any node is (Figure 6.1):

$$e_k = \theta_{l-1} + b_k - \theta_l \tag{6.3}$$

where θ_{l-1} and θ_l are the temperatures in the nodes $l-1$ and l, connecting branch k via resistance R_k and b_k is the temperature source. The term b_k can be either an external temperature source, such as outside air temperature, or an internal temperature source (part of internal heat source).

As a building or a single room consists of multiple walls, the heat balance has a number of thermal circuits presented mathematically by differential equations. These equations are coupled as it is convenient to represent all thermal circuits in state space. The temperature difference over all nodes in Figure 6.1 is presented in matrix form:

$$\mathbf{e} = -\mathbf{A}\boldsymbol{\theta} + \mathbf{b} \tag{6.4}$$

where

$\mathbf{e} = [e_1, e_2, \ldots \ldots . e_n]^T$ is the vector of temperature drop across a resistor,

$\boldsymbol{\theta} = [\theta_1, \theta_2 \ldots \ldots . \theta_n]^T$ is the vector of temperature nodes,

$\mathbf{b} = [b_1, b_2, \ldots \ldots . b_n]^T$ is the vector of temperature sources on each branch.

The matrix $\mathbf{A}$ is the incidence matrix whose elements show the presence of resistances and direction of heat flows towards or away from the node. The rows of the incidence matrix show the heat flow branches between two nodes; the columns show the nodes of thermal circuit. In a row corresponding to a branch, 1 or 0 presents whether the branch is connected to a particular node or not. The sign of the node shows whether heat is entering or leaving the node. The element $\boldsymbol{a}_{kl}$ of the matrix **A** corresponding to branch k and node l is:

$$a_{kl} = \begin{cases} 0, & \text{if branch is not connected to node} \\ +1, & \text{if heat is flowing towards node} \\ -1, & \text{if heat is moving away from node} \end{cases} \quad (6.5)$$

Heat transfer across any thermal resistor/branch is

$$q_k = R_k^{-1} e_k \quad (6.6)$$

where R_k is the thermal resistance. For the wall presented in Figure 6.1, the insulation and the brick layers form the branches. The number of branches and nodes depend on the number of slices of each wall layer of material. Accounting for all heat transfers the matrix form of equation (6.6) is

$$\mathbf{q} = \mathbf{G}e \quad (6.7)$$

where

$\mathbf{q} = [q_1 \ldots q_k, \ldots \ldots . q_m]^T$ is the vector of heat rates in branches;

$\mathbf{G} = \begin{bmatrix} R_1^{-1} & 0 & 0 \\ 0 & \ddots & 0 \\ 0 & 0 & R_m^{-1} \end{bmatrix}$, is a diagnol matrix of conductivities

The heat balance for any node consists of the sum of heat entering and leaving the nodes and the heat sources connected to a node is

$$C_l \dot{\theta}_l = \sum_l q_l + f_l \tag{6.8}$$

where C_l is the capacitance of the node, q_l represents heat entering or leaving the node and f_l is the heat source, input to the node. The heat balance for all the nodes is

$$\mathbf{C}\dot{\boldsymbol{\theta}} = \mathbf{A^T q} + \mathbf{f} \tag{6.9}$$

The matrix of capacitances is:

$$\mathbf{C} = \begin{bmatrix} C_1 & 0 & 0 \\ 0 & \ddots & 0 \\ 0 & 0 & C_n \end{bmatrix}$$

where $\mathbf{A^T}$, the transpose of the incidence matrix, represents the algebraic sum of all heat exchange rates,

$\mathbf{f} = [f1, f_2, \dots f_l \dots . f_n]^T$, is the vector of heat sources across nodes.

By substituting in equation (6.10), we obtain:

$$\mathbf{C}\dot{\boldsymbol{\theta}} = -\mathbf{A^T G A \theta} + \mathbf{A^T G b} + \mathbf{f} \tag{6.10}$$

The matrices in equation (6.10), can be partitioned based on nodes with capacitances and without capacitance as

$$\begin{bmatrix} 0 & 0 \\ 0 & \mathbf{C}_c \end{bmatrix} \begin{pmatrix} \dot{\boldsymbol{\theta}}_o \\ \dot{\boldsymbol{\theta}}_c \end{pmatrix} = \begin{bmatrix} \mathbf{K}_{11} & \mathbf{K}_{12} \\ \mathbf{K}_{21} & \mathbf{K}_{22} \end{bmatrix} \begin{bmatrix} \boldsymbol{\theta}_o \\ \boldsymbol{\theta}_c \end{bmatrix} + \begin{bmatrix} \mathbf{K}_{b1} \\ \mathbf{K}_{b2} \end{bmatrix} b + \begin{bmatrix} \mathbf{I}_{11} & 0 \\ 0 & \mathbf{I}_{22} \end{bmatrix} \begin{bmatrix} \mathbf{f}_o \\ \mathbf{f}_c \end{bmatrix} \tag{6.11}$$

The state space form of the equation depends on the air capacitance. If it is non-negligible, than $\boldsymbol{\theta}_a$(air temperature) can be obtained as output of the state space model

$$\begin{aligned} \dot{\boldsymbol{\theta}}_c &= \mathbf{A}_s \boldsymbol{\theta}_c + \mathbf{B}_s \mathbf{u} \\ \boldsymbol{\theta}_a &= \mathbf{C}_s \boldsymbol{\theta}_c + \mathbf{D}_s \mathbf{u} \end{aligned} \tag{6.12}$$

where

$\mathbf{A}_s = \mathbf{C}_c^{-1}[-\mathbf{K}_{21}\mathbf{K}_{11}^{-1}\mathbf{K}_{12} + \mathbf{K}_{22}\,]$,
$\mathbf{B}_s = \mathbf{C}_c^{-1}[-\mathbf{K}_{21}\mathbf{K}_{11}^{-1}\mathbf{K}_{b1} + \mathbf{K}_{b2} - \mathbf{K}_{21}\mathbf{K}_{11}^{-1}\,\mathbf{I}_{22}\,]$,
$\boldsymbol{u} = [b\ f_0\ f_c]^T$ is the input vector,
$\boldsymbol{\theta}_a$ is the air temperature
$\mathbf{D}_s$ is feedthrough matrix that is zero in case of non-negligible air capacity and
$\mathbf{C}_s$ extracts the air temperature $\boldsymbol{\theta}_a$.

In case of negligible air capacity,

$$\boldsymbol{\theta}_0 = \mathbf{C}_s \boldsymbol{\theta}_c + \mathbf{D}_s \mathbf{u} \tag{6.13}$$

where

$\mathbf{C}_s = -\mathbf{K}_{21}\mathbf{K}_{11}^{-1}$ and $\mathbf{D}_s = \mathbf{K}_{11}^{-1}[\mathbf{K}_{b1}\ \mathbf{I}_{11}\ 0]$.
$\boldsymbol{\theta}_a$ is obtained from the vector of $\boldsymbol{\theta}_0$.

6.4 Assembling the thermal circuits

It is easy and convenient to obtain thermal circuits for different elements of the building (walls, floors, windows, doors, etc.). Then, the model of a whole building may be obtained by

assembling the elements. Assembling is different from coupling. In coupling, the models of the elements form a set of equations which is solved numerically; in assembling, the model of the whole building is obtained first and then the system of equations is solved. The advantage of assembling is that the model can be analyzed: the eigenvalues and the eigenvectors of the whole system can be obtained.

The problem of circuit assembling is to obtain the thermal circuit TC by knowing that some nodes of the elementary circuits $TC_1,\ TC_2, \dots,\ TC_n$ are common to several circuits. Since a thermal circuit is described by the set of arrays, $TC = \{\mathbf{A}, \mathbf{G}, \mathbf{b}, \mathbf{C}, \mathbf{f}, \mathbf{y}\}$, the aim of assembling is to form the global system:

$$\begin{bmatrix} \mathbf{G}^{-1} & \mathbf{A} \\ -\mathbf{A}^T & \mathbf{C}_S \end{bmatrix} \begin{bmatrix} \mathbf{q} \\ \boldsymbol{\theta} \end{bmatrix} = \begin{bmatrix} \mathbf{b} \\ \mathbf{f} \end{bmatrix} \tag{6.14}$$

or, by using the notations:

$$\mathbf{K} \equiv \begin{bmatrix} \mathbf{G}^{-1} & \mathbf{A} \\ -\mathbf{A}^T & \mathbf{C}_S \end{bmatrix};\ \mathbf{u} \equiv \begin{bmatrix} \mathbf{q} \\ \boldsymbol{\theta} \end{bmatrix};\ \mathbf{a} \equiv \begin{bmatrix} \mathbf{b} \\ \mathbf{f} \end{bmatrix} \tag{6.15}$$

to form the equation:

$$\mathbf{K}\mathbf{u} = \mathbf{a} \tag{6.16}$$

from the models of the elementary systems (walls, floors, doors, windows, etc.):

$$\begin{bmatrix} \mathbf{G}_i^{-1} & \mathbf{A}_i \\ -\mathbf{A}_i^T & \mathbf{C}_i S \end{bmatrix} \begin{bmatrix} \mathbf{q}_i \\ \boldsymbol{\theta}_i \end{bmatrix} = \begin{bmatrix} \mathbf{b}_i \\ \mathbf{f}_i \end{bmatrix} \tag{6.17}$$

We can write equation (6.16) as

$$\mathbf{K}_i \mathbf{u}_i = \mathbf{a}_i \tag{6.18}$$

where

$$\mathbf{K}_i \equiv \begin{bmatrix} \mathbf{G_i^{-1}} & \mathbf{A}_i \\ -\mathbf{A_i^T} & \mathbf{C}_i s \end{bmatrix}; \mathbf{u}_i \equiv \begin{bmatrix} \mathbf{q}_i \\ \boldsymbol{\theta}_i \end{bmatrix}; \mathbf{a}_i \equiv \begin{bmatrix} \mathbf{b}_i \\ \mathbf{f}_i \end{bmatrix} \tag{6.19}$$

Let's note the dissembled block matrix $\mathbf{K}_d$ and the disassembled block vectors $\mathbf{u}_d$, $\mathbf{a}_d$, the matrix and the vectors obtained by simply placing in order the matrices and the vectors of the elementary models described by equation (6.20) **Erreur ! Source du renvoi introuvable.**:

$$\mathbf{K}_d \equiv \begin{bmatrix} \mathbf{K}_1 & \dots & \mathbf{0} \\ \vdots & \ddots & \vdots \\ \mathbf{0} & \dots & \mathbf{K}_n \end{bmatrix} \mathbf{u}_d \equiv \begin{bmatrix} \mathbf{u}_1 \\ \vdots \\ \mathbf{u}_n \end{bmatrix}; \ \mathbf{a}_d \equiv \begin{bmatrix} \mathbf{a}_1 \\ \vdots \\ \mathbf{a}_n \end{bmatrix} \tag{6.20}$$

There is a disassembling matrix $\mathbf{A}_d$ which transforms the assembled vectors $\mathbf{a}$ and $\mathbf{u}$ into the dissembled vectors $\mathbf{a}_d$ and $\mathbf{u}_d$ as:

$$\mathbf{a}_d = \mathbf{A}_d \mathbf{a}; \mathbf{u}_d = \mathbf{A}_d \mathbf{u}. \tag{6.21}$$

The relations between the global and the elementary matrices and vectors are:

$$\mathbf{K} = \mathbf{A}_d^T \mathbf{K}_d \mathbf{A}_d \tag{6.22}$$

$$\mathbf{u} = \mathbf{A}_d^T \mathbf{u}_d \tag{6.23}$$

$$\mathbf{a} = \mathbf{A}_d^T \mathbf{a}_d \tag{6.24}$$

The elements of the assembled circuit, $TC = \{\{\mathbf{A}, \mathbf{G}, \mathbf{b}, \mathbf{C}, \mathbf{f}, \mathbf{y}\}$, are then obtained from the partition of the arrays:

$$\mathbf{K} = \begin{bmatrix} \mathbf{G}^{-1} & \mathbf{A} \\ -\mathbf{A}^{\mathbf{T}} & \mathbf{C}s \end{bmatrix}; \mathbf{u} = \begin{bmatrix} \mathbf{q} \\ \boldsymbol{\theta} \end{bmatrix}; \mathbf{a} = \begin{bmatrix} \mathbf{b} \\ \mathbf{f} \end{bmatrix} \tag{6.25}$$

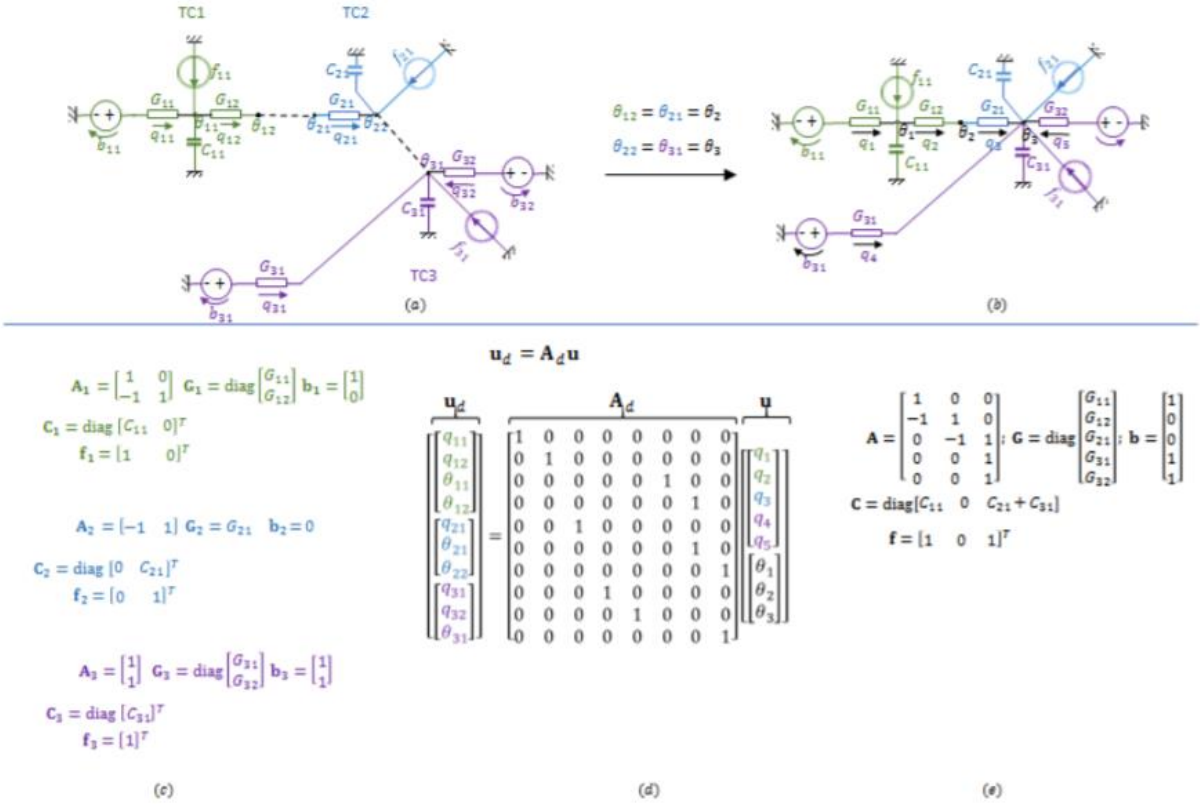

Figure 6.2 Simple example for the assembling of thermal circuits: a) three disassembled circuits with local indexing of nodes and branches (the dashed lines show the nodes which are in common); b) the assembled circuit with local and global indexing of nodes and branches; c) the matrices and the vectors characterizing the disassembled thermal circuits; d) the disassembling matrix and the transformation of the assembled vector into disassembled vectors; e) the matrices and the vectors characterizing the assembled thermal circuit.

An illustrative example is given in Figure 6.2. There are three circuits:

- TC1 with two branches and two nodes,
- TC2 with one branch and two nodes,
- TC3 with two branches and one node.

The second node of TC1 is put in common with the first node of TC2 and the second node of TC2 is put in common with the first node of TC3 (Figure 6.2a). The local indexes of the dissembled circuits correspond to global indexes in the assembled circuit (Figure 6.2b). Each disassembled circuit is characterized by the set of arrays $TC_i = \{\mathbf{A}_i, \mathbf{G}_i, \mathbf{b}_i, \mathbf{C}_i, \mathbf{f}_i, \mathbf{y}_i\}$, where $i = 1, 2, 3$, with values given by equations of each circuit (Figure 6.2c). The disassembling matrix, $\mathbf{A}_d$, transforms the assembled variables, $\mathbf{u}$, into disassembled variables, $\mathbf{u}_d$ (Figure 6.2d). Finally, the assembled circuit is characterized by a set of arrays, $TC = \{\mathbf{A}, \mathbf{G}, \mathbf{b}, \mathbf{C}, \mathbf{f}, \mathbf{y}\}$ (Figure 6.2e).

6.5 Extract state-space model from thermal circuits

If the thermal circuit contains nodes without heat capacity, the matrix $\mathbf{C}$ is singular. In order to obtain the state-space model, the equations corresponding to the nodes without heat capacity need to be eliminated from the system of equations (6.10). By partitioning the matrix $\mathbf{C}$,

$$\mathbf{C} = \begin{bmatrix} \mathbf{0} & \mathbf{0} \\ \mathbf{0} & \mathbf{C}_C \end{bmatrix} \tag{6.26}$$

where $\mathbf{C}_C$ corresponds to the nodes having capacities, the set of equations (6.10) may be written as:

$$\begin{bmatrix} \mathbf{0} & \mathbf{0} \\ \mathbf{0} & \mathbf{C}_C \end{bmatrix} \begin{bmatrix} \dot{\boldsymbol{\theta}}_0 \\ \dot{\boldsymbol{\theta}}_C \end{bmatrix} = \begin{bmatrix} \mathbf{K}_{11} & \mathbf{K}_{12} \\ \mathbf{K}_{21} & \mathbf{K}_{22} \end{bmatrix} \begin{bmatrix} \boldsymbol{\theta}_0 \\ \boldsymbol{\theta}_C \end{bmatrix} + \begin{bmatrix} \mathbf{K}_{b1} \\ \mathbf{K}_{b1} \end{bmatrix} \mathbf{b} + \begin{bmatrix} \mathbf{I}_{11} & \mathbf{0} \\ \mathbf{0} & \mathbf{I}_{22} \end{bmatrix} \begin{bmatrix} \mathbf{f}_0 \\ \mathbf{f}_C \end{bmatrix} \tag{6.26}$$

where:

$\boldsymbol{\theta}_0$ and $\mathbf{f}_0$ correspond to the nodes without thermal capacity;

$\boldsymbol{\theta}_C$ and $\mathbf{f}_C$ correspond to the nodes with thermal capacity;

$\mathbf{C}_C$ is the bloc of the partitioned matrix $\mathbf{C}$ for which the elements on the diagonal are non-zero;

$\mathbf{K}_{11}$, $\mathbf{K}_{12}$, $\mathbf{K}_{21}$, and $\mathbf{K}_{22}$ are blocs of the partitioned matrix $\mathbf{K}$ obtained according to the partioning of the matrix $\mathbf{C}$;

$\mathbf{K}_{b1}$ and $\mathbf{K}_{b2}$ are blocs of the partitioned matrix $\mathbf{K}_b$ obtained according to the partitioning of the matrix $\mathbf{C}$;

$\mathbf{I}_{11}$ and $\mathbf{I}_{22}$ are identity matrices.

The state equation of the state-space model is:

$$\dot{\boldsymbol{\theta}}_C = \mathbf{A}_S\boldsymbol{\theta}_C + \mathbf{B}_S\mathbf{u} \qquad (6.27)$$

where the state matrix is:

$$\mathbf{A}_S = \mathbf{C}_C^{-1}(-\mathbf{K}_{21}\mathbf{K}_{11}^{-1}\mathbf{K}_{12} + \mathbf{K}_{22}) \qquad (6.27)$$

and the input matrix is:

$$\mathbf{B}_S = \mathbf{C}_C^{-1}[-\mathbf{K}_{21}\mathbf{K}_{11}^{-1}\mathbf{K}_{b1} + \mathbf{K}_{b2} \quad -\mathbf{K}_{21}\mathbf{K}_{11}^{-1} \quad \mathbf{I}] \qquad (6.28)$$

If the outputs are temperatures of nodes with capacities, the observation matrix $\mathbf{C}_S$ extracts their values from the state vector and the feed-through matrix is $\mathbf{D}_S = \mathbf{0}$. If the outputs are temperatures from nodes without capacities, the observation equation can be obtained from the first row of equation (5.26):

$$\begin{aligned}\boldsymbol{\theta}_0 &= -\mathbf{K}_{\mathbf{11}}^{-\mathbf{1}}(\mathbf{K}_{12}\boldsymbol{\theta}_C + \mathbf{K}_{b1}\mathbf{b} + \mathbf{I}_{11}\mathbf{f}_0) \\ &= -\mathbf{K}_{\mathbf{11}}^{-\mathbf{1}}\left(\mathbf{K}_{12}\boldsymbol{\theta}_C + [\mathbf{K}_{b1} \quad \mathbf{I}_{11} \quad \mathbf{0}]\begin{bmatrix}\mathbf{b}\\ \mathbf{f}_0\\ \mathbf{f}_C\end{bmatrix}\right)\end{aligned} \tag{6.29}$$

Then, the output equation is:

$$\mathbf{C}_S = -\mathbf{K}_{11}^{-1}\,\mathbf{K}_{12} \tag{6.30}$$

and the feed through matrix is:

$$\mathbf{D}_S = -\mathbf{K}_{11}^{-1}[-\mathbf{K}_{b1} \quad \mathbf{I}_{11} \quad \mathbf{0}] \tag{6.31}$$

6.6 Model construction by assembling: a proposal for BIM application

In Building Information Modelling (BIM), the building components (such as walls, doors, windows, etc.) are software "objects" with specific properties (such as thermal characteristics). These "objects" need to be parametrizable, i.e. adjust their width, position, number of meshes for numerical discretization, etc. [155].

The assembling method proposed in this paper can be used for BIM objects. For the model of a house, six types of BIM "objects" may be defined (Figure 6.3). The outdoor walls have as boundary conditions on the outdoor surface the temperature, T_o, and short-wave and long-wave thermal radiation, Φ_o, and on the indoor surface the short-wave and long-wave thermal radiation, Φ_i. The wall can be composed of an arbitrary number of materials, such as brick and insulation, each one discretized in an arbitrary number of meshes, depending on the frequency to which the model needs to respond (Figure 6.3 Type 1: Outdoor wall). The model

for each mesh, composed by two thermal resistances and a thermal capacity, is obtained by the finite volume method [112].

The inner wall is defined in a similar way as the outdoor wall, with the difference that the boundary conditions are heat flow rates (Figure 6.3, Type 2: Inner wall). The doors and windows are considered without a thermal capacity (Figure 6.3, Types 3 and 4).

Ventilation is modelled as a conductance with the value

$$G = \dot{m}_{inf} c_a \tag{6.32}$$

where $\dot{m}_{inf}$ is the mass flow rate of the air and c_a is the specific heat of the air.

A complex model can be obtained by assembling the parameterizable types to form rooms; the transformation from the set of "objects" to an assembled circuit is done by the dissembling matrix, $\mathbf{A}_d$, as indicated in equations (6.21)-(6.24). For example, Figure 6.3 shows a single room, the living room. The air in the room (object 13) is connected to 12 other objects through convective resistances; e.g. node 9 of object 13 is connected to node *end* of object 9 of type 1. The outdoor temperature, T_o, and the convective heater, $\dot{Q}_{heater}$, are inputs for the indoor air Figure 6.3.

Once the model of a room is done, it can be assembled with the model of another room. For example, Figure 6.5 shows the assembling of the living room, and shows the assembling of seven thermal zones.

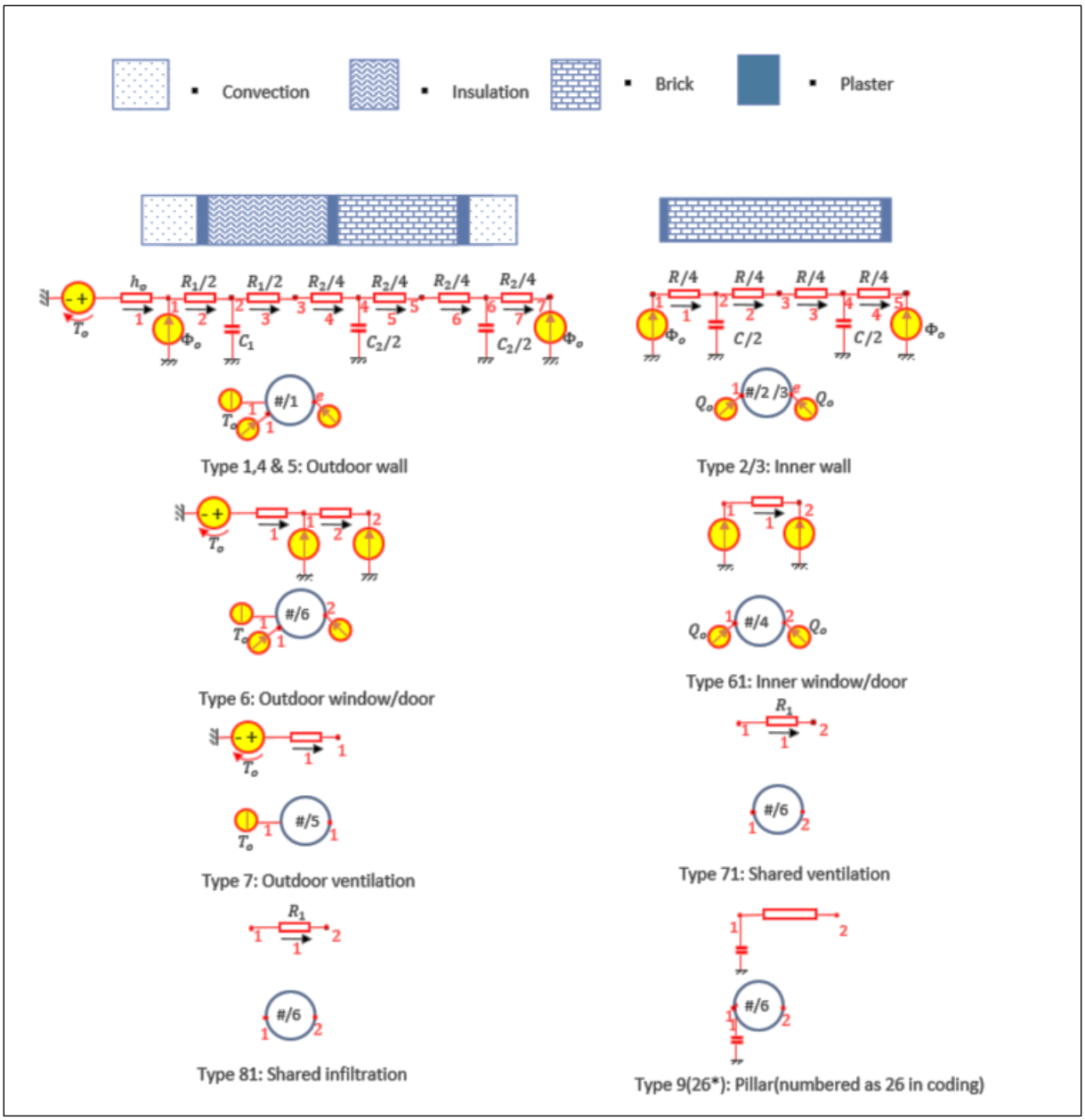

Figure 6.3: Building components, thermal circuits and their symbols

6.7 Eigenvalues, time step and response time

An important advantage of the assembling over coupling is that in assembling a single circuit is obtained, which can be transformed in state-space representation. This allows us to obtain the eigenvalues and the eigenvectors of the state matrix, which have many applications.

The time step of the simulation depends on the frequency spectrum of the inputs and on the frequencies to which the output needs to be analyzed. The eigenvalues of the state matrix were used to determine the maximum time step for simulation,

$$\Delta t \leq \min \frac{T_i}{2} \tag{6.33}$$

where the time constants, T_i, are found from the eigenvalues, λ_i:

$$T_i = -\frac{1}{\lambda_i} \tag{6.34}$$

Considering, for example, the living room. If the dynamics of the air into the room need to be modelled, the time step needs to be less than 360 s or 6 min. This time step requires that the insulation of the outdoor wall is divided in 4 meshes and the brick is divided in 8 meshes.

Another important application of the eigenvalues is to find the response time, which is 3 … 4 times the largest time constant. For the model of the living room, the largest time constant is 234 h = 9.7 days. It means that simulations need to be done for about 30 days in order to obtain the good initial conditions.

6.8 Experimental protocol

The state space model developed in sections (6.2,6.3,6.4 and 6.5) is validated by using data from the IEA,EBC annex-58 (the Twin House experiment). The experiment setup is discussed in details in chapter 0. The experiment was conducted for 41 days in summer 2013 starting with an initialization period of 7 days followed by a period of 7 days with a heating set point of 30 °C in all rooms. The constant temperature period was followed by a Randomly Ordered Logarithmic Binary Sequence of heat inputs (ROLBS) for 15 days. A 500 W heating power was supplied only in the living room during the ROLBS period. The time period for heat pulses

ranged from 1 hour to 90 hours. The ROLBS period was followed by a re-initialization period for 7 days with a heating set point of 25 °C in all rooms. For the final 11 days of the experiment, no heat input was supplied and the temperature was allowed to float freely [156].

6.9 Model of the Twin House

The experimental house consists of seven thermal zones: kitchen, living room, doorway, bedroom 1, bathroom, corridor and bedroom 2. Internal temperature is simulated for living room (single zone), kitchen & living room (two zones), and entire twin house (seven zones), respectively.

A thermal circuit for each building element (wall, roof, window, door, etc.) is obtained by using techniques discussed in section (6.2) (Figure 6.4). The spatial discretization of the building elements can be changed according to the frequency response desired for the system. The wall thermal capacity is located in the middle of each mesh.

All thermal properties are considered constant in time. In simulation, the solar radiation on walls and windows is taken from measurements done directly on the building surface and from calculations from the measurement on a horizontal surface; both approaches give very similar results.

Solar radiation entering the twin house through windows is calculated as a function of varying solar transmittance that changes with the angle of incidence of the solar radiation. According to the manufacturer, the heat from heaters is split in thirty percent radiation and seventy percent convection [102]. The same split of heat input from the heater is considered in simulation. A detailed description of the twin house construction, experiments and data is given in Annex 11-11

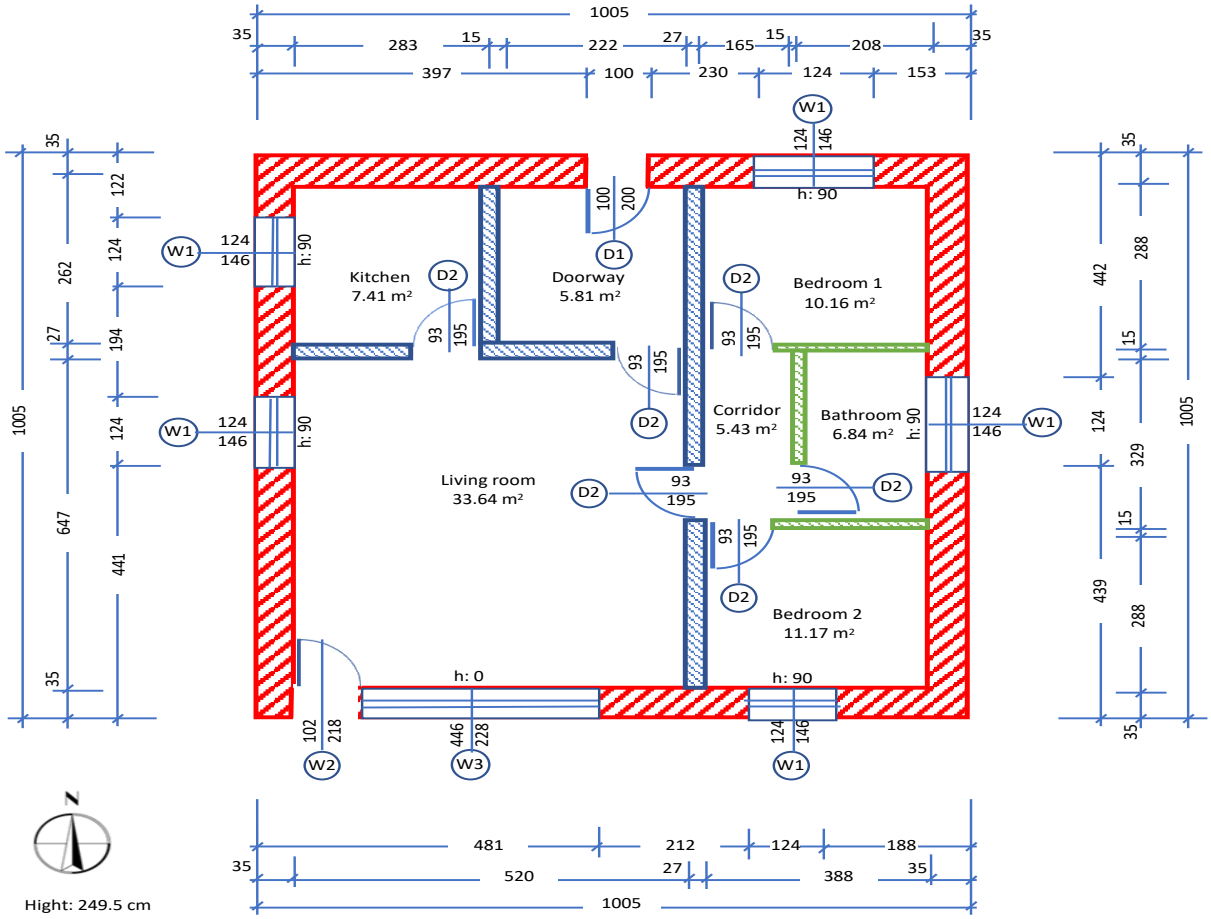

Figure 6.4 Layout and dimensions of ground floor of twin house

The thermal circuits generated for each zone are assembled as discussed in sections 6.3 and 6.4. The state space model for the assembled circuits is generated as discussed in section 6.5. The measured data has a time step of 10 minutes. The simulation is done at a time step of 5 minutes.

6.9.1 Single zone model (Living room)

Living room is modelled as a single thermal zone. The conditions of spaces adjacent to living room are considered as boundary zones, as shown in Figure 6.5. The living room is bounded by kitchen wall, kitchen door, doorway wall, doorway door, corridor wall, bedroom wall, Southern external wall, southern window, Eastern wall and Eastern window.

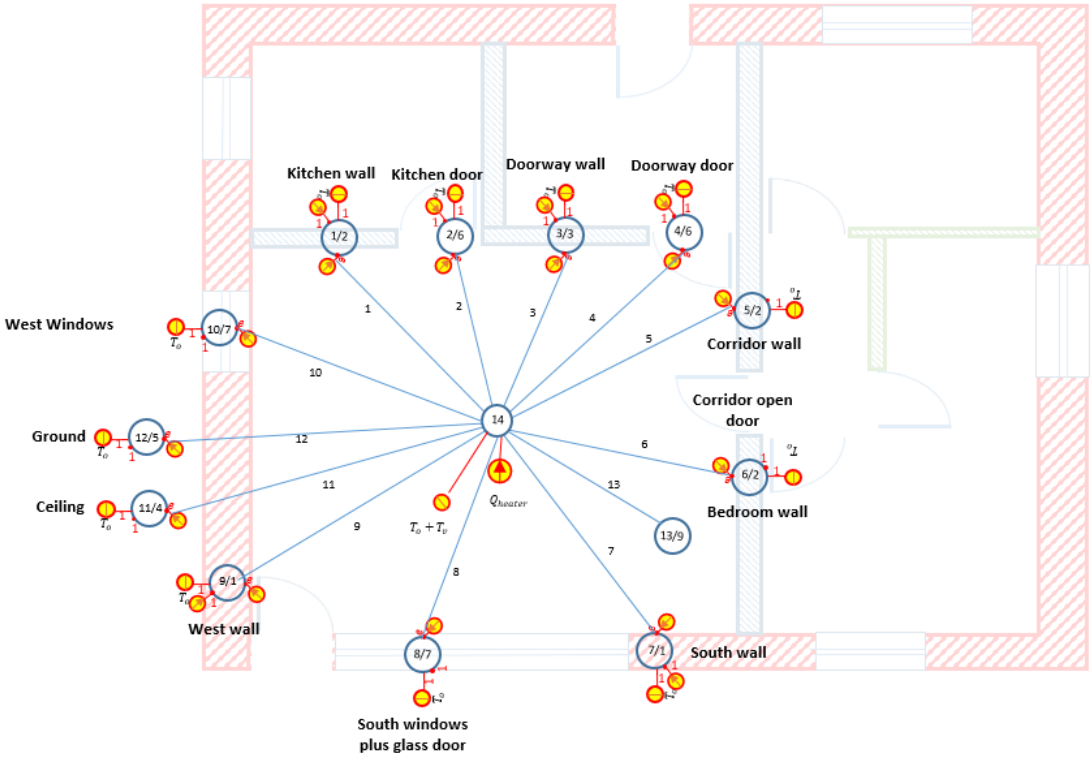

Figure 6.5: Thermal circuit connections for living room zone

Figure 6.5 shows the connection of each thermal circuit (wall, windows, ceiling etc.) with room air. The model of the living room consists of 13 thermal circuits (building elements). The numbering of each circuit and the position of each input to thermal circuit is shown in Figure 6.5. Thermal circuit number 13 represents the air node, which receives heat transferred from 12 thermal circuits that model the building elements.

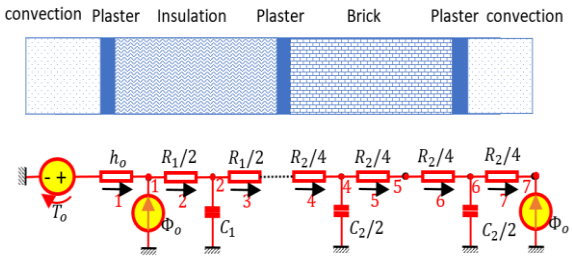

Figure 6.6 Representation of a wall heat transfer by a thermal circuit

Each wall is modelled as an RC (resistances and capacitances) circuit with adjustable number of slices. The air inside the living room is modelled as homogeneous node exchanging heat with different surfaces via branches as shown in Figure 6.7

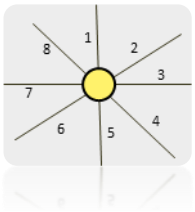

Figure 6.7: Air nodes with braches connecting different walls and components of living room

All the circuits once modelled are assembled and connected with the air node. The indoor temperature is simulated using three methods numerical integration methods: Euler explicit, Euler Implicit and exponential.

In Figure 6.8, the simulation results (in red) as compared to the actual measured internal temperature (in green). The histogram show that errors are within range of $\pm 0.5℃$

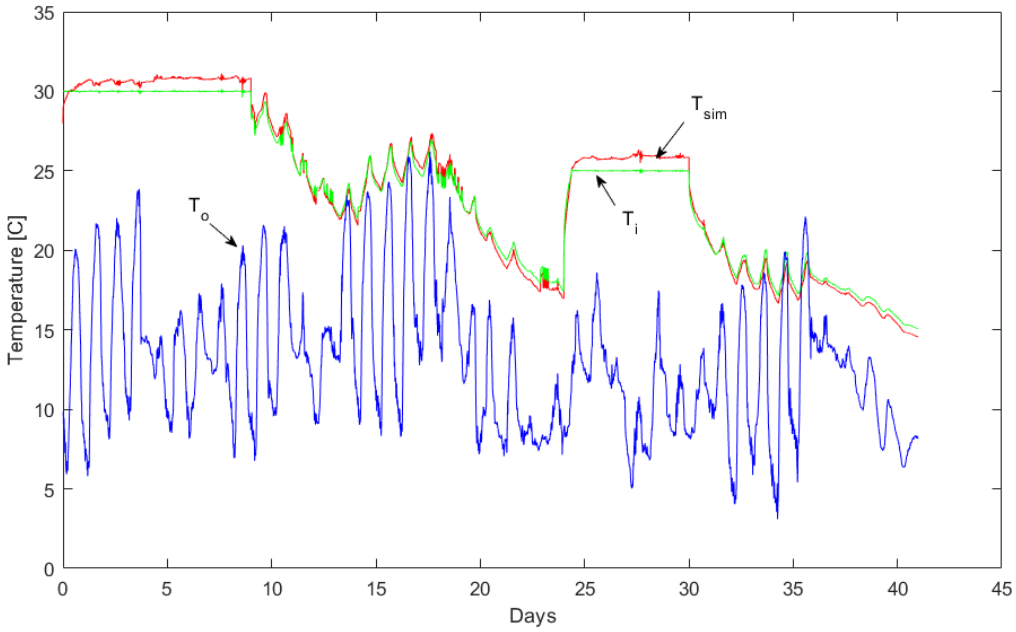

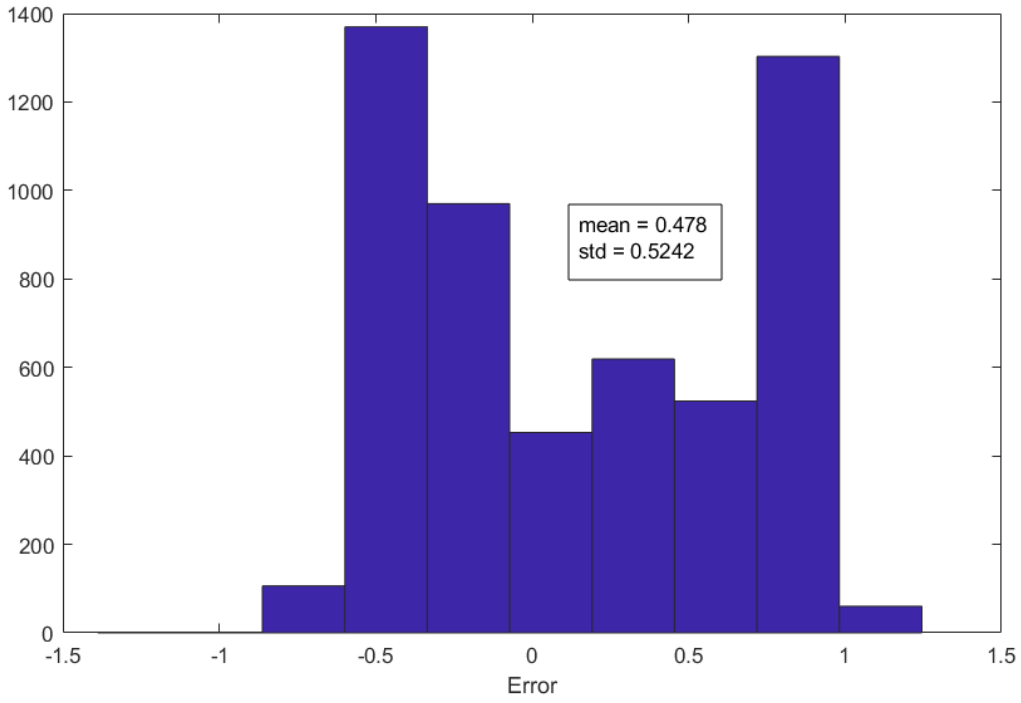

Figure 6.8: Temperature simulation and histogram of errors, showing that error is between -0.5 and +0.5

6.9.2 Two zones model (Kitchen and Living room)

The kitchen and the living room were modelled together to validate the assembling and the state-space methodologies discussed in sections (6.2,6.3,6.4 and 6.5). The kitchen and the living room share an internal wall and a door. Although the shared door is sealed, there is infiltration of air between the two rooms, equivalent to 1/3rd of the infiltration between North and South zones. The ventilation supply duct passing through the kitchen is uninsulated and is responsible for loss of heat from the kitchen. The heat losses to ventilation duct are provided in the experimental data and are incorporated in the simulation.

The total number of thermal circuits for the two zones is nineteen (Figure 6.9). All zones external to the kitchen and the living room are considered boundary conditions for the model. The number of state variables in the assembled model is 57.

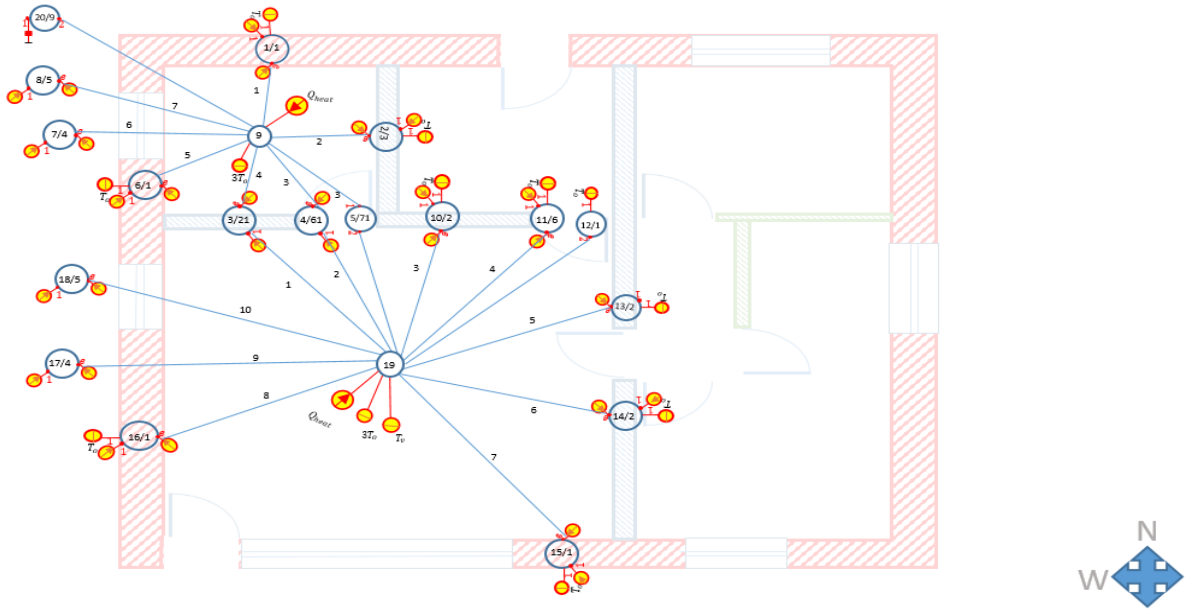

Figure 6.9: Thermal circuit diagram for living room and kitchen

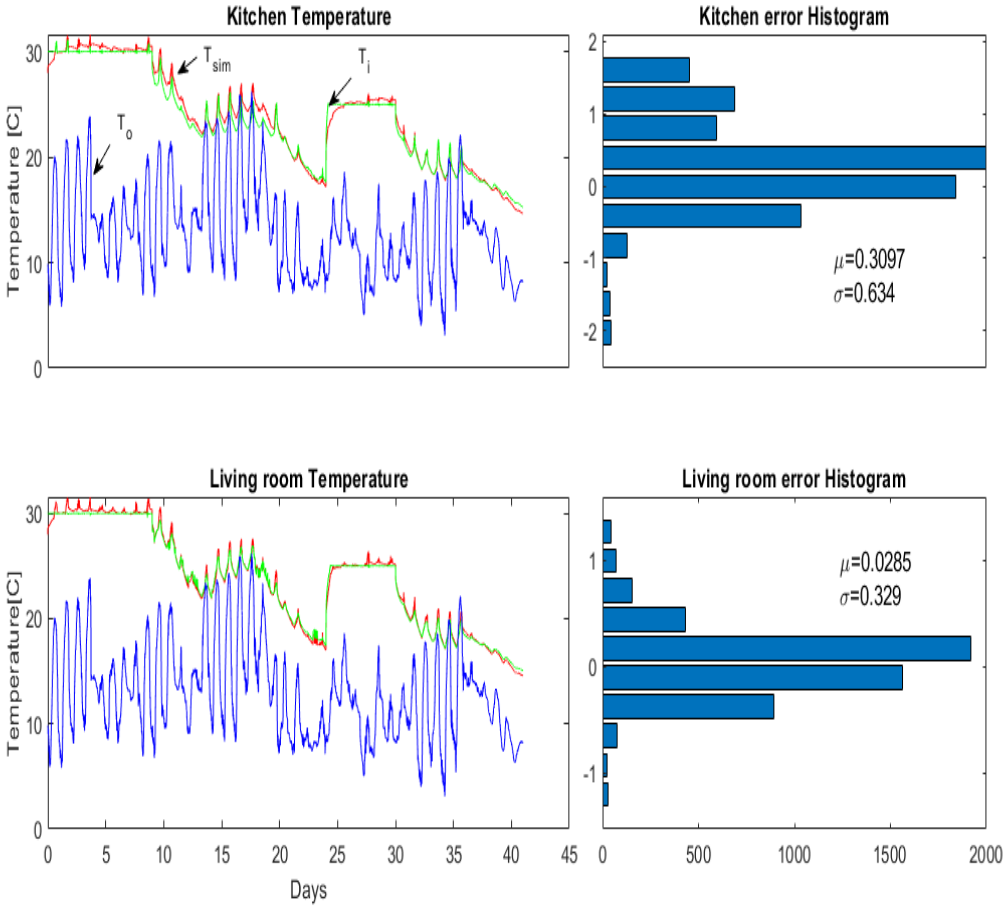

Figure 6.10: Simulation of living room and kitchen temperatures

The results of simulation for two zones along with error histogram are shown in Figure 6.10. The modelling errors lie within -1 to $+1.5℃$. The increase in error coincide with the peak solar radiation hours.

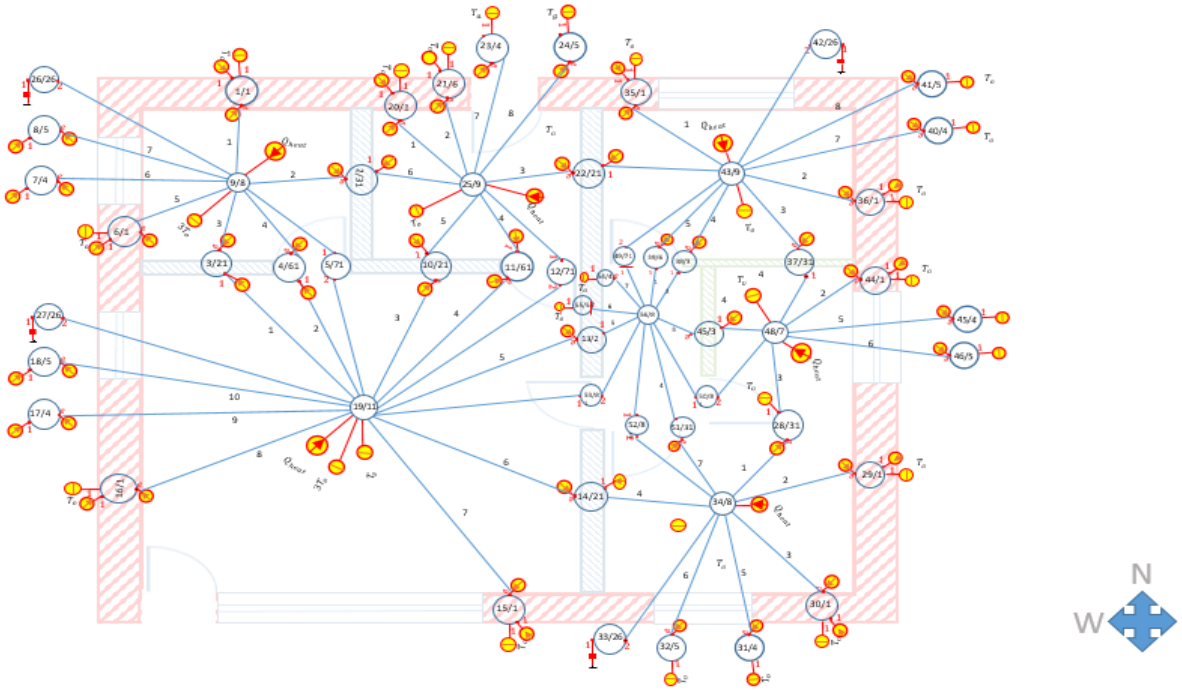

Figure 6.11: Thermal circuit diagram for all zones of twin house

6.9.3 All zones model

The model for the whole house consists of seven thermal zones that are modelled by assembling 56 thermal circuits (Figure 6.11). The number of states in the final state-space model is 109. The simulation error increases with the number of zones, which is explained by the errors induced in the values of boundary conditions (Figure 6.12). For example, when only the living room is simulated, the boundary temperatures are the measurements of the temperatures of adjacent rooms (Figure 6.7); when the whole house is simulated, the boundary temperatures for the living room are state variables that are simulated with an error (Figure 6.12). The simulation results show that, for every zone, three quantiles of simulated temperature lie within $\pm 1℃$. These results are similar to the best results obtained in a benchmark of 21 modelling teams using commercial and research simulation programmes (Strachan, et al., 2016).

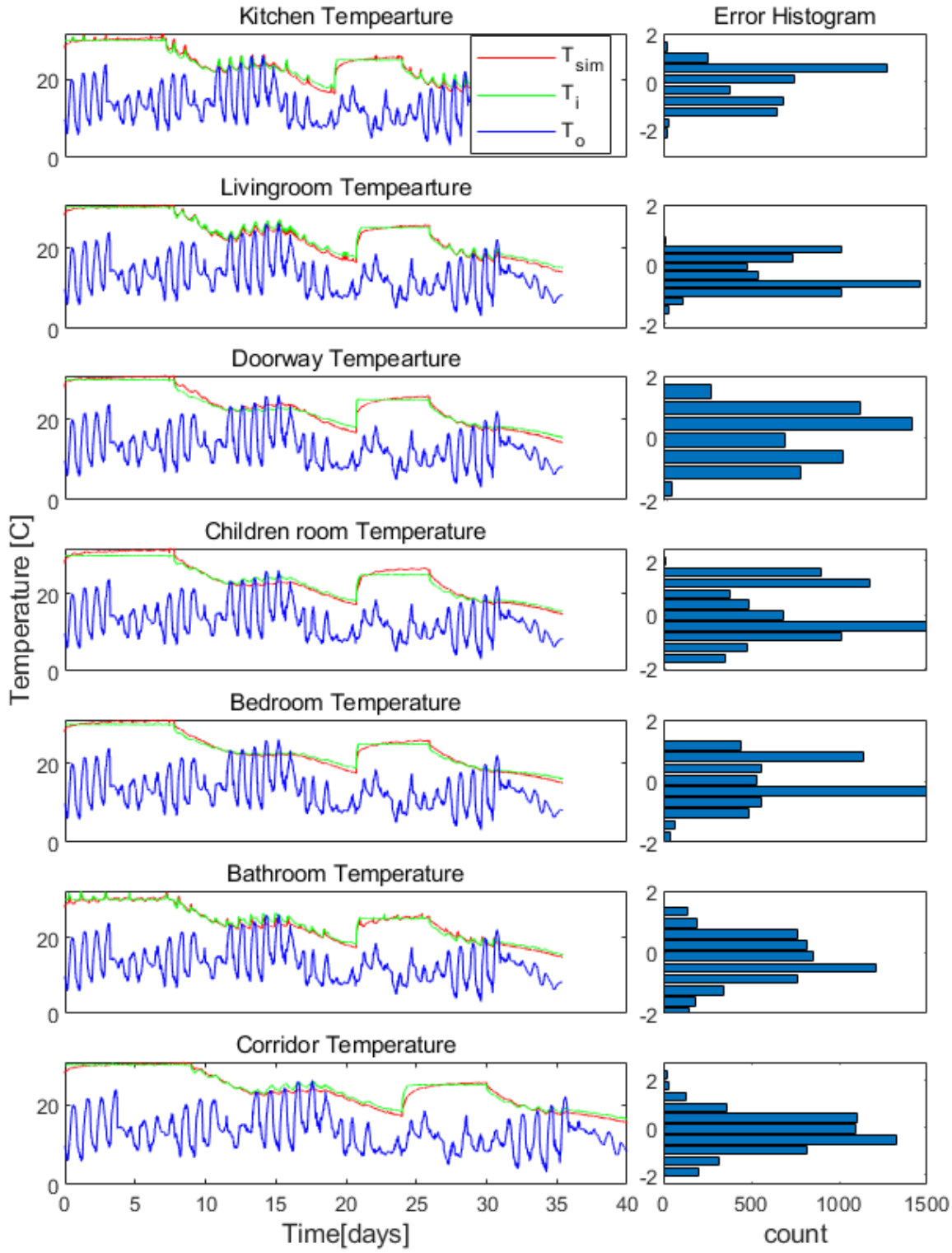

Figure 6.12: The simulation results of all the rooms in twin house and the corresponding error histograms

6.10 Conclusions

This chapter discussed the theoretical background for the state space modelling. The thermal circuit presentation of the individual components of the building is explained with reference to the Twin House construction details. The component thermal circuits are then assembled to generate a single thermal circuit for the entire building. A state space model is developed using the input data (outdoor temperature, solar radiations etc.) and the assembled thermal circuit. The model is validated with the measured data. The error histogram ranges between $\pm 2℃$. Three quartiles of simulation errors lie within $\pm 1℃$.

The state-space representation can be effectively obtained from thermal circuits, even for very large models. This is specifically suited to detailed thermal models of buildings. The state-space models, although linear, can be used also for non-linear models if the linearity is considered for a time step. State-space models are completely equivalent to thermal circuits from which they were obtained. The assembling of elementary thermal circuits allows us to obtain only one thermal circuit for the whole building; therefore, the state-space model can model in detail a whole building. Since assembling can be used to create large models from individual elements, it can find applications in the emerging technologies of Building Information Modelling (BIM). Obtaining state-space representation from very large thermal networks can have applications in model order reduction and the synthesis of control algorithms for complex buildings.

The model developed is used for the analysis of QUB method in next chapter. The QUB experiments are designed with different level of power, time duration and weather data with the help of the state space model developed in this chapter. The state space model has the advantage of using flexible number of meshes for better validation of the model. It allows us to determine the minimum time step required for simulation. The eigen values obtained with the state space model help us identify the significant time constants that govern the evolution of temperature during the QUB experiments. The state of the building surfaces dictates the behavior of air temperature and the corresponding error of the QUB experiment. The state space model helps us to achieve the realistic status of the building in simulation.

7 Design of experiments for QUB test method

The previous chapter discussed in detail the variations in results of QUB tests during experiments can be due to the influence of different variables, such as input power, time duration, level of insulation, outdoor temperature, solar radiation, wind speed, measurement errors etc. Like any other experiment QUB test is also performed under controlled set of inputs. The level of inputs depend on the weather conditions and the level of insulation of building. The process of selection of input values for an experiment is commonly known as design of experiment (DOE). The DOE for QUB experiment is to find the optimal value of power and time duration for different outdoor weather conditions and construction types.

The steps for DOE of QUB experiment as discussed in [93] are:

- Obtain a state space model for the given building and determine the steady state value of heat loss coefficient using equation.
- Use the same state space model to simulate the temperature response to QUB input.
- Estimate the slope of the response (heating and cooling period).
- Determine the QUB value from the slopes and power level.
- Repeat the estimation of QUB value for different levels of input power and time duration.
- Draw the contour map that gives error at the given power level and the time duration and outdoor weather conditions.

This chapter explains these steps to simulate QUB experiments for a building with weather data and different levels of inputs. Several numerical experiments are performed with variation of boundary conditions (solar radiation and outdoor temperature) and initial conditions (temperature distribution inside building surfaces and indoor air temperature).

7.1 Simulation of QUB experiments for the twin house

The IEA, EBC annex-58 provides full data set that includes: construction details along with dimensions and thermal properties, weather measurements, and the experimental indoor measurements. The Twin House data provides a good opportunity to generate and validate the building simulation models.

With the model of Twin House it is possible to design optimal conditions (time and power level) for the QUB experiment. The model was generated for ground portion only that includes seven zones: living room, kitchen, doorway, bedroom, corridor, bathroom and children's room. The conditions below the floor (ground) and above the ceiling (attic) was considered as boundary condition at the outdoor temperature.

A state space model

$$\dot{x} = Ax + Bu \qquad (7.1)$$
$$y = Cx + Du$$

was generated for the twin house, where x represents all the states of the twin house (109 in this case), y represents the desired outputs, which in our case were the indoor temperatures of all the seven thermal zones (rooms) of the twin house. The model was validated using the indoor temperature measurement data from the experiment.

The steady state value for heat loss coefficient of a building maintained at a constant temperature by supplying heating power is defined as [93]:

$$H \equiv \frac{P}{\theta_{indoor} - T_o} \qquad (7.2)$$

where

H – overall heat loss coefficient,

P– steady state power supplied,

θ_i– indoor air temperature,

T_o– outdoor air temperature.

Since the steady state is never achieved, the global conductance is estimated by the integral in time

$$H \equiv \frac{\int_0^{t_{final}} P dt}{\int_0^{t_{final}} (\theta_{indoor} - T_o) dt} \tag{7.3}$$

When several different boundary conditions are present, the indoor temperature θ_{indoor} is the result of the gains from the different boundary temperatures T_i and can be obtained by changing the indoor temperature in equation (7.2*)*:

$$\theta_{indoor} = \sum_i K_i T_i + K_p P \tag{7.4}$$

where K_i is the sate gain of boundary temperatures T_i and K_p is the static gain for power. Equation (7.4) is valid whether the boundary temperatures are same or not, $\forall_i, T_i = T_o$. However, it is important to note that when the boundary temperatures are not the same, the heat loss coefficient value using equation (7.2) will give errors.

In case of multiple zones, it is important to find the single equivalent mean temperature $\overline{\theta}_{indoor}$, as representative of all zones temperature, to be used in equation (7.2) for θ_{indoor}. The equivalent mean temperature in case of zones with equal height can be determined as:

$$\overline{\theta}_{indoor} = \frac{\sum_i A_i \theta_i}{A_i} \tag{7.5}$$

The steady state heat loss coefficient H, is then estimated as [93]:

$$H = \frac{\sum_i P_i}{\frac{\sum_i A_i \theta_i}{\sum_i A_i} - T_o} \tag{7.6}$$

where

- P_i is the power supplied to each zone
- A_i is the area of each zone
- θ_i is the temperature of each zone in the steady state vector y_{ss}
- T_o is the outdoor temperature

In QUB experiment, heating power is applied as a step input in all zones. The power in each zone is tailored according to the surface area of each zone. This generates uniform temperature across all zones. The response of the twin house is modelled using discrete exponential method

$$\begin{aligned} X_{k+1} &= \Phi X_k + \Gamma u_k \\ y_k &= C X_k + D u_k \end{aligned} \tag{7.7}$$

where

$$\begin{aligned} \Phi &= e^{A\Delta t} \\ \Gamma &= \frac{B}{A}(e^{A\Delta t} - I) \end{aligned} \tag{7.8}$$

The QUB experiments are simulated by using weather and construction data from IEA, EBC Annex-58 [102]. The numerical QUB experiments are simulated for the ground floor of the twin house that consist of living room, kitchen, children's room, bathroom, two doorways and a bedroom. The outdoor ventilation is zero whereas the outdoor infiltration rate of 1.62 m^3/h is considered for simulation. The values for outdoor and indoor convection heat transfer coefficient of 23 and 8 ($\frac{W}{m^2 K}$) are considered for simulation. The shutters for windows and

doors on Southern face are closed. The QUB experiments are simulated for the weather data of 40 days (Experiment-1, IEA, EBC Annex-58) of data given in [102]. The 40 days weather data show a good variation of weather with sunny, cloudy and partly cloudy days.

The average outdoor temperature during the QUB experiment nights varies between 6 to 16 ℃. Let us note already here that the conditions in which some of the QUB experiments were performed are known not to be the optimal one. A large temperature difference (e.g. 10 °C) in between the set point temperature (20 °C) and the outdoor temperature during the night is indeed known to increase the accuracy of the method.

As a first step, a QUB experiment is performed with constant outdoor temperature and assumed initial conditions (no solar radiations before the start of experiment) at different levels of power and time duration. The contour error for twin house are similar to those obtained previously in literature [93], showing that QUB error is predictable at given power and time Figure 7.1(a). The contour valleys of the error as a function of power and time duration show that consistent QUB values can be obtained even if the power and time duration vary Figure 7.1(a).

Figure 7.1 (b) shows the rise and fall of temperatures in different rooms of the experimental house during the simulated QUB experiment. It is evident that there is a slight variation (± 1℃) in temperature of different rooms during the QUB experiment. It is therefore important to take weighted average temperature in case of a house with multiple thermal zones (black circles for heating and pink circles for cooling phase of the QUB experiment in Figure 7.1(b)).

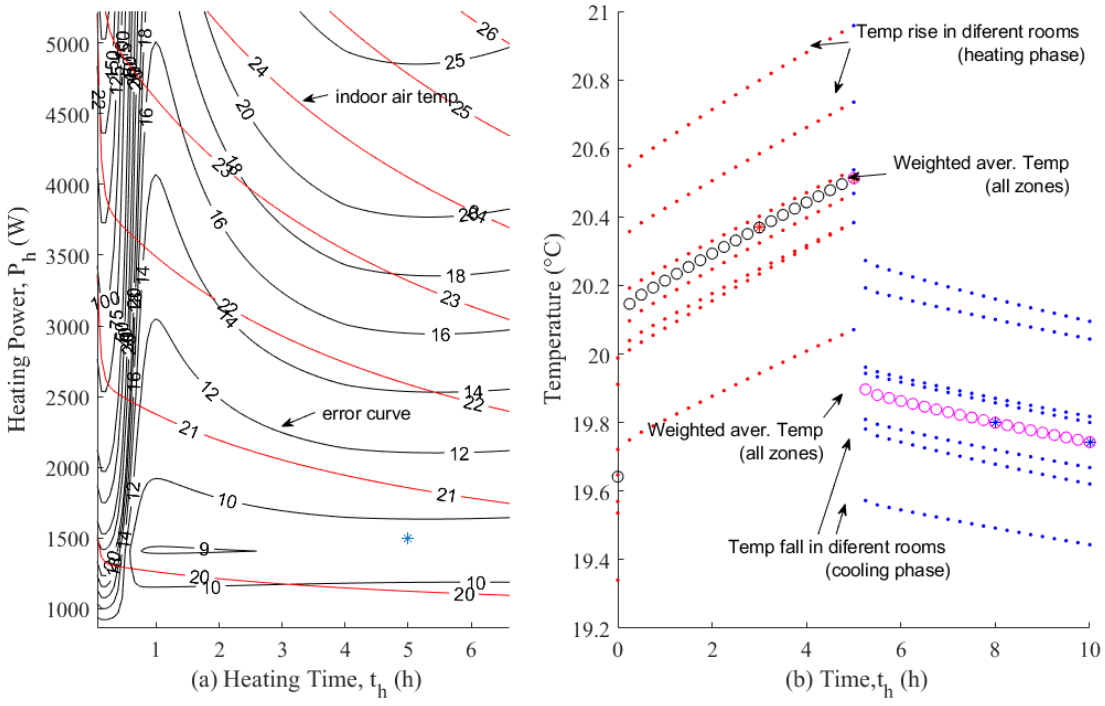

Figure 7.1: Design of the QUB experiment: (a) Heating power and time duration: error curves (black) and internal temperature (red); the blue star shows the error when the experiment is performed at 1500 W and 5 hour duration for the each phase of the QUB experiment; (b) the exponential response of seven zones of the house for 1500 W and 5 hours: fall of temperature during the two stages of QUB experiments (dotted line), weighted average temperature rise during heating (the black circles show the) and weighted average temperature rise during cooling (pink).

The numerical QUB experiments are conducted with the different conditions of weather given in EBC Annex-58. The power during heating phase is estimated using equation (7.9). A low power of 200 W is kept during the cooling phase of QUB experiments.

$$P_{optimum} \sim 2H_{ref}(T_i - T_o) \qquad (7.9)$$

The results for three days i.e. 3, 4, 18, 28 and 33 are the extreme outliers in the experiment set with an in the range of 30 % to 40 %,. The corresponding slopes during these days show that the slopes were extremely small during the heating and cooling phases showing a failure of experiment during these days. The experiment on day 18 failed as the slope is positive

during the cooling phase. The day 33 and 28 show a high difference of slope during two phases (higher than $2\mathrm{E}-05$). The outliers corresponding to the days 3, 4, 18, 28 and 33 are removed for further analysis in this work.

7.2 Influence of variation of optimal power on design of experiment (DOE) results

It is evident from the plot of error curves (Figure 7.1) that variation in input power changes the output of the QUB method. The optimum power for QUB experiment on any day with reference to the initial power can be estimated by using equation (7.9) [100]:

The effect of variation of the optimum power could be investigated by generating error curves for the twin house with ± 20 % of the optimum power ($P_{optimum}$) value. In this case the error curves were almost vertical (Figure 7.2). The advantage of this behavior was that the variation in QUB error (with ± 20 % variation in power) was limited (maximum variation of 6 % in QUB error). For example, the QUB error would vary by 3 % when the optimum power varied from 2100 to 2600 W (blue vertical line in Figure 7.2).

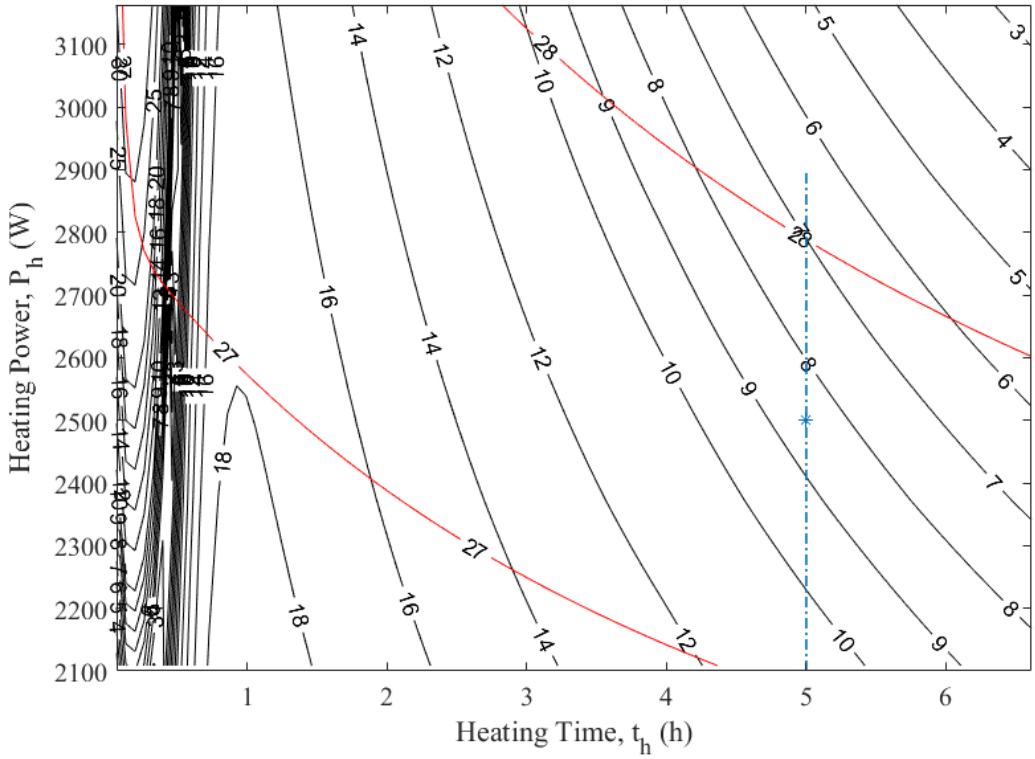

Figure 7.2: QUB errors generated with variation of the optimum power: error curves (black) and indoor temperature (red). The blue vertical line shows error for QUB experiments at different levels of power but for the same duration of the experiment.

7.2.1 Design of experiment time duration for QUB test

It is interesting to see that H-values with small errors could be obtained with QUB tests having short heating duration. This is evident from Figure 7.3 showing that H_{QUB} value within ± 20 % of the reference value could be obtained during the first half hour of QUB experiment. The error curves however were very sensitive to power level if the duration of the experiment was short.

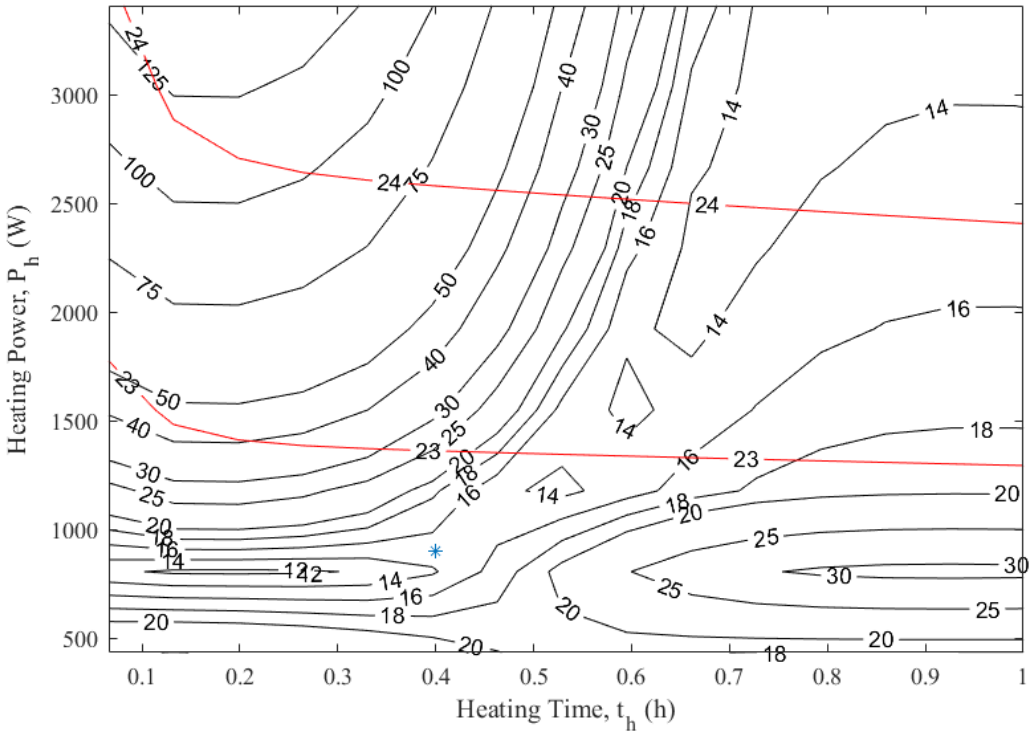

Figure 7.3: QUB error curves (black) and indoor temperature curves (red) during the first 1.5 hours of the QUB experiment

The variation in error with the time duration of QUB test could be further explored by performing QUB experiments with different time durations. The dependency of QUB errors with time was generated by repeating a QUB experiment with time duration ranging from 20 min to 5 h (Figure 7.4). It can be seen that initially the error was large (30 %) but it reduced significantly during the next twenty minutes. The error remains almost constant after 1–2 h of the QUB experiment, which was in accordance with previously published results [93]. This

behavior was explained by the important contribution of the exponentials corresponding to medium time constants (1 … 2 h), which have significant coefficients [93].

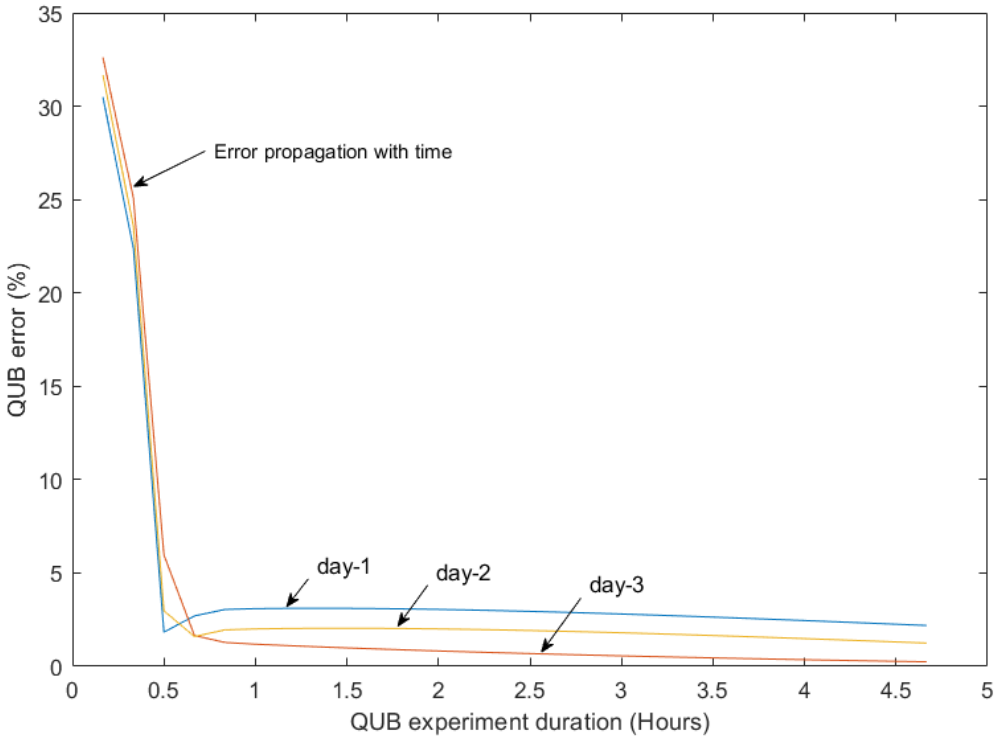

Figure 7.4: Variation of QUB error with change in time duration of QUB experiment

7.3 Conclusions

This chapter discussed the steps for the design of QUB experiments. Using design of experiment the QUB experiment were simulated with varying level of power and time duration. The error curves generated at varying level of power and time duration can help us predict the QUB error. The optimum power for the QUB experiment given by equation (7.9) depends on the overall heat transfer coefficient H_{ref}, a quantity estimated with stated thermos physical properties. It is verified that $\pm$ 20 % variation in optimum power causes only $\pm$ 3 % variation in QUB results. The QUB experiments can produce accurate results with durations shorter than half hour, however, the results are prone to large variation with small change in power during heating phase. It was shown that after 3 hours the results of experiments only slightly improve with increase in duration of QUB experiments.

This page is intentionally blank

8 Influence of boundary and initial conditions on QUB experiments

The QUB experiment begin after the sunset, the solar radiation absorbed by the building envelope might influence the results of QUB experiment.The expression used for the calculation of overall heat transfer coefficient H_{QUB}, does not take into account the solar radiation. It is important to see how the error in QUB results vary with respect to the solar radiation. Since the QUB method is an experiment with short duration of time the initial condition before the start of QUB experiment can have influence results. This chapter analyses the variation of QUB results with boundary conditions (solar radiation) and initial conditions (initial power).

8.1.1 Timing of QUB experiment: before or after the sunset

To explore the effect of the solar radiation delayed by the transmission through the walls, the QUB experiment was performed at different starting times with respect to sunset. Figure 8.1 shows the errors of QUB experiment (black curves) and the indoor temperature (red curves) when the QUB experiment was done for heating power ranging from 500 to 3500 W and time duration between 0 and 6 h. When the time duration was shorter than 30 min., the measurement was very sensitive to the heating power: there was a large variation of error with a small variation of heating power. The errors became less sensitive with power if the time duration was about 5–6 h. When QUB experiment was performed half an hour before the sunset, in the same conditions of power and duration (1500 W and 5 h), the error was 13 % (blue star in Figure 8.1). There was a reduction of the error to 10.5 % when the experiment was performed one hour after the sunset (Figure 8.2). There was no further reduction of error when the starting time of QUB experiment was further delayed. It could be inferred that the solar radiation influenced QUB results.

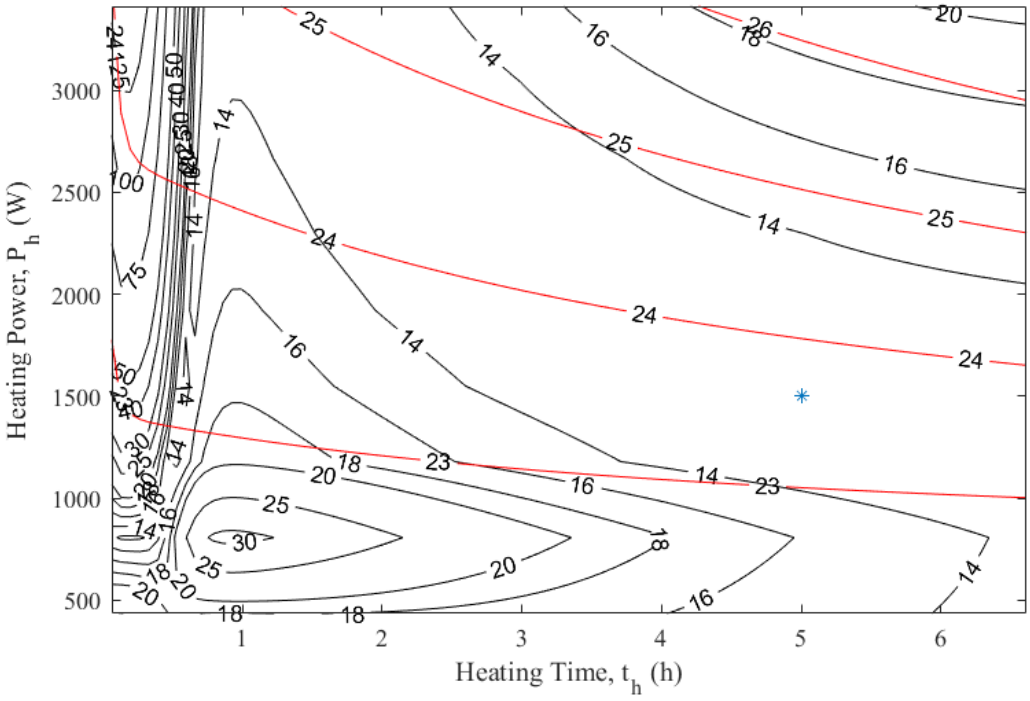

Figure 8.1: Error (blue star) when the experiment is performed half an hour before the sunset time (at 1500 W and 5 h of heating); error of measured overall heat loss coefficient (black curves), indoor temperature (red curves).

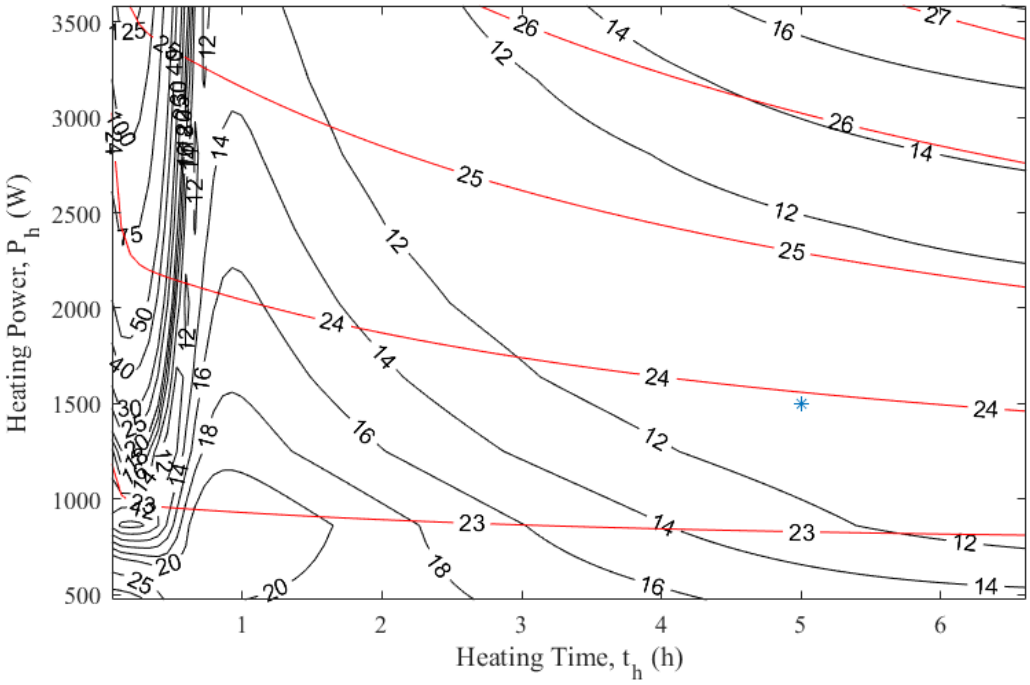

Figure 8.2: Results (blue star) when the experiment is performed one hour after the sunset (at 1500 W and 5 h of heating); error of overall heat loss coefficient (black curves), indoor temperature (red curves).

8.1.2 Influence of the day type: sunny, cloudy or partly cloudy

The experimental data offer an opportunity to investigate the impact of the day type (sunny, cloudy or partly cloudy) on the results of the QUB experiment. To perform the analysis, days are classified based on the average global Horizontal solar radiation. The QUB numerical experiments are performed with the weather data, optimal power and time duration of five hours. For each day, the initial conditions are simulated with respect to the conditions of all the days before the QUB experiment. The days are categorized as sunny days (average solar radiation>350 W/m^2), partly cloudy days (average solar radiation>152 W/m^2) and cloudy days (average solar radiation<153 W/m^2). It can be observed that results for sunny days show high variation as compared to cloudy and partly cloudy days (Figure 8.3). The 2nd and 3rd quartile of the QUB results on cloudy days are close to the steady state H-value as compared

to the QUB results on sunny days (Figure 8.3). However, the variation in QUB results on cloudy, partly cloudy and sunny days show that not all the errors can be explained with respect to solar radiation.

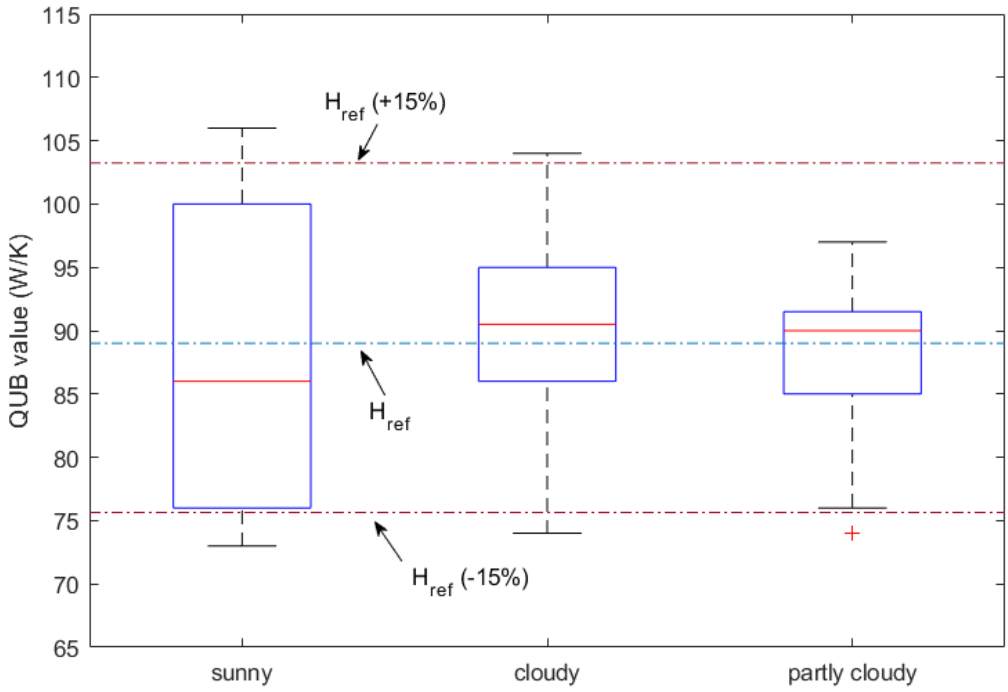

Figure 8.3: QUB value variation as a function of day type: sunny, cloudy and partly cloudy. Dashed horizontal line (blue) is the steady state reference value

To explore further the effects of solar radiation on the QUB measurement, experiments were simulated on a sunny day. The simulations were started assuming that the temperature in the external walls was constant and equal to 10 °C. Then, simulations were repeated with the weather data of a given day in order to obtain the initial conditions. Figure 8.4 shows the results when the same day was repeated 1, 2, …, 40 times. It could be observed that the initial conditions of temperature distribution in the walls highly influenced the errors of QUB measurement. If initially the temperature in the walls was 10 °C, the error of QUB experiment was 140 %. However, this type of arbitrary initial conditions was specific to a numerical experiment; the simulations need to be repeated for more days in order to obtain values of the state variables, which are not influenced by the “arbitrary” initial conditions. It can be noticed in Figure 8.4 that the errors entered in a range after 15–17 days.

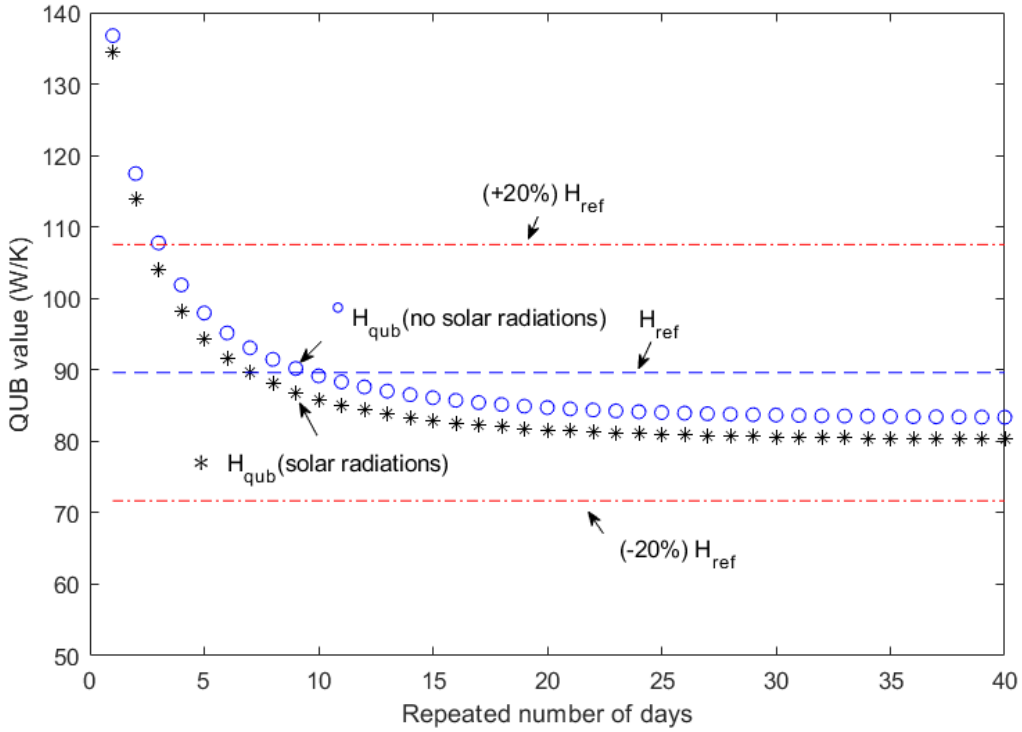

Figure 8.4: Convergence of QUB test when experiment is repeated without solar radiations (blue circles) and with solar radiations (black asterisk). In absence of solar radiations (blue circles) the QUB test settles at a value closer to H_{ref}. Blue dashed line the reference/steady state over all heat transfer coefficient (H_{ref}), upper dashed red line (+20% H_{ref}), lower dashed red line (-20% H_{ref})

This error can be explained by the power of solar radiation in the over-all heat transfer coefficient for steady state conditions

$$H = \frac{P_{heater} + P_{solar\ radiations}}{A\Delta T} \tag{8.1}$$

In case of QUB method the heater power input is the only power considered for estimation of over-all heat transfer coefficient. The QUB over all heat transfer coefficient is estimated using formula

$$H_{QUB} = \frac{\alpha_1 P_2 - \alpha_2 P_1}{\alpha_1 T_2 - \alpha_2 T_1}$$	(8.2)

where P_1 is the heater power during the heating period. The expression gives a good value when there are no solar radiation. However, for a sunny day, the power of the heater is not the only power contributing to the rise in temperature during the heating phase. On a sunny day, the surfaces of a building continuously receive solar radiation that are partially absorbed and stored. As the QUB experiment starts immediately after the sunset and the heating continues for a short duration of time after the sunset, the contribution of delayed solar radiation transferred to the room air via building surfaces cannot be ignored. This is evident from the equation (8.1*)*; when evaluated with no solar power added, the overall heat transfer coefficient will always result in a value smaller than its reference values for steady state. The input power (heating phase) for QUB calculations can be corrected as:

$$P_1 = P_{heater} + P_{solar\ corrective} \quad (8.3)$$

In absence of solar radiations the evolution of indoor temperature during the QUB experiment is different as shown in (Figure 8.5). The temperature profile in case of no delayed solar radiations via walls (orange line) is different from the profile (blue line) when delayed solar radiations from the wall are considered. The slope of temperature line with no solar radiations (orange) is different from the temperature line (blue) with delayed solar radiations. In order for the both lines to have the same the same evolution profile an additional power needs to be added to the indoor air temperature line with no solar radiations (orange line).

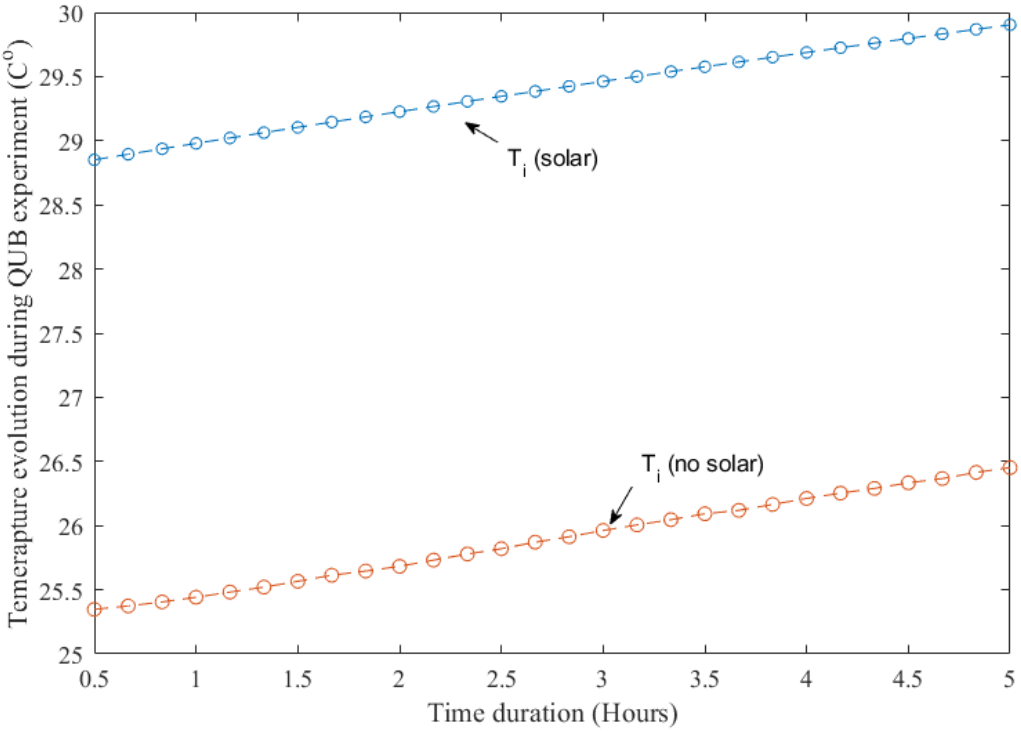

Figure 8.5: Temperature evolution during the QUB heating phase with no solar radiations (orange line) and with solar radiations (blue)

The correction for solar radiation requires the calculation of delayed heat flow to indoor air due to solar radiation absorbed by the building envelope. In order to solve this problem, two calculations are performed (Figure 8.6):

1) The heat flow from the building envelope to the room air, considering both outdoor temperature and solar radiation as inputs, is calculated in order to obtain the temperature of the walls and the temperature of the air during the heating phase of QUB experiment. The heat flow from the envelope to the room air is calculated by the convective heat transfer due to temperature difference between room air and walls (Figure 8.6 a).
2) The heat flow from the building envelope to the room air is calculated by considering only the outdoor temperature (no solar radiation) as input from the boundary conditions (Figure 8.6 b). A controller is added to introduce the additional heat flow necessary to obtain the indoor temperature, θ_K (Figure 8.6 b) that is same as indoor temperature, θ_i, obtained in the first step (i. e. with solar radiation, (Figure 8.6a). The heat flow rate Q_2 introduced by the controller represents the contribution of the solar radiation (Figure 8.6 b).

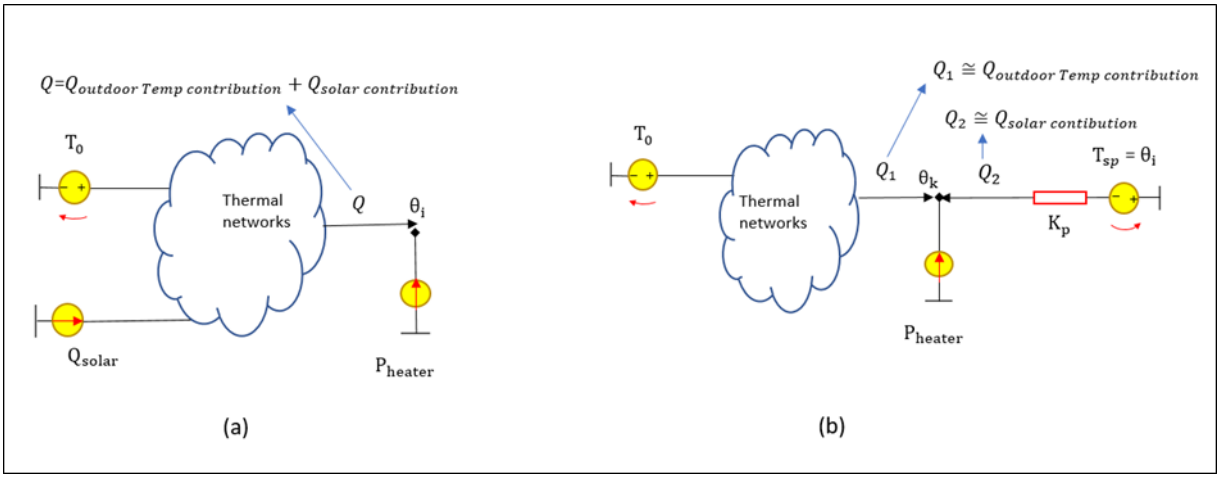

Figure 8.6: QUB experiment with (a) indoor temperature evolution as a function of solar radiations, outdoor temperature and heater power; (b) temperature evolution as function of outdoor temperature, heater power and a controller

The controller power required to keep the controlled temperature θ_k (no solar radiations) equal to the indoor temperature θ_i (with solar radiation) is the contribution of solar radiation to the indoor temperature evolution (Figure 8.7). The average power from the controller in such case is equal to 110 W. This is considered as the corrective power needed to be added to power P_1 (power during heating phase) in QUB expression for H in equation (8.2*)*.

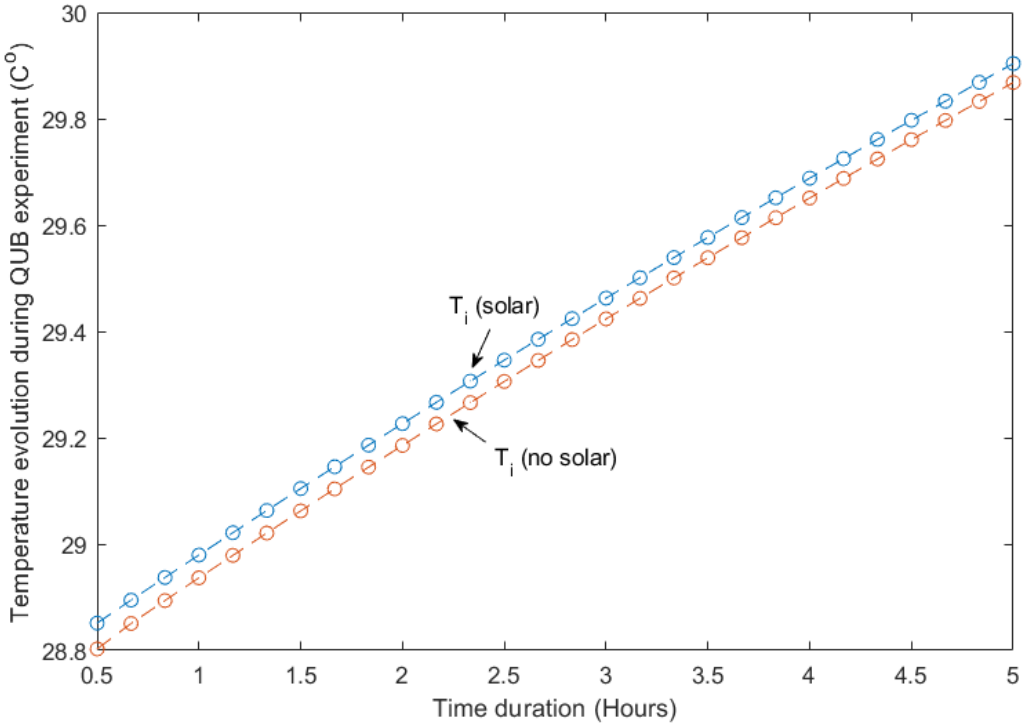

Figure 8.7: Temperature evolution during the QUB heating phase with no solar radiations and controller heat (orange line) and with solar radiations (blue)

When this corrective power is added as compensation for solar radiations, it reduces errors from 8% (Figure 8.4) to 5% (Figure 8.8). The average power contributed by the walls to inside air is 110 Watts.

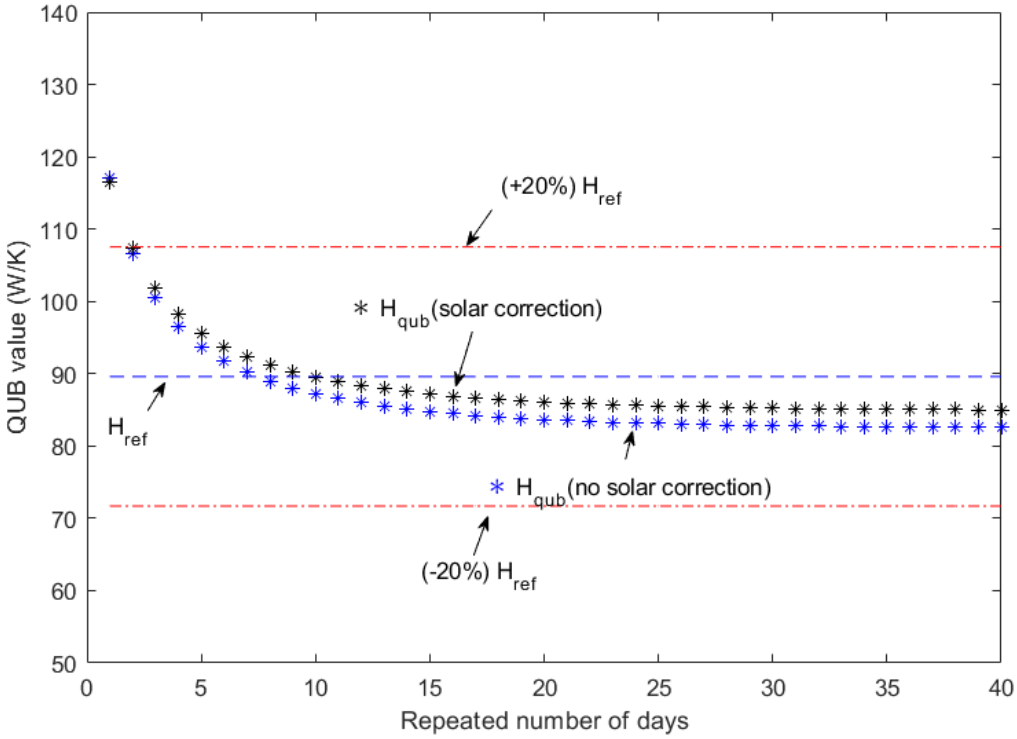

Figure 8.8: Convergence of error to a value closer to reference value when a day with sunny conditions is repeated with solar power correction factor

8.2 Influence of initial conditions

The optimal error curves for the experimental house change with the initial conditions. The QUB method error increases (Figure 8.9(a)) when there is no initial power before the start of QUB experiment, the error is large. The error curves converge when house is supplied with a steady heating power before the QUB experiment ((Figure 8.9b)).

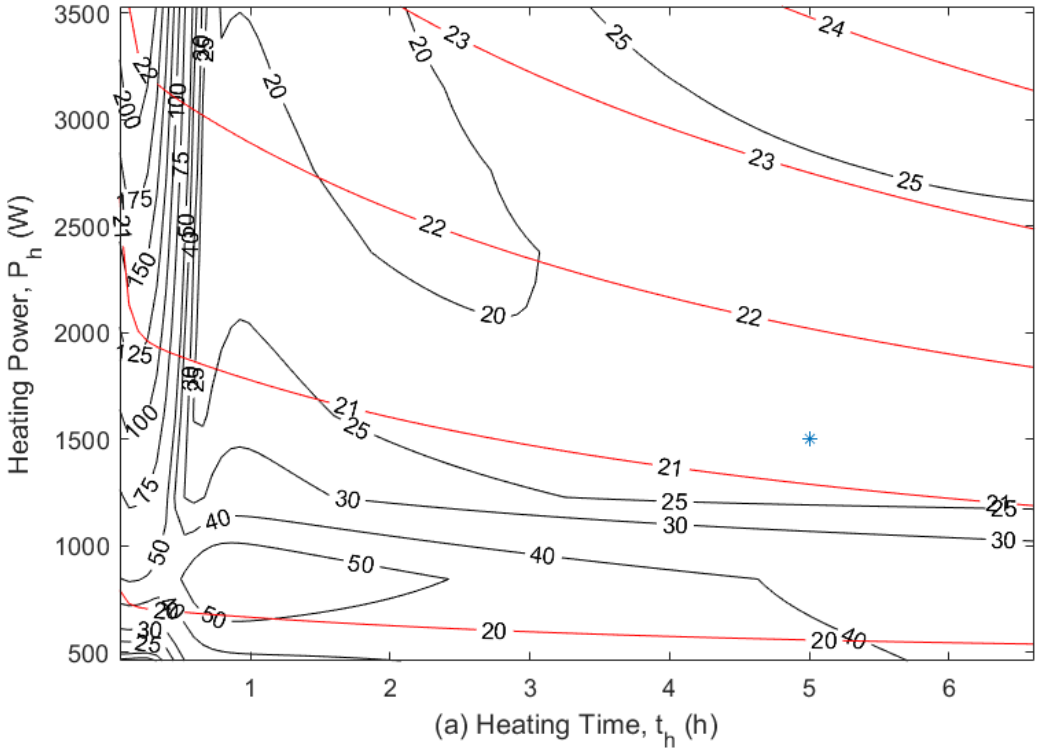

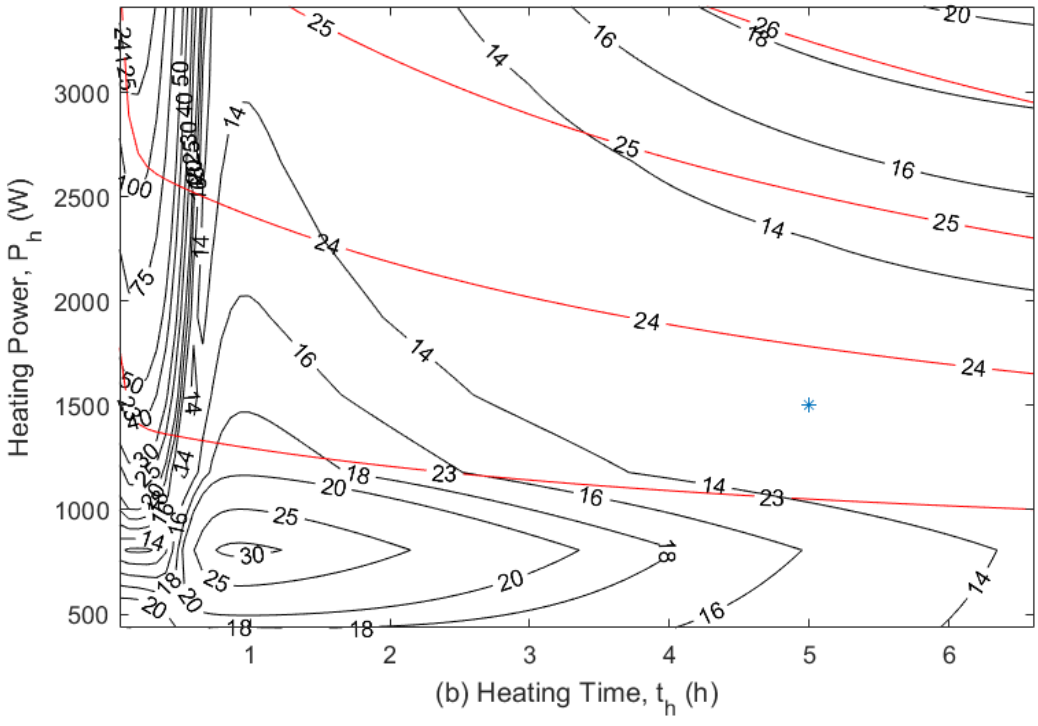

*Figure 8.9: QUB error curves for the experimental house (**a**) no initial power before the experiment, the curves move towards increased error (**b**) initial power before the experiment, the curves converge, red curves show the indoor air temperature and black curve show the error curves.*

Figure 8.10 shows the results of QUB experiment when no power was used before the experiment (panel a) and when power of 600 W was used before the experiment. It can be seen that the errors persist after 15 days when there was no power before the experiment (Figure 8.10a); if the building was heated before the experiment, the errors of QUB experiment decreased, being in the range ± 20 % Figure 8.10(b).

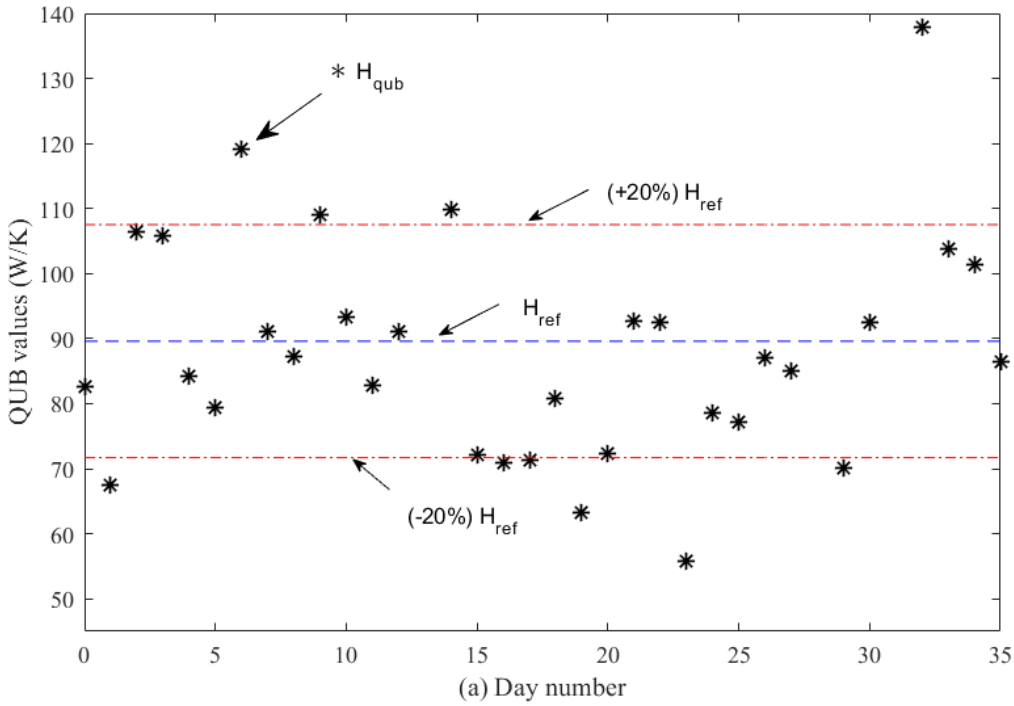

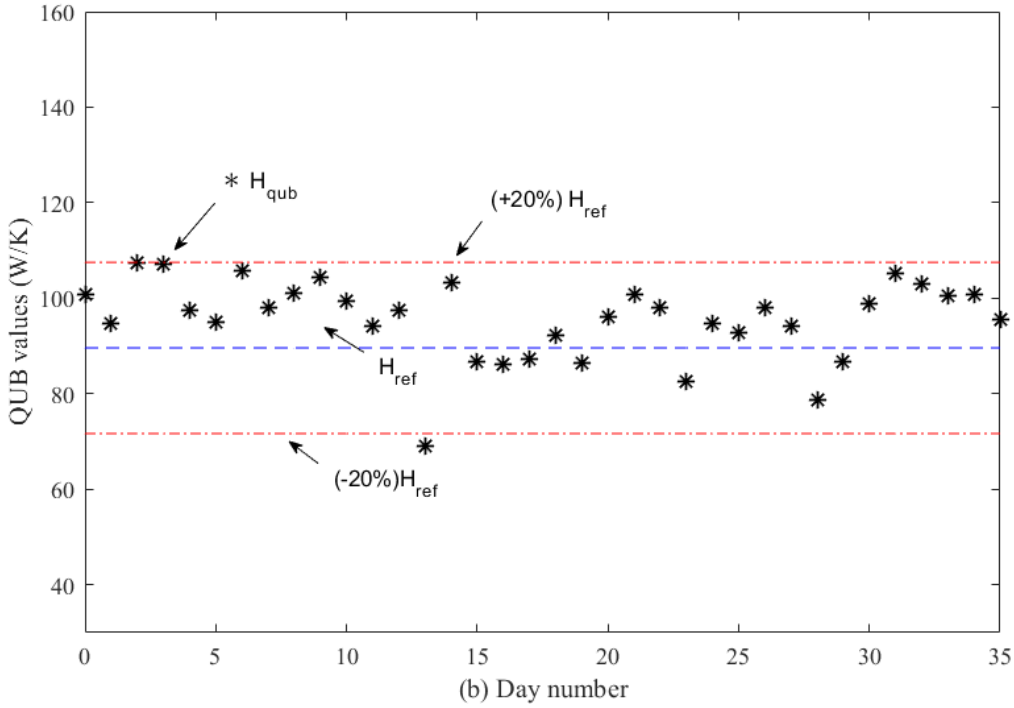

*Figure 8.10: QUB values obtained for simulations for forty days **a**) no initial power before the QUB experiment and **b**) initial power before QUB experiment. Blue dashed line the reference/steady state over all heat transfer coefficient (H_{ref}), upper dashed red line (+20 % H_{ref}) and lower dashed red line (−20 % H_{ref}).*

8.3 Conclusions

The IEA ECB Annex experiment provides good data to simulate a model of temperature variation inside a house. The simulated temperature lies well within ± 1°C of the measured temperature; the error outliers (± 2°C) are obtained during the initialisation period only. The model is also validated with real QUB experiments performed on the twin house.

The validated model is then used to perform QUB experiment with different levels of power, boundary and initial conditions. The weather data of forty days was used to simulate QUB experiment. The following conclusions can be drawn from the results of QUB experiments:

- Heating building with steady state power before the experiment improved QUB results. The error curves show a large error when there was no initial power before

the QUB experiment. The error curves converged to smaller error when the building was supplied with power before the experiment.

- The starting time of the QUB experiment before or after the sunset affected the results. A QUB experiment half an hour before the sunset gave an error of 14 % that was reduced to 11 % when the experiment was conducted one hour after the sunset.
- Comparison of QUB results for sunny and cloudy days revealed that at a given power and time duration of the QUB experiment the results on cloudy days showed less variation as compared to sunny days.
- QUB errors on sunny days were due to solar radiation absorbed by the walls of the building. The absorbed solar radiation contributes as a delayed heat input to the evolution of air temperature during heating phase. This paper proposed a method to estimate the delayed solar radiation and to correct the input power during the heating phase. The solar correction factor, when added to the heating power P_1 in the QUB expression, reduced the error by 2 %.

9 Posterior error analysis

Design of experiment (DOE) can be used to estimate the optimum power and time duration for the QUB experiment that can give low errors [93]. The design of experiment depends on the overall heat loss coefficient used, a quantity that depends on the stated or calculated value using building material properties. The stated or calculated value of the overall heat loss coefficient is different from the one measured on the real building due to material property deterioration, missing insulation layers, moisture transfer and the quality of workmanship. It is therefore important to investigate how the results of the QUB method change when the overall heat loss coefficient value used in the design of the experiment is different from the real overall heat loss coefficient of the building, which in general is larger than the designed value.

Three cases were studied in which the value of H (used for the design of the experiment) and the real value of H were different:

1) The outer wall insulation for design of QUB experiment was two times higher than that of the real wall ($8\ \%$ error in assumed H_{ref} compared to the real envelope).
2) The real wall insulation is completely missing whereas in the design of QUB experiment the outer wall has insulation ($50\ \%$ error in assumed H_{ref} compared to the real envelope).
3) The real wall had no insulation and the roof insulation was smaller as compared to the wall and roof insulation used in the design of QUB experiment ($100\ \%$ error in assumed H_{ref} compared to the real envelope).

For the cases discussed above, the a priori error is defined as the error when the real H-value was used for designing the experiment, whereas the a posteriori error is defined as the error when a supposed H-value (obtained, for example from building specifications), which is different of the real H-value, was used for designing the experiment. Figure 9.1 shows the results of 32 QUB experiments conducted on different days. The results show that when $8\ \%$ error of H-value was used in the design of the experiment (Figure 9.1a), the increase in a posteriori error was not significant (shown by the blue bar slightly higher than the red bar).

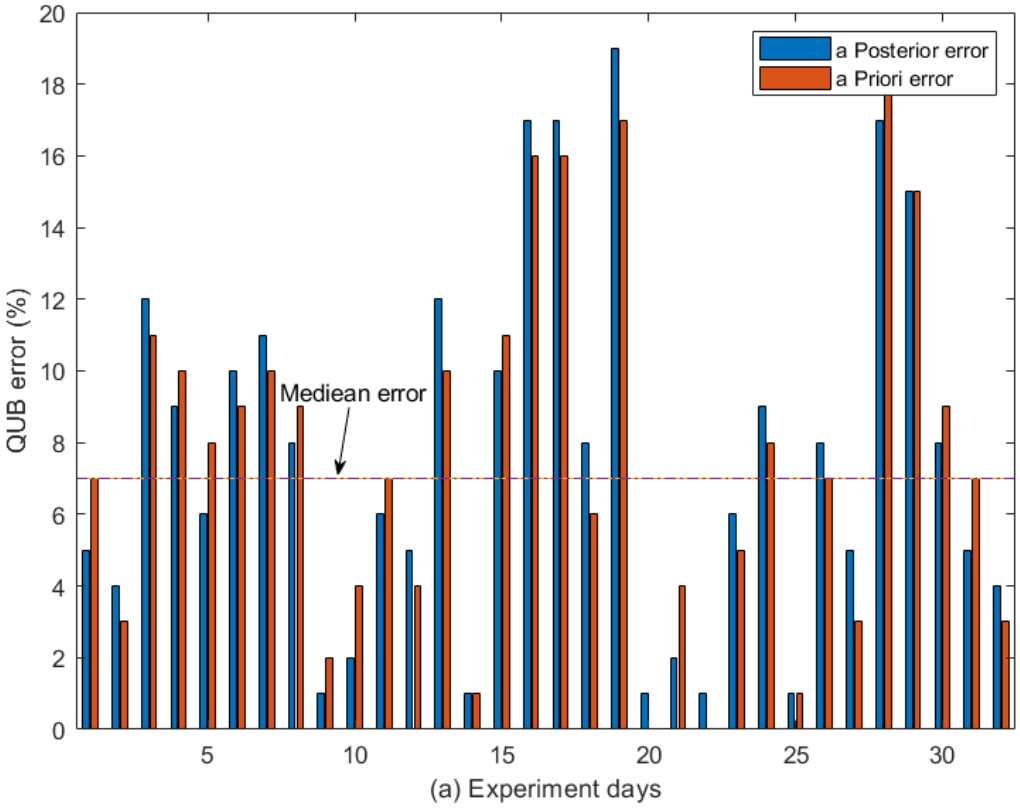

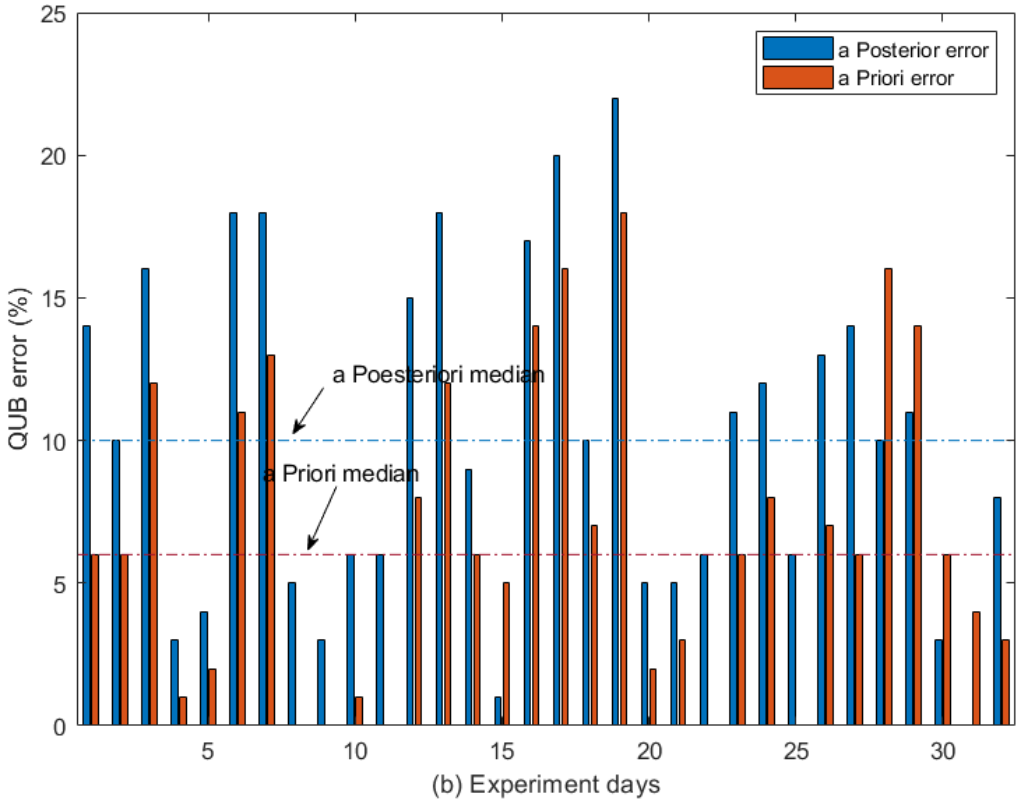

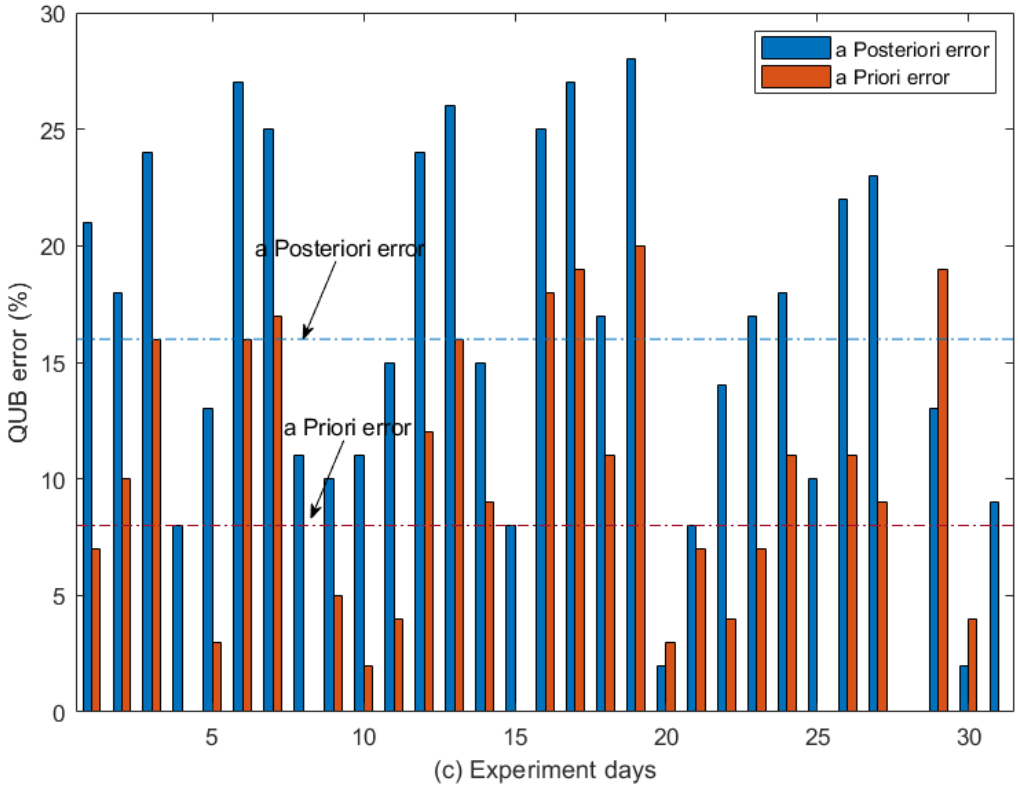

*Figure 9.1: A posteriori error analysis for three case studies: (**a**) outer wall insulation is reduced (8 % error in H-value), (**b**) outdoor wall insulation is completely removed (50 % error in H-value) and (**c**) outdoor wall insulation removed and roof insulation reduced (100 % error in H-value). Red bars show error with real envelope and blue bars show QUB error with assumed envelope.*

Figure 9.1b shows that with no outer wall insulation (H_{ref} error of 50 %), the a posteriori error was higher than the a priori error, with a median of a posteriori errors 10 % as compared to median error of 6 % for a priori errors. The majority of errors still lied within ± 15 %. In case of no wall insulation and reduced roof insulation ($\mathrm{H_{ref}}$ error of 100%) the a posteriori error was significantly higher as compared to a priori error, with a median of a posteriori errors of 16 % as compared to a priori median error of 8 % (Figure 9.1c). Nevertheless, in this case the error made with the QUB method (median error of 16 %) was significantly smaller than the error made on the initial estimate of the overall heat loss coefficient (100 %).

This also means that, in practice, the experimentalist will clearly notice that “something went wrong” in the sense that the measured value of the heat loss coefficient is very different from the assumed value (median difference being 100 % – 16 % = 84 %). The experimentalist can then suspect that there is an important gap between the theoretical design of the building and its actual state. This could also trigger another QUB experiment, using for the design of experiment the measured value of the heat loss coefficient instead of the theoretical (or stated by design) value. In this case, the measured and the assumed values would be much closer, confirming the important gap between theoretical and actual thermal performance.

9.1 Ideal conditions for the QUB experiment

The derivation of equation is based on the evolution of indoor temperature as a single RC circuit:

$$C\frac{dT_i}{dt} = P - H(T_i - T_o), \tag{9.1}$$

The conditions for the derivation of QUB equation are that the outdoor temperature should remain constant during heating and cooling phases and the heating and cooling durations should be of equal length [97]. A constant value of power is maintained before the experiment [82]. The power dissipated during the cooling phase should be zero i.e. $Q_2 = 0$. The method assumes a homogeneous internal temperature to be maintained inside the building i.e. in case of a house with many rooms, the temperature during heating and cooling phases inside each room should be ideally the same, a condition that is difficult to achieve in real experiments. There should be no air stratification (temperature difference along the height of the room) inside individual zones. The test should be carried without any occupants inside the house [92].

The ideal conditions for QUB experiment are that it should start from the steady state conditions. The literature however does not mention how long before the QUB test an initial steady state should be maintained [92].

The temperature evolution during the QUB experiment depends on the initial internal air temperature as well as the distribution of different temperatures inside the building envelope. Before the start of the QUB experiment, the building should be in steady state [82]. The power input should be in the form of a simple electric heater as the heating from gas or boiler requires conversion efficiencies for power calculation that can lead to increase in errors. [82].

To reduce the variation of QUB results, a dimensionless quantity alpha (also known as alpha criterion) is introduced. Alpha is the ratio of power between initial power (before the start of QUB experiment to achieve steady state conditions) P_o and the power applied with the start of QUB experiment P_1:

$$\alpha = 1 - P_o/P_1 \tag{9.2}$$

where the initial power P_o , before the start of QUB experiment is given as [94]

$$P_o = HLC_{ref}\Delta T_o \tag{9.3}$$

where $\Delta T_o = T_{io} - T_{eh}$ is the temperature difference between internal and external temperature at the beginning of the QUB test. Ideally, this difference should be around 10 K. Since HLC_{ref} in equation (9.3) is determined from the stated thermos physical properties [96].The power should be optimized based on the α criteria [96]. The heating and cooling phases should be of equal durations. The theoretical model shows a strong dependence on the alpha value. For experiments, it is recommended that alpha should be between 0.4 and 0.7; the power during heating phase can be between $1.7P_0$ to $3.3P_0$[97].

A method for the design of experiment of QUB method was introduced by [93] where the error can be predicted at any power (heating phase) and time duration. The power input should be in the form of a simple electric heater as the heating from gas or boiler requires conversion efficiencies for power calculation that can lead to increase in errors. The power should be optimized based on the α criterion [82]. The heating and cooling phases should be of equal durations.

A desired indoor temperature was maintained at real house using thermostatically controlled heaters [92]. The house was tested between the end of September until the end of April. The experimental reported errors for QUB test conducted in real house were within $\pm 10\,\%$. However, few tests above this limit were also reported. There is no influence of α criteria on

the results provided that the alpha value stays in the range: $0.4 < \alpha < 0.6$ [92]. When α was greater than 0.7, the results stayed consistently within $+10\%$ region. At reduced infiltration rate, the alpha criterion has no influence up to the value of 0.8. The result of a single experiment performed on real house shows that there is no correlation between the wind speed and H-value of the QUB method, although it was argued that the house was sheltered from three sides and only West side of the house was exposed [92]. Some of the variance (with a determination coefficient of 0.21 to 0.16) in QUB results can be attributed to external temperature where an increased external temperature can increase the H-value measured with QUB method.

QUB experiments have generally shown good results. However, with limited experiment sets it should be repeated under different weather conditions to improve understanding of the method. The variation in results with change in test conditions and wall configuration should be established. The performance of the method when ideal conditions are not respected during the experiment should be analyzed further [82]. In the next section, QUB experiments under non-ideal conditions are simulated for further analysis. The QUB experiments are also simulated for winter and summer seasons to analyze the suitability of particular season for QUB experiments.

9.2 Assumption of constant outdoor temperature

The derivation of the QUB experiments assume that the external temperature should remain constant during heating and cooling phases [97]. This condition may not be respected in real experiments where the temperature can vary during both phases. It is interesting to find the impact of variation in outdoor temperature on the QUB results when the perfect conditions of constant outdoor temperature are not respected during the test. Two sets of QUB experiments are performed for winter months starting from November to end of March (150 days) for the weather data of Munich, Germany, and the construction data form IEA, EBC Annex-58 (one of the twin houses). One set of experiments is performed with constant outdoor temperature and the other set is performed with varying outdoor temperature during the QUB experiments.

Figure 9.2 shows the results when the QUB experiments are performed:

a) at the real outdoor temperature with normal variation during the QUB night and
b) at the assumed constant outdoor temperature during the experiment night.

It is evident form the figure Figure 9.2 that, with the exception of two outliers, the results of QUB experiments for both conditions (a) and (b) lie within $\pm 20\ \%$ of the steady state overall heat transfer coefficient. It can be inferred, with constant outdoor temperature, the QUB results show that with both constant and variable outdoor temperature, the QUB results are relatively similar.

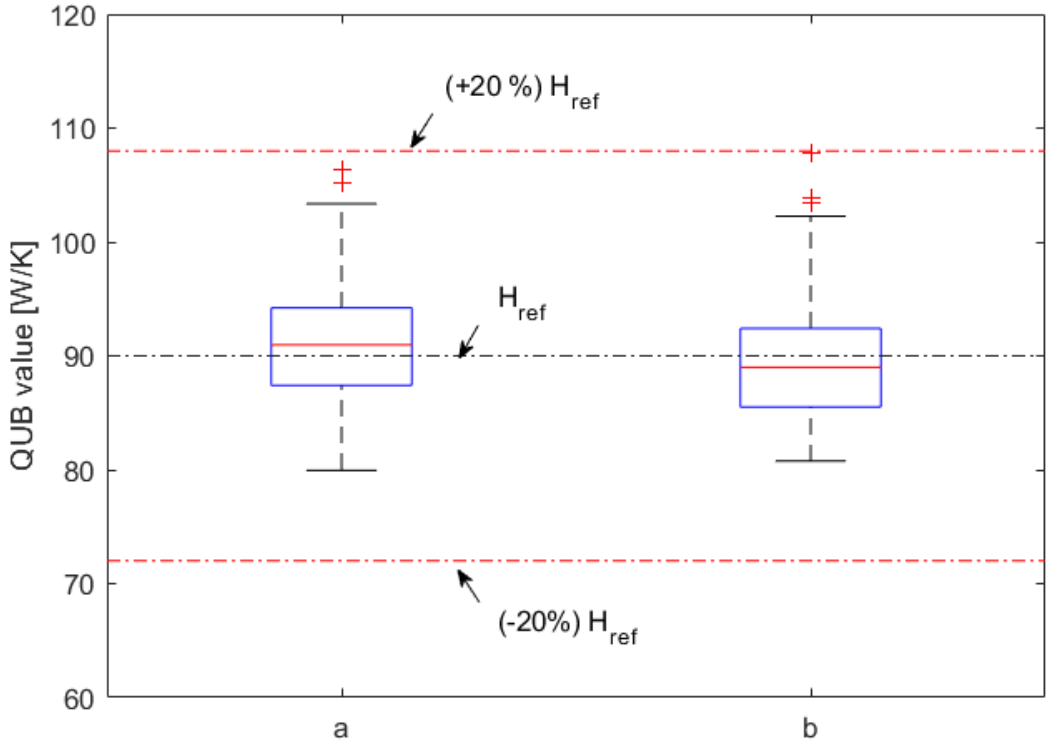

Figure 9.2: Comparison between QUB results at (a) variable outdoor temperature and (b) varying outdoor temperature. The black dashed line shows the steady state overall heat transfer coefficient and the two red dashed lines show $(\pm 20\ \%)$ *of the steady state overall heat transfer coefficient.*

9.3 Variation in Design of experiment (DOE) QUB results

The method of predicting the errors of the QUB at a given power and time was discussed in [93]. The method has potential to be used as a tool for design of experiments provided that we have the simulation model of the building and the weather data is known. For any simulation model, to accurately predict the outcome end the error in QUB experiment, it is important that simulation starts with the true states, i.e. temperatures of the building surfaces and layers. The inability to realize the true states of the building envelope can lead to erroneous predictions. This is shown by generating error curves of the QUB method by repeating the QUB experiments at different levels of power and time duration. The error curves in Figure 9.3 are generated for the same house at the same outdoor temperature and power levels during the QUB experiment. However, the states i.e. the temperature of the surfaces and layers of building were different during each simulation. The results of simulation show that with the changed states, the QUB error also changes (Figure 9.3a). The error curves in Figure 9.3b are generated for the same building but with different temperature/states of the building envelope. The red dashed line show that an experiment at the same power, outdoor temperature, and time duration will result is different errors. A design of experiment therefore may not be relied upon if the real states of the building are not taken into account. This also helps us understand that with the changed, states every time a QUB experiment is repeated, the results will be changed.

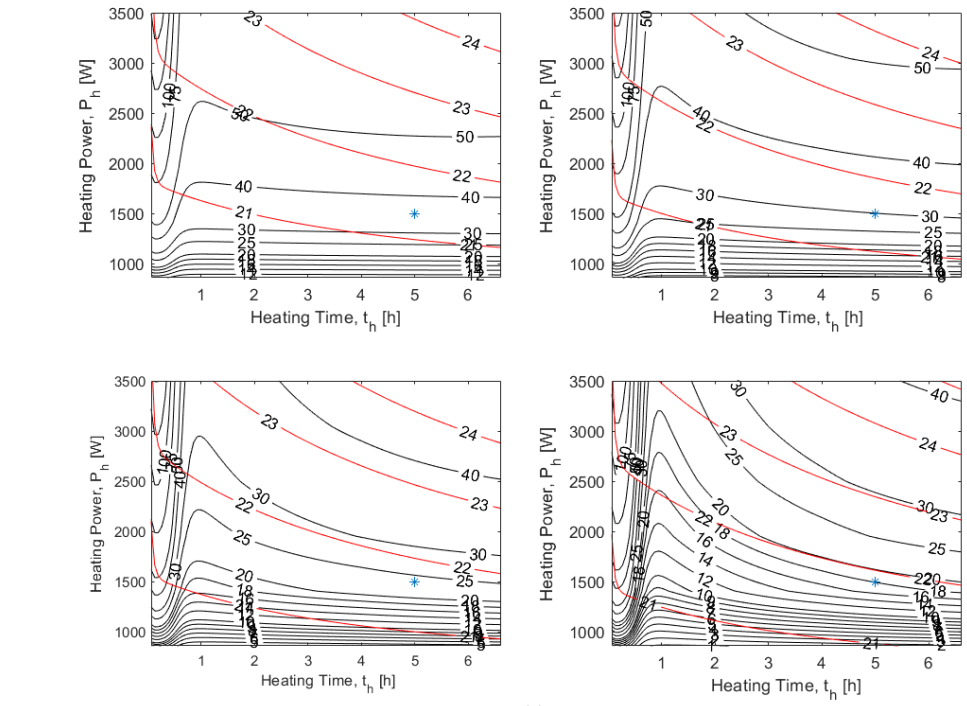

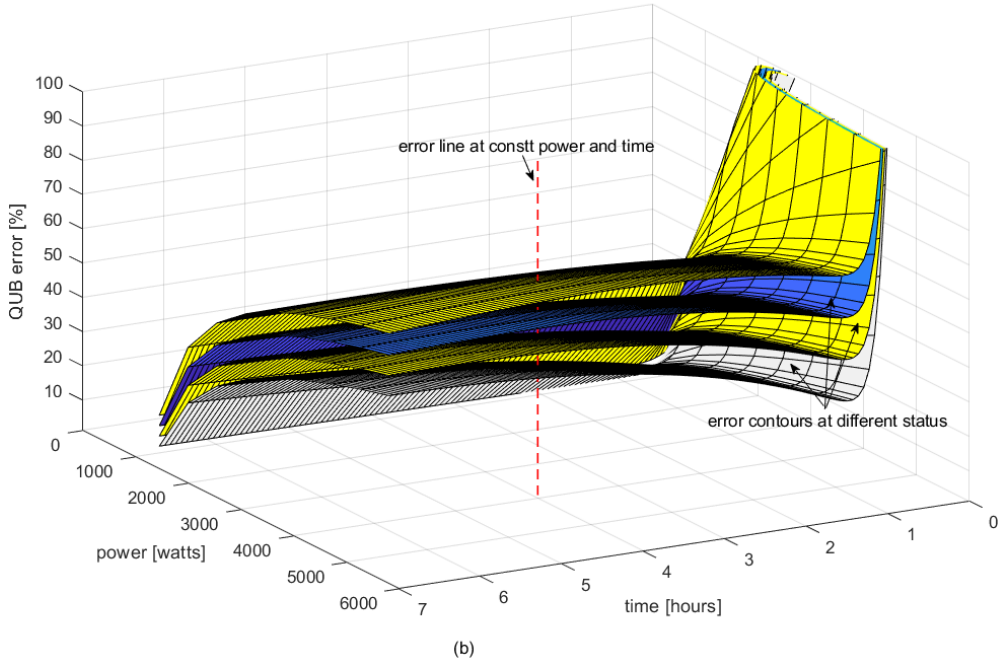

Figure 9.3: QUB error when the states in simulation are changed although the outdoor temperature and power are the same during the QUB experiment. (i) top left 35 %, (ii) top right 30 %, (iii) bottom left 24 % and (iv) error is 12 %. (b) The error curves in 3D an experiment conducted at the same level of power and time duration with different errors as shown by red vertical line

9.4 Change in temperature during the QUB experiment

The change in meteorological conditions during the QUB experiment can influence the results. The design of experiment depends on the predicted temperature during the experiment. It is expected that outdoor conditions can deviate from the predicted weather conditions. The effects of meteorological uncertainties can be reduced by performing QUB experiment at high level of power [128]. To analyze the effect of meteorological uncertainty, a QUB experiment was simulated at power level of 5'000 W during the heating phase. The experiment was simulated at the predicted outdoor temperature and then repeated at the ± 20 % of the predicted temperature (Figure 9.4). It can be observed that the responses at different outdoor temperatures are only slightly different (Figure 9.4). The QUB results with variation of outdoor temperature show a variation of $\pm 5\%$.

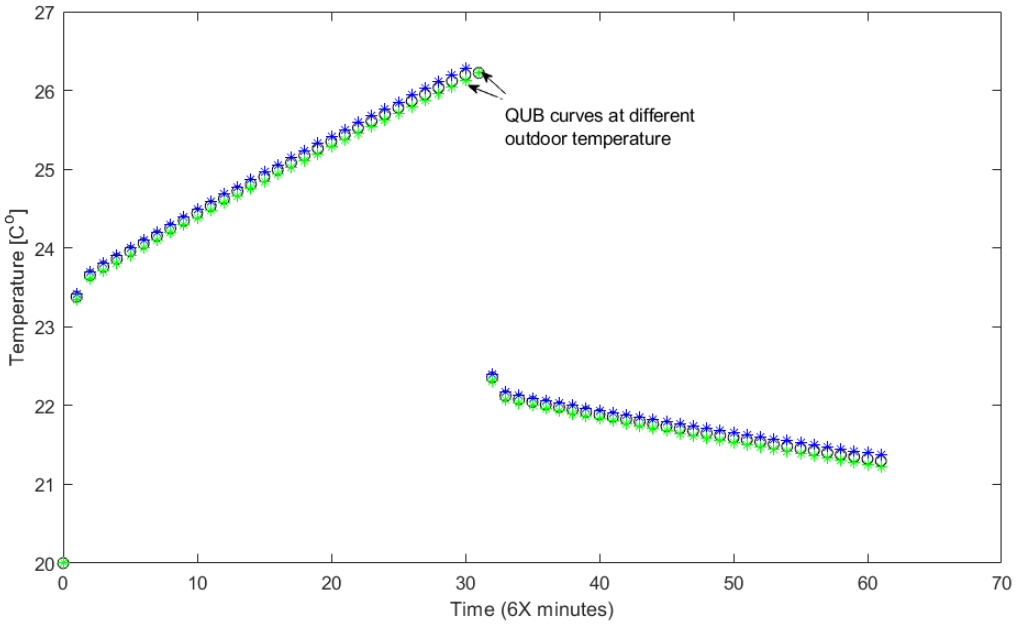

Figure 9.4: The indoor air temperature response when temperature during QUB experiment at different outdoor temperatures i.e. at predicted temperature (black circles), at -20% of the predicted temperature (green asterisks) and at $+20\%$ of the predicted temperature (blue asterisks)

9.5 QUB experiments during winter and summer seasons

The QUB experiments can be potentially performed during the entire year. The literature review does not show the impact of different seasons of the year on QUB test. To verify this, QUB experiments were simulated during winter, spring and summer seasons. An hourly EnergyPlus weather data for the city of Munich was used to simulate the QUB experiment on a house specified in IEA, EBC Annex-58 [102]. The data was interpolated to generate 10 minute data. The applied power was optimized using alpha criteria of 0.5 with no power during the cooling phase. Figure 9.5 shows the results for November to March and June to August. The experiments start at 20:00 PM and end at 05:00 AM, with a length of 4.5 hours for heating and cooling phase. The results of the experiment show that in winter season (November to March) the QUB experiments have less error and variation. The majority of the results are within $\pm$ 15 % of the reference overall heat transfer coefficient with only few outliers near $\pm$20 % (Figure 9.5). For the summer season (June, July, August), the QUB experiments show relatively large variation, majority of the results show under estimation (Figure 9.5). The set temperature before the start of QUB experiments was maintained at 20℃ during these experiments. It may be mentioned that the majority of the in-situ overall heat transfer coefficient testing methods are recommended for seasons where a minimum temperature difference of 10 K can be maintained between indoor and outdoor temperature, a condition that is difficult to achieve during summer time. The outliers during the summer season coincide with high outdoor temperatures during QUB experiments. Figure 9.6 shows the temperature difference before the start of QUB experiments during summer months and the QUB error. It is evident that the small temperature difference between outdoor and indoor temperature results in increasing of the errors. It can be seen that with the temperature difference above 10 K, the error remains within $\pm$20 %.

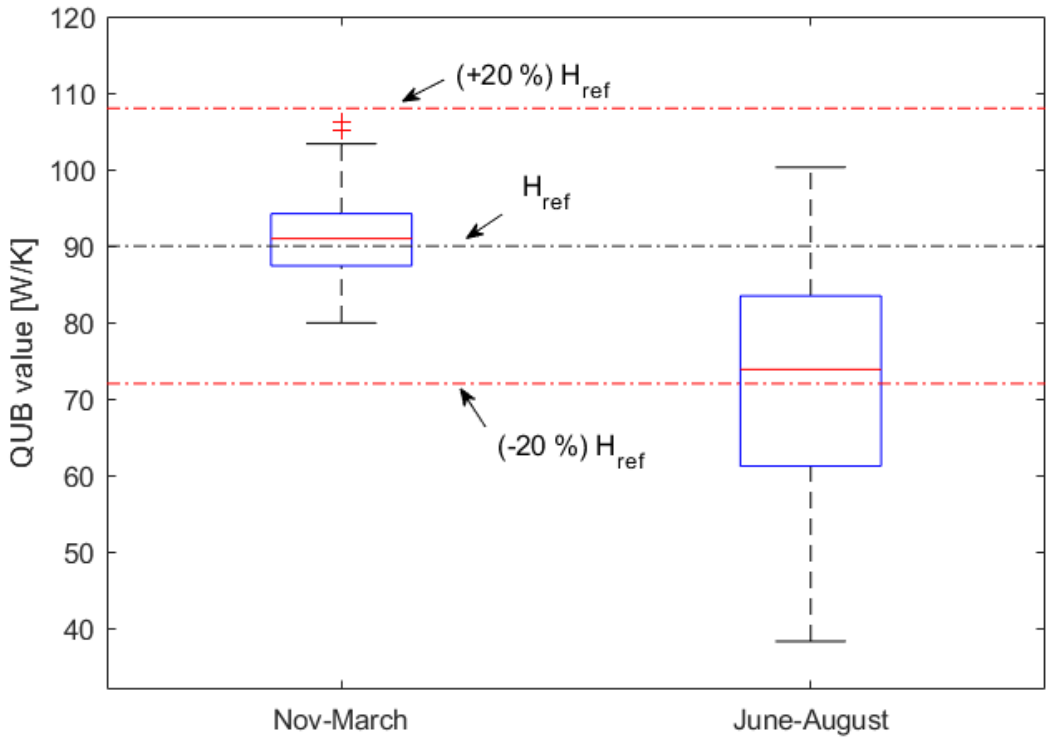

Figure 9.5: QUB experiments when performed during three seasons: winter and summers. The black dashed line shows the steady state overall heat transfer coefficient and the two red dashed lines show $(\pm 20\ \%)$ *of the steady state overall heat transfer coefficient.*

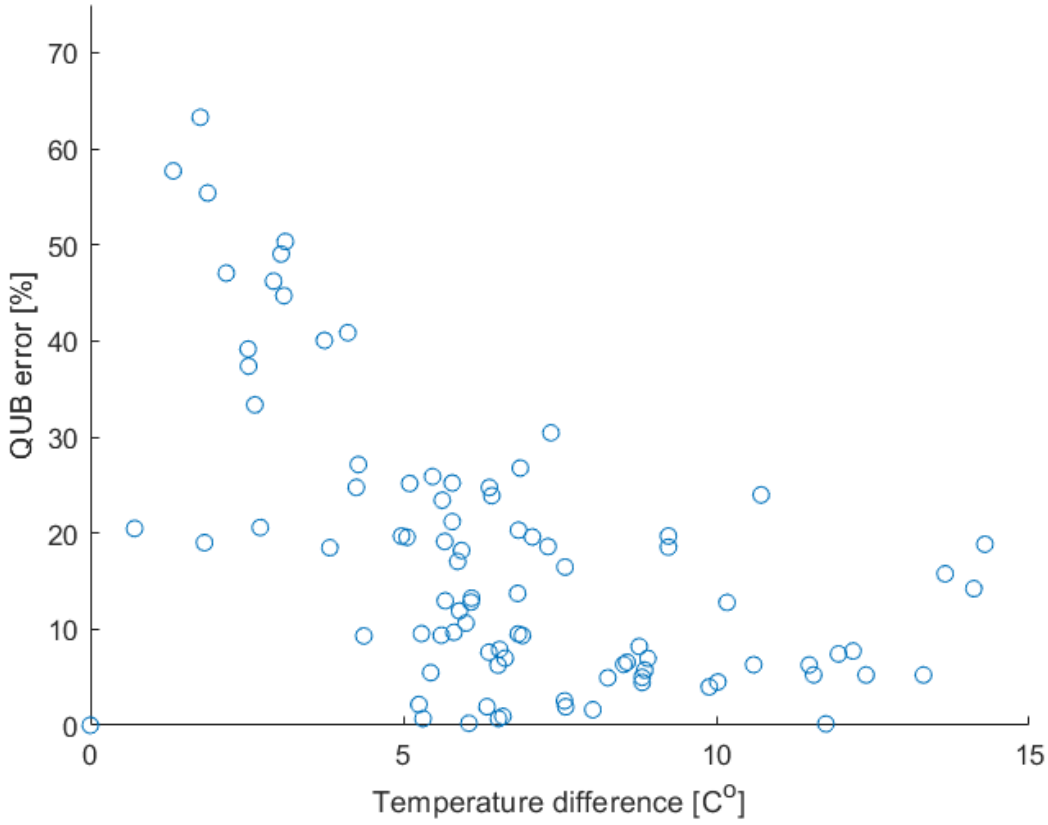

Figure 9.6: QUB error as a function of difference between outdoor and indoor temperature before the start of experiment

It can be concluded that winters is a better seasons for the QUB experiment. In summer, the variation and error in QUB experiment is relatively large due to small temperature difference between indoor and outdoor temperatures.

In order to increase the temperature difference in summer, QUB experiments during summers were repeated with a high set point temperature of $25\ ℃$ before the start of the experiment. The results of QUB experiments show (Figure 9.7) that, at high indoor set temperature, the results of QUB experiment improve. The majority of the QUB results are within $\pm 20\ \%$ of the steady state overall heat transfer coefficient with few outliers. The results are further improved by increasing the power ratio ($\alpha = 0.7$, n=3), an increase in power ratio, α above 0.7 results in over estimation of QUB results.

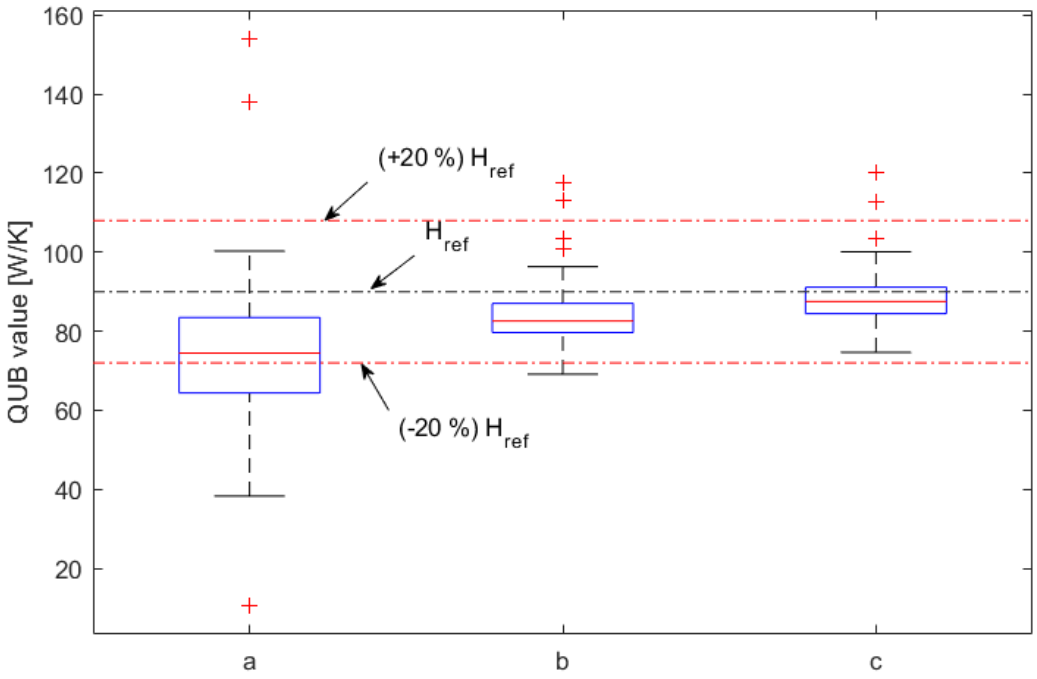

Figure 9.7: QUB experiments when simulated at (a) 20C set point temperature and alpha = 0.5 (n=2), (b) 25C set point temperature and alpha = 0.5 (n=2) (c) 25C set point temperature and alpha = 0.67 (n=3)

9.6 Conclusions

It is possible that the overall heat loss coefficient value H_{ref} used for calculation of optimum power for QUB experiment is not known with accuracy, e.g. there may be a missing insulation layer inside the wall or the thickness of the real wall insulation may be higher than the stated value. To check the robustness of QUB method, three scenarios were replicated to perform a posteriori error analysis:

- The real outer wall insulation was twice the assumed value: the real H_{ref} value of the house was $8\,\%$ less than the value used for QUB experiment design. QUB method (without knowing the real situation) responded well to the changed H-value. The error remained well within 15 % for most of the days of QUB experiment.
- The real outer wall insulation was missing (50 % change in value as compared to the assumed H-value for QUB method): QUB method, without knowing the real condition of outer wall, responded with 4 % increase in error compared to the

situation when the real condition of the outer wall was known. The error remained within ± 20 % for most of the days of QUB experiment.

- The real outer wall insulation was missing and the roof insulation was reduced (100 % changed value as compared to the assumed H-value for the QUB method). Though the QUB method responded to the changed situation, the error increased significantly (12.5 %). Still, even in this extreme case, we noted that the error made with the QUB method was significantly smaller than the error made originally. In this situation, although the accuracy of the method was deteriorated, the method still clearly showed the important fact that the assumed value of heat loss coefficient was far smaller than the true one.

QUB experiments with variable and constant outdoor temperature were simulated. Majority of the errors for variable and constant outdoor temperature (during QUB experiment) lie within$\pm 15\%$. The variation of QUB results for variable outdoor temperature is relatively similar.

The simulation results of QUB experiment can vary with change in the initial states/temperature of the building envelope. This explains why a QUB experiment for the same house but under different initial conditions will generate different results, a reason why two QUB experiments are most likely to have different outcomes.

The meteorological conditions can vary, i.e. the outdoor temperature can increase or decrease during QUB night. A $\pm 20\%$ variation in outdoor temperature vary the QUB results within ± 5 %.

Winter can be considered as suitable for QUB experiments. Experiments conducted for the month of November, December, January, February and March show that the majority of the errors lie within$\pm 15\%$ with few outliers around ± 20 %.

The QUB experiments for summer months (June, July and August) show large variation (errors). However, it is possible to predict the experiment outcome by observing the difference between indoor temperature and outdoor temperature during the QUB experiment. The experiments give large errors when the temperature difference between the initial indoor and outdoor temperature is smaller than 10K. With set point of 20℃ the difference between indoor and outdoor temperature for few days remained smaller than 10K, the experiments in such conditions generated large errors. The results during summer days were improved by using a high set point temperature (25 ℃), such that majority of the errors remained within ± 20 ℃ of the steady state overall heat transfer coefficient.

This page is intentionally blank

10 Conclusions and perspectives

Energy (supply and consumption) constitute the major source of global greenhouse gas emissions. Different projections show continuous growth in consumption and associated emissions in future. Buildings contribute 21 % to the global energy consumption and 2/3rd of the greenhouse gas emissions. In developed regions, like EU and US, buildings constitute 40 % and 34 % of the total energy consumption, respectively. The International Energy Agency projected an annual growth of 1.1 % between 2015 and 2040.

Two approaches are used to reduce emissions due to building energy consumption: supply side management and demand side management. Demand side management includes all steps to reduce building energy consumption, such as improving thermal resistance of envelope, reducing infiltration losses, improving efficiency of heating and cooling equipment etc. A systematic and predictable way to achieve energy efficiency is to introduce building energy regulations that put limit on energy standards for different building components. Majority of the countries have now adopted building energy regulations.

The positive impacts of regulations are difficult to assess because of the multiple factors impacting building energy consumption. However, some studies [11], [14] have confirmed the potential savings, although the savings are either underestimated or overestimated. The building energy consumption is usually assessed using mathematical models or thermal performance tests. The models can either calculate the energy consumption of the building under different set of conditions or estimate performance measurement parameters.

This work discusses the mathematical methods for parameter identification. The modelling methods can be categorized as statistical modelling, physical/forward modelling and hybrid modelling. The focus of this work is on parameter identification models. The parameter identification models can be categorized as steady state modelling and dynamic modelling. Both steady state and dynamic models have their advantages and disadvantages. The

multiplicity of modelling performance criteria, i.e. criteria over which modelling performance can be evaluated, makes it difficult to prefer one method over the other. However, the dynamic models can be preferred for their ability to estimate dynamic characteristics of building. A short duration experimental data is usually required for dynamic analysis.

The performance prediction of building's energy consumption is based on simulation. The performance predictions are either underestimated or overestimated. This prediction discrepancy is termed as "Performance Gap". Some of the reasons of performance gap are deterioration of building thermal properties, reduction in efficiency of equipment, operation off the designed values, changing weather pattern, changes in operation schedule, occupancy and inability of simulation tools to cover complete dynamics of building.

A better measure for building performance is to determine the building parameters, such as overall heat transfer coefficient, solar aperture and building time constants etc., known as the intrinsic performance measurement. These measures remain fairly stable with changing weather conditions, operation schedule etc. The identification models can be either based on pre designed/supervised onsite (in-situ) experiments, such as co-heating, or they can be based on unsupervised experiments, such as smart metering data where the coefficient of regression analysis provide different parameters.

In case of supervised experiments, the thermal performance of building or building components is evaluated using onsite (in-situ) testing methods. Most of the test methods developed are aimed at thermal performance verification of building envelope by using measurements and estimation techniques to verify the claimed characteristics. The methods discussed in this work are ISO 9869 (flow meter) method, calorimetric method, co-heating testing methods, etc. These methods are known as long term methods.

The long term methods require a long testing period that can range from two to four weeks, with the least reported measurement period being three days. Most of the tests produce precise results when applied on unoccupied buildings. The season of the year during which the tests can be conducted is limited to heating season only when external temperatures are

low and effects of solar radiations are minimal. These shortcomings make long term methods impractical to be employed at large scale in practice.

Short term in-situ thermal characterization methods are developed that have much smaller duration of time as compared to the long term methods. QUB, PSTAR/STEM, ISABELE, EPM (Excitation pulse method) and HYBRID methods are some of the short term methods reported in various literature sources. With short duration, they have the potential to be employed at large scale in practice. However, the validation of these methods is limited to small number of simulation and experimental results. These methods need critical analysis, significant simulations and real time tests on buildings, before they can be generalized in practice.

Among the short methods, QUB is a dynamic in-situ thermal characterization test method that has the potential to be conducted in the shortest duration; the theoretical background of the method offers an understanding of the correctness of the method. The method is tested on small scale buildings, on full scale house with controlled environment and a full scale house with real weather conditions. The method is robust; the over-all heat transfer coefficient value (H) measured using QUB method lies within ± 20 % of the steady state value. It is important to understand the variation of QUB method with variation in boundary conditions (solar radiations, outdoor temperature and outdoor temperature variation during QUB test night) and initial conditions (initial power before QUB experiment). The robustness of QUB method with uncertainty in power level (during QUB heating phase) and uncertainty in H_{ref} (overall heat transfer coefficient) needs to be established with real time data.

To model the QUB method, a dynamic sate space modelling method is explained and tested in this work. The state space modelling involves generating thermal circuit for each component of building (walls, fenestration, ventilation etc.). The thermal circuits are then combined to generate a single circuit for the entire building. The state space model is validated using measured data of a full scale house (the Twin House). With a data of 10 min. time step size, the state space model simulated the interior temperature of the entire house (seven zones), the errors varied between ± 2 ℃, The three quartiles of the errors lied within ± 1 ℃.

The state space model is validated with QUB experimental data, with modelling errors well within± 0.5 ℃.

Simulation of QUB experiment with the Twin House data shows that the method has only slight variation with uncertainty in power; for example, a 30 % error in optimum power can cause an error within 3 % of the reference value. The QUB method can be considered as robust with variation in power.

A priori analyses are achieved without the justification of experimental or real observations whereas A posteriori analyses are performed after obtaining experimental observations. A priori error analyses are done by performing the QUB experiments in a situation where the real envelope has different characteristics (without the knowledge of real envelope). These results are then compared with a posteriori errors, a situation in which QUB experiments are performed with the knowledge of the real envelope. The error analysis shows that with 50 % error in H_{ref} value (missing wall insulation situation), the QUB method results in an increased error of 3 % only. The method can be considered as robust within the range of 50 % error in H_{ref}.

The QUB method was tested with reference to variation in solar radiation. QUB results on cloudy days show lesser variation as compared to sunny days. It was shown that the heat transfer from the delayed solar radiation entering through the walls of the building has an effect on the temperature evolution during the QUB experiment. This can lead to an increased error in QUB method. A method was used to estimate the contribution of solar radiation and to calculate a solar corrective factor that can reduce the error of QUB method. The impact of corrective factor depends on the solar radiation before the QUB experiment and the thermal capacitance of the building envelope.

In this work, the QUB experiments were initially performed with a limited seasonal variation, that is a season between the months of August and September. The twin house can be considered as a full scale real house. The QUB method has a good potential to be employed on commercial scale. It is therefore important to conduct QUB experiment during different

seasons of the year, such as winter and summer. The repetition of experiments during winter and summer seasons show that winter season is a preferred season for QUB experiments. The summer months show large variation (errors) in results when the temperature difference between indoor and outdoor conditions is smaller than 10 K. The QUB results during summer month can be improved by using a high set point temperature before the start of QUB experiments.

The analysis and results in the current work were performed using simulations. The simulation model was validated on IEA, EBC Annex-58 data. Some of the conditions, such as power levels and time duration, weather data etc., were varied with help of simulations. It will be interesting to repeat the real QUB experiment with the variation in power and time duration. This will help validate the simulation results. The QUB method should be further tested on different constructions, such as apartment buildings, houses with low and high insulation levels as well. In the current simulation, the weather data from European region is used. It will be interesting to test the QUB method with construction and weather data from regions with temperate and hot climates, as well.

This page is intentionally blank

11 Annexes

11.1 Description of the Twin House experiments

The Twin House experiments were conducted as part of Annex 58: *Reliable building energy performance characterization based on full scale dynamic measurements* of the International Energy Agency Energy in Buildings and Communities program (IEA EBC) [50]. The purpose of Annex 58 was to collect the existing tools, knowledge and experimental setups that can be used for dynamic thermal characterization of building components and whole building. The Subtask 4 of IEA EBC Annex 58 dealt with the characterization of an the entire building and involves verification of building energy models (thermal characterization) based on in situ tests [102].

The purpose of Twin House experiment was to generate a good quality data set that can be used to verify the performance of building energy models. The aim was to simulate real conditions inside a real house and generate number of measurements that can be used for simulation and estimation of thermal characteristics. In order to simplify the simulation conditions, the two identical houses were non-occupied during the experiment. Both houses were equipped with instruments that might not be possible to install/use in normal occupied house. The experiment details are given in section 5.2

11.1.1 Construction details of the Twin Houses

Location: Holzkirchen, Germany, 47.874 N, 11.728 E, 680 m altitude

Constant temperatures: cellar 19.5 °C, attic 25 °C

South façade roller blinds: down for building N_5, up for building O_5.

Internal height: 2.495 m

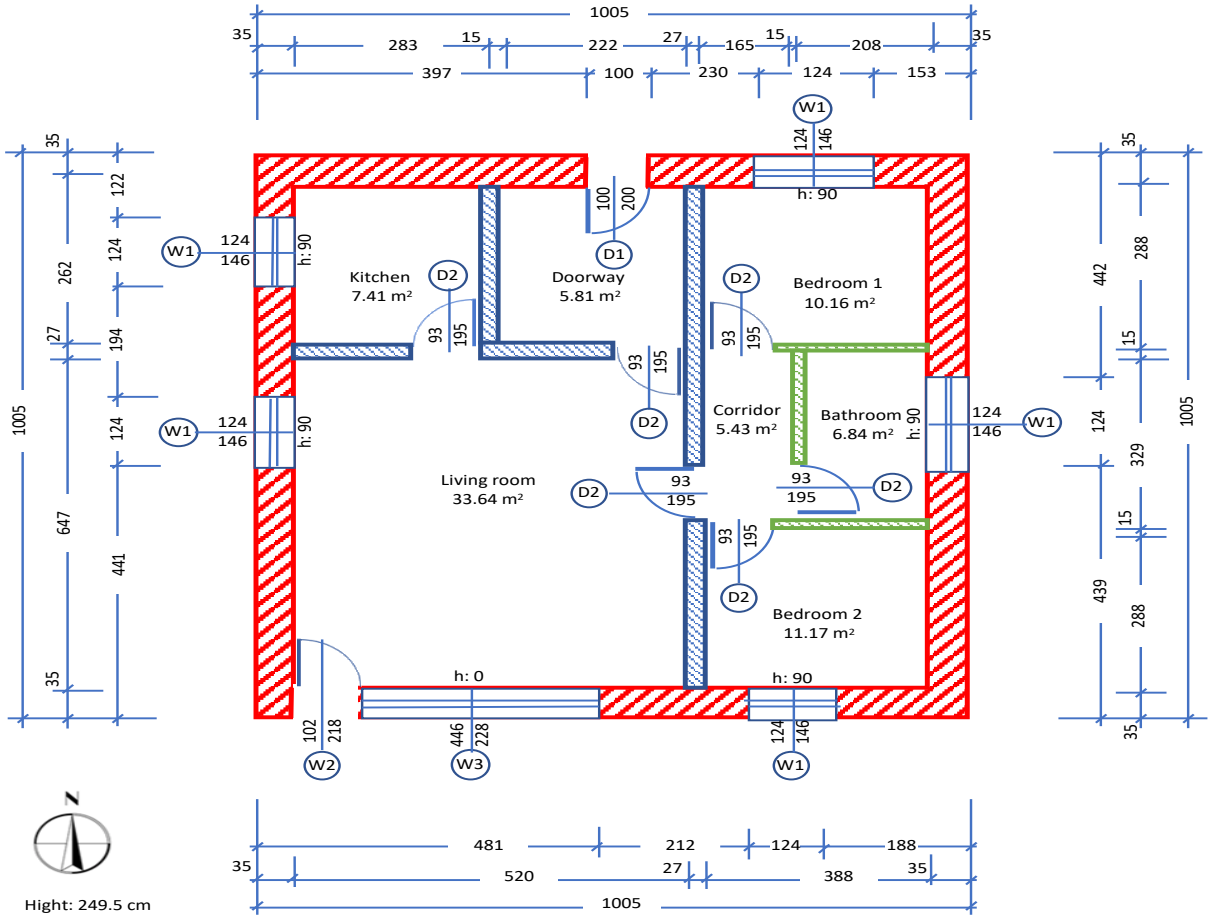

Figure 11.1 Layout and dimensions of ground floor of twin house

Table 11-1 Window dimensions

Window type	Overall dimensions with roller blinds	Overall dimensions without roller blinds	Glass dimensions
W1	1.24 x 1.74	1.24 x 1.46	1.00 x 1.30
W2	1.02 x 2.38	1.02 x 2.18	2.00 x 0.90
W3	4.46 x 2?58	4.46 x 2.28	3 x 1.00 x 1.40

Table 11-2 Walls and doors

	Wall type	Layer	Thickness (m)	Cond. (W/mK)	Dens. (kg/m^3)	Sp. heat (J/kg K)	Absorp SW	Emiss LW
P1	External wall (red) U = 0.2	Ext. plaster	0.01	0.80	1200	1000	0.23	0.90
		Insulation	0.12	0.035	80	840		
		Plaster	0.01	1.00	1200	1000		
		Brick	0.20	0.22	800	1000		
		Int. plaster	0.01	1.00	1200	1000	0.17	0.90
P2	Internal wall (blue)	Plaster	0.01	0.35	1200	1000	0.17	0.90
		Brick	0.25	0.33	1000	1000		
		Plaster	0.01	0.35	1200	1000	0.17	0.90
P3	Internal wall (green)	Plaster	0.01	0.35	1200	1000	0.17	0.90
		Brick	0.13	0.33	1000	1000		
		Plaster	0.01	0.35	1200	1000	0.17	0.90
P4	Ceiling U = 0.25	Screed	0.04	1.40	2000	2000	0.60	0.90
		Insulation	0.04	0.04	80	840		
		Concrete	0.22	2.00	2400	1000		
		Plaster	0.01	1.00	1200	1000		
		Insulation	0.10	0.035	80	840	0.17	0.90
P5	Ground U = 0.32	Concrete	0.22	2.10	2400	1000	0.60	0.90
		Fill	0.03	0.06	80	840		
		Insulation	0.03	0.025	80	840		
		Panel	0.03	0.023	80	840		
		Screed	0.06	1.40	2000	1000	0.60	0.90
D1	External door	Wood	0.04	0.13	600	1000	0.60	0.90
D2	Internal door	Wood with glass	0.04	0.13	600	1000	0.60	0.90

Windows

Double glazing with low emissivity and argon fill. U-value (EN ISO 10077_1): U = 1.2 W/m^{2}K. Hemispheric solar transmittance 0.43. Hemispheric solar absorptance: 0.11.

Thermal bridges

Junction	ψ – value (W/m K)
External wall – floor	0.107
External wall – ceiling	0.084
External wall – external wall	0.093
Internal wall – floor	0.378
Internal wall – ceiling	0.204
Window sill	0.140

Ventilation

The living room is ventilated with outside air at the rate of 120 m^3/h. There two exhaust ducts inside the bathroom and bedroom with an exhaust rate of 60 m^3/h, each. The ventilation air enters through basement and passes through kitchen to the ceiling of living room. The ventilation duct passing through kitchen is uninsulated and therefore receives heat from the kitchen air. This must be taken into consideration during simulation.

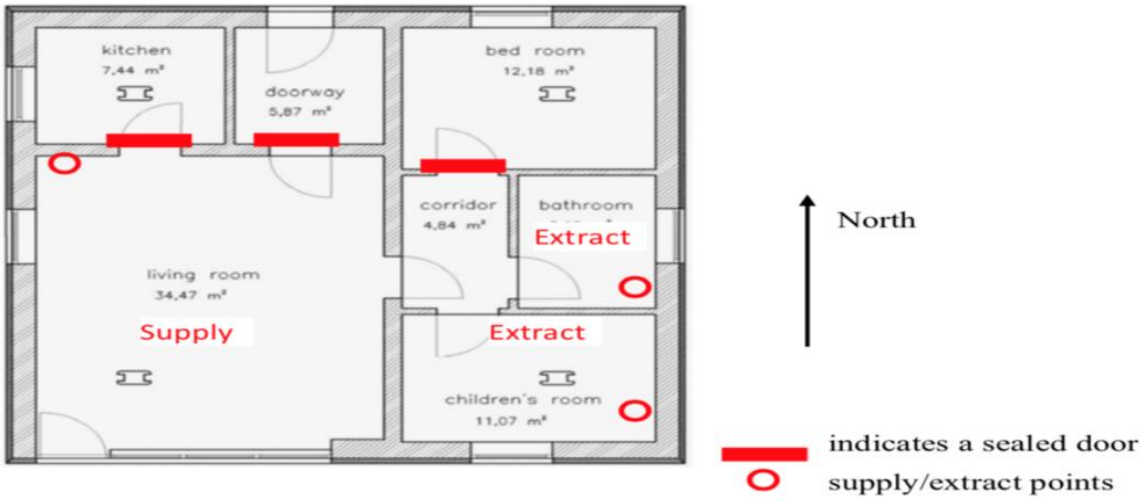

Figure 11.2: Exhaust and intake ports for ventilation

Supply flow rates and temperatures are supplied with data. The air is distributed equally to both extractors.

Heating / cooling

Electric heater 30 % radiative and 70 % convective.

Time response of the heater: 1 – 2 minutes.

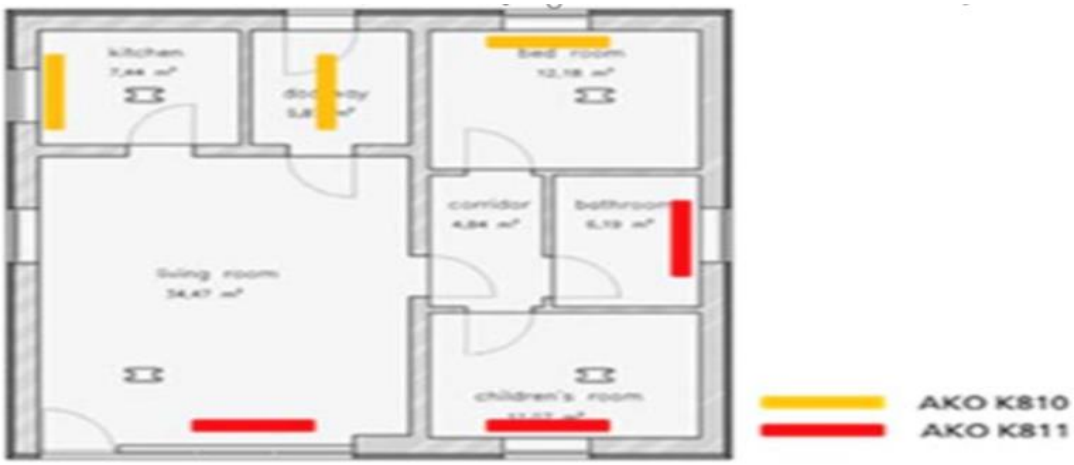

Figure 11.3: Heater locations in Twin house

Air leakage

Whole ground floor

Twin House N2 (northern house): n_{50} = 1.62 ACH

Twin House O5 (southern house): n_{50} = 1.54 ACH

Living room-corridor-bathroom-children's room with doors sealed:

Twin House N2 (northern house): n_{50} = 2.2 ACH

Twin House O5 (southern house): n_{50} = 2.3 ACH

Ground reflectivity: 0.23

Table 11-3 Surfaces

	Position		Type		Surface
1	North	wall	P1	10.05*2.49 - 2*0.35 - 1.00*2.00 - 1.24*1.46	20.51
2		door	D1	1.00*2.00	2.00

3		window	W1	1.24*1.46	1.81
4	East	wall	P1	10.05*2.49 - 2*0.35 - 1.24*1.46	22.51
5		window	W1	1.24*1.46	1.81
6	South	wall	P1	10.05*2.49 - 2*0.35 - 1.24*1.46 - 4.46*2.28 -1.02*2.18	10.12
7		window	W1	1.24*1.46	1.81
8		window	W2	1.02*2.18	2.22
9		window	W3	4.46*2.28	10.17
10	West	wall	P1	10.05 - 2*0.35 - 2*1.24*1.46	5.72
11		window	W1	2*1.24*1.46	3.62
12	Indoor	wall	P2	2.49*(3.97 + 2.62 + 10.05 - 2*0.35) - 3*0.93*1.95	34.25
13		wall	P3	2.49*(2*2.08 + 3.29) - 0.93*1.95	16.74

11.1.2 Data

The twin house experiment provides two data files. One with measurement of all the inside temperatures and heat input from the heaters along with other measurements. The file is named as `Twin_house_exp1_house_N2_10min_ductwork_correction.xls`. The second file contains data from the weather station measurements, such as outdoor temperature, solar radiations, wind speed, wind direction etc.

The file is named as `Twin_house_exp1_weather_data_all_measurements_10min.xls`

The procedure to load data in MATLAB:

- delete the header (first two lines)
- change date and hour in numbers
- take care to use decimal point
- copy from A1 :AJ5905 and paste in a new sheet
- save as .csv

1	1	2	3	4	5	6	7	8
2	Date	Time	N2_attic_east_AT	N2_attic_west_AT	N2_cellar_AT	N2_living_AT_h67cm	N2_living_AT_h125cm	N2_living_AT_h187cm
3	dd.MM.yyyy	HH:mm:ss	°C	°C	°C	°C	°C	°C
4	21/08/2013	00:00:00	24,135921	24,057659	20,144239	29,531048	29,986008	31,134912
5	21/08/2013	00:10:00	24,12431	24,038069	20,13871	29,547962	30,000132	31,15799
6	21/08/2013	00:20:00	24,110592	24,020189	20,131298	29,54632	29,972891	31,184851

	I	J	K	L	M	N	O	P
1	9	10	11	12	13	14	15	16
2	N2_corridor_AT	N2_bath_AT	N2_child_AT	N2_kitchen_AT	N2_doorway_AT	N2_bedroom_AT	N2_living_rH_h125cm	N2_westfacade_S_IS_T
3	°C	°C	°C	°C	°C	°C	%	°C
4	30,049305	29,979389	29,99707	29,986731	30,012228	30,000942	32,82666	29,403091
5	30,057949	30,0056	30,006847	29,99439	29,999079	29,998449	32,73769	29,403967
6	30,067911	30,00235	30,002213	30,00835	29,985352	30,000271	32,673229	29,420502

1	17	18	19	20	21	22
2	N2_westfacade_S_IS_HF	N2_westfacade_S_BL1_T	N2_westfacade_S_BL1_HF	N2_westfacade_S_ES_T	N2_heat_elP_living_room	N2_heat_elP_bath_room
3	W/m²	°C	W/m²	°C	W	W
4	-5,42798	23,11824	-8,122489	7,441233	1148,295898	195,525391
5	-5,436573	23,088718	-8,203476	7,30115	1159,407959	197,555878
6	-5,588989	23,06073	-8,235997	7,364199	1174,606934	192,249298

1	23	24	25	26	27	28	29
2	N2_heat_elP_children_room	N2_heat_elP_kitchen	**N2-Heat-Input-Kitchen**	N2_heat_elP_doorway	N2_heat_elP_bedroom	N2_vent_ODA_AT	N2_vent_SUA_AT
3	W	W	W	W	W	°C	°C
4	362,478455	316,952423	-147,4558946	181,835098	262,006775	12,0888	14,122999
5	362,155701	323,893127	-148,8728733	181,458313	266,2659	11,94253	13,998851
6	356,349487	318,024597	-149,8112527	184,004181	261,460388	11,87324	13,926028

1	30	31	32	33	34	35	36
2	**N2_vent_SUA_corr**	N2_vent_EHA_AT	N2_vent_SUA_VFR	N2_vent_EHA_VFR	N2_vent_SUA_fan_elP	N2_vent_EHA_fan_elP	N2_vent_thP
3	°C	°C	m³/h	m³/h	W	W	W
4	17,60345897	30,50737	120,032494	120,069397	51,31963	62,448448	-661,163208
5	17,50940971	30,539021	120,024002	119,975388	51,350929	62,469982	-667,194641
6	17,45614642	30,520077	120,045204	119,9879	51,047638	62,144032	-669,467102

The measured data inside the house is as:

1	1	2	3	4	5	6	7	8	9
2	Date	Time	Ambient temperature	Solar radiation: global h	Solar radiation: di	Solar radiation: g	Solar radiation:	Solar radiation: g	Solar radiation: g
3	dd.MM.yyyy	HH:mm:ss	°C	W/sqrm	W/sqrm	W/sqrm	W/sqrm	W/sqrm	W/sqrm
4	21/08/2013	00:00:00	9.863076	0	0	0.000667	0.158132	0.020885	0.033397
5	21/08/2013	00:10:00	9.8295	0	0	0.054833	0.186	0.006	0.112
6	21/08/2013	00:20:00	9.806328	0	0	0.042842	0.201919	0.021382	0.231267

1	10	11	12	13	14	15	16	17	18
2	Longwave radiation horiz	Longwave radiation vert	Wind speed	Wind direction	Relative humidity	Ground temperature (0cm)	Ground temperature (50cm)	Ground temperature (100cm)	Ground temperature (200cm)
3	W/sqrm	W/sqrm	m/s	deg	%rel.H.	°C	°C	°C	°C
4	311.48999	339.994904	0.980333	78.949989	99.660141	16.78117	18.899998	17.800001	14.800001
5	314.247986	340.939758	0.942	64.820015	100	16.675671	18.899998	17.800001	14.800001
6	316.124695	341.495209	0.802	70.011665	99.579666	16.58017	18.899998	17.800001	14.800001

The data files are loaded as (`KithcenLivngrmnew.m`)

```
4 -     H = dlmread('TwinHouse.csv');    % house
5 -     W = dlmread('TwinWeather.csv'); % weather
```

Desired weather data such as outdoor temperature, solar radiations and data for any room temperature or input heat from heater is loaded as

```
305        % Inputs
306 -      Ti  = H(:,7);      % temperature in living at 125 cm (output)
307 -      Tk  = H(:,12);     % kitchen
308 -      Td  = H(:,13);     % doorway
309 -      Tc  = H(:,9);      % corridor
310 -      Tb2 = H(:,11);     % bedroom 2
311 -      Ta  = H(:,4);      % attic
312 -      Tg  = H(:,5);      % cellar
313 -      Tv  = H(:,30);     % ventilation supply air
314 -      To  = W(:,3);      % outdoor
315 -      Qs  = W(:,8);      % specific global solar vert. South
316 -      Qw  = W(:,9);      % specific global solar vert. West
317 -      Qi  = H(:,21);     % el. power living
318
```

11.2 Thermal model of the Twin House

11.2.1 Modeling of single zone model (Living room)

Script file `s02THLiving01Rad.m`

Living room is modelled as a single room of twin house, the conditions of areas adjacent to living room are considered as boundary zones as shown in figure. The living room is bounded by kitchen wall, kitchen door, doorway wall, doorway door, corridor wall, bedroom wall, Southern external wall, southern window, Eastern wall and Eastern window.

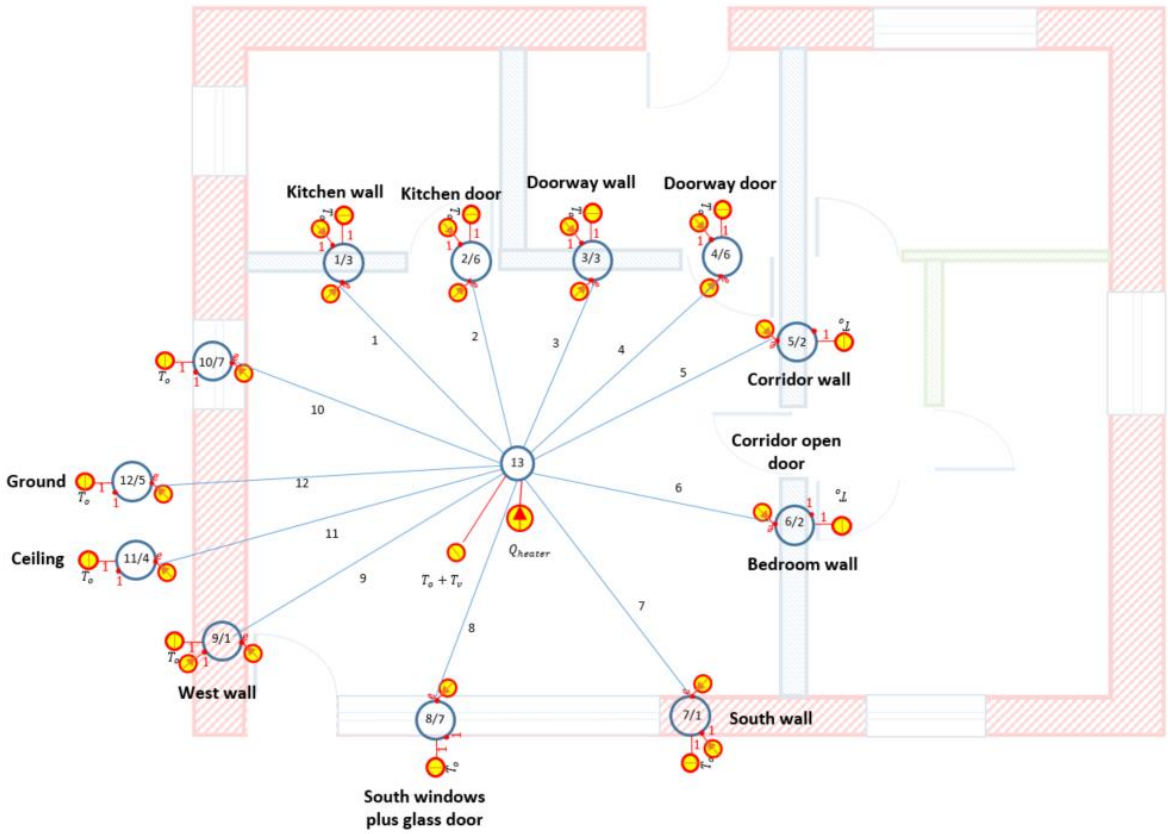

Figure 11.4: Thermal circuit connections for living room zone

Figure 11.5 shows the connection of each thermal circuit (wall, windows, ceiling etc.) with room air. The thermal circuit for each component of living room (wall, windows, ceiling etc.) is as shown in figure

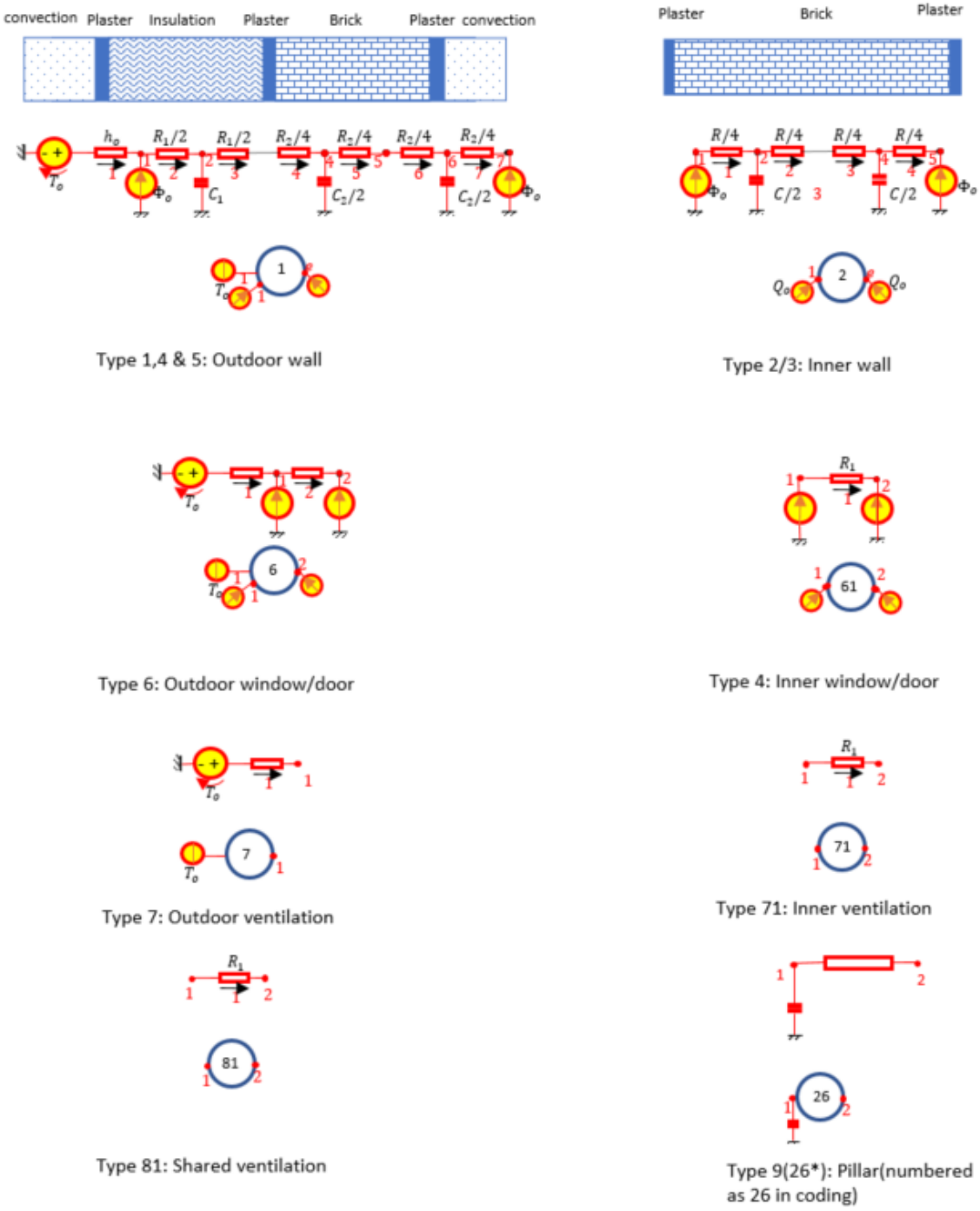

Figure 11.5: Building components, thermal circuits and their symbols

Each wall is modelled as RC circuit with adjustable number of slices (Resistances and Capacitances) as

```
15      % Wall type P1: external [insulation; brick]
16 -    nm1 = [4 8]';              % for wall P1, number of meshes in layer 1, 2, ...
17 -    w1 = [0.12 0.20]';         % width [m]
18 -    lam1 = [0.035 0.22]';      % conductivity [W/m K]
19 -    rho1 = [80 800]';          % density [kg/m3]
20 -    c1 = [840 1000]';          % specific heat [J/kg K]
21
22 -    G1 = lam1./w1;
23 -    C1 = rho1.*c1.*w1;
24 -    G1m1 = 2*nm1(1)*G1(1)*ones(2*nm1(1),1); % meshed insulation
25 -    G1m2 = 2*nm1(2)*G1(2)*ones(2*nm1(2),1); % meshed brick
26 -    C1m1 = C1(1)/nm1(1)*mod(0:2*nm1(1)-1,2)';% meshed insulation
27 -    C1m2 = C1(2)/nm1(2)*mod(0:2*nm1(2)-1,2)';% meshed brick
28
29 -    G1 = [ho; 0.8/0.01; G1m1; 1/0.03; G1m2;1/0.01];
30 -    C1 = [0; C1m1; 0; C1m2;0;0];
31 -    nt = length(G1); nq = nt;        % no. temperatures; no. flows
32 -    A1 = diff(eye(nt+1));
33 -    A1(:,1) = [];                     % delete 1st node = reference temperature
34 -    b1 = zeros(nq,1); b1(1) = 1;      % Temp source on branch 1: Tout
35 -    f1 = zeros(nt,1); f1(1) = 1;      % Flow source in node 1: Qsolar
36 -    f1(end) = 1;                      % radiation on surface
37 -    y1 = zeros(nt,1);                 % No output
```

The air inside living room is modelled as homogeneous node exchanging heat with different surfaces via branches as shown in Figure 11.6

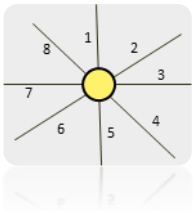

Figure 11.6: Air nodes with braches connecting different walls and components of living room

The air node for each room/zone is modelled as (s02THLiving01Rad.m)

```
% Indoor air
Va = 120/3600;      % volumetric air flow [m3/s]
Infil=1.62/3600; %Infiltration per hour per floor area 81.69
sg=81.69;
Infil1=0.75*2.22/3600;
S13=2.662; %Surface area of Pillar
G8 = hi*[S1; S2; S3; S4; S5;S7; S8; S9; S10; S11; S12; S12];
G8 = [G8; rhoa*Va*ca;Infil/23*sg*rhoa*ca;Infil1/23*sg*rhoa*ca;Va*rhoa*ca;2.495*0.093]; %Inculding thermal bridge
A8 = -eye(13); A8=[A8;zeros(1,13);zeros(1,13);zeros(1,13);zeros(1,13)]; A8(:,13) = 1;
C8 = zeros(13,1); C8(13) = rhoa*6.47*5.20*2.495*ca;
b8 = zeros(17,1); b8(13) = 1;b8(14) = 1;b8(15)=1;b8(16)=1;b8(17)=1;  % in: source Tout
f8 = zeros(13,1); f8(13) = 1;   % in: source heat flow in air volume
y8 = zeros(13,1); y8(13) = 1;   % out: indoor air

TCd{13} = {A8,diag(G8),b8,diag(C8),f8,y8};              % indoor air
```

All the circuits once modelled are assembled and connected with air node using Matlab function `fTCAssAll.`

```
    % Assembling and ss-model
    % ***********************************
    AssX = [1  length(f2)  14  1;...
            2  length(f6)  14  2;...
            3  length(f2)  14  3;...
            4  length(f6)  14  4;...
            5  length(f2)  14  5;...
            6  length(f2)  14  6;...
            7  length(f1)  14  7;...
            8  length(f7)  14  8;...
            9  length(f1)  14  9;...
            10 length(f7)  14  10;...
            11 length(f4)  14  11;
            12 length(f5)  14  12;
            14 13 13 length(f9)];

    [TCa, Idx] = fTCAssAll(TCd, AssX);
```

The input temperature, heat flow sources and solar radiations are modelled as:

```
% SW radiative sources on walls: distributed uniformely
Sliv = 2*(6.47+5.20)*2.495 + 2*6.47*5.20; % total area living room
% radiative gain through closed blinds
Qr = [S1 S2 S3 S4 S5 S7 S8 S9 S10 S11 S12 S12]/Sliv.*(1.29*Qw*0.427+0.3*Qi)*0.8 ;

T = [Tk'; Tk'; Td'; Td'; Tc';Tb2';...
    To'; To'; To'; To';...
    Ta'; Tg'; Tv';To';Tk';Tc';To';To';Tk'];

Q=[Qr'; 0.7*Qi'+(1.29*Qw'*0.427+0.3*Qi')*0.20];
u=[T;Q];
u = [u(1:25,:); S8*0.23*Qs'; u(26,:); u(27,:); ...
    S10*0.23*Qw'; u(28,:); u(29,:); u(30:end,:)];
```

The indoor temperature is simulated using all the three methods namely Euler Explicit, Euler Implicit and exponential methods as:

```
336 —     n = length(H(:,1));
337 —     Time = 0:dt:(n-1)*dt;              % time
338 —     nth = size(A,1);                   % no states
339       % initial conditions
340 —     th = 28*ones(nth,n); thi = th; the = th;
341 —     Ae = (eye(nth) + dt*A);            % Euler explicit
342 —     Ai = inv((eye(nth) - dt*A));       % Euler implicit
343 —     Ad = expm(A*dt);                   % exp. matrix
344 —     Bd = (Ad-eye(size(A)))*inv(A)*B;
345 —   for k = 1:n-1
346 —     th(:,k+1) = Ae*th(:,k) + dt*B*u(:,k);      % Euler explicit
347 —     thi(:,k+1) = Ai*(thi(:,k) + dt*B*u(:,k));  % Euler implicit
348 —     the(:,k+1) = Ad*the(:,k)+Bd*u(:,k);        % matrix exponential
349 —   end
350 —   ye = C*th + D*u;          % Euler explicit
351 —   yi = C*thi + D*u;         % Euler implicit
352 —   yE = C*the + D*u;         % exponential
```

11.2.2 The Twin house two zones model (Kitchen and Living room)

Script File `KithcenLivngrmnew.m`

The model of two zones is the same as single zone except that there will be a shared wall or door between the two zones and now the temperature of two zones will be simulated. In our two zones model we modelled two zones Kitchen and Living room. The shared zones are door and wall between the two zones. Infiltration is also shared between the two zones.

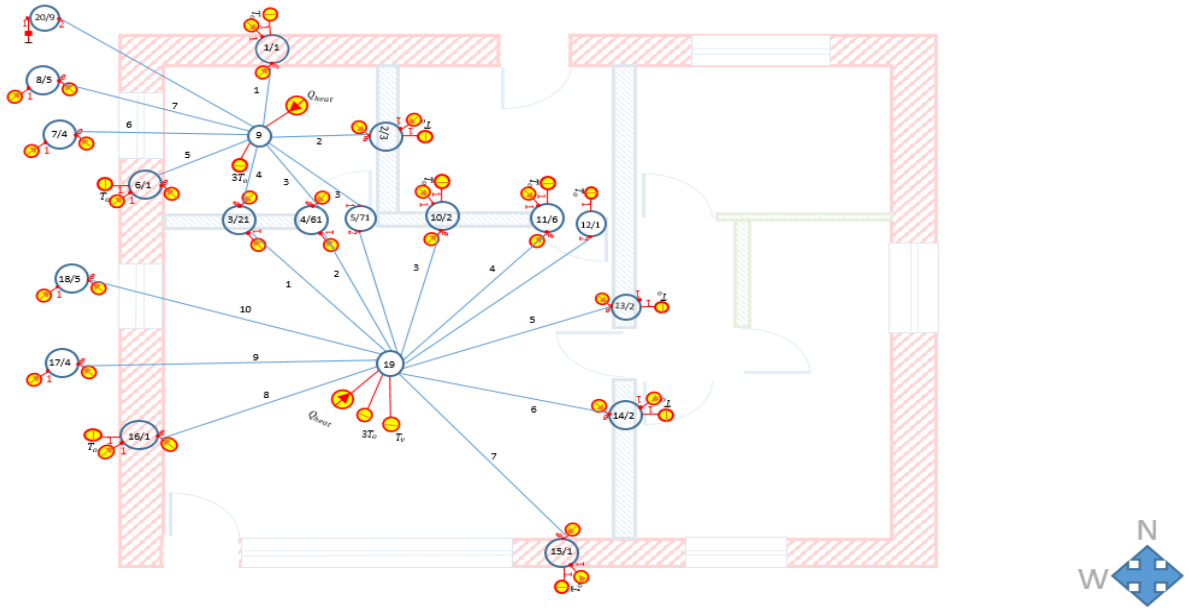

Figure 11.7: Thermal circuit diagram for living room and kitchen

The shared walls are modelled as

```
117      % Shared Internal thin Wall type P3: internal [brick]
118 -    nm3 = 2;       % number of meshes in layer
119 -    w3 = 0.115;     % width
120 -    lam3 = 0.33;   % conductivity [W/m K]
121 -    rho3 = 1000;   % density [kg/m3]
122 -    c3 = 1000;     % specific heat [J/kg K]
123
124 -    G31 = lam3./w3;
125 -    C31 = rho3.*c3.*w3;
126 -    G3m = 2*nm3*G31*ones(2*nm3,1);          % meshed brick
127 -    C3m = C31/nm3*mod(0:2*nm3-1,2)';   % meshed brick
128 -    G31 = [0.35/0.01;G3m;0.35/0.01];%With plaster layers
129 -    C31 = [0;C3m;0;0];
130 -    nt = length(C31); nq = length(G31);      % no. temperatures; no. flows
131 -    A31 = diff(eye(nt));
132 -    b31 = zeros(nq,1); b31(1) = 1;     % Temp source on branch 1: Troom
133 -    f31 = zeros(nt,1);f31(1)=1; f31(end) = 1;   % Rad. flow on int. surface
134 -    y31 = zeros(nt,1);                % No output
```

The shared door is modelled as

```
211      %Shared Door
212 -    nm6 = 1;       % number of meshes in layer
213 -    w6 = 0.04;     % width [m]
214 -    lam6 = 0.13;   % conductivity [W/m K]
215 -    rho6 = 600;   % density [kg/m3]
216 -    c6 = 1000;      % specific heat [J/kg K]
217      %c6 = 0;       % changes dt = 49 s -> dt = 3920 s
218
219 -    G61 = lam6./w6;
220 -    C61 = rho6.*c6;
221 -    G6m = 2*nm6*G61*ones(2*nm6,1);          % meshed wood
222 -    C6m = C61/nm6*mod(0:2*nm6-1,2)';   % meshed wood
223 -    G61 = [G6m];
224 -    C61 = [C6m; 0];
225 -    nt = length(C61); nq = length(G61);      % no. temperatures; no. flows
226 -    A61 = diff(eye(nt));
227 -    b61 = zeros(nq,1);
228 -    f61 = zeros(nt,1);    % Rad. flow on int. surface
```

Each wall is modelled as a thermal circuit according to the input heat flows and temperature sources as

```
355 -    S3 = 2.225*2.495 - 0.93*1.95;
356 -    b2(1)=1;
357 -    f2(1)=1;
358 -    f2(end)=1;
359 -    TCd{10} = {A2,S3*diag(G2),b2,S3*diag(C2),f2,y2};   % Living-doorway internal wall
```

11.3 MATLAB code for modelling

11.3.1 MATLAB code for single zone (living room)

Files `s02THLiving01Rad.m`, `fTC2SSold.m`, `ftrans1.m`, `fTCAssAll.m`

```
% Equivalent to s02THLiving01.m
clear all, clc
% Read data
```

```
H = dlmread('TwinHouse.csv');   % house
W = dlmread('TwinWeather.csv'); % weather

% Physical values
% ***************************************
ho = 23;                % outdoor convection coefficient
hi = 8;                 % indoor convection coefficent
rhoa = 1.2; ca = 1000;  % indoor air density; heat capacity
Kp = 1000;              % controller

% Conductances and capacities per unit surface
% Wall type P1: external [insulation; brick]
nm1 = [4 8]';           % for wall P1, number of meshes in layer 1, 2, ...
w1 = [0.12 0.20]';      % width [m]
lam1 = [0.035 0.22]';   % conductivity [W/m K]
rho1 = [80 800]';       % density [kg/m3]
c1 = [840 1000]';       % specific heat [J/kg K]

G1 = lam1./w1;
C1 = rho1.*c1.*w1;
G1m1 = 2*nm1(1)*G1(1)*ones(2*nm1(1),1); % meshed insulation
G1m2 = 2*nm1(2)*G1(2)*ones(2*nm1(2),1); % meshed brick
C1m1 = C1(1)/nm1(1)*mod(0:2*nm1(1)-1,2)';% meshed insulation
C1m2 = C1(2)/nm1(2)*mod(0:2*nm1(2)-1,2)';% meshed brick

G1 = [ho; 0.8/0.01; G1m1; 1/0.03; G1m2;1/0.01];
C1 = [0; C1m1; 0; C1m2;0;0];
nt = length(G1); nq = nt;       % no. temperatures; no. flows
A1 = diff(eye(nt+1));
A1(:,1) = [];                   % delete 1st node = reference temperature
b1 = zeros(nq,1); b1(1) = 1;    % Temp source on branch 1: Tout
f1 = zeros(nt,1); f1(1) = 1;    % Flow source in node 1: Qsolar
f1(end) = 1;                    % radiation on surface
y1 = zeros(nt,1);               % No output

% A1'*diag(G1)*A1 + A1'*diag(G1)*b1 + diag(C1)*f1 + y1

% Wall type P2: internal [brick]
%nm2 = 1;      % number of meshes in layer
%w2 = 0.25;    % width
%lam2 = 0.33;  % conductivity [W/m K]
%rho2 = 1000;  % density [kg/m3]
%c2 = 1000;    % specific heat [J/kg K]
%
%G2 = lam2./w2;
%C2 = rho2.*c2.*w2;
%G2m = 2*nm2*G2*ones(2*nm2,1);         % meshed brick
%C2m = [C2/nm2*mod(0:2*nm2-1,2)'; 0];  % meshed brick
%
%nt = 1+2*sum(nm2); nq = nt - 1;   % no. flows; no. temperatures
%A2 = diff(eye(nt));
```

```
%G2 = G2m;
%b2 = zeros(nq,1);
%C2 = C2m;
%f2 = zeros(nt,1);
%y2 = zeros(nt,1);

nm2 = 3;      % number of meshes in layer
w2 = 0.24;    % width
lam2 = 0.33;  % conductivity [W/m K]
rho2 = 1000;  % density [kg/m3]
c2 = 1000;    % specific heat [J/kg K]

G2 = lam2./w2;
C2 = rho2.*c2.*w2;
G2m = 2*nm2*G2*ones(2*nm2,1);    % meshed brick
C2m = C2/nm2*mod(0:2*nm2-1,2)';  % meshed brick

nt = 1+2*sum(nm2); nq = nt;     % no. temperatures; no. flows
A2 = diff(eye(nt+1));
A2(:,1) = [];                   % delete 1st node = reference temperature
G2 = [hi; G2m];
b2 = zeros(nq,1); b2(1) = 1;    % Temp source on branch 1: Troom
C2 = [C2m; 0];
f2 = zeros(nt,1); f2(end) = 1;  % Rad. flow on int. surface
y2 = zeros(nt,1);               % No output

% A2'*diag(G2)*A2 + A2'*diag(G2)*b2 + diag(C2)*f2 + y2

% Wall type P3: internal [brick]
nm3 = 1;      % number of meshes in layer
w3 = 0.115;    % width
lam3 = 0.33;  % conductivity [W/m K]
rho3 = 1000;  % density [kg/m3]
c3 = 1000;    % specific heat [J/kg K]

G3 = lam3./w3;
C3 = rho3.*c3.*w3;
G3m = 2*nm3*G3*ones(2*nm3,1);         % meshed brick
C3m = C3/nm3*mod(0:2*nm3-1,2)';  % meshed brick

nt = 1+2*sum(nm3); nq = nt;     % no. temperatures; no. flows
A3 = diff(eye(nt+1));
A3(:,1) = [];                   % delete 1st node = reference temperature
G3 = [hi; G3m];
b3 = zeros(nq,1); b3(1) = 1;    % Temp source on branch 1: Troom
C3 = [C3m; 0];
f3 = zeros(nt,1); f3(end) = 1;  % Rad. flow on int. surface
y3 = zeros(nt,1);               % No output

% A3'*diag(G3)*A3 + A3'*diag(G3)*b3 + diag(C3)*f3 + y3
```

```
% Wall type P4: ceiling [concrete & insulation]
nm4 = [3 1]';          % for wall P4, number of meshes in layer 1, 2, ...
w4 = [0.22 0.10]';     % width [m]
lam4 = [2.00 0.035]'; % conductivity [W/m K]
rho4 = [2400 80]';     % density [kg/m3]
c4 = [1000 840]';      % specific heat [J/kg K]

G4 = lam4./w4;
C4 = rho4.*c4.*w4;
G4m1 = 2*nm4(1)*G4(1)*ones(2*nm4(1),1); % meshed concrete
G4m2 = 2*nm4(2)*G4(2)*ones(2*nm4(2),1); % meshed insulation
C4m1 = C4(1)/nm4(1)*mod(0:2*nm4(1)-1,2)';% meshed concrete
C4m2 = C4(2)/nm4(2)*mod(0:2*nm4(2)-1,2)';% meshed insulation

%nt = 1+2*sum(nm4); nq = nt;      % no. temperatures; no. flows
A4 = diff(eye(nt+1));
A4(:,1) = [];                    % delete 1st node = reference temperature
G4 = [ho;1.4/0.4;0.04/0.04; G4m1;1.0/0.01; G4m2];
nt = length(G4); nq = nt;      % no. temperatures; no. flows
A4 = diff(eye(nt+1));
A4(:,1) = [];                    % delete 1st node = reference temperature
b4 = zeros(nq,1); b4(1) = 1;     % Temp source on branch 1: Tceiling
C4 = [0;0;C4m1;0;C4m2;0];
f4 = zeros(nt,1); f4(end) = 1;   % Rad. flow on int. surface
y4 = zeros(nt,1);                % No output

% A4'*diag(G4)*A4 + A4'*diag(G4)*b4 + diag(C4)*f4 + y4

% Wall type P5: ground (concrete & insulation & screed)
nm5 = [3 1 1]';          % for wall P4, number of meshes in layer 1, 2, ...
w5 = [0.22 0.03 0.065]';     % width [m]
lam5 = [2.10 0.025 1.40]'; % conductivity [W/m K]
rho5 = [2400 80 2000]';     % density [kg/m3]
c5 = [1000 840 1000]';      % specific heat [J/kg K]

G5 = lam5./w5;
C5 = rho5.*c5.*w5;
G5m1 = 2*nm5(1)*G5(1)*ones(2*nm5(1),1);    % meshed concrete
G5m2 = 2*nm5(2)*G5(2)*ones(2*nm5(2),1);    % meshed insulation
G5m3 = 2*nm5(3)*G5(3)*ones(2*nm5(3),1);    % meshed screed
C5m1 = C5(1)/nm5(1)*mod(0:2*nm5(1)-1,2)'; % meshed concrete
C5m2 = C5(2)/nm5(2)*mod(0:2*nm5(2)-1,2)'; % meshed insulation
C5m3 = C5(3)/nm5(3)*mod(0:2*nm5(3)-1,2)'; % meshed insulation


G5 = [ho;G5m1;0.060/0.029;G5m2;0.023/0.030; G5m3];
nt = length(G5); nq = nt;      % no. temperatures; no. flows
A5 = diff(eye(nt+1));
A5(:,1) = [];                    % delete 1st node = reference temperature
b5 = zeros(nq,1); b5(1) = 1;     % Temp source on branch 1: Tground
C5 = [C5m1;0; C5m2;0; C5m3; 0];
```

```
f5 = zeros(nt,1); f5(end) = 1;  % Rad. flow on int. surface
y5 = zeros(nt,1);               % No output

% A5'*diag(G5)*A5 + A5'*diag(G5)*b5 + diag(C5)*f5 + y5

% Door type D1 & D2: wood
nm6 = 1;      % number of meshes in layer
w6 = 0.04;    % width [m]
lam6 = 0.13;  % conductivity [W/m K]
rho6 = 600;  % density [kg/m3]
c6 = 1000;     % specific heat [J/kg K]
%c6 = 0;      % changes dt = 49 s -> dt = 3920 s

G6 = lam6./w6;
C6 = rho6.*c6;
G6m = 2*nm6*G6*ones(2*nm6,1);         % meshed wood
C6m = C6/nm6*mod(0:2*nm6-1,2)';  % meshed wood

nt = 1+2*sum(nm6); nq = nt;     % no. temperatures; no. flows
A6 = diff(eye(nt+1));
A6(:,1) = [];                   % delete 1st node = reference temperature
G6 = [hi; G6m];
b6 = zeros(nq,1); b6(1) = 1;    % Temp source on branch 1: Troom
C6 = [C6m; 0];
f6 = zeros(nt,1); f6(end) = 1;  % Rad. flow on int. surface
y6 = zeros(nt,1);

% A6'*diag(G6)*A6 + A6'*diag(G6)*b6 + diag(C6)*f6 + y6

% Window
A7 = 1;
G7 = 1.2; % 1.2;
C7 = 0;
b7 = 1;
f7 = 1;
y7 = 0;

% A7'*diag(G7)*A7 + A7'*diag(G7)*b7 + diag(C7)*f7 + y7
% Window
rhoa=1.2;
ca=1000;
A8 = 1;
G8 = 2.2/23*rhoa*ca; % 1.2;
C8 = 0;
b8 = 1;
f8 = 0;
y8 = 0;
%Thermal Bridge
rhoa=1.2;
ca=1000;
A9 = 1;
```

```
G9 = 2.495*0.093; % 1.2;
C9 = 0;
b9 = 1;
f9 = 0;
y9 = 0;


% Dissambled thermal circuits
% ***********************************************
S1 = (3.97 - 0.35)*2.495 - 0.93*1.95;
TCd{1} = {A2,S1*diag(G2),b2,S1*diag(C2),f2,y2};   % Living-kitchen internal wall

S2 = 0.93*1.95;
TCd{2} = {A6,S2*diag(G6),b6,S2*diag(C6),f6,y6};  % Living-kitchen door

S3 = 2.22*2.495 - 0.93*1.95;
TCd{3} = {A2,S3*diag(G2),b2,S3*diag(C2),f2,y2};   % Living-doorway internal wall

S4 = 0.93*1.95;
TCd{4} = {A6,S4*diag(G6),b6,S4*diag(C6),f6,y6};       % Living-doorway door

S5 = 3.29*2.495 - 0.93*1.95;
TCd{5} = {A2,S5*diag(G2),b2,S5*diag(C2),f2,y2};       % Living - corridor wall

S6 = 0.93*1.95;
%TCd{6} = {A6,S6*diag(G6),b6,S6*diag(C6),f6,y6};       % Living-corridor door

S7 = 2.28*2.495;
TCd{6} = {A2,S7*diag(G2),b2,S7*diag(C2),f2,y2};       % Living - bedroom2 wall

S8 = 5.290*2.495 - 8.66;
TCd{7} = {A1,S8*diag(G1),b1,S8*diag(C1),f1,y1};       % Living - extern. South wall

S9 = 8.66;
TCd{8} = {A7,S9*diag(1.05),b7,S9*diag(C7),f7,y7};       % Living - South windows

S10 = 6.47*2.495 - 2.14;
TCd{9} = {A1,S10*diag(G1),b1,S10*diag(C1),f1,y1};    % Living - extern. West wall

S11 = 2.14;
TCd{10} = {A7,S11*diag(G7),b7,S11*diag(C7),f7,y7};     % Living - West window

S12 = 6.47*5.20;
TCd{11} = {A4,S12*diag(G4),b4,S12*diag(C4),f4,y4};     % Living - Attic

TCd{12} = {A5,S12*diag(G5),b5,S12*diag(C5),f5,y5};     % Living - Cellar

% Indoor air
Va = 120/3600;      % volumetric air flow [m3/s]
Infil=1.62/3600; %Infiltration per hour per floor area 81.69
sg=81.69;
```

```
Infil1=0.75*2.22/3600;
S13=2.662; %Surface area of Pillar
G8 = hi*[S1; S2; S3; S4; S5;S7; S8; S9; S10; S11; S12; S12];
G8    =    [G8;    rhoa*Va*ca;Infil/23*sg*rhoa*ca;Infil1/23*sg*rhoa*ca;Va*rhoa*ca;2.495*0.093];
%Inculding thermal bridge
A8 = -eye(13); A8=[A8;zeros(1,13);zeros(1,13);zeros(1,13);zeros(1,13)]; A8(:,13) = 1;
C8 = zeros(13,1); C8(13) = rhoa*6.47*5.20*2.495*ca;
b8 = zeros(17,1); b8(13) = 1;b8(14) = 1;b8(15)=1;b8(16)=1;b8(17)=1;  % in: source Tout
f8 = zeros(13,1); f8(13) = 1;   % in: source heat flow in air volume
y8 = zeros(13,1); y8(13) = 1;   % out: indoor air

TCd{13} = {A8,diag(G8),b8,diag(C8),f8,y8};              % indoor air

% Assembling and ss-model
% ***********************************
AssX = [1 length(f2) 13 1;...
        2 length(f6) 13 2;...
        3 length(f2) 13 3;...
        4 length(f6) 13 4;...
        5 length(f2) 13 5;...
        6 length(f2) 13 6;...
        7 length(f1) 13 7;...
        8 length(f7) 13 8;...
        9 length(f1) 13 9;...
        10 length(f7) 13 10;...
        11 length(f4) 13 11;
        12 length(f5) 13 12 ];

[TCa, Idx] = fTCAssAll(TCd, AssX);
A = TCa{1}; G = TCa{2}; b = TCa{3}; C = TCa{4}; f = TCa{5}; y = TCa{6};

% ************************************
% State-space
% ************************************
% Model
[A,B,C,D] = fTC2SSold(A,G,b,C,f,y);
% Inputs
Ti = H(:,7);    % temperature in living at 125 cm (output)
Tk = H(:,12);   % kitchen
Td = H(:,13);   % doorway
Tc = H(:,9);    % corridor
Tb2 = H(:,11);  % bedroom 2
Ta = H(:,4);    % attic
Tg = H(:,5);    % cellar
Tv = H(:,30);   % ventilation supply air
To = W(:,3);    % outdoor
Qs = W(:,8);    % specific global solar vert. South
Qw = W(:,9);    % specific global solar vert. West
Qi = H(:,21);   % el. power living

% SW radiative sources on walls: distributed uniformely
```

```
Sliv = 2*(6.47+5.20)*2.495 + 2*6.47*5.20; % total area living room
% radiative gain through closed blinds
Qr = [S1 S2 S3 S4 S5 S7 S8 S9 S10 S11 S12 S12]/Sliv.*(1.29*Qw*0.427+0.3*Qi)*0.8 ;

T = [Tk'; Tk'; Td'; Td'; Tc';Tb2';...
    To'; To'; To'; To';...
    Ta'; Tg'; Tv';To';Tk';Tc';To'];

Q=[Qr'; 0.7*Qi'+(1.29*Qw'*0.427+0.3*Qi')*0.20];
u=[T;Q];
u = [u(1:23,:); S8*0.23*Qs'; u(24,:); u(25,:); ...
    S10*0.23*Qw'; u(26,:); u(27,:); u(28:end,:)];

disp(['max dt = ',num2str(min(-2./eig(A))),'[s]'])

dt = 10*60;                     % time step: 10 min
n = length(H(:,1));
Time = 0:dt:(n-1)*dt;           % time
nth = size(A,1);                % no states
% initial conditions
th = 28*ones(nth,n); thi = th; the = th;
Ae = (eye(nth) + dt*A);         % Euler explicit
Ai = inv((eye(nth) - dt*A));    % Euler implicit
Ad = expm(A*dt);                % exp. matrix
Bd = (Ad-eye(size(A)))*inv(A)*B;
for k = 1:n-1
 th(:,k+1) = Ae*th(:,k) + dt*B*u(:,k);     % Euler explicit
 thi(:,k+1) = Ai*(thi(:,k) + dt*B*u(:,k));  % Euler implicit
 the(:,k+1) = Ad*the(:,k)+Bd*u(:,k);        % matrix exponential
end
ye = C*th + D*u;        % Euler explicit
yi = C*thi + D*u;       % Euler implicit
yE = C*the + D*u;       % exponential

figure(1)
Time = Time/3600/24;
% plot(Time,ye,Time,yi,Time,yE,'r',Time,Ti, Time, To,'b')
% plot(Time,yi, Time,yE,'r',Time,Ti,'g', Time, To,'b')
plot(Time,yE,'r', Time,Ti,'g', Time,To,'b')
ylabel('Temperature [C]')
legend('T_s_i_m','T_i','T_o')
% subplot(212)
% plot(Time,Qi)
% xlabel('Time [h]'),ylabel('P_e_l[W]')
delta=yi'-Ti;
delta=delta(500:5905,:);
Time=Time(:,500:5905);
%plot(Time,delta,'r')
% Statics of error
[mean(delta) std(delta) max(delta) min(delta)]
figure(2)
```

```
hist(delta)
```

11.4 MATLAB code for two zones(kitchen and living room)

Files KithcenLivngrmnew.m, fTC2SSold.m, ftrans1.m, fNumInOut.m, fTCAssAll.m

```
% Equivalent to s02THLiving01.m
clear all, clc
% Read data
H = dlmread('TwinHouse.csv');   % house
W = dlmread('TwinWeather.csv'); % weather
ft=xlsread('f1');
% Physical values
% ***************************************
ho = 23;                % outdoor convection coefficient
hi = 8;                 % indoor convection coefficent
rhoa = 1.2; ca = 1000;  % indoor air density; heat capacity
Kp = 1000;              % controller

% Inputs
Ti = H(:,7);    % temperature in living at 125 cm (output)
Tk = H(:,12);   % kitchen
Td = H(:,13);   % doorway
Tc = H(:,9);    % corridor
Tb2 = H(:,11);  % Children room
Tb1=H(:,14);    %Bed room
Ta = H(:,4);    % attic
Tg = H(:,5);    % cellar
Tv = H(:,30);   % ventilation supply air
To = W(:,3);    % outdoor
Qn = W(:,6);
Qs = W(:,8);    % specific global solar vert. South
Qw = W(:,9);    % specific global solar vert. West
Qi = H(:,21);   % el. power living
Qk=H(:,24)+H(:,25); %Kithcne power input minus duct losses
Qd=H(:,26); %Doorway Heater
QB=H(:,27); %Bedroom Heater

% Conductances and capacities per unit surface
% Wall type P1: external [insulation; brick]
nm1 = [4 2]';           % for wall P1, number of meshes in layer 1, 2, ...
w1 = [0.12 0.20]';      % width [m]
lam1 = [0.035 0.22]';   % conductivity [W/m K]
rho1 = [80 800]';       % density [kg/m3]
c1 = [840 1000]';       % specific heat [J/kg K]

G1 = lam1./w1;
C1 = rho1.*c1.*w1;
G1m1 = 2*nm1(1)*G1(1)*ones(2*nm1(1),1); % meshed insulation
G1m2 = 2*nm1(2)*G1(2)*ones(2*nm1(2),1); % meshed brick
```

```
C1m1 = C1(1)/nm1(1)*mod(0:2*nm1(1)-1,2)';% meshed insulation
C1m2 = C1(2)/nm1(2)*mod(0:2*nm1(2)-1,2)';% meshed brick

G1 = [ho; 0.8/0.01; G1m1; 1/0.03; G1m2;1/0.01];
C1 = [0; C1m1; 0; C1m2;0;0];
nt = length(G1); nq = nt;       % no. temperatures; no. flows
A1 = diff(eye(nt+1));
A1(:,1) = [];                   % delete 1st node = reference temperature
b1 = zeros(nq,1);              % Temp source on branch 1: Tout
f1 = zeros(nt,1);               % Flow source in node 1: Qsolar
y1 = zeros(nt,1);               % No output

%Internal thick wall
nm2 = 3;      % number of meshes in layer
w2 = 0.24;    % width
lam2 = 0.33;  % conductivity [W/m K]
rho2 = 1000;  % density [kg/m3]
c2 = 1000;    % specific heat [J/kg K]

G2 = lam2./w2;
C2 = rho2.*c2.*w2;
G2m = 2*nm2*G2*ones(2*nm2,1);    % meshed brick
C2m = C2/nm2*mod(0:2*nm2-1,2)';  % meshed brick
G2 = [hi;0.35/0.01;G2m;0.35/0.01];
C2 = [0;C2m;0;0];
nt = length(G2); nq = nt;     % no. temperatures; no. flows
A2 = diff(eye(nt+1));
A2(:,1) = [];                   % delete 1st node = reference temperature
b2 = zeros(nq,1); b2(1) = 1;    % Temp source on branch 1: Troom

f2 = zeros(nt,1);f2(1)=1; f2(end) = 1;  % Rad. flow on int. surface
y2 = zeros(nt,1);               % No output

%Shared wall with livingroom
nm2 = 2;      % number of meshes in layer
w2 = 0.24;    % width
lam2 = 0.33;  % conductivity [W/m K]
rho2 = 1000;  % density [kg/m3]
c2 = 1000;    % specific heat [J/kg K]
G21 = lam2./w2;
C21 = rho2.*c2.*w2;
G2m = 2*nm2*G21*ones(2*nm2,1);    % meshed brick
C2m = C21/nm2*mod(0:2*nm2-1,2)';  % meshed brick
G21 = [0.35/0.01;G2m;0.35/0.01];
C21 = [0;C2m;0;0];
nt = length(C21); nq =length(G21);     % no. temperatures; no. flows
A21 = diff(eye(nt));
b21 = zeros(nq,1);
f21 = zeros(nt,1);
y21 = zeros(nt,1);               % No output
```

```
% Internal thin Wall type P3: internal [brick]
nm3 = 1;      % number of meshes in layer
w3 = 0.115;    % width
lam3 = 0.33;  % conductivity [W/m K]
rho3 = 1000;  % density [kg/m3]
c3 = 1000;    % specific heat [J/kg K]

G3 = lam3./w3;
C3 = rho3.*c3.*w3;
G3m = 2*nm3*G3*ones(2*nm3,1);         % meshed brick
C3m = C3/nm3*mod(0:2*nm3-1,2)';  % meshed brick
G3 = [hi;0.35/0.01;G3m;0.35/0.01];%With plaster layers
C3 = [0;C3m;0;0];
nt = length(G3); nq = nt;     % no. temperatures; no. flows
A3 = diff(eye(nt+1));
A3(:,1) = [];                   % delete 1st node = reference temperature
b3 = zeros(nq,1); b3(1) = 1;    % Temp source on branch 1: Troom
f3 = zeros(nt,1);f3(1)=1; f3(end) = 1;  % Rad. flow on int. surface
y3 = zeros(nt,1);               % No output

% Shared Internal thin Wall type P3: internal [brick]
nm3 = 2;      % number of meshes in layer
w3 = 0.115;    % width
lam3 = 0.33;  % conductivity [W/m K]
rho3 = 1000;  % density [kg/m3]
c3 = 1000;    % specific heat [J/kg K]

G31 = lam3./w3;
C31 = rho3.*c3.*w3;
G3m = 2*nm3*G31*ones(2*nm3,1);         % meshed brick
C3m = C31/nm3*mod(0:2*nm3-1,2)';  % meshed brick
G31 = [0.35/0.01;G3m;0.35/0.01];%With plaster layers
C31 = [0;C3m;0;0];
nt = length(C31); nq = length(G31);     % no. temperatures; no. flows
A31 = diff(eye(nt));
b31 = zeros(nq,1); b31(1) = 1;    % Temp source on branch 1: Troom
f31 = zeros(nt,1);f31(1)=1; f31(end) = 1;  % Rad. flow on int. surface
y31 = zeros(nt,1);               % No output


% Wall type P4: ceiling [concrete & insulation]
nm4 = 2;         % for wall P4, number of meshes in layer 1, 2, ...
w4 = 0.22;    % width [m]
lam4 = 2.00; % conductivity [W/m K]
rho4 =2400;    % density [kg/m3]
c4 =1000;     % specific heat [J/kg K]

G4 = lam4./w4;
C4 = rho4.*c4.*w4;
G4m1 = 2*nm4(1)*G4(1)*ones(2*nm4(1),1); % meshed concrete
```

```
C4m1 = C4(1)/nm4(1)*mod(0:2*nm4(1)-1,2)';% meshed concrete
G4 = [ho;1.4/0.4;0.04/0.04; G4m1;1.0/0.01;0.035/0.1];
C4 = [0;0;C4m1;0;0;0];
nt = length(G4); nq = nt;     % no. temperatures; no. flows
A4 = diff(eye(nt+1));
A4(:,1) = [];                   % delete 1st node = reference temperature
b4 = zeros(nq,1); b4(1) = 1;    % Temp source on branch 1: Tceiling

f4 = zeros(nt,1); f4(end) = 1;  % Rad. flow on int. surface
y4 = zeros(nt,1);               % No output

% A4'*diag(G4)*A4 + A4'*diag(G4)*b4 + diag(C4)*f4 + y4

% Wall type P5: ground (concrete & insulation & screed)
nm5 = [1 1 4]';         % for wall P4, number of meshes in layer 1, 2, ...
w5 = [0.22 0.03 0.065]';    % width [m]
lam5 = [2.10 0.025 1.40]'; % conductivity [W/m K]
rho5 = [2400 80 2000]';    % density [kg/m3]
c5 = [1000 840 1000]';     % specific heat [J/kg K]

G5 = lam5./w5;
C5 = rho5.*c5.*w5;
G5m1 = 2*nm5(1)*G5(1)*ones(2*nm5(1),1);   % meshed concrete
G5m2 = 2*nm5(2)*G5(2)*ones(2*nm5(2),1);   % meshed insulation
G5m3 = 2*nm5(3)*G5(3)*ones(2*nm5(3),1);   % meshed screed
C5m1 = C5(1)/nm5(1)*mod(0:2*nm5(1)-1,2)'; % meshed concrete
C5m2 = C5(2)/nm5(2)*mod(0:2*nm5(2)-1,2)'; % meshed insulation
C5m3 = C5(3)/nm5(3)*mod(0:2*nm5(3)-1,2)'; % meshed insulation


G5 = [ho;G5m1;0.060/0.029;G5m2;0.023/0.030; G5m3];
nt = length(G5); nq = nt;     % no. temperatures; no. flows
A5 = diff(eye(nt+1));
A5(:,1) = [];                   % delete 1st node = reference temperature
b5 = zeros(nq,1); b5(1) = 1;    % Temp source on branch 1: Tground
C5 = [C5m1;0; C5m2;0; C5m3; 0];
f5 = zeros(nt,1); f5(end) = 1;  % Rad. flow on int. surface
y5 = zeros(nt,1);               % No output

% A5'*diag(G5)*A5 + A5'*diag(G5)*b5 + diag(C5)*f5 + y5

% Door type D1 & D2: wood
nm6 = 1;      % number of meshes in layer
w6 = 0.04;    % width [m]
lam6 = 0.13;  % conductivity [W/m K]
rho6 = 600;  % density [kg/m3]
c6 = 1000;     % specific heat [J/kg K]

G6 = lam6./w6;
C6 = rho6.*c6;
G6m = 2*nm6*G6*ones(2*nm6,1);         % meshed wood
```

```
C6m = C6/nm6*mod(0:2*nm6-1,2)';  % meshed wood

nt = 1+2*sum(nm6); nq = nt;     % no. temperatures; no. flows
A6 = diff(eye(nt+1));
A6(:,1) = [];                   % delete 1st node = reference temperature
G6 = [hi; G6m];
b6 = zeros(nq,1);     % Temp source on branch 1: Troom
C6 = [C6m; 0];
f6 = zeros(nt,1);   % Rad. flow on int. surface
y6 = zeros(nt,1);

% A6'*diag(G6)*A6 + A6'*diag(G6)*b6 + diag(C6)*f6 + y6

%Shared Door
nm6 = 1;      % number of meshes in layer
w6 = 0.04;    % width [m]
lam6 = 0.13;  % conductivity [W/m K]
rho6 = 600;  % density [kg/m3]
c6 = 1000;     % specific heat [J/kg K]
%c6 = 0;      % changes dt = 49 s -> dt = 3920 s

G61 = lam6./w6;
C61 = rho6.*c6;
G6m = 2*nm6*G61*ones(2*nm6,1);         % meshed wood
C6m = C61/nm6*mod(0:2*nm6-1,2)';  % meshed wood
G61 = [G6m];
C61 = [C6m; 0];
nt = length(C61); nq = length(G61);     % no. temperatures; no. flows
A61 = diff(eye(nt));
b61 = zeros(nq,1);
f61 = zeros(nt,1);   % Rad. flow on int. surface
y61 = zeros(nt,1);

% Shared Infiltration
A7 =1;
G7 = 1.62/3600*rhoa*ca;
C7 = 0;
b7 = 0;
f7 = 0;
y7 = 0;

% Shared Infiltration
A71 =[-1 1];
G71 = 1.62/3600*rhoa*ca;
C71 = [0;0];
b71 = 0;
f71 = [0;0];
y71 = [0;0];

% % A7'*diag(G7)*A7 + A7'*diag(G7)*b7 + diag(C7)*f7 + y7
%Pillar
```

```
rhoc=2400;
cc=1000;
S20=0.3048*0.23; %Cross sectional area of concrete
Hc=2.495; %Hieght of concrete
A20 = [-1 1];
G20 =0.5; % 1.2;
C20 =[rhoc*cc*S20*Hc;0];
b20 = 0;
f20 = [0;0];
y20 = [0;0];
TCd{20}={A20,diag(G20),b20,diag(C20),f20,y20};

%**************************%
%Kitchen zones
%**************************%
S1 = 2.8355*2.495;
b1(1)=1;
f1(1)=1;
f1(end)=1;
TCd{1} = {A1,S1*diag(G1),b1,S1*diag(C1),f1,y1};   % Kitchen Northern wall

S2 = 2.625*2.495;
b3(1)=1; %Doorway Temperature
f3(1)=0;
f3(end)=1;
TCd{2} = {A3,S2*diag(G3),b3,S2*diag(C3),f3,y3};  % Kitchen Eastern wall shared with doorwy

S3=2.835*2.495; % Kithcen wall shared with livngrm
b21(1)=0;
f21(1)=1;
f21(end)=1;
TCd{3} = {A21,S3*diag(G21),b21,S3*diag(C21),f21,y21};

S4=0.935*1.95;
b61(1)=0;
f61(1)=1;
f61(end)=1;
TCd{4} = {A61,S4*diag(G61),b61,S4*diag(C61),f61,y61};  % Door shared with livngrm

Sg = 81.69;%Infiltration between two zones
b71(1)=0;
f71(1)=0;
f71(end)=0;
TCd{5} = {A71,Sg*diag(G71),b71,diag(C71),f71,y71};  % Infiltration

S5 =2.625*2.495;%West wall
b1(1)=1;
f1(1)=1;
f1(end)=1;
TCd{6} = {A1,S5*diag(G1),b1,S5*diag(C1),f1,y1};  % Kithcen west wall
```

```
S6 = 7.44;
f4(1)=0;
b4(1)=1;
f4(end)=1;
TCd{7}={A4,S6*diag(G4),b4,S6*diag(C4),f4,y4};       % Kitchen cieling

S7=7.44;
f5(1)=0;
b5(1)=1;
f5(end)=1;
TCd{8} = {A5,S7*diag(G5),b5,S7*diag(C5),f5,y5};       % Kitchen Ground

% Indoor air

Infil=1.62/3600; %Infiltration per hour per floor area 81.69
sg=7.44;
Infil1=1/3*2.22/3600;

G9 = hi*[S1; S2; S3; S4; S5;S6;S7];
Gwind=1.2*2.14; %Window resistance
Ginfil=Infil/10*sg*rhoa*ca; %External
Gextwall=0.091*2.495; %Thermal bridge b.w ext-ext wall
Gt=Gwind+Ginfil+Gextwall;%Total

G9 = [G9;Gt];

A9 = -eye(8);  A9(:,8) = 1;
C9 = zeros(8,1); C9(8) = rhoa*sg*2.495*ca;
b9 = zeros(8,1); b9(8) = 1; % in: source Tout
f9 = zeros(8,1); f9(8) = 1;   % in: source heat flow in air volume
y9 = zeros(8,1); y9(end) = 1;   % out: indoor air

TCd{9} = {A9,diag(G9),b9,diag(C9),f9,y9};              % indoor air

% SW radiative sources on walls: distributed uniformely
Skith = 2*(2.625+2.835)*2.495 + 2*2.625*2.835; % total area Kitchen room
% radiative gain through closed blinds
%Splr=2*2.495*(0.3048+0.203);
Z=90;
trns1=ftrans1(Z);
Qr = [S1 S2 S3 S4 S5 S6 S7]/Skith.*(1.29*Qw*0.427.*trns1+0.3*Qk);
Tkith = [To';Td';To';Ta';Tg';To'];
Qr=Qr';

Qsolkith=[S1*0.23*Qn';Qr(1:4,:);S2*0.23*Qw';Qr(5:end,:);0.9*0.7*Qk'];
%Qheaterkith=0.9*0.7*Qk'+(1.29*Qw'*0.427*0.8+0.3*Qk')*0.25;

%**********************%
    %Livingroom Zone%
%**********************%
S1 = (3.97 - 0.35)*2.495 - 0.93*1.95;%Livng shared wall with Kithcen
```

```
S2 = 0.93*1.95; % Living-kitchen door


S3 = 2.225*2.495 - 0.93*1.95;
b2(1)=1;
f2(1)=1;
f2(end)=1;
TCd{10} = {A2,S3*diag(G2),b2,S3*diag(C2),f2,y2};   % Living-doorway internal wall

S4 = 0.93*1.95;
b6(1)=1;
f6(1)=1;
f6(end)=1;
TCd{11} = {A6,S4*diag(G6),b6,S4*diag(C6),f6,y6};       % Living-doorway door

Sg = 81.69;%Infiltration between two zones
b7(1)=1;
f7(1)=0;
f7(end)=0;
TCd{12} = {A7,Sg*diag(G7),b7,diag(C7),f7,y7};  % Infiltration between zones

S5 = 3.29*2.495 - 0.93*1.95;
b2(1)=1;
f2(1)=0;
f2(end)=1;
TCd{13} = {A2,S5*diag(G2),b2,S5*diag(C2),f2,y2};       % Living - corridor wall

S6 = 2.28*2.495;
b2(1)=1;
f2(1)=1;
f2(end)=1;
TCd{14} = {A2,S6*diag(G2),b2,S6*diag(C2),f2,y2};       % Living - bedroom2 wall

S7 = 5.290*2.495 - 8.66;
f1(1)=1;
f1(end)=1;
b1(1)=1;
b1(end)=0;
TCd{15} = {A1,S7*diag(G1),b1,S7*diag(C1),f1,y1};       % Living - extern. South wall

S8 = 6.47*2.495 - 2.14;
f1(1)=1;
f1(end)=1;
b1(1)=1;
b1(end)=0;
TCd{16} = {A1,S8*diag(G1),b1,S8*diag(C1),f1,y1};    % Living - extern. West wall

S9 = 6.47*5.20;
f4(1)=0;
f4(end)=1;
```

```
b4(1)=1;
TCd{17} = {A4,S9*diag(G4),b4,S9*diag(C4),f4,y4};     % Living - Attic

S10 = 6.47*5.20;
f5(1)=0;
f5(end)=1;
b5(1)=1;
TCd{18} = {A5,S10*diag(G5),b5,S10*diag(C5),f5,y5};     % Living - Cellar

% Indoor air
Va = 120/3600;      % volumetric air flow [m3/s]
Infil=1.62/3600; %Infiltration per hour per floor area 81.69
sg=81.69;
Infil1=1/3*2.22/3600;
%S13=2.662; %Surface area of Pillar
G10 = hi*[S1; S2; S3; S4; S5;S6;S7; S8; S9; S10];
%Last three terms consist of thermal bridges:Ext-Ext wall, Extwall-Ground
%and Internal wall ground

Gsouthwin=8.66*1.05; %South window
Gwestwin=2.14*1.2;   %West window
Infil=Infil/10*33.65*rhoa*ca;%External Infiltration
Gt=Gsouthwin+Gwestwin+Infil;
G10 = [G10;Gt;rhoa*Va*ca;];
%G10 = [G10;8.66*1.05;2.14*1.2;rhoa*Va*ca;Infil/10*33.65*rhoa*ca];
A10 = -eye(11); A10=[A10;zeros(1,11)]; A10(:,11) = 1;
C10 = zeros(11,1); C10(11) = rhoa*6.47*5.20*2.495*ca;
b10 = zeros(12,1); b10(11) = 1;b10(12) = 1;  % in: source Tout
f10 = zeros(11,1); f10(end) = 1;   % in: source heat flow in air volume
y10 = zeros(11,1); y10(11) = 1;   % out: indoor air

TCd{19} = {A10,diag(G10),b10,diag(C10),f10,y10};  % indoor air
%Radiations on wall of Living room
Sliv = 2*(6.465+5.205)*2.495 + 2*6.465*5.205;
Qr = [S1 S2 S3 S4 S5 S6 S7 S8 S9 S10]/Sliv.*(1.29*Qw*0.427.*trns1+0.3*Qi);
Qr=Qr';
Tliv = [Td';Td';Td';Tc';Tb2';To';To';Ta';Tg';To';Tv'];
Qsolliv=[Qr(1:2,:);0.3*Qd'/8;Qr(3,:);0.3*Qd'/10;Qr(4:5,:);0.3*QB'/7;Qr(6,:);S7*0.23*Qs';Qr(7,:
);S8*0.23*Qw';Qr(8:end,:);0.9*0.7*Qi'];
%Qsolliv=[S7*0.23*Qs';S8*0.23*Qw'];
%Qheaterliv=0.9*0.7*Qi'+(1.29*Qw'*0.427+0.3*Qi')*0.25;


% Assembling and ss-model
% *********************************
%Kitchen
AssXkith=[1 length(TCd{1}{5}) 9 1;...
        2 length(TCd{2}{5}) 9 2;...
        3 length(TCd{3}{5}) 9 3;...
        4 length(TCd{4}{5}) 9 4;...
        6 length(TCd{6}{5}) 9 5;...
```

```
        7 length(TCd{7}{5}) 9 6;...
        8 length(TCd{8}{5}) 9 7;9 length(TCd{9}{5}) 20 length(TCd{20}{5});9 length(TCd{9}{5}) 5
length(TCd{5}{5})];
%Living Room
AssXliv = [3 1 19 1;...
        4 1 19 2;...            %Kithcen door
        19 length(TCd{19}{5}) 5 1;...  %Infiltration between zones
        10 length(TCd{10}{5}) 19 3;...      %Doorway wall
        11 length(TCd{11}{5}) 19 4;...      %Doorway door
        13 length(TCd{13}{5}) 19 5;...         % Corridor wall
        14 length(TCd{14}{5}) 19 6;...         %Children room wall
        15 length(TCd{15}{5}) 19 7;...         % South wall
        16 length(TCd{16}{5}) 19 8;...         %West wall
        17 length(TCd{17}{5}) 19 9;...         %Cieling
        18 length(TCd{18}{5}) 19 10;19 length(TCd{19}{5}) 12 length(TCd{12}{5})];           %
Ground
AssX=[AssXkith;AssXliv];
[TCa1, Idx1] = fTCAssAllold(TCd, AssX);
A1 = TCa1{1}; G1 = TCa1{2}; b1 = TCa1{3}; C1 = TCa1{4}; f1 = TCa1{5}; y1 = TCa1{6};

[TCa, Idx] = fTCAssAll(TCd, AssX);
A = TCa{1}; G = TCa{2}; b = TCa{3}; C = TCa{4}; f = TCa{5}; y = TCa{6};
[InTN, InFN, OutN] = fNumInOut(TCa, Idx);
%f=ft(1,1:160);
%f=f';
% *************************************
% State-space
% *************************************
% Model
[A,B,C,D] = fTC2SSold(A,G,b,C,f,y);
disp(['max dt = ',num2str(min(-2./eig(A))),'[s]'])

% *************************************
%               Inputs                  %
% *************************************
u=[Tkith;Tliv;Qsolkith;Qsolliv];

dt = 10*60;                     % time step: 10 min
n = length(H(:,1));
Time = 0:dt:(n-1)*dt;           % time
nth = size(A,1);                % no states
% initial conditions
th = 28*ones(nth,n); thi = th; the = th;
Ae = (eye(nth) + dt*A);         % Euler explicit
Ai = inv((eye(nth) - dt*A));    % Euler implicit
Ad = expm(A*dt);                % exp. matrix
Bd = (Ad-eye(size(A)))*inv(A)*B;
for k = 1:n-1
 th(:,k+1) = Ae*th(:,k) + dt*B*u(:,k);     % Euler explicit
 thi(:,k+1) = Ai*(thi(:,k) + dt*B*u(:,k));  % Euler implicit
 the(:,k+1) = Ad*the(:,k)+Bd*u(:,k);        % matrix exponential
```

```
end
ye = C*th + D*u;         % Euler explicit
yi = C*thi + D*u;        % Euler implicit
yE = C*the + D*u;        % exponential

%subplot(211)
figure(1)
Time = Time/3600/24;
plot(Time,ye,Time,yi,Time,yE,'r',Time,Ti, Time, To,'b')
plot(Time,yi, Time,yE,'r',Time,Ti,'g', Time, To,'b')
plot(Time,yE(1,:),'r', Time,Tk,'g', Time,To,'b')
ylabel('Temperature [C]')
legend('T_s_i_m','T_i','T_o')
%subplot(212)
figure(2)
plot(Time,yE(2,:),'r', Time,Ti,'g', Time,To,'b')
delta=yE(1,:)'-Tk;
delta=delta(700:5905,:);
Time=Time(:,700:5905);
%plot(Time,delta,'r')
% Statics of error
[mean(delta) std(delta) max(delta) min(delta)]
figure(3)
hist(delta)
title('Kitchen Histogram')

delta=yE(2,:)'-Ti;
delta=delta(700:5905,:);
%Time=Time(:,700:5905);
%plot(Time,delta,'r')
% Statics of error
[mean(delta) std(delta) max(delta) min(delta)]
figure(4)
hist(delta)
title('Living room Histogram')
```

11.5 MATLAB Code for all Zones

Files `sevenzonessinglegraph.m, fTC2SSold.m, ftrans1.m, fNumInOut.m, fTCAssAll.m`

```
% Equivalent to s02THLiving01.m
clear all, clc
% Read data
H = dlmread('TwinHouse.csv');   % house
W = dlmread('TwinWeather.csv'); % weather

% Physical values
% ************************************
ho = 23;                % outdoor convection coefficient
hi = 8;                 % indoor convection coefficent
rhoa = 1.2; ca = 1000;  % indoor air density; heat capacity
Kp = 1000;              % controller

% Inputs
Ti = H(:,7);    % temperature in living at 125 cm (output)
Tk = H(:,12);   % kitchen
Td = H(:,13);   % doorway
Tc = H(:,9);    % corridor
Tbh=H(:,10);    % Bathroom Temperature
Tb2 = H(:,11);  % Children room
Tb1=H(:,14);    %Bed room
Ta = H(:,4);    % attic
Tg = H(:,5);    % cellar
Tv = H(:,30);   % ventilation supply air
To = W(:,3);    % outdoor
Qn = W(:,6);    % Solar radiations on North wall
Qe = W(:,7);    % Solar radiations on East wall
Qs = W(:,8);    % specific global solar vert. South
Qw = W(:,9);    % specific global solar vert. West
Qi = H(:,21);   % el. power living
Qk=H(:,24)+H(:,25); %Kithcne power input minus duct losses
Qbh=H(:,22);    %Bathroom heater
Qch=H(:,23); %Children room heater
Qd=H(:,26); %Doorway Heater
QB=H(:,27); %Bedroom Heater

% Conductances and capacities per unit surface
% Wall type P1: external [insulation; brick]
nm1 = [1 2]';           % for wall P1, number of meshes in layer 1, 2, ...
w1 = [0.12 0.20]';      % width [m]
lam1 = [0.035 0.22]';   % conductivity [W/m K]
rho1 = [80 800]';       % density [kg/m3]
c1 = [840 1000]';       % specific heat [J/kg K]

G1 = lam1./w1;
C1 = rho1.*c1.*w1;
G1m1 = 2*nm1(1)*G1(1)*ones(2*nm1(1),1); % meshed insulation
G1m2 = 2*nm1(2)*G1(2)*ones(2*nm1(2),1); % meshed brick
C1m1 = C1(1)/nm1(1)*mod(0:2*nm1(1)-1,2)';% meshed insulation
C1m2 = C1(2)/nm1(2)*mod(0:2*nm1(2)-1,2)';% meshed brick
```

```
G1 = [ho; 0.8/0.01; G1m1; 1/0.03; G1m2;1/0.01];
C1 = [0; C1m1; 0; C1m2;0;0];
nt = length(G1); nq = nt;       % no. temperatures; no. flows
A1 = diff(eye(nt+1));
A1(:,1) = [];                   % delete 1st node = reference temperature
b1 = zeros(nq,1);              % Temp source on branch 1: Tout
f1 = zeros(nt,1);               % Flow source in node 1: Qsolar
y1 = zeros(nt,1);               % No output

%Internal thick wall
nm2 = 2;      % number of meshes in layer
w2 = 0.24;    % width
lam2 = 0.33;  % conductivity [W/m K]
rho2 = 1000;  % density [kg/m3]
c2 = 1000;    % specific heat [J/kg K]

G2 = lam2./w2;
C2 = rho2.*c2.*w2;
G2m = 2*nm2*G2*ones(2*nm2,1);    % meshed brick
C2m = C2/nm2*mod(0:2*nm2-1,2)';  % meshed brick
G2 = [hi;0.35/0.01;G2m;0.35/0.01];
C2 = [0;C2m;0;0];
nt = length(G2); nq = nt;     % no. temperatures; no. flows
A2 = diff(eye(nt+1));
A2(:,1) = [];                   % delete 1st node = reference temperature
b2 = zeros(nq,1); b2(1) = 1;    % Temp source on branch 1: Troom

f2 = zeros(nt,1);f2(1)=1; f2(end) = 1;  % Rad. flow on int. surface
y2 = zeros(nt,1);               % No output

%Shared wall with livingroom
nm2 = 2;      % number of meshes in layer
w2 = 0.24;    % width
lam2 = 0.33;  % conductivity [W/m K]
rho2 = 1000;  % density [kg/m3]
c2 = 1000;    % specific heat [J/kg K]
G21 = lam2./w2;
C21 = rho2.*c2.*w2;
G2m = 2*nm2*G21*ones(2*nm2,1);    % meshed brick
C2m = C21/nm2*mod(0:2*nm2-1,2)';  % meshed brick
G21 = [0.35/0.01;G2m;0.35/0.01];
C21 = [0;C2m;0;0];
nt = length(C21); nq =length(G21);     % no. temperatures; no. flows
A21 = diff(eye(nt));
b21 = zeros(nq,1);
f21 = zeros(nt,1);
y21 = zeros(nt,1);               % No output


% Internal thin Wall type P3: internal [brick]
nm3 = 2;      % number of meshes in layer
```

```
w3 = 0.115;    % width
lam3 = 0.33;  % conductivity [W/m K]
rho3 = 1000;  % density [kg/m3]
c3 = 1000;    % specific heat [J/kg K]

G3 = lam3./w3;
C3 = rho3.*c3.*w3;
G3m = 2*nm3*G3*ones(2*nm3,1);         % meshed brick
C3m = C3/nm3*mod(0:2*nm3-1,2)';  % meshed brick
G3 = [hi;0.35/0.01;G3m;0.35/0.01];%With plaster layers
C3 = [0;C3m;0;0];
nt = length(G3); nq = nt;     % no. temperatures; no. flows
A3 = diff(eye(nt+1));
A3(:,1) = [];                    % delete 1st node = reference temperature
b3 = zeros(nq,1); b3(1) = 1;    % Temp source on branch 1: Troom
f3 = zeros(nt,1);f3(1)=1; f3(end) = 1;  % Rad. flow on int. surface
y3 = zeros(nt,1);               % No output

% Shared Internal thin Wall type P3: internal [brick]
nm3 = 2;      % number of meshes in layer
w3 = 0.115;    % width
lam3 = 0.33;  % conductivity [W/m K]
rho3 = 1000;  % density [kg/m3]
c3 = 1000;    % specific heat [J/kg K]

G31 = lam3./w3;
C31 = rho3.*c3.*w3;
G3m = 2*nm3*G31*ones(2*nm3,1);         % meshed brick
C3m = C31/nm3*mod(0:2*nm3-1,2)';  % meshed brick
G31 = [0.35/0.01;G3m;0.35/0.01];%With plaster layers
C31 = [0;C3m;0;0];
nt = length(C31); nq = length(G31);     % no. temperatures; no. flows
A31 = diff(eye(nt));
b31 = zeros(nq,1); b31(1) = 1;    % Temp source on branch 1: Troom
f31 = zeros(nt,1);f31(1)=1; f31(end) = 1;  % Rad. flow on int. surface
y31 = zeros(nt,1);               % No output


% Wall type P4: ceiling [concrete & insulation]
nm4 = 2;         % for wall P4, number of meshes in layer 1, 2, ...
w4 = 0.22;    % width [m]
lam4 = 2.00; % conductivity [W/m K]
rho4 =2400;    % density [kg/m3]
c4 =1000;     % specific heat [J/kg K]

G4 = lam4./w4;
C4 = rho4.*c4.*w4;
G4m1 = 2*nm4(1)*G4(1)*ones(2*nm4(1),1); % meshed concrete
C4m1 = C4(1)/nm4(1)*mod(0:2*nm4(1)-1,2)';% meshed concrete
G4 = [ho;1.4/0.4;0.04/0.04; G4m1;1.0/0.01;0.035/0.1];
C4 = [0;0;C4m1;0;0;0];
```

```
nt = length(G4); nq = nt;     % no. temperatures; no. flows
A4 = diff(eye(nt+1));
A4(:,1) = [];                   % delete 1st node = reference temperature
b4 = zeros(nq,1); b4(1) = 1;    % Temp source on branch 1: Tceiling

f4 = zeros(nt,1); f4(end) = 1;  % Rad. flow on int. surface
y4 = zeros(nt,1);               % No output

% A4'*diag(G4)*A4 + A4'*diag(G4)*b4 + diag(C4)*f4 + y4

% Wall type P5: ground (concrete & insulation & screed)
nm5 = [2 1 1]';         % for wall P4, number of meshes in layer 1, 2, ...
w5 = [0.22 0.03 0.065]';    % width [m]
lam5 = [2.10 0.025 1.40]'; % conductivity [W/m K]
rho5 = [2400 80 2000]';    % density [kg/m3]
c5 = [1000 840 1000]';     % specific heat [J/kg K]

G5 = lam5./w5;
C5 = rho5.*c5.*w5;
G5m1 = 2*nm5(1)*G5(1)*ones(2*nm5(1),1);   % meshed concrete
G5m2 = 2*nm5(2)*G5(2)*ones(2*nm5(2),1);   % meshed insulation
G5m3 = 2*nm5(3)*G5(3)*ones(2*nm5(3),1);   % meshed screed
C5m1 = C5(1)/nm5(1)*mod(0:2*nm5(1)-1,2)'; % meshed concrete
C5m2 = C5(2)/nm5(2)*mod(0:2*nm5(2)-1,2)'; % meshed insulation
C5m3 = C5(3)/nm5(3)*mod(0:2*nm5(3)-1,2)'; % meshed insulation


G5 = [ho;G5m1;0.060/0.029;G5m2;0.023/0.030; G5m3];
nt = length(G5); nq = nt;     % no. temperatures; no. flows
A5 = diff(eye(nt+1));
A5(:,1) = [];                   % delete 1st node = reference temperature
b5 = zeros(nq,1); b5(1) = 1;    % Temp source on branch 1: Tground
C5 = [C5m1;0; C5m2;0; C5m3; 0];
f5 = zeros(nt,1); f5(end) = 1;  % Rad. flow on int. surface
y5 = zeros(nt,1);               % No output

% A5'*diag(G5)*A5 + A5'*diag(G5)*b5 + diag(C5)*f5 + y5

% Door type D1 & D2: wood
nm6 = 1;      % number of meshes in layer
w6 = 0.04;    % width [m]
lam6 = 0.13;  % conductivity [W/m K]
rho6 = 600;  % density [kg/m3]
c6 = 1000;     % specific heat [J/kg K]

G6 = lam6./w6;
C6 = rho6.*c6;
G6m = 2*nm6*G6*ones(2*nm6,1);         % meshed wood
C6m = C6/nm6*mod(0:2*nm6-1,2)';  % meshed wood

nt = 1+2*sum(nm6); nq = nt;     % no. temperatures; no. flows
```

```
A6 = diff(eye(nt+1));
A6(:,1) = [];                    % delete 1st node = reference temperature
G6 = [hi; G6m];
b6 = zeros(nq,1);      % Temp source on branch 1: Troom
C6 = [C6m; 0];
f6 = zeros(nt,1);    % Rad. flow on int. surface
y6 = zeros(nt,1);

% A6'*diag(G6)*A6 + A6'*diag(G6)*b6 + diag(C6)*f6 + y6

%Shared Door
nm6 = 1;       % number of meshes in layer
w6 = 0.04;     % width [m]
lam6 = 0.13;   % conductivity [W/m K]
rho6 = 600;   % density [kg/m3]
c6 = 1000;      % specific heat [J/kg K]
%c6 = 0;       % changes dt = 49 s -> dt = 3920 s

G61 = lam6./w6;
C61 = rho6.*c6;
G6m = 2*nm6*G61*ones(2*nm6,1);          % meshed wood
C6m = C61/nm6*mod(0:2*nm6-1,2)';   % meshed wood
G61 = [G6m];
C61 = [C6m; 0];
nt = length(C61); nq = length(G61);      % no. temperatures; no. flows
A61 = diff(eye(nt));
b61 = zeros(nq,1);
f61 = zeros(nt,1);    % Rad. flow on int. surface
y61 = zeros(nt,1);

% Shared Infiltration
A7 =1;
G7 = 2.22/3600*rhoa*ca*2.495;
C7 = 0;
b7 = 0;
f7 = 0;
y7 = 0;

% Shared Infiltration
A71 =[-1 1];
G71 = 1/3*2.22/3600*rhoa*ca*2.495;
C71 = [0;0];
b71 = 0;
f71 = [0;0];
y71 = [0;0];

% Shared Ventilation
A81 =[-1 1];
G81 = 60/3600*rhoa*ca*2.495;
C81 = [0;0];
b81 = 0;
```

```
f81 = [0;0];
y81 = [0;0];

% % A7'*diag(G7)*A7 + A7'*diag(G7)*b7 + diag(C7)*f7 + y7
% %Pillar
% rhoc=2400;
% cc=1000;
% S9=0.3048*0.23; %Cross sectional area of concrete
% Hc=2.495; %Hieght of concrete
% A9 = [-1 1];
% G9 =0.5; % 1.2;
% C9 =[rhoc*cc*S9*Hc;0];
% b9 = 0;
% f9 = [0;0];
% y9 = [0;0];

%**************************%
%Kitchen zones
%**************************%
S1k = 2.8355*2.495;
b1(1)=1;
f1(1)=1;
f1(end)=1;
TCd{1} = {A1,S1k*diag(G1),b1,S1k*diag(C1),f1,y1};   % Kitchen Northern wall

S2k = 2.625*2.495;
b31(1)=0; %Doorway Temperature
f31(1)=1;
f31(end)=1;
TCd{2} = {A31,S2k*diag(G31),b31,S2k*diag(C31),f31,y31};   % Kitchen Eastern wall shared with
doorwy

S3k=2.835*2.495; % Kithcen wall shared with livngrm
b21(1)=0;
f21(1)=1;
f21(end)=1;
TCd{3} = {A21,S3k*diag(G21),b21,S3k*diag(C21),f21,y21};

S4k=0.935*1.95;
b61(1)=0;
f61(1)=1;
f61(end)=1;
TCd{4} = {A61,S4k*diag(G61),b61,S4k*diag(C61),f61,y61};  % Door shared with livngrm

Sg = 81.69;%Infiltration between two zones
b71(1)=0;
f71(1)=0;
f71(end)=0;
TCd{5} = {A71,Sg*diag(G71),b71,diag(C71),f71,y71};  % Infiltration

S5k =2.625*2.495;%West wall
```

```
b1(1)=1;
f1(1)=1;
f1(end)=1;
TCd{6} = {A1,S5k*diag(G1),b1,S5k*diag(C1),f1,y1};  % Kithcen west wall

S6k = 7.44;
f4(1)=0;
b4(1)=1;
f4(end)=1;
TCd{7}={A4,S6k*diag(G4),b4,S6k*diag(C4),f4,y4};       % Doorway cieling

S7k=7.44;
f5(1)=0;
b5(1)=1;
f5(end)=1;
TCd{8} = {A5,S7k*diag(G5),b5,S7k*diag(C5),f5,y5};       % Kitchen Ground

% Indoor air

Infil=1.62/3600; %Infiltration per hour per floor area 81.69
sg=7.44;


G9 = hi*[S1k; S2k; S3k; S4k; S5k;S6k;S7k];
Gb1=0.089*11.67; % Thermal bridge Ext wall cieling
Gb2=0.110*11.67; % Thermal bridge Ext wall ground
Gb3=2*0.093*2.495; % Thermal bridge Ext wall-wall
Gwin=2.14*1.2; %West Window
GInfil=Infil/30*sg*2.495*rhoa*ca; % External infiltration
Gt=Gwin+GInfil;
G9 = [G9;Gt];
%Last   three   terms   Extwall-Ground   Thermal-bridge,Extwall-cieling   bridge,shared-wall-
kithcen/ground bridge
A9 = -eye(8);  A9(:,8) = 1;
C9 = zeros(8,1); C9(8) = rhoa*sg*2.495*ca;
b9 = zeros(8,1); b9(8) = 1; % in: source Tout
f9 = zeros(8,1); f9(8) = 1;   % in: source heat flow in air volume
y9 = zeros(8,1); y9(end) = 1;   % out: indoor air

TCd{9} = {A9,diag(G9),b9,diag(C9),f9,y9};              % indoor air
% SW radiative sources on walls: distributed uniformely
Skith = 2*(2.625+2.835)*2.495 + 2*2.625*2.835; % total area Kitchen room
% radiative gain through closed blinds
%Splr=2*2.495*(0.3048+0.203);
%Qheaterkith=0.9*0.7*Qk'+(1.29*Qw'*0.427*0.8+0.3*Qk')*0.25;

%********************%
    %Livingroom Zone%
%********************%
S1l = (3.97 - 0.35)*2.495 - 0.93*1.95;%Livng shared wall with Kithcen
```

```
S2l = 0.93*1.95; % Living-kitchen door


S3l = 2.225*2.495 - 0.93*1.95;
b21(1)=0;
f21(1)=1;
f21(end)=1;
TCd{10} = {A21,S3l*diag(G21),b21,S3l*diag(C21),f21,y21};   % Living-doorway internal wall

S4l = 0.93*1.95;
b61(1)=0;
f61(1)=1;
f61(end)=1;
TCd{11} = {A61,S4l*diag(G61),b61,S4l*diag(C61),f61,y61};       % Living-doorway door

Sg = 81.69;%Infiltration between two zones
b71(1)=0;
f71(1)=0;
f71(end)=0;
TCd{12} = {A71,Sg*diag(G71),b71,diag(C71),f71,y71};  % Infiltration between zones

S5l = 3.31*2.495 - 0.93*1.95;
b21(1)=0;
f21(1)=0;
f21(end)=1;
TCd{13} = {A21,S5l*diag(G21),b21,S5l*diag(C21),f21,y21};       % Living - corridor wall

S6l = 2.88*2.495;
b21(1)=0;
b21(end)=0;
f21(1)=1;
f21(end)=1;
TCd{14} = {A21,S6l*diag(G21),b21,S6l*diag(C21),f21,y21};       % Living - bedroom2 wall

S7l = 5.290*2.495 - 8.66;
f1(1)=1;
f1(end)=1;
b1(1)=1;
b1(end)=0;
TCd{15} = {A1,S7l*diag(G1),b1,S7l*diag(C1),f1,y1};       % Living - extern. South wall

S8l = 6.47*2.495 - 2.14;
f1(1)=1;
f1(end)=1;
b1(1)=1;
b1(end)=0;
TCd{16} = {A1,S8l*diag(G1),b1,S8l*diag(C1),f1,y1};    % Living - extern. West wall

S9l = 6.47*5.20;
f4(1)=0;
f4(end)=1;
```

```
b4(1)=1;
TCd{17} = {A4,S9l*diag(G4),b4,S9l*diag(C4),f4,y4};     % Living - Attic

S10l = 6.47*5.20;
f5(1)=0;
f5(end)=1;
b5(1)=1;
TCd{18} = {A5,S10l*diag(G5),b5,S10l*diag(C5),f5,y5};     % Living - Cellar

% Indoor air
Va = 120/3600;      % volumetric air flow [m3/s]
Infil=1.62/3600; %Infiltration per hour per floor area 81.69
%S13=2.662; %Surface area of Pillar
G10 = hi*[S1l; S2l; S3l; S4l; S5l;S6l;S7l; S8l; S9l; S10l];
%Last three terms consist of thermal bridges:Ext-Ext wall, Extwall-Ground
Gb1=0.089*11.67; % Thermal bridge Ext wall cieling
Gb2=0.110*11.67; % Thermal bridge Ext wall ground
Gb3=0.093*2.495; % Thermal bridge Ext wall-wall
Ginf=Infil/23*33.65*2.495*rhoa*ca
Gt=Ginf+Gb1+Gb2+Gb3; % Total resistance
%and Internal wall ground
%        S window W window Ventilation  Infiltration   Air-exchange corridr
G10 = [G10;8.66*1.05;2.14*1.2;rhoa*Va*ca;Gt];
A10 = -eye(11); A10=[A10;zeros(1,11);zeros(1,11);zeros(1,11)]; A10(:,11) = 1;
C10 = zeros(11,1); C10(11) = rhoa*6.47*5.20*2.495*ca;
b10 = zeros(14,1); b10(11) = 1;b10(12) = 1;b10(13) = 1;b10(14) = 1;  % in: source Tout
f10 = zeros(11,1); f10(end) = 1;   % in: source heat flow in air volume
y10 = zeros(11,1); y10(11) = 1;   % out: indoor air

TCd{19} = {A10,diag(G10),b10,diag(C10),f10,y10};  % indoor air

%Radiations on wall of Living room
Sliv = 2*(6.465+5.205)*2.495 + 2*6.465*5.205;
%Qsolliv=[S7*0.23*Qs';S8*0.23*Qw'];
%Qheaterliv=0.9*0.7*Qi'+(1.29*Qw'*0.427+0.3*Qi')*0.25;
%**********************%
    %Doorway Zone%
%**********************%
S20d=2.225*2.495-2.0;  % Doorway Northwall
f1(1)=1;
f1(end)=1;
b1(1)=1;
b1(end)=0;
TCd{20}={A1,S20d*diag(G1),b1,S20d*diag(C1),f1,y1}; % Doorway Northwall

S21d=1.0*2.0;  % Doorway Door
f6(1)=1;
f6(end)=1;
b6(1)=1;
b6(end)=0;
TCd{21}={A6,S21d*diag(G6),b6,S21d*diag(C6),f6,y6}; % Doorway Door
```

```
S22d=2.625*2.495;  % Doorway wall shared with Bedroom
f21(1)=1;
f21(end)=1;
b21(1)=0;
b21(end)=0;
TCd{22}={A21,S22d*diag(G21),b21,S22d*diag(C21),f21,y21}; % Doorway wall shared with Bedroom

S23d=0.935*1.95; %Doorway door shared with Livingrm

S24d=2.225*2.495-0.935*1.95; %Area of shared wall/Livingrm

S25d=2.625*2.495; %Wall shared with Kitchen

S26d=5.84;  % Doorway Ceiling
f4(1)=0;
f4(end)=1;
b4(1)=1;
b4(end)=0;
TCd{23}={A4,S26d*diag(G4),b4,S26d*diag(C4),f4,y4}; % Doorway Ceiling

S27d=5.84;  % Doorway Ground
f5(1)=0;
f5(end)=1;
b5(1)=1;
b5(end)=0;
TCd{24}={A5,S27d*diag(G5),b5,S27d*diag(C5),f5,y5}; % Doorway Ground

%Doorway Air node

%Infil=1.62/3600; %Infiltration per hour per floor area 81.69
%S13=2.662; %Surface area of Pillar
G11 = hi*[S20d; S21d; S22d; S23d; S24d;S25d;S26d; S27d];
Ginf=Infil/23*5.84*2.495*rhoa*ca;
% Gb1=0.089*2.22; % Thermal bridge Ext wall cieling
% Gb2=0.110*2.22; % Thermal bridge Ext wall ground
%Gb3=0.093*2.495; % Thermal bridge Ext wall-wall
Gt=Ginf; % Total resistance
%Last three terms consist of thermal bridges:Ext-Ext wall, Extwall-Ground
%and Internal wall ground
%        S window W window Ventilation  Infiltration   Air-exchange corridr
G11 = [G11;Gt];
A11 = -eye(9);  A11(:,9) = 1;
C11 = zeros(9,1); C11(9) = rhoa*5.84*2.495*ca;
b11 = zeros(9,1); b11(9) = 1;  % in: source Tout
f11 = zeros(9,1); f11(end) = 1;   % in: source heat flow in air volume
y11 = zeros(9,1); y11(9) = 1;   % out: indoor air
TCd{25}={A11,diag(G11),b11,diag(C11),f11,y11};
%Radiations on wall of Living room
%Qsolliv=[S7*0.23*Qs';S8*0.23*Qw'];
%Qheaterliv=0.9*0.7*Qi'+(1.29*Qw'*0.427+0.3*Qi')*0.25;
```

```
% Pillar
% Kitchen Pillar
rhoc=2400;
cc=1000;
S26=0.3048*0.23; %Cross sectional area of concrete
Hc=2.495; %Hieght of concrete
A26 = [-1 1];
G26 =0.5; % 1.2;
C26 =[rhoc*cc*S26*Hc;0];
b26 = 0;
f26 = [0;0];
y26 = [0;0];
TCd{26}={A26,diag(G26),b26,diag(C26),f26,y26};
% Livingroom Pillar
TCd{27}={A26,diag(G26),b26,diag(C26),f26,y26};

% **********************************
        %Children's Room
% **********************************
S1C = 2.09*2.495 - 0.935*1.95;
f31(1)=1;
f31(end)=1;
b31(1)=0;
b31(end)=0;
TCd{28} = {A31,S1C*diag(G31),b31,S1C*diag(C31),f31,y31};  % Childrnrm wall shared with Bathroom


S2C = 2.88*2.495;
f1(1)=1;
f1(end)=1;
b1(1)=1;
b1(end)=0;
TCd{29} = {A1,S2C*diag(G1),b1,S2C*diag(C1),f1,y1};  % Childrenrm Eastern wall

S3C=3.885*2.495 - 2.14;
f1(1)=1;
f1(end)=1;
b1(1)=1;
b1(end)=0;
TCd{30} = {A1,S3C*diag(G1),b1,S3C*diag(C1),f1,y1};  % Childrenrm South wall

S4C=2.88*2.495;
% f2(1)=1;
% f2(end)=1;
% b2(1)=1;
% b2(end)=0;
% TCd{31} = {A2,S4C*diag(G2),b2,S4C*diag(C2),f2,y2};  % Childrnrm wall shared with livngrm

S5C =11.19;
f4(1)=0;
f4(end)=1;
```

```
b4(1)=1;
b4(end)=0;
TCd{31} = {A4,S5C*diag(G4),b4,S5C*diag(C4),f4,y4};     % Childrnrm - Attic

S6C = 11.19;
f5(1)=0;
f5(end)=1;
b5(1)=1;
b5(end)=0;
TCd{32} = {A5,S6C*diag(G5),b5,S6C*diag(C5),f5,y5};     % Childrnrm- Cellar

TCd{33} = {A26,diag(G26),b26,S6C*diag(C26),f26,y26};     % Plillar

% Indoor air
Va = 60/3600;
rhoa=1.2;
ca=1000;
Infil=1.62/3600; %Infiltration per hour per floor area 81.69
sg=11.19;
G34 = hi*[S1C; S2C; S3C; S4C; S5C;S6C;1.65*2.495];
Gwin=2.14*1.05; %Window
Gven=0.9*Va*rhoa*ca;
Gbe=0.107*6.765+0.084*6.765; %External wall-ground+cieling bridge
Gbil=0.378*2.88+0.204*2.88;%Internal Floor and Cieling thermal bridge shared with livingroom
Gbibh=0.243*3.885+0.131*3.885; %Intermal floor and ceiling thermal bridge shared with Bathroom
Ginfil=Infil/20*sg*2.495*rhoa*ca+0.01*Va*rhoa*ca; %Outdoor Infiltration
Gextwall=0.091*2.495; %Thermal bridge b.w ext-ext wall
Gt=Gwin+Ginfil+Gextwall+Gbe; %Total

G34 = [G34;Gt;Gbil;Gbibh];
%Last   three   terms   Extwall-Ground   Thermal-bridge,Extwall-cieling   bridge,shared-wall-
kithcen/ground bridge
A34 = -eye(8);A34=[A34;zeros(1,8);zeros(1,8)];  A34(:,8) = 1;
C34 = zeros(8,1); C34(8) = rhoa*sg*2.495*ca;
b34 = zeros(10,1);  b34(8) = 1;b34(9) = 1;b34(10) = 1; % in: source Tout
f34 = zeros(8,1); f34(8) = 1;   % in: source heat flow in air volume
y34 = zeros(8,1); y34(8) = 1;   % out: indoor air

TCd{34} = {A34,diag(G34),b34,diag(C34),f34,y34};              % indoor air

%Qsolcdrm=[0.17*0.3*Qbh'/6;Qr(1,:);Qe'*0.23*S2;Qr(2,:);Qs'*0.23*S3;Qr(3,:);0.17*0.3*Qi'/12;Qr(
4:end,:);0.9*0.7*Qch'];

% **********************************
        %Bedroom Room
% **********************************
S1b = 3.885*2.495 - 2.14;
f1(1)=1;
f1(end)=1;
b1(1)=1;
b1(end)=0;
```

```
TCd{35} = {A1,S1b*diag(G1),b1,S1b*diag(C1),f1,y1};   % Bedroom Northern wall



S2b = 2.88*2.495;
f1(1)=1;
f1(end)=1;
b1(1)=1;
b1(end)=0;
TCd{36} = {A1,S2b*diag(G1),b1,S2b*diag(C1),f1,y1};  % Bedroom Eastern wall

S3b=2.09*2.495;
f31(1)=1;
f31(end)=1;
b31(1)=0;
b31(end)=0;
TCd{37} = {A31,S3b*diag(G31),b31,S3b*diag(C31),f31,y31};  % Bedroom wall shared with Bathroom

S4b=1.65*2.495-0.935*1.95;
f31(1)=0;
f31(end)=1;
b31(1)=0;
b31(end)=0;
TCd{38} = {A31,S4b*diag(G31),b31,S4b*diag(C31),f31,y31};  % Bedrrom wall shared with Corridor


S5b =0.935*1.95;
f61(1)=0;
f61(end)=1;
b61(1)=0;
b61(end)=0;
TCd{39} = {A61,S5b*diag(G61),b61,S5b*diag(C61),f61,y61};    % Bedroom door shared with corridor

S6b = 2.88*2.495;
% f21(1)=0;
% f21(end)=1;
% b21(1)=0;
% b21(end)=0;
% TCd{6} = {A21,S6b*diag(G21),b21,S6b*diag(C21),f21,y21}; % Bedroom wall shared with Doorwy

S7b =11.19;
f4(1)=0;
f4(end)=1;
b4(1)=1;
b4(end)=0;
TCd{40} = {A4,S7b*diag(G4),b4,S7b*diag(C4),f4,y4};     % Bedrrom - Attic

S8b = 11.19;
f5(1)=0;
f5(end)=1;
b5(1)=1;
```

```
b5(end)=0;
TCd{41} = {A5,S8b*diag(G5),b5,S8b*diag(C5),f5,y5};     % Bedroom- Cellar

TCd{42} = {A26,diag(G26),b26,diag(C26),f26,y26};     % Pillar
% Indoor air
rhoa=1.2;
ca=1000;
 %Infiltration per hour per floor area 81.69
sg=11.19;
GInfil=1.62/3600*sg*2.495*rhoa*ca;
%GInfil1=1/3*2.22/3600*sg*2.495*rhoa*ca;
Gwin=2.14*1.2;
Gextwall=0.091*2.495; %Thermal bridge b.w ext-ext wall
Gt=Gwin+GInfil/20+Gextwall;
G8 = hi*[S1b; S2b; S3b; S4b; S5b;S6b;S7b;S8b];

G8 = [G8;Gt];
%Last   three   terms   Extwall-Ground   Thermal-bridge,Extwall-cieling   bridge,shared-wall-
kithcen/ground bridge
A8 = -eye(9);  A8(:,9) = 1;
C8 = zeros(9,1); C8(9) = rhoa*sg*2.495*ca;
b8 = zeros(9,1); b8(9) = 1;  % in: source Tout
f8 = zeros(9,1);  f8(9) = 1;   % in: source heat flow in air volume
y8 = zeros(9,1); y8(9) = 1;   % out: indoor air

TCd{43} = {A8,diag(G8),b8,diag(C8),f8,y8};              % indoor air

% **********************************
        %Bathroom Room
% **********************************
S1bh=2.09*2.495; % Wall shared with Bedroom

S2bh = 3.31*2.495; % Bathroom East External wall
f1(1)=1;
f1(end)=1;
b1(1)=1;
b1(end)=0;
TCd{44} = {A1,S2bh*diag(G1),b1,S2bh*diag(C1),f1,y1};   % Bedroom East wall

S3bh=2.09*2.495; %Wall shared with Children room

S4bh =3.31*2.495-0.935*1.95; % Bathroom wall shared with corridor
f31(1)=0;
f31(end)=1;
b31(1)=0;
b31(end)=0;
TCd{45} = {A31,S4bh*diag(G31),b31,S4bh*diag(C31),f31,y31};

S5bh =6.92; % Bathroom Cieling
f4(1)=0;
f4(end)=1;
```

```
b4(1)=1;
b4(end)=0;
TCd{46} = {A4,S5bh*diag(G4),b4,S5bh*diag(C4),f4,y4};

S6bh =6.92; % Bathroom Ground
f5(1)=0;
f5(end)=1;
b5(1)=1;
b5(end)=0;
TCd{47} = {A5,S6bh*diag(G5),b5,S6bh*diag(C5),f5,y5};

% Indoor air
rhoa=1.2;
ca=1000;
%Infiltration per hour per floor area 81.69
sg=6.92;
Va=60/3600; % Ventilation
Gvent=Va*rhoa*ca; % Ventilation
GInfil=1.62/3600*sg*2.495*rhoa*ca+0.01*Va*rhoa*ca;
Gwin=2.14*1.2;
Gt=Gwin+GInfil/20;

G8 = hi*[S1bh;S2bh;S3bh;S4bh;S5bh;S6bh];
G8 = [G8;Gt];

A8 = -eye(7);  A8(:,7) = 1;
C8 = zeros(7,1); C8(7) = rhoa*sg*2.495*ca;
b8 = zeros(7,1); b8(7) = 1;  % in: source Tout
f8 = zeros(7,1);  f8(7) = 1;   % in: source heat flow in air volume
y8 = zeros(7,1); y8(7) = 1;   % out: indoor air

TCd{48} = {A8,diag(G8),b8,diag(C8),f8,y8};              % Indoor air
%Bathroom
% ***********************************
        %Corridor
% ***********************************
S1cr=0.935*1.95; %Shared door area

S2cr=1.65*2.495-0.935*1.95; % Shared wall between corridor and bedrm

S3cr=3.31*2.495-0.935*1.95; % Shared wall between corridor and bathroom

S4cr=1.65*2.495-0.935*1.95; %Shared wall between Children rm and corridor

S5cr=3.31*2.495-0.935*1.95; %Shared wall between living rm and corridor

f71(1)=0; %Infiltration between Bedrm and Corridor
f71(end)=0;
b71(1)=0;
b71(end)=0;
TCd{49} = {A71,diag(G71),b71,diag(C71),f71,y71};
```

```
f81(1)=0; %Infiltration between Bathrm and Corridor
f81(end)=0;
b81(1)=0;
b81(end)=0;
TCd{50} = {A81,diag(G81),b81,diag(C81),f81,y81};

S4cr=1.65*2.495-0.935*1.95; %Shared wall between Bathrm and corridor
f31(1)=0;
f31(end)=0;
b31(1)=0;
b31(end)=0;
TCd{51} = {A31,S4cr*diag(G31),b31,S4cr*diag(C31),f31,y31};

f81(1)=0;%Shared Infiltration between corridor and chldrn rm
f81(end)=0;
b81(1)=0;
b81(end)=0;
TCd{52} = {A81,diag(G81),b81,diag(C81),f81,y81};

f81(1)=0;%Shared Infiltration between corridor and Livngrm
f81(end)=0;
b81(1)=0;
b81(end)=0;
TCd{53} = {A81,2*diag(G81),b81,diag(C81),f81,y81};

S6cr =5.46; % Corridor Cieling
f4(1)=0;
f4(end)=0;
b4(1)=1;
b4(end)=0;
TCd{54} = {A4,S6cr*diag(G4),b4,S6cr*diag(C4),f4,y4};

S7cr =5.46; % Bathroom Ground
f5(1)=0;
f5(end)=0;
b5(1)=1;
b5(end)=0;
TCd{55} = {A5,S7cr*diag(G5),b5,S7cr*diag(C5),f5,y5};

% Indoor air
rhoa=1.2;
ca=1000;
%Infiltration per hour per floor area 81.69
sg=5.46;
% Va=60/3600; % Ventilation
% Gvent=Va*rhoa*ca; % Ventilation
% GInfil=1.62/3600*sg*2.495*rhoa*ca;
% Gwin=2.14*1.2;
% Gt=Gwin+GInfil/20;
```

```
G8 = hi*[S1cr;S2cr;S3cr;S4cr;S5cr;S6cr;S7cr];

A8 = -eye(8);A8(8,:)=[]; A8(:,8) = 1;
C8 = zeros(8,1); C8(8) = rhoa*sg*2.495*ca;
b8 = zeros(7,1);   % in: source Tout
f8 = zeros(8,1);
y8 = zeros(8,1); y8(8) = 1;   % out: indoor air

TCd{56} = {A8,diag(G8),b8,diag(C8),f8,y8};              % Indoor air

% **********************************
            %Assembly
% **********************************

AssX=[1 length(TCd{1}{5}) 9 1;...
          2 1 25 6;...
          2 length(TCd{2}{5}) 9 2;...
          3 1 19 1;...
          3 length(TCd{3}{5}) 9 3;...
          4 1 19 2;...
          4 length(TCd{4}{5}) 9 4;...
          9 length(TCd{9}{5}) 5 length(TCd{5}{5});...
          6 length(TCd{6}{5}) 9 5;...
          7 length(TCd{7}{5}) 9 6;...
          8 length(TCd{8}{5}) 9 7;...
          9 length(TCd{9}{5}) 26 length(TCd{26}{5});...
          10 1 25 5;...
          10 length(TCd{10}{5}) 19 3;...
          11 1 25 4;...
          11 length(TCd{11}{5}) 19 4;...
          13 1 56 5;...
          13 length(TCd{13}{5}) 19 5;...
          14 length(TCd{14}{5}) 19 6;...
          14 1 34 4;...
          15 length(TCd{15}{5}) 19 7;...
          16 length(TCd{16}{5}) 19 8;...
          17 length(TCd{17}{5}) 19 9;...
          18 length(TCd{18}{5}) 19 10;...
          19 length(TCd{19}{5}) 5 1;...
          19 length(TCd{19}{5}) 12 length(TCd{12}{5});...
          19 length(TCd{19}{5}) 27 length(TCd{27}{5});...
          20 length(TCd{20}{5}) 25 1;...
          21 length(TCd{21}{5}) 25 2;...
          22 length(TCd{22}{5}) 25 3;...
          22 1 43 6;...
          23 length(TCd{23}{5}) 25 7;...
          24 length(TCd{24}{5}) 25 8;...
          25 length(TCd{25}{5}) 12 1;...
          28 length(TCd{28}{5}) 34 1;...
          28 1 48 3;...
          29 length(TCd{29}{5}) 34 2;...
```

```
          30 length(TCd{30}{5}) 34 3;...
          31 length(TCd{31}{5}) 34 5;...
          32 length(TCd{32}{5}) 34 6;...
          34 length(TCd{34}{5}) 33 length(TCd{33}{5});...
          35 length(TCd{35}{5}) 43 1;...
          36 length(TCd{36}{5}) 43 2;...
          37 length(TCd{37}{5}) 43 3;...
          37 1 48 1;...
          38 1 56 2;...
          38 length(TCd{38}{5}) 43 4;...
          39 1 56 1;...
          39 length(TCd{39}{5}) 43 5;...
          40 length(TCd{40}{5}) 43 7;...
          41 length(TCd{41}{5}) 43 8;...
          43 length(TCd{43}{5}) 42 length(TCd{42}{5});...
          44 length(TCd{44}{5}) 48 2;...
          45 1 56 3;...
          45 length(TCd{45}{5}) 48 4;...
          46 length(TCd{46}{5}) 48 5;...
          47 length(TCd{47}{5}) 48 6;...
          48 length(TCd{48}{5}) 50 length(TCd{50}{5});...
          43 length(TCd{43}{5}) 49 1;...
          56 length(TCd{56}{5}) 49 length(TCd{49}{5});...
          56 length(TCd{56}{5}) 50 1;...
          51 length(TCd{51}{5}) 34 7;...
          51 1 56 4;...
          34 length(TCd{34}{5}) 52 1;...
          56 length(TCd{56}{5}) 52 length(TCd{52}{5});...
          19 length(TCd{19}{5}) 53 length(TCd{53}{5});...
          56 length(TCd{56}{5}) 53 1;...
          54 length(TCd{54}{5}) 56 6;...
          55 length(TCd{55}{5}) 56 7];

[TCa, Idx] = fTCAssAll(TCd, AssX);
A = TCa{1}; G = TCa{2}; b = TCa{3}; C = TCa{4}; f = TCa{5}; y = TCa{6};
[InTN, InFN, OutN] = fNumInOut(TCa, Idx);
% ************************************
% Inputs
% ************************************
Z=90;
trns1=ftrans1(Z);
Qrkith = [S1k S2k S3k S4k S5k S6k S7k]/Skith.*(1.29*Qw.*trns1+0.3*Qk)*0.70; %Kithcen
Tkith = [To';To';Ta';Tg';To'];
Qrkith=Qrkith';
%Qsolkith=[S1k*0.23*Qn';Qrkith(1:4,:);S5k*0.23*Qw';Qrkith(5:end,:);0.7*Qk'+(1.29*Qw'.*trns1'+0
.3*Qk')*0.30];
%Living room

Qrliv = [S1l S2l S3l S4l S5l S6l S7l S8l S9l S10l]/Sliv.*(1.29*Qw.*trns1+0.3*Qi)*0.70;
Qrliv=Qrliv';
Tliv = [To';To';Ta';Tg';To';To';Tv';To'];
```

```
%Qsolliv=[Qr(1:6,:);Qr(7,:);Qr(8:end,:);0.7*Qi'+(1.29*Qw'*0.427.*trns1'+0.3*Qi')*0.30];
%Doorway
Sdrwy = 2*(2.625+2.225)*2.495 + 2*2.625*2.225;
Qrdrwy = [S20d S21d S22d S23d S24d S25d S26d S27d]/Sdrwy.*(0.9*0.3*Qd);
Qrdrwy=Qrdrwy';
Tdrwy = [To';To';Ta';Tg';To'];

% SW Children's room
Scdrm = 2*(3.885+2.88)*2.495 + 2*3.885*2.88; % Children's room
% Childre's room temperature
Tcdrm=[To';To';Ta';Tg';To';Ti';Tbh'];
% Childre's room internal radiations
Qrcdrm = [S1C S2C S3C S4C S5C S6C]/Scdrm.*(0.85*0.3*Qch);
Qrcdrm=Qrcdrm';

%Bedroom
Sbdrm = 2*(3.885+2.88)*2.495 + 2*3.885*2.88; % total area Doorway room
% radiative gain through closed blinds
Tbdrm=[To';To';Ta';Tg';To'];
Z=180;
trns1=ftrans1(Z);

Qbdrm = [S1b S2b S3b S4b S5b S6b S7b S8b]/Sbdrm.*(Qn.*trns1*1.29+0.90*0.30*QB)*0.7;
Qbdrm=Qbdrm';
%Qsol=[S1*0.23*Qn';Qr(1,:);S2*0.23*Qn';Qr(2:end,:)];
%Qheaterdrwy=0.70*QB'+(Qn'*0.427*1.29+0.90*0.30*QB')*0.7;

%Bathroom
Sbthrm = 2*(2.09+3.31)*2.495 + 2*2.09*3.31; % total area Doorway room
% radiative gain through closed blinds
Tbthrm=[To';Ta';Tg';To'];
Z=-90;
trns1=ftrans1(Z);

Qbthrm = [S1bh S2bh S3bh S4bh S5bh S6bh]/Sbdrm.*(Qe.*trns1*1.29+0.90*0.30*Qbh)*0.7;
Qbthrm=Qbthrm';

%Corridor
Tcrrdr=[Ta';Tg'];

Q=[S1k*0.23*Qn';Qrkith(1,:);Qrdrwy(6,:);Qrkith(2,:);Qrliv(1,:);...
   Qrkith(3,:);Qrliv(2,:);Qrkith(4,:);S5k*0.23*Qw';Qrkith(5:end,:);...
   0.7*Qk'+(1.29*Qw'*0.427+0.3*Qk')*0.30;Qrdrwy(5,:);Qrliv(3,:);...
   Qrdrwy(4,:);Qrliv(4:5,:);Qrcdrm(4,:);Qrliv(6,:);S7l*0.23*Qs';Qrliv(7,:);S8l*0.23*Qw';...
   Qrliv(8:end,:);0.7*Qi'+(1.29*Qw'*0.427+0.3*Qi')*0.30;S20d*0.23*Qn';...
   Qrdrwy(1,:);S21d*0.23*Qn';Qrdrwy(2,:);Qbdrm(6,:);Qrdrwy(3,:);Qrdrwy(7:8,:);0.9*0.7*Qd';...
   Qbthrm(3,:);Qrcdrm(1,:);S2C*0.23*Qe';Qrcdrm(2,:);S3C*0.23*Qs';Qrcdrm(3,:);...
   Qrcdrm(5:6,:);0.85*0.7*Qch';Qn'*0.23*S1b;Qbdrm(1,:);Qe'*0.23*S2b;...
   Qbdrm(2,:);Qbthrm(1,:);Qbdrm(3:5,:);Qbdrm(7:8,:);...
   0.9*0.70*QB'+(Qn'.*trns1'*1.29+0.90*0.30*QB')*0.3;Qe'*0.23*S2bh;...
   Qbthrm(2,:);Qbthrm(4:6,:);0.9*0.7*Qbh'+(Qe'.*trns1'*1.29+0.90*0.30*Qbh')*0.3];
```

```
% ************************************
%           State Space
% ************************************

% Model
[A,B,C,D] = fTC2SSold(A,G,b,C,f,y);
disp(['max dt = ',num2str(min(-2./eig(A))),'[s]'])

% ************************************
%               Inputs                 %
% ************************************
u=[Tkith;Tliv;Tdrwy;Tcdrm;Tbdrm;Tbthrm;Tcrrdr;Q];

dt = 10*60;                     % time step: 10 min
n = length(H(:,1));
Time = 0:dt:(n-1)*dt;           % time
nth = size(A,1);                % no states
% initial conditions
th = 28*ones(nth,n); thi = th; the = th;
Ae = (eye(nth) + dt*A);         % Euler explicit
Ai = inv((eye(nth) - dt*A));    % Euler implicit
Ad = expm(A*dt);                % exp. matrix
Bd = (Ad-eye(size(A)))*inv(A)*B;
for k = 1:n-1
 th(:,k+1) = Ae*th(:,k) + dt*B*u(:,k);     % Euler explicit
 thi(:,k+1) = Ai*(thi(:,k) + dt*B*u(:,k));  % Euler implicit
 the(:,k+1) = Ad*the(:,k)+Bd*u(:,k);        % matrix exponential
end
ye = C*th + D*u;        % Euler explicit
yi = C*thi + D*u;       % Euler implicit
yE = C*the + D*u;       % exponential

figure(1)
Time = Time/3600/24;
% plot(Time,ye,Time,yi,Time,yE,'r',Time,Ti, Time, To,'b')
% plot(Time,yi, Time,yE,'r',Time,Ti,'g', Time, To,'b')
plot(Time,yE(1,:),'r', Time,Tk,'g', Time,To,'b')
ylabel('Temperature [C]')
legend('T_s_i_m','T_i','T_o')
title('Kitchen Tempearture')

delta=yE(1,:)'-Tk;

delta=delta(500:5905,:);
Time=Time(:,500:5905);

% Statics of error
[mean(delta) std(delta) max(delta) min(delta)]
figure(2)
hist(delta)
```

```
title('Kithcen Histogram')

figure(3)
Time = 0:dt:(n-1)*dt;
plot(Time,yE(2,:),'r', Time,Ti,'g', Time,To,'b')
ylabel('Temperature [C]')
legend('T_s_i_m','T_i','T_o')
title('Livingroom Tempearture')
delta=yE(2,:)'-Ti;

delta=delta(500:5905,:);
Time=Time(:,500:5905);

% Statics of error
[mean(delta) std(delta) max(delta) min(delta)]
figure(4)
hist(delta)
title('Livingroom Error Histogram')
figure(5)
Time = 0:dt:(n-1)*dt;
plot(Time,yE(3,:),'r', Time,Td,'g', Time,To,'b')
ylabel('Temperature [C]')
legend('T_s_i_m','T_i','T_o')
title('Doorway Tempearture')
delta=yE(3,:)'-Td;

delta=delta(500:5905,:);
Time=Time(:,500:5905);

% Statics of error
[mean(delta) std(delta) max(delta) min(delta)]
figure(6)
hist(delta)
title('Doorway Error Histogram')

figure(7)
Time = 0:dt:(n-1)*dt;
plot(Time,yE(4,:),'r', Time,Tb2,'g', Time,To,'b')
ylabel('Temperature [C]')
legend('T_s_i_m','T_i','T_o')
title('Children room Temperature')
delta=yE(4,:)'-Tb2;

delta=delta(500:5905,:);
Time=Time(:,500:5905);

% Statics of error
[mean(delta) std(delta) max(delta) min(delta)]
figure(8)
hist(delta)
title('Childrenroom Error Histogram')
```

```
figure(9)
Time = 0:dt:(n-1)*dt;
plot(Time,yE(5,:),'r', Time,Tb1,'g', Time,To,'b')
ylabel('Temperature [C]')
legend('T_s_i_m','T_i','T_o')
title('Bedroom Temperature')
delta=yE(5,:)'-Tb1;

delta=delta(500:5905,:);
Time=Time(:,500:5905);

% Statics of error
[mean(delta) std(delta) max(delta) min(delta)]
figure(10)
hist(delta)
title('Bedroom Error Histogram')

figure(11)
Time = 0:dt:(n-1)*dt;
plot(Time,yE(6,:),'r', Time,Tbh,'g', Time,To,'b')
ylabel('Temperature [C]')
legend('T_s_i_m','T_i','T_o')
title('Bathroom Temperature')
delta=yE(6,:)'-Tbh;

delta=delta(500:5905,:);
Time=Time(:,500:5905);

% Statics of error
[mean(delta) std(delta) max(delta) min(delta)]
figure(12)
hist(delta)
title('Bathroom Error Histogram')

figure(13)
Time = 0:dt:(n-1)*dt;
plot(Time,yE(7,:),'r', Time,Tc,'g', Time,To,'b')
ylabel('Temperature [C]')
legend('T_s_i_m','T_i','T_o')
title('Corridor Temperature')
delta=yE(6,:)'-Tc;

delta=delta(500:5905,:);
Time=Time(:,500:5905);

% Statics of error
[mean(delta) std(delta) max(delta) min(delta)]
figure(14)
hist(delta)
title('Corridor Error Histogram')
```

This page is intentionally blank

12 References

[1] Energy Information Administration - EIA - Official Energy Statistics from the U.S. Government EIA - "International Energy Outlook 2019".Retrieved from official website of US Energy Information administration website: www.eia.gov/outlooks/ieo/pdf/ieo2019.pdf

[2] Intergovernmental Panel on Climate Change, Climate Change: Mitigation of Climate Change. Contribution of Working Group III to the Fifth Assessment Report of the Intergovernmental Panel on Climate Change. 2014 Mitig. Clim. Chang. Contrib. Work. Gr. III to Fifth Assess. Rep., pp. 1–31, 2014.

[3] United Nations “Population 2030: Demographic challenges and opportunities for sustainable development planning,” 2014 United Nations(2015)(ST/ESA/SE 58).

[4] O. Lucon *et al.*, “Buildings,” in *Climate Change: Climate Change Mitigiation Contribution of Working Group III to Fifth Assess. Report. Intergovernmental. Panel on Climate Chang.*, vol. 33, pp. 1–66, 2014.

[5] International Energy Agency, “Energy Efficiency 2017,” Retrieved from official website of International Energy Agnecy official website : https://www.iea.org/reports/world-energy-outlook-2019.

[6] Hepher B, “Energy Pathways,” *Cambridge University Press,* pp. 64–103, 2010.

[7] J. B. S. Qi Li∗, Godfried Augenbroe, “Assessment of linear emulators in lightweight Bayesian calibration of dynamic building energy models for parameter estimation and performance prediction,” *Energy Build.*, vol. 124, pp. 194–202, Jul. 2016.

[8] S. C. M. Hui, “Building Energy Efficiency Standards in Hong Kong and Mainland China,” In Proc. of the 2000 ACEEE Summer Study on Energy Efficiency in Buildings, 20-25 August 2000, Pacific Grove, California.

[9] S. B. Forgotten and E. D. O. Fernandes, “Building Thermal Regulations : Why Has Summer Been Forgotten?”, In book: Solar Energy in Architecture and Urban Planning Proceedings, Florence, Italy 17-21 May 1993, Chapter: Proposals for a new working frame, Publisher: H.S. Stephens & Associates, Editors: Sir Norman Foster, Hermann

Scheer, pp.626-630.

[10] R. Bartlett, M. A. Halverson, and D. L. Shankle, “Understanding Building Energy Codes and Standards,” 2003.

[11] G. D. Jacobsen and M. J. Kotchen, “ARE BUILDING CODES EFFECTIVE AT SAVING ENERGY? EVIDENCE FROM RESIDENTIAL BILLING DATA IN FLORIDA,” 2013.

[12] ALLIANCE, “The History of Energy Efficiency Alliance Commission on National Energy Efficiency Policy,” 2013.

[13] “New York | Building Energy Codes Program,” 2016. [Online]. Available: https://www.energycodes.gov/adoption/states/new-york. [Accessed: 06-Jan-2018].

[14] E. Doris, J. Cochran, and M. Vorum, “Energy Efficiency Policy in the United States: Overview of Trends at Different Levels of Government,” 2009.

[15] U. Berardi*, “Building Energy.” 2010.

[16] EU, “Directive 2010/31/EU of the European Parliament and of the Council of 19 May 2010 on the energy performance of buildings,” 2010.

[17] S. Roaf, F. Nicol, M. Humphreys, P. Tuohy, and A. Boerstra, “Twentieth century standards for thermal comfort: promoting high energy buildings,” *Archit. Sci. Rev.*, vol. 53, no. 1, pp. 65–77, 2010.

[18] L. Pérez-Lombard, J. Ortiz, R. González, and I. R. Maestre, “A review of benchmarking, rating and labelling concepts within the framework of building energy certification schemes,” *Energy Build.*, vol. 41, no. 3, pp. 272–278, Mar. 2009.

[19] F. Anagnostopoulos *et al.*, “A MAPPING OF NATIONAL APPROACHES ENERGY PERFORMANCE CERTIFICATES ACROSS THE EU,” 2014.

[20] S. Wang, C. Yan, and F. Xiao, “Quantitative energy performance assessment methods for existing buildings,” *Energy Build.*, vol. 55, pp. 873–888, 2012.

[21] S. Attia, M. Hamdy, W. O’Brien, and S. Carlucci, “Assessing gaps and needs for integrating building performance optimization tools in net zero energy buildings design,” *Energy Build.*, vol. 60, pp. 110–124, May 2013.

[22] P. Rajagopalan and C. Y. Leung Tony, “Progress on building energy labelling techniques,” *Adv. Build. Energy Res.*, vol. 6, no. 1, pp. 61–80, 2012.

[23] “How BREEAM Certification Works – BREEAM,” 2017. [Online]. Available: https://www.breeam.com/discover/how-breeam-certification-works/. [Accessed: 16-

Jan-2018].

[24] X. Gao and A. Malkawi, “A new methodology for building energy performance benchmarking: An approach based on intelligent clustering algorithm,” *Energy Build.*, vol. 84, pp. 607–616, 2014.

[25] P. de Wilde, “The gap between predicted and measured energy performance of buildings: A framework for investigation,” *Autom. Constr.*, vol. 41, pp. 40–49, May 2014.

[26] IPMVP, “Measurement and Verification,” vol.no.1, January, 2012.

[27] E. Burman, D. Mumovic, and J. Kimpian, “Towards measurement and verification of energy performance under the framework of the European directive for energy performance of buildings,” *Energy*, vol. 77, pp. 153–163, 2014.

[28] M. (2008) Turner, C. & Frankel, “Energy performance of LEED for New Construction Buildings,” 2008.

[29] M. Sunikka-Blank and R. Galvin, “Building Research & Information Introducing the prebound effect: the gap between performance and actual energy consumption,” 2012.

[30] R. Galvin, “Making the ‘rebound effect’ more useful for performance evaluation of thermal retrofits of existing homes: Defining the ‘energy savings deficit’ and the ‘energy performance gap,’” *Energy Build.*, vol. 69, pp. 515–524, Feb. 2014.

[31] C. Demanuele, T. Tweddell, and M. Davies, “Bridging the gap between predicted and actual energy performance in schools,” 2010.

[32] W. L. Lee* and F. W. H. Yik, “Regulatory and voluntary approaches for enhancing building energy efficeincy.” pp. 477–499, 2004.

[33] M. A. Jamison, “Encyclopedia of Energy Engineering and Technology,” no. October, pp. 1–18, 2005.

[34] C.-H. Consulting, “20120314_1400_Ad van der Aa Simurex April 14 2012 definitief.” 2012.

[35] A. Foucquier, S. Robert, F. Suard, L. Stéphan, and A. Jay, “State of the art in building modelling and energy performances prediction: A review,” *Renew. Sustain. Energy Rev.*, vol. 23, pp. 272–288, 2013.

[36] N. Fumo, “A review on the basics of building energy estimation,” *Renew. Sustain. Energy Rev.*, vol. 31, pp. 53–60, 2014.

[37] H. Zhao and F. Magoulès, “A review on the prediction of building energy consumption,”

Renew. Sustain. Energy Rev., vol. 16, no. 6, pp. 3586–3592, Aug. 2012.

[38] ASHRAE, "Energy Estimating and Modeling Methods," *ASHREA Handbook. Fundam.*, no. 1, pp. 19.1-38, 2009.

[39] a. Rabl, "Parameter Estimation in Buildings: Methods for Dynamic Analysis of Measured Energy Use," *J. Sol. Energy Eng.*, vol. 110, no. 1, p. 52, 1988.

[40] D. Coakley, P. Raftery, and M. Keane, "A review of methods to match building energy simulation models to measured data," *Renew. Sustain. Energy Rev.*, vol. 37, pp. 123–141, 2014.

[41] M. Manfren, N. Aste, and R. Moshksar, "Calibration and uncertainty analysis for computer models" A meta-model based approach for integrated building energy simulation," *Appl. Energy*, vol. 103, pp. 627–641, 2013.

[42] A. H. Neto and F. A. S. Fiorelli, "Comparison between detailed model simulation and artificial neural network for forecasting building energy consumption," *Energy Build.*, vol. 40, no. 12, pp. 2169–2176, 2008.

[43] Lennart Ljung, "DEVELOPMENT OF SYSTEM IDENTIFICATION Department of Electrical Engineering, Linkoping University Linkoping, Sweden. Emai t: Ljung~isy. liu. se," in *13th Tric:nnial World Congress. San Francisco. USA*, 1996.

[44] V. Balakrishnan, "System identification: theory for the user (second edition)," *Automatica*, vol. 38, no. 2, pp. 375–378, 2002.

[45] J. L. Crassidis and J. L. Junkins, *Optimal estimation of dynamic systems*. 2011.

[46] A. Janssens, *Statistical Guidelines:Reliable building energy performance characterisation based on full scale dynamic measurements in Buildings Background : Renewed interest in full scale testing Interest*, no. May. 2014.

[47] M. J. Jiménez, B. Porcar, and M. R. Heras., "2008. Estimation of UA and gA values of building components from outdoor tests in warm and moderate weather conditions. Solar Energy. 82(7), pp. 573-587.," *Sol. Energy. 79(3), pp. 302-310.*, vol. 79, no. 3, pp. 302–310, 2008.

[48] D. Kim, J. Cai, J. E. Braun, and K. B. Ariyur, "System Identification for Building Thermal Systems under the Presence of Unmeasured Disturbances in Closed Loop Operation: Theoretical Analysis and Application," *Energy Build.*, 2017.

[49] P. Bacher and H. Madsen, "Identifying suitable models for the heat dynamics of

buildings," *Energy Build.*, vol. 43, no. 7, pp. 1511–1522, Jul. 2011.

[50] IEA, *Report of Subtask 4b: Towards a characterisation of buildings based on in situ testing and smart meter readings and potential for applications in smart grids*, no. May. 2014.

[51] X. Li and J. Wen, "Review of building energy modeling for control and operation," *Renew. Sustain. Energy Rev.*, vol. 37, pp. 517–537, 2014.

[52] X. Lu, D. Clements-Croome, and M. Viljanen, "Past, present and future mathematical models for buildings," *Intell. Build. Int.*, vol. 1, no. 1, pp. 23–38, 2009.

[53] I. E. Agency, "Reliable building energy performance characterisation based on full scale dynamic measurements," 2014.

[54] M. De Rosa, V. Bianco, F. Scarpa, and L. A. Tagliafico, "Historical trends and current state of heating and cooling degree days in Italy," *Energy Convers. Manag.*, vol. 90, pp. 323–335, 2015.

[55] S. Danov, J. Carbonell, J. Cipriano, and J. Martí-Herrero, "Approaches to evaluate building energy performance from daily consumption data considering dynamic and solar gain effects," *Energy Build.*, vol. 57, pp. 110–118, 2013.

[56] S. Danov, J. Carbonell, J. Cipriano, and J. Martí-Herrero, "Approaches to evaluate building energy performance from daily consumption data considering dynamic and solar gain effects," *Energy Build.*, vol. 57, pp. 110–118, 2013.

[57] C. Ghiaus, "Experimental estimation of building energy performance by robust regression," *Energy Build.*, vol. 38, no. 6, pp. 582–587, Jun. 2006.

[58] Q. Meng and M. Mourshed, "Degree-day based non-domestic building energy analytics and modelling should use building and type specific base temperatures," *Energy Build.*, vol. 155, pp. 260–268, 2017.

[59] R.Bouche, "Methodologies for the Assessment of Intrinsic Energy Performance of Buildings Envelope," Performer, March 2015.

[60] Y. Zhang, Z. O'Neil, B. Dong, G. Augenbroe, "Comparisons of inverse modeling approaches for predicting building energy performance," *Build. Env.*, vol. 86, pp. 177–190, 2015.

[61] J. S. Park, S. J. Lee, K. H. Kim, K. W. Kwon, and J.-W. Jeong, "Estimating thermal performance and energy saving potential of residential buildings using utility bills,"

Energy Build., vol. 110, pp. 23–30, 2016.

[62] Z. An Verbai, A. Lakatos, and F. Kalm, “Prediction of energy demand for heating of residential buildings using variable degree day,” *Energy*, vol. 76, pp. 780–787, 2014.

[63] A.-H. Deconinck and S. Roels, “Comparison of characterisation methods determining the thermal resistance of building components from onsite measurements,” *Energy Build.*, vol. 130, pp. 309–320, 2016.

[64] A. Anjomshoaa and M. Salmanzadeh, “Estimation of the changeover times and degree-days balance point temperatures of a city using energy signatures,” *Sustain. Cities Soc.*, vol. 35, pp. 538–543, 2017.

[65] M. De Rosa, V. Bianco, F. Scarpa, and L. A. Tagliafico, “Heating and cooling building energy demand evaluation; a simplified model and a modified degree days approach,” *Appl. Energy*, vol. 128, pp. 217–229, 2014.

[66] Y. Heo, R. Choudhary, and G. A. Augenbroe, “Calibration of building energy models for retrofit analysis under uncertainty,” *Energy Build.*, vol. 47, pp. 550–560, Apr. 2012.

[67] L. Webster *et al.*, “M&V Guidelines: Measurement and Verification for Performance-Based Contracts Version 4.0,” 2015.

[68] T. A. Reddy, “Literatue Review on Calibration of Building Energy Simulation Programs: Uses,Problems,Procedures,Uncetainty, and Tools,” *ASHRE Trans.*, p. 112:126, 2006.

[69] P. Taylor, R. T. Hodapp, and R. T. Hodapp, “Encyclopedia of Energy Engineering and Technology LEED-EB : Leadership in Energy and Environmental Design for Existing Buildings,” , pp. 37–41, April 2011.

[70] E. Fabrizio and V. Monetti, “Methodologies and advancements in the calibration of building energy models,” *Energies*, vol. 8, no. 4, pp. 2548–2574, 2015.

[71] P. Raftery, M. Keane, and A. Costa, “Calibrating whole building energy models: Detailed case study using hourly measured data,” *Energy Build.*, vol. 43, pp. 3666–3679, 2011.

[72] K. Subbarao, “PSTAR: Primary and secondary terms analysis and renormalization: A unified approach to building energy simulations and short-term monitoring,” Golden, CO (United States), Sep. 1988.

[73] J. Sun and T. A. Reddy, “Calibration of Building Energy Simulation Programs Using the Analytic Optimization Approach (RP-1051),” *HVAC&R Res.*, vol. 12, no. 1, pp. 177–196, Jan. 2006.

[74] W. Tian, “A review of sensitivity analysis methods in building energy analysis,” *Renew. Sustain. Energy Rev.*, vol. 20, pp. 411–419, 2013.

[75] Y. Gan *et al.*, “A comprehensive evaluation of various sensitivity analysis methods: A case study with a hydrological model,” 2014.

[76] S. Yang, W. Tian, E. Cubi, Q. Meng, Y. Liu, and L. Wei, “ScienceDirect Comparison of Sensitivity Analysis Methods in Building Energy Assessment,” *Procedia Eng.*, vol. 146, pp. 174–181, 2016.

[77] G. Allesina, E. Mussatti, F. Ferrari, and A. Muscio, “A calibration methodology for building dynamic models based on data collected through survey and billings,” *Energy Build.*, vol. 158, pp. 406–416, Jan. 2018.

[78] M. J. Jiménez and H. Bloem, “Energy performance assessment of buildings and building components. Guidelines for data analysis from dynamic experimental campaigns part 1: physical aspects,” *Energy Procedia*, vol. 78, pp. 3306–3311, 2015.

[79] Matalas N.C.(U.S. Geological Survey Arlington), “Time Series Analysis,” *Water Resour. Res.*, vol. 3, no. 3, pp. 5–6, 1967.

[80] F. Edition, R. S. Figliola, and D. E. Beasley, *Theory and Design for Mechanical Measurements*. 2011.

[81] D. Myers, *KALMAN FILTERING Theory:Theory and Practice Using MATLAB*. 2002.

[82] A.Florent, G. Pandraud, and R. Fitton, “QUB: a fast dynamic method for in-situ measurement of the whole building heat loss,” *Energy Build.*, vol. 174, pp. 124–133, 2018.

[83] A. Brun, A. Florent, P. Boisson, and S. Thebault, “Short methodologies for in-situ assessment of the intrisinc thermal performance of the building envelope,” in *Sustainable Places*, 2014, no. October.

[84] “ISO - ISO 9869-1:2014 - Thermal insulation — Building elements — In-situ measurement of thermal resistance and thermal transmittance — Part 1: Heat flow meter method.” [Online]. Available: https://www.iso.org/standard/59697.html. [Accessed: 04-Mar-2020].

[85] A. Rasooli, L. Itard, and C. I. Ferreira, “A response factor-based method for the rapid in-situ determination of wall’s thermal resistance in existing buildings,” *Energy Build.*, vol. 119, pp. 51–61, 2016.

[86] M. J. Jiménez and .M.R. Heras, “Application of multi-output ARX models to estimate the U and g values of building components from outdoors testing,” *Sol. Energy. 79(3), pp. 302-310.*, vol. 3, no. 79, pp. 302–310, 2005.

[87] M. J. Jiménez and H. Madsen, “Models for describing the thermal characteristics of building components,” *Build. Environ.*, vol. 43, no. 2, pp. 152–162, Feb. 2008.

[88] C. Lodi, P. Bacher, J. Cipriano, and H. Madsen, “Modelling the heat dynamics of a monitored Test Reference Environment for Building Integrated Photovoltaic systems using stochastic differential equations,” *Energy Build.*, vol. 50, pp. 273–281, 2012.

[89] G. Bauwens and S. Roels, “Co-heating test: A state-of-the-art,” *Energy Build.*, vol. 82, pp. 163–172, 2014.

[90] G. Bauwens and S. Roels, “Co-heating test: A state-of-the-art,” *Energy Build.*, 2014.

[91] S. Stamp, H. Altamirano-Medina, and R. Lowe, “Assessing the Relationship between Measurement Length and Accuracy within Steady State Co-Heating Tests,” *Buildings*, vol. 7, no. 4, p. 98, 2017.

[92] V. Sougkakis, J. Meulemans, F. Alzetto, C. Wood, and T. Cox, “An assessment of the QUB method for predicting the whole building thermal performance under actual operating conditions,” vol. 2015, no. September, pp. 13–14, 2017.

[93] C. Ghiaus and A. Florent, “Design of experiments for Quick U-building method for building energy performance measurement,” *J. Build. Perform. Simul.*, vol. 0, no. 0, pp. 1–15, 2019.

[94] J. Meulemans, F. Alzetto, D. Farmer, and C. Gorse, “QUB/e: A novel transient experimental method for in situ measurements of the thermal performance of building fabrics,” *Build. Inf. Model. Build. Performance, Des. Smart Constr.*, no. September 2016, pp. 14–15, 2017.

[95] E. Mangematin, G. Pandraud, and D. Roux, “Author ’ s personal copy Comptes Rendus Physique Quick measurements of energy e ffi ciency of buildings Mesures rapides de l ’ e ffi cacité énergétique des bâtiments,” 2012.

[96] A. Florent, G. Didier, and P. Guillaume, “Mesure rapide du coefficient de perte thermique des bâtiments Bases théoriques,” no. 1, pp. 1–10, 2014.

[97] G. Pandraud, G. Didier, and F. Alzetto, “Experimental optimization of the QUB method,” in *IEA–EBC Annex 58, 6th Expert meeting*, 2014, no. 1.

[98] H.Madesen and J.Hoist, “Estimation of continuous-time models for the heat dynamics of building,” vol. 22, pp. 67–79, 1995.

[99] G. Pandraud and R. Fitton, “QUB: Validation of a Rapid Energy Diagnosis Method for Buildings,” in *Interanational Energy Agency Annexe 58*, 2014, pp. 1–6.

[100] A.Florent, D. Farmer, R. Fitton, T. Hughes, and W. Swan, “Comparison of whole house heat loss test methods under controlled conditions in six distinct retrofit scenarios,” *Energy Build.*, vol. 168, pp. 35–41, Jun. 2018.

[101] A. Florent, Gossard D, “Mesure rapide du coefficient de perte thermique des bâtiments, , 19-20 mars 2014, Paris.,” in *Congrès Sciences et Technique Ecobat*, 2014, pp. 19–20.

[102] P. Strachan, I. Heusler, M. Kersken, and M. J. Jiménez, “Empirical Whole Model Validation Modelling Specification Validation of Building Energy Simulation Tools,” 2016.

[103] H. Wang and Z. (John) Zhai, “Advances in building simulation and computational techniques: A review between 1987 and 2014,” *Energy Build.*, vol. 128, pp. 319–335, Sep. 2016.

[104] S. Bruning, P. James, and R. Doeffinger., *Nonresidential Cooling and Heating Load Calculation Procedures*, 18.1-18.66. Atlanta, 2017.

[105] “Heating systems in buildings - Method for calculation of the design heat load," EN 12831, European Committee for Standardization,Brussels, 2003.

[106] CEN, *Thermal performance of buildings-calculation of energy use for space heating and cooling-General criteria and validation procedures (Energy need calculations-heating and cooling)"*, EN 15265., European Committee for Standardization, Brussels,2007.

[107] CEN, *Heating systems in buildings - Method for calculation of the design heat load", EN 12831*. European Committee for Standardization, Brussels,2003.

[108] IBPSA-USA, “Building Energy Software Tools.” [Online]. Available: https://www.buildingenergysoftwaretools.com/?__cf_chl_jschl_tk__=5c7a2e0fd09b138d1e4971146a21dcc291498c5c-1579703694-0-AU7MXXr9NGcpQMabW7HZtAoxEWrjHBg4Xfd-yJrbkq09EfD4pICk1Z6MZfwosmduMZjxB7jej4CBOgt1jdPdLQSO-jyuCOlHAW4bgwBxKuaAIkbhhLGvm6nw8R8gmKO2ZlKm4bvA. [Accessed: 22-Jan-2020].

[109] TRNSYS 16, “Mathematical Reference.” WI: Solar Energy Laboratory, University of Wisconsin-Madison, Madison, 2009.

[110] EnergyPlus, “EnergyPLus Engineering Reference,” University of Illinois and Lawrence Berkeley National Laboratory, 2013.

[111] P. Sahlin, L. Eriksson, P. Grozman, H. Johnsson, A. Shapovalov, and M. Vuolle, “Whole-building simulation with symbolic DAE equations and general purpose solvers,” in *Building and Environment*, 2004, vol. 39, no. 8 SPEC. ISS., pp. 949–958.

[112] J. Clarke, *Energy Simulation in Building Design*. Oxford:Butterworth Heinmann, 2001.

[113] A. H. Fakra, F. Miranville, H. Boyer, and S. Guichard, “Development of a new model to predict indoor daylighting: Integration in CODYRUN software and validation,” Dec. 2012.

[114] K. S.- Energy and undefined 2010, “Advanced software tool for the dynamic analysis of heat transfer in buildings; applications to Syria,” *Elsevier*.

[115] M. Chung and H. C. Park, “Development of a software package for community energy system assessment - Part I: Building a load estimator,” *Energy*, vol. 35, no. 7, pp. 2767–2776, 2010.

[116] A. Buonomano and A. Palombo, “Building energy performance analysis by an in-house developed dynamic simulation code: An investigation for different case studies,” *Appl. Energy*, vol. 113, pp. 788–807, 2014.

[117] D. W. U. Perera, D. Winkler, and N. O. Skeie, “Multi-floor building heating models in MATLAB and Modelica environments,” *Appl. Energy*, vol. 171, pp. 46–57, Jun. 2016.

[118] P. Michalak, “The development and validation of the linear time varying Simulink-based model for the dynamic simulation of the thermal performance of buildings,” *Energy Build.*, vol. 141, pp. 333–340, Apr. 2017.

[120] M. Wetter, “Modelica-based modelling and simulation to support research and development in building energy and control systems,” *J. Build. Perform. Simul.*, vol. 2, no. 2, pp. 143–161, Jun. 2009.

[121] V. S. K. V. Harish and A. Kumar, “A review on modeling and simulation of building energy systems,” *Renewable and Sustainable Energy Reviews*, vol. 56. Elsevier Ltd, pp. 1272–1292, 01-Apr-2016.

[122] Y. Wang, J. Kuckelkorn, and Y. Liu, “A state of art review on methodologies for control

strategies in low energy buildings in the period from 2006 to 2016," *Energy Build.*, vol. 147, pp. 27–40, Jul. 2017.

[123] Z. Afroz, G. M. Shafiullah, T. Urmee, and G. Higgins, "Modeling techniques used in building HVAC control systems: A review," *Renewable and Sustainable Energy Reviews*, vol. 83. Elsevier Ltd, pp. 64–84, 01-Mar-2018.

[124] P. Bacher and H. Madsen, "Identifying suitable models for the heat dynamics of buildings," *Energy Build.*, vol. 43, pp. 1511–1522, 2011.

[125] CEN, "Thermal performance of buildings-Sensible room cooling load calculation – General criteria and validation procedures EN 15255," in *Thermal performance of buildings*, Brussels: European Committee for Standardization.

[126] O. Alhaj Hasan, D. Defer, and I. Shahrour, "A simplified building thermal model for the optimization of energy consumption: Use of a random number generator," *Energy Build.*, vol. 82, pp. 322–329, 2014.

[127] V. S. K. V. Harish and A. Kumar, "Reduced order modeling and parameter identification of a building energy system model through an optimization routine," *Appl. Energy*, vol. 162, pp. 1010–1023, Jan. 2016.

[128] A. Florent, J. Meulemans, G. Pandraud, and D. Roux, "A perturbation method to estimate building thermal performance," 2018.

[129] C. Andrade-Cabrera, D. Burke, W. J. N. Turner, and D. P. Finn, "Ensemble Calibration of lumped parameter retrofit building models using Particle Swarm Optimization," *Energy Build.*, vol. 155, pp. 513–532, Nov. 2017.

[130] S. Rouchier, "Solving inverse problems in building physics: An overview of guidelines for a careful and optimal use of data," *Energy and Buildings*, vol. 166. Elsevier Ltd, pp. 178–195, 01-May-2018.

[131] S. Rouchier, M. Rabouille, and P. Oberlé, "Calibration of simplified building energy models for parameter estimation and forecasting: Stochastic versus deterministic modelling," *Build. Environ.*, vol. 134, pp. 181–190, Apr. 2018.

[132] A. Zekar and S. El Khatib, "Development and assessment of simplified building representations under the context of an urban energy model: Application to arid climate environment," *Energy Build.*, vol. 173, pp. 461–469, Aug. 2018.

[133] E. J. Kim, G. Plessis, J. L. Hubert, and J. J. Roux, "Urban energy simulation: Simplification

and reduction of building envelope models," *Energy Build.*, vol. 84, pp. 193–202, 2014.

[134] M. Robillart, P. Schalbart, F. Chaplais, and B. Peuportier, "Model reduction and model predictive control of energy-efficient buildings for electrical heating load shifting," *J. Process Control*, vol. 74, pp. 23–34, Feb. 2019.

[135] O. Mejri, E. Palomo Del Barrio, and N. Ghrab-Morcos, "Energy performance assessment of occupied buildings using model identification techniques," *Energy Build.*, vol. 43, no. 2–3, pp. 285–299, Feb. 2011.

[136] I. Naveros and C. Ghiaus, "Order selection of thermal models by frequency analysis of measurements for building energy efficiency estimation," *Appl. Energy*, vol. 139, pp. 230–244, Feb. 2015.

[137] J. Široký, F. Oldewurtel, J. Cigler, and S. Prívara, "Experimental analysis of model predictive control for an energy efficient building heating system," *Appl. Energy*, vol. 88, no. 9, pp. 3079–3087, Sep. 2011.

[138] E. O'Dwyer, L. De Tommasi, K. Kouramas, M. Cychowski, and G. Lightbody, "Prioritised objectives for model predictive control of building heating systems," *Control Eng. Pract.*, vol. 63, pp. 57–68, Jun. 2017.

[139] I. Hazyuk, C. Ghiaus, and D. Penhouet, "Optimal temperature control of intermittently heated buildings using Model Predictive Control: Part II - Control algorithm," *Build. Environ.*, vol. 51, pp. 388–394, 2012.

[140] J. Figueiredo and J. Sá Da Costa, "A SCADA system for energy management in intelligent buildings," *Energy Build.*, vol. 49, pp. 85–98, Jun. 2012.

[141] Z. Váňa, J. Cigler, J. Široký, E. Žáčeková, and L. Ferkl, "Model-based energy efficient control applied to an office building," *J. Process Control*, vol. 24, no. 6, pp. 790–797, 2014.

[142] S. Mahendra, P. Stephane, and W. Frederic, "Modeling for reactive building energy management," in *Energy Procedia*, 2015, vol. 83, pp. 207–215.

[143] H. Viot, A. Sempey, L. Mora, J. C. Batsale, and J. Malvestio, "Model predictive control of a thermally activated building system to improve energy management of an experimental building: Part I—Modeling and measurements," *Energy Build.*, vol. 172, pp. 94–103, Aug. 2018.

[144] S. Yang *et al.*, "A state-space thermal model incorporating humidity and thermal

comfort for model predictive control in buildings," *Energy Build.*, vol. 170, pp. 25–39, Jul. 2018.

[145] M. Luzi, M. Vaccarini, and M. Lemma, "A tuning methodology of Model Predictive Control design for energy efficient building thermal control," *J. Build. Eng.*, vol. 21, pp. 28–36, Jan. 2019.

[146] V. Kirubakaran, C. Sahu, T. K. Radhakrishnan, and N. Sivakumaran, "Energy efficient model based algorithm for control of building HVAC systems," *Ecotoxicol. Environ. Saf.*, vol. 121, pp. 236–243, Nov. 2015.

[147] M. Maasoumy, M. Razmara, M. Shahbakhti, and A. S. Vincentelli, "Handling model uncertainty in model predictive control for energy efficient buildings," *Energy Build.*, vol. 77, pp. 377–392, 2014.

[148] J. Hu and P. Karava, "A state-space modeling approach and multi-level optimization algorithm for predictive control of multi-zone buildings with mixed-mode cooling," *Build. Environ.*, vol. 80, pp. 259–273, 2014.

[149] T. Martinez-Marin, "State-space formulation for circuit analysis," *IEEE Trans. Educ.*, vol. 53, no. 3, pp. 497–503, Aug. 2010.

[150] K. R. Uren and G. Van Schoor, "State space model extraction of thermohydraulic systems - Part I: A linear graph approach," *Energy*, vol. 61, pp. 368–380, Nov. 2013.

[151] "Hydro-Québec, SimPowerSystems, Natick, MA: The MathWorks, Inc., 2003 - Google Search." [Online]. Available: https://www.google.com/search?q=Hydro-Québec%2C+SimPowerSystems%2C+Natick%2C+MA%3A+The+MathWorks%2C+Inc.%2C+2003&rlz=1C1EJFA_frFR823FR823&oq=Hydro-Québec%2C+SimPowerSystems%2C+Natick%2C+MA%3A+The+MathWorks%2C+Inc.%2C+2003&aqs=chrome..69i57.927j0j4&sourceid=chrome&ie=UTF-8. [Accessed: 22-Jan-2020].

[152] I. Naveros, C. Ghiaus, and D. P. Ruiz, "THERMAL NETWORKS CONSIDERING GRAPH THEORY AND THERMODYNAMICS."

[153] G.Strang ,"Intorduction to Linear Algebra", Welleseley-Cambride Press,Welleseley,MA, Fifth edition,2009.GhiaFloreAlze

[154] C. Ghiaus, "Causality issue in the heat balance method for calculating the design heating and cooling load," *Energy*, vol. 50, no. 1, pp. 292–301, 2013.

[155] C. Eastman, P. Teicholz, R. Sacks, and K. Liston, *BIM Handbook*. John Wiley & Sons, Inc., 2008.

[156] P. Strachan, K. Svehla, M. Kersken, and I. Heusler, “Reliable building energy performance characterisation based on full scale dynamic measurements Report of Subtask 4a: Empirical validation of common building energy simulation models based on in situ dynamic data,” 2014.

FOLIO ADMINISTRATIF

THESE DE L'UNIVERSITE DE LYON OPEREE AU SEIN DE L'INSA LYON

NOM : AHMAD DATE de SOUTENANCE : 08/07/2020

Prénoms : Naveed

TITRE : Measurement of Energy Performance: Analysis of QUB method

NATURE : Doctorat Numéro d'ordre : 2020LYSEI051

Ecole doctorale : Mécanique, énergétique, génie civil, acoustique (MEGA)

Spécialité :

Thermique et Energetique de Batiment et de leur de Environment

RESUME : The quick U-building (QUB) method is used to measure the overall heat loss coefficient of buildings during one to two nights by applying heating power and by measuring the indoor and the outdoor temperatures. In this work numerical QUB experiments are performed with different initial conditions (initial power), boundary conditions (solar radiation) and designs of QUB experiment (heating power and time duration). In order to simulate the QUB experiments a dynamic state space model is developed. The developed model is validated using IEA EBC Annex 58 data for a single story house. The QUB experiments are simulated for this house, using different initial conditions, boundary conditions and different seasons. QUB method shows robustness to variation in the value of the overall heat loss coefficient for which the experiment was designed and in the variation of optimum power for the QUB experiments. The variations in the QUB method results are smaller on cloudy than on sunny days, the error being reduced from about 10 % to about 7 %. A correction is proposed for the solar radiation absorbed by the wall that contributes to the evolution of air temperature during the heating phase. The QUB results with variable outdoor temperature during the test show relatively high variation and error as compared to the conditions when temperature is constant. A ±20% increase or decrease in the outdoor temperature during the QUB experiment can change the results of test by ±5%. The QUB results for QUB experiments simulated during the winter months show error within ±15%. The QUB results during the months of summers show relatively large variation. The median error of multiple QUB experiments in summers can be reduced by increasing the set point temperature before the start of QUB experiment.

MOTS-CLÉS : energy efficiency, overall heat transfer coefficient, buildings energy, QUB, IEA EBC Annex-58,data analysis, a prioiri, a posteriori analysis, buildings, energy perfromance

Laboratoire (s) de recherche :Centre D'ENERGETIQUE ET DE THERMIQUE DE LYON

Directeur de thèse: GHIAUS, Christian : Professeur des Universités, INSA Lyon, France.

Président de jury : SAELENS, Dirk : Professeur des Universités, KU Leuven, Belgique, examinateur

Composition du jury :
JIMENEZ, Maria Jose : Directrice de recherche, CIEMAT, Espagne, rapporteuse
IBOS, Laurent : MCF, HDR, CERTES, Université Paris-Est Créteil, France, rapporteur